Selective Low Temperature Oxidation of Methane with Hydrogen Peroxide by Quasi-Heterogeneous Catalysis

Thesis submitted in accordance with the requirements of the University of Cardiff for the degree of doctor of philosophy by

Rebecca Una McVicker

2014

Declaration

This work has not been submitted in substance for any other degree or award at this or any other university or place of learning, nor is being submitted concurrently in candidature for any degree or other award.

Signed …… (candidate) Date ……

STATEMENT 1

This thesis is being submitted in partial fulfillment of the requirements for the degree of …… (insert MCh, MD, MPhil, PhD etc, as appropriate)

Signed …… (candidate) Date ……

STATEMENT 2

This thesis is the result of my own independent work/investigation, except where otherwise stated.
Other sources are acknowledged by explicit references. The views expressed are my own.

Signed …… (candidate) Date ……

STATEMENT 3

I hereby give consent for my thesis, if accepted, to be available online in the University's Open Access repository and for inter-library loan, and for the title and summary to be made available to outside organisations.

Signed …… (candidate) Date ……

STATEMENT 4: PREVIOUSLY APPROVED BAR ON ACCESS

I hereby give consent for my thesis, if accepted, to be available online in the University's Open Access repository and for inter-library loans **after expiry of a bar on access previously approved by the Academic Standards & Quality Committee.**

Signed …… (candidate) Date ……

Summary

Methane is our most abundant hydrocarbon. However, this natural resource is not being effectively utilised. Currently, its primary industrial use is the manufacture of methanol through the intermediate formation of synthesis gas (H_2 and CO). This is an energy intensive process requiring temperatures of up to 850 ^{0}C and pressures of up to 100 atm. Clearly, a direct method of converting methane to methanol under mild conditions would provide many advantages. Au-Pd/TiO_2 has already been shown to be an effective catalyst for the oxidation of methane with H_2O_2 at low temperature (50 °C). In this work, the intrinsic activity of the Au-Pd nanoparticles and the role of the support in this reaction are investigated. This is achieved by comparing, in detail, the activity of Au-Pd/TiO_2 with that of unsupported Au-Pd nanoparticles. The unsupported nanoparticles are not only found to be active for this reaction but in fact display superior activity compared to the supported nanoparticles. The basis for this difference in activity is investigated and shown to be caused by an increase in H_2O_2 decomposition which occurs when the particles are supported thus reducing oxidant availability for the methane oxidation reaction. Further investigations into the intrinsic activity of the unsupported Au-Pd nanoparticles, and the factors affecting it, are then carried out. A study was also carried out into the use of methyl hydroperoxide (a methane oxidation product) in combination with H_2O_2 to activate methane. The first stage of this study was to establish a method of producing methyl hydroperoxide and to this end several copper catalysts were prepared and tested. Cu/ZSM-5 was selected for this purpose and was used thereafter to produce methyl hydroperoxide for subsequent reactions with methane without the presence of a solid catalyst. The reaction conditions for the methyl hydroperoxide system were optimised and some preliminary investigations of the reaction mechanism were carried out.

Acknowledgements

Firstly, I would like to thank my supervisor, Prof. Graham Hutchings for giving me the opportunity to carry out my PhD at the Cardiff Catalysis Institute. I would also like to thank him for the advice, support and encouragement he has given me over the last three years.

I'd like to say a special thanks to Dr. Robert Jenkins for help with all things NMR. And also for always giving useful advice when things went wrong. I'd like to thank my mentor Prof. Stuart Taylor for his helpful input over the last three years. I gratefully acknowledge Dr. Chris Kiely and his staff at Lehigh University for some of the wonderful TEM images in this thesis. All other TEM analysis was carried out by Dr. Georgi Lalev in the School of Optometry at Cardiff University who I'd also like to thank. And I'd like to thank Dr. David Morgan for running all of the XPS analysis reported in this thesis and his help and advice regarding the analysis of the spectra. Steve Morris is especially deserving of my thanks for keeping my reactors running and for always fixing them faster than I expected no matter how I managed to break them.

I'd like to thank the post-docs and PhD students that I've worked with at Cardiff University. In particular the people I worked with as part of the alkane oxidation team. Dr. Mike Forde, Dr. Nikolaos Dimitratos, Dr. Greg Shaw and Dr. Robert Armstrong. I owe a special thanks to Dr. Simon Freakley for reading this thesis, offering corrections and advice and for keeping me calm during the write up period. And to Virginie Peneau, for being a wonderful friend and teammate.

I'd like to thank my school science teacher Ms. Daly for sparking my interest in science and always being happy to answer questions that weren't in the book.

I'd like to thank my brothers, Barry and Lyle, who are accepting thesis acknowledgements in lieu of birthday presents this year. And my parents, without out their support (both financial and emotional) none of this would have been possible. I'd like to thank all the new friends I made in Cardiff (and the ones who came with me from Ireland) for not only helping me through the last three years but making also making them far more enjoyable.

Finally I would like to thank Charlie, for everything.

Table of Contents

6 *Conclusions and Future Work*

Introduction 1

1.1 Introduction to Selective Methane Oxidation

Methane, as the most abundant hydrocarbon, is both available and affordable. It is the primary component of natural gas, accounting for 70-90% of its total composition depending on source.[1] As of January 1, 2013, it was estimated that the total worldwide volume of natural gas reserves are 6,846 trillion cubic feet.[2] In addition, the recent development of hydraulic fracking processes to release hydrocarbons from rock formations has led to the availability of shale gas, of which methane has also been found to be a major constituent.[3]

However, this natural resource is difficult to effectively utilise. Currently, the primary industrial utilisation of methane involves the indirect conversion of methane to methanol via the intermediate formation of synthesis gas (a mixture of CO and H_2). This process requires high temperatures (up to 850 °C) and pressures (up to 100 atm) making it both expensive and energy intensive. As such a one-step process for the activation and transformation of methane under mild conditions would be advantageous. The activation of methane is technically challenging as it is the least reactive of all hydrocarbons. The inertness of the molecule is the result of a combination of factors. It has perfect symmetry and poor coordinative ability due to the low polarity of its C-H bonds. This low polarity is the result of the similar electronegativity values of carbon and

hydrogen (χ_C = 2.55; χ_H = 2.20).[4] The main difficulty is the high C-H bond dissociation energy value of methane (439 kJ mol^{-1}).[5] The problem is further complicated by the likelihood of over- oxidation. As the methane molecule is highly inert, the target species are generally much more reactive than methane. For example, the C-H bonds of methanol are much weaker than those of methane (C-H bond dissociation 373.5 kJ mol^{-1}). As such the selectivity of methane oxidation systems is often limited by the tendency to produce deeper oxidation products. [6]

The effective use of methane is also hindered by the difficulties surrounding the transportation of this flammable and highly volatile gas. This has led to the practice of flaring natural gas at well heads, which results in high amounts of CO_2 entering the environment. Improvements have been made in this area through the use of the LNG (liquefied natural gas) process, which involves cooling natural gas to -162 °C in order to liquefy it so as to make it more transportable.[7] However the process is considered hazardous, and also requires considerable energy input.

The oxidative upgrading of methane into more useful chemicals has attracted significant academic attention for some time, particularly as petroleum recovery becomes more difficult and the demand for chemicals and energy increases.[8] The direct conversion of methane to methanol would represent an ideal method of exploiting natural gas reserves, as methanol is easily transportable and can be used as a chemical feedstock to produce a wide variety of high value hydrocarbons.

1.2 Biological Methane Oxidation

Despite these difficulties a highly selective method to oxidise methane to methanol at low temperature in aqueous media already exists in nature. Methanotrophic bacteria have the ability to utilise methane as their sole source of both carbon and energy. The initial step in their respiration process is the oxidation of methane to methanol (equation 1.1).[9]

$$CH_4 + NADH + H^+ + O_2 \rightarrow CH_3OH + NAD^+ + H_2O$$

Equation 1.1

This reaction is catalysed by the non-heme enzyme system methane monooxygenase (MMO). The majority of methanotrophic bacteria express the particulate form of MMO which is membrane-bound (pMMO), while the expression of the soluble form (sMMO) is less common.[9] However sMMO has been fully characterised, whereas pMMO is less well understood since the instability of the enzyme creates difficulties for purification. The most studied variations of sMMO are those isolated from *Methylococcus capsulatus* (Bath) and *Metylosinus trichosporium* OB3b. sMMO has been found to be a multi-enzyme complex composed of three protein units: a hydroxylase unit, a reductase unit, and a regulatory protein.[9] The oxidation of methane by molecular oxygen occurs at the active site, a di-iron μ-oxo species (shown in figure 1.1), which is located within the hydroxylase unit.[10] The active site is flexible, allowing the oxidation state of both iron centres to vary between 2+ and 4+ during the redox cycle. It is believed that the hydroxylation of an un-activated methane C-H bond occurs by a non-radical mechanism that involves the formation of a high valent ferryl ion.[11, 12]

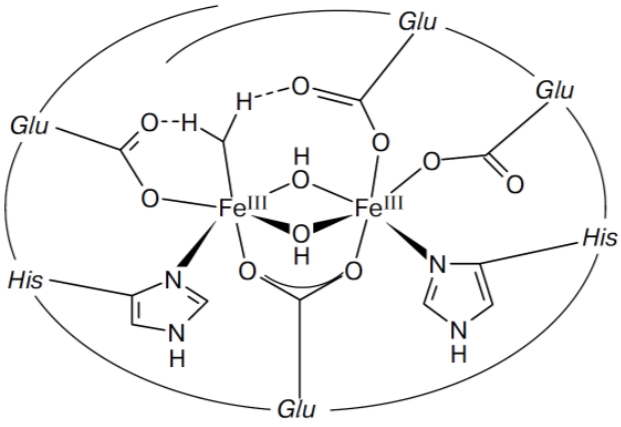

Figure 1.1 The active site of a methane monooxygenase enzyme complex.[10]

The seminal work carried out by Dalton *et al.* found that sMMO is a non-specific monooxygenase enzyme that can efficiently oxidise not only methane but

also other n-alkanes up to C8 as well as cyclic and aromatic alkanes, alkenes, and ether.[13] It was found to be highly selective; the only products formed from the oxidation of C1-C8 n-alkanes were 1- or 2-alcohols with no over-oxidation detected.[9, 13] The productivity of sMMO for methane oxidation with molecular oxygen was found to be 5.05 $mol_{(methanol)}kg_{(protein)}^{-1}$ h^{-1}, which is often used as an academic benchmark for the low temperature oxidation of methane.[13]

Methane monooxygenase enzymes with active sites that contained metals other than iron have also been studied. Although not as well understood as sMMO, it is known that the active site of pMMO contains copper. The enzyme contains 12 – 15 copper atoms, but it is unclear how many are present within the hydroxylase active site. Various studies have suggested that a mono-, di-, or tri-copper moiety could be responsible for methane hydroxylation.[14-16] A Au-protein from the aurophilic bacteria *Micrococcus luteus* has also been reported to display activity for the selective oxidation of methane.[17] This enzyme, however, has not been extensively studied.

These biological systems are unlikely to be employed to oxidise methane on an industrial scale due to the high costs associated with expressing and purifying the proteins. Additional disadvantages associated with an enzymatic system include limited working temperature range, stability issues and, in the case of MMO, the need to prevent subsequent oxidation of methanol which occurs as part of the respiration process of methanotrophs.[18] As opposed to providing an industrially viable option for the oxidation of methane, the purpose of the study of these enzymatic systems is to provide insights that may inform the development of synthetic catalysts.

1.3 Industrial Use of Methane

At this time the use of methane as a raw material for chemical synthesis on an industrial scale requires that it first be converted to synthesis gas, or syngas, which is mixture of molecular hydrogen and carbon monoxide. The syngas can then be used either as a source of CO and H_2 for hydroformylation, hydrogenation, and ammonia synthesis, or the syngas itself can be used to

manufacture diesel fuel through the Fischer-Tropsch process.[4] Its primary use, however, is the manufacture of methanol. This process requires a CO: $2H_2$ syngas composition.

There are two methods currently for the conversion of methane to syngas. The first is the steam reforming of methane (equation 1.2) over a nickel catalyst, which is a highly endothermic reaction carried out at 850 °C and a pressure of 40 atm.[19, 20] There are several drawbacks to this process, including the tendency of the catalyst to undergo coking which leads to deactivation. In addition the process produces syngas with a CO: $3H_2$ composition, which then requires further processing.

$$CH_4 + H_2O \rightarrow CO + 3H_2$$

Equation 1.2

$$CH_4 + \frac{1}{2}O_2 \rightarrow CO + 2H_2$$

Equation 1.3

Both of these factors are mitigated in the industrial process by carrying out the steam reforming of methane in combination with the partial oxidation of methane to carbon monoxide and hydrogen (equation 1.3). This reaction is exothermic and so provides some of the heat energy needed to produce steam for the reforming. The combination of these reactions is known as autothermal reforming. The partial oxidation pathway is not used independently of the steam reforming process because of the difficulties and safety hazards surrounding the separation of oxygen from air, and the storage of mixtures of methane and oxygen. Even when these two processes are used in combination achieving the desired syngas composition for methanol synthesis incurs further costs. In addition to the syngas having the correct composition it is necessary to ensure it is free from any impurities that can poison the catalyst, such as sulfur or chloride compounds.

The syngas goes on to be converted to methanol through the reaction shown in equation 1.4. This reaction is catalysed by a Cu-ZnO-Al_2O_3 catalyst, and is carried out at temperatures ranging from 240 – 260 °C and pressures of 50 – 100

bar.[4, 21] This process generates methanol very selectively and at high yields, however the high pressures and temperatures employed make this process very expensive.

$$CO + 2H_2 \rightarrow CH_3OH$$

Equation 1.4

This process of converting methane to methanol involves the complete dissociation of all four C-H bonds of methane (1755 kJ mol^{-1}).[5] It would be more efficient to achieve this conversion using a single-step, direct method that avoided unnecessary financial and energetic expenditure. Carrying out this process at the well head would also avoid the problem of transporting methane. Although this has been achieved in nature, an industrially viable direct method has yet to be identified. This is due to the intrinsic difficulty associated with the activation of methane.

1.4 Academic Approaches to Direct Selective Methane Oxidation

Despite extensive investigation there are currently no commercially viable methods of converting methane directly to methanol. There have, however, been many studies of academic interest that have shown promising results. A number of these are detailed below with an emphasis on liquid phase, heterogeneous systems.

1.4.1 High Temperature Systems

High temperature (> 500 °C) methane oxidation systems generally involve a complex radical pathway and tend to generate coupling products from radical recombination.[22] Under these conditions the desired oxygenated products are significantly more reactive than methane. This leads to over-oxidation, thus limiting the selectivity of the system to partial oxygenates. As such CO_2 acts as a thermodynamic sink for oxidised methane. By combining high temperatures and

low partial pressures of methane Hargreaves *et al*. were able to selectivity produce formaldehyde.[23] Reducing the methane partial pressure reduced the concentration of methyl radicals in the system, which reduced competition with coupling reactions. A number of other studies have adopted this high temperature/ low pressure approach, however it was found that methanol was only selectively produced when methane conversion was <1%.[24, 25] In order to overcome these disadvantages more recent work has focused on low temperature systems.

1.4.2 Low Temperature Homogeneous Systems

The main disadvantage of low temperature (< 250 °C) systems is that because of the inherent difficulties associated with the activation of methane the catalytic system must be especially active. Therefore the use of an oxidant, such as H_2O_2, that is more reactive than molecular oxygen is generally required as this eliminates the need for a very active catalyst. Molecular oxygen, however, is the preferred oxidant from both a financial and environmental stand point.

The electrophilic activation of methane over high valent transition metal electrophiles is one of the most effective low temperature methods for the oxidation of methane. A generalised mechanism for this type of reaction is shown in figure 1.2.[8] It was first demonstrated by the seminal work of Shilov *et al*. using aqueous chloroplatinum complexes.[26] This homogeneous system required the reaction medium to be highly acidic (e.g. oleum).

Typical catalysts include transition metal complexes of Hg^{2+}, Pt^{2+}, Pd^{2+}, Tl^{2+}, Au^{1+}, Au^{3+} or Co^{3+} but this reaction can also be catalysed by I_2.[27-29] The main disadvantage of this method is that methane was not directly converted to methanol. A methanol derivative such as methyl bisulfate,[28, 29] methane sulfonic acid[30, 31] or methyl triflouroacetate[32] (depending on the identity of the oxidative species employed) was produced. This prevented over-oxidation occurring but a subsequent reaction was required to generate methanol. The most effective version of this catalytic system was reported by Periana *et al*.[28] A methane conversion of 90% was achieved with a selectivity of 81% to the product methyl

bisulphate using a Pt-bipyrimidine complex and conducting the reaction in oleum (SO_3/H_2SO_4), which acted as both a solvent and as an oxidant.

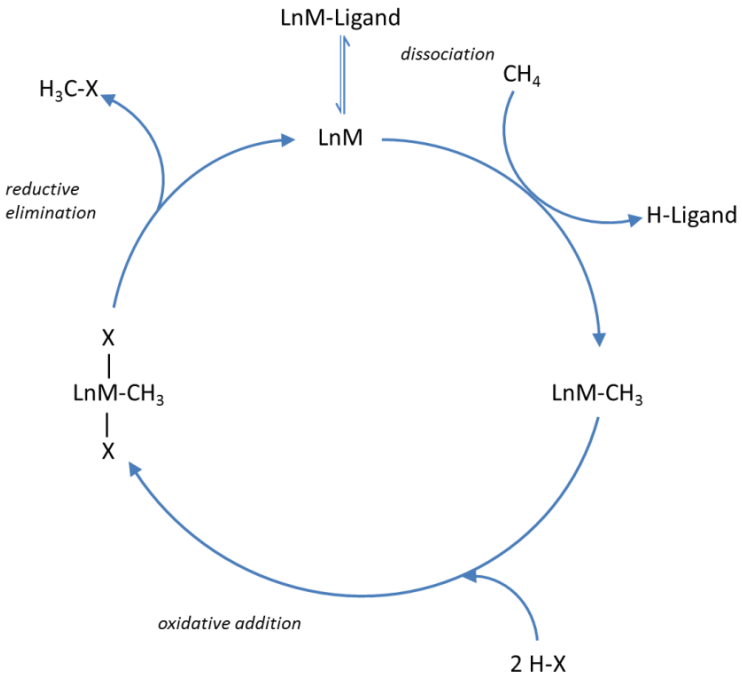

Figure 1.2 Reaction scheme for the electrophilic activation of methane over high valent transition metal electrophiles. [8]

Apart from the need to carry out a secondary reaction to generate methanol there are other disadvantages associated with this system. The use of highly acidic solvents is environmentally unfavourable and in addition there have been reports of the transition metals deactivating. This occurred when the metal was irreversibly reduced to the metallic oxidation state during the reaction. This was reported by Kalucki *et al.*[33] for a palladium based catalyst and by Jones *et al.*[34] for gold based catalysts.

In 2007 Yuan *et al.*[35] reported a homogeneous catalytic system for the oxidation of methane that utilised an environmentally favourable oxidant and solvent. In this system methane activation occurred via the formation of hydroxyl- and hydroperoxy radicals through the interaction of H_2O_2 with the catalyst as opposed to electrophilic activation. These reactions were carried out

in water with H_2O_2 as an oxidant and produced methanol, methyl hydroperoxide, formaldehyde and carbon dioxide. The ability of a range of transition metal chlorides to catalyse this reaction was demonstrated at low temperature (<150 °C). $OsCl_3$ and $HAuCl_4$ were found to be the most active of the catalysts tested, displaying turnover frequencies of 10 and 12 h^{-1} respectively.

1.4.3 Low Temperature Heterogeneous Systems

It is preferable that that the direct conversion of methane to methanol takes place by heterogeneous catalysis because of the advantages as regards ease of separation and reusability when compared to a homogenous system. With this in mind heterogeneous analogues of the Periana catalyst (a Pt-bipyrimidine complex) were produced by Palkovits *et al.*[36, 37] They consisted of polymer frameworks coordinated to a Pt centre, where the Pt is co-ordinated to a covalent triazine-based framework (figure 1.3). These catalysts were reusable and more active than the homogeneous system. However they still required a highly acidic solvent.

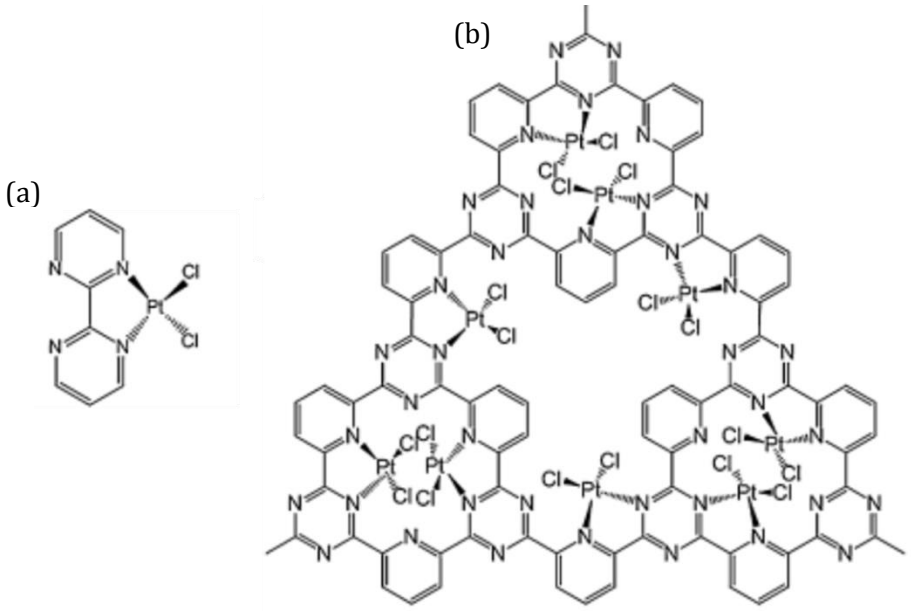

Figure 1.3 (a) Periana's homogeneous catalyst, a Pt-bipyrimidine complex and (b) one of Palkovits' heterogeneous analogues.

To avoid this issue other studies have focused on the use of more favourable oxidants. One alternative possibility is H_2O_2. The small difference in value between methane and methanol makes the use of pre-formed H_2O_2 un-economical unless very efficient usage is achieved. However, with the right catalyst it is possible to generate H_2O_2 *in situ* from gaseous hydrogen and oxygen. A system that generated H_2O_2 *in situ* for the activation of methane was first reported by Lin and Sen.[38] The system utilised a Pd/C catalyst along with CO as a co-reductant. The Pd/C catalysed three concurrent reactions: a water gas shift reaction that produced H_2 from H_2O and CO, the H_2 then reacted with added O_2 to form H_2O_2 which went on to oxidise methane. They found that the CO could be replaced with H_2 such that only H_2O_2 synthesis and methane activation occurred. They observed turnover numbers in the range of 80-160 moles products/moles surface metal atoms. However the major product of this reaction was formic acid, which is less desirable than methanol. In addition they found the formic acid to be unstable in the system as it tended to undergo decomposition and over-oxidation. Further research into using H_2O_2 generated *in situ* to oxidise methane has been carried out by Hutchings *et al*.[39] using Au-Pd/TiO_2 and is discussed in section 1.4.4.

Since the ability of MMO to oxidise methane at low temperature using O_2 as an oxidant has been demonstrated, the design of several other heterogeneous catalysts took the active centre ($Fe_2(\mu\text{-}O)_2$) into consideration.[13] Phthalocyanine complexes of Fe and Cu encapsulated within zeolites were used by Raja *et al* [40] to catalyse the oxidation of methane. Using the Fe catalyst and a combination of molecular oxygen and *tert*-butyl hydroperoxide (TBHP) as an oxidant they produced a mixture of C1 oxygenates with 53% selectivity to methanol at 0 °C. However, the maximum yield of methanol was only 2% over 12 h. Further research in this area was carried out by Sorokin *et al.*[41, 42] who supported the metal phthalocyanine complexes on SiO_2. They reported the formation of methanol, formaldehyde and formic acid from the oxidation of methane with an Fe-phthalocyanine complex and H_2O_2 as an oxidant.[42] However selectivity to methanol was limited by over-oxidation and the catalysts tend to be unstable, undergoing metal leaching as the supporting ligand decomposed. This resulted in

both a loss of activity and may have contributed to the amount of oxygenated products detected.[43]

Two other low temperature heterogeneous catalyst systems for the oxidation of methane (which were utilised during the course of this project) are described in detail in this chapter. Supported Au-Pd nanoparticles are discussed in section 1.4.4 and ZSM-5 based catalysts are discussed in the following section.

1.4.4 ZSM-5 for Methane Oxidation

ZSM-5 is a type of zeolite which are microporous, crystalline aluminosilicates.[44] They are composed of SiO_4 and AlO_4^- tetrahedra which are connected by bridging oxygen atoms. In order to maintain the overall electroneutrality of the framework, the negative charge of the AlO_4^- tetrahedra must be balanced by extra-framework cations (such as Na^+ or H^+). These cations are exchangeable, giving rise to the diverse ion-exchange chemistry associated with these materials. Zeolite composition can be manipulated to achieve high levels of Brønsted acidity (when H^+ is the extra-framework counter-cation) or Lewis acidity (through the dealumination of the zeolite framework).[44, 45] The pore structure of zeolites is such that interconnected channels exist throughout the framework. These enable zeolites to be used for both molecular sieving (separating molecules by size/shape) and shape-selective catalysis. The selectivity of shape-selective reactions catalysed by zeolites may be based upon the shape of the substrate, the product, or a transition state which is formed during the reaction.[44, 45]

ZSM-5 was first patented by the Mobil Oil Company in 1975 and is widely used as a solid acid catalyst in both the fine and bulk chemical industries.[46] It has an MFI-type zeolite structure. The structure of this class of zeolite is based on a 5-membered pentasil unit. The full framework structure (figure 1.4) is composed of two intersecting 10-ring tunnel systems.[47, 48] One is a straight channel with dimensions of 5.4 × 5.6 Å that runs along the (010) axis, while the other runs along the (100) in a sinusoidal fashion with dimensions of 5.1 × 5.5 Å

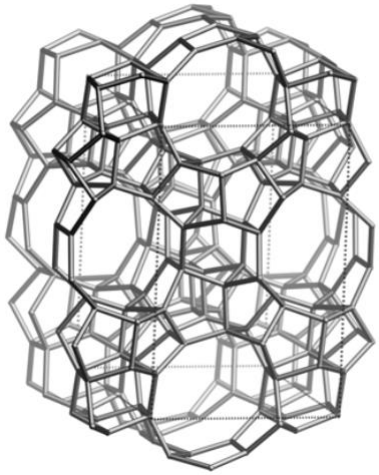

Figure 1.4 ZSM-5 framework viewed along (010) face[47]

Work published by the Hutchings group reported the activity of Cu-Fe/ZSM-5 (30) for the low temperature oxidation of methane in water using H_2O_2 as oxidant.[49, 50] It was reported that commercial H-ZSM-5 (30) which had been subjected to high temperature (550 °C) displayed significant activity for the oxidation of methane with H_2O_2, achieving a conversion of 0.3% with a selectivity of 95% to oxygenated products. The ability of H-ZSM-5(30) to selectively produce formic acid from the oxidation of methane had previously been reported.[51] Elemental analysis carried out on samples of the commercial H-ZSM-5(30) revealed the presence of trace amounts of iron in the zeolite. Previous studies showed that iron within the zeolite framework exhibited activity for benzene oxidation.[52, 53] The addition of extra-framework iron to form 2.5wt% Fe/ZSM-5(30) by solid state ion exchange led to an increase in catalytic activity, with the conversion of methane increasing to 0.7%.[50] A combination of EXAFS experiments and DFT calculations were used to elucidate a model for the active site. The hypothesised structure was a di-iron complex (shown figure 1.5). Despite the similarities between the active site and that of sMMO (figure 1.1) it was not possible to replace the oxidant with molecular oxygen in this process. Nevertheless the turnover frequency of the H-ZSM-5(30)/ H_2O_2 system (2278 h^{-1}) compares favourably with that of sMMO (95 h^{-1}).[50]

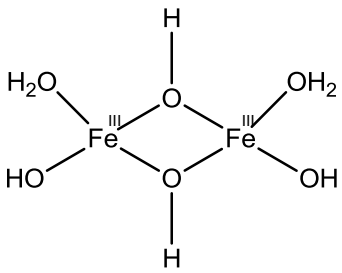

Figure 1.5 Proposed active site for methane oxidation in Fe/ZSM-5(30).[50]

The reaction pathway that was determined for the oxidation of methane with H_2O_2 by H-ZSM-5(30) is shown in figure 1.6.[50]

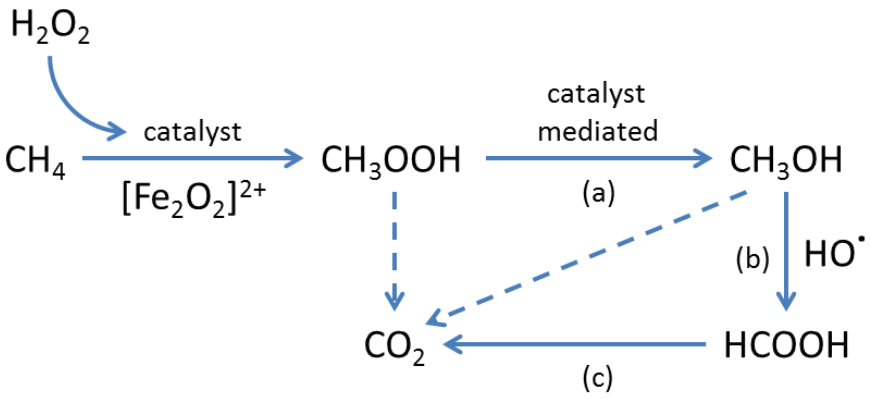

Figure 1.6 Reaction scheme for the oxidation of methane with ZSM-5(30). The primary reaction product, MeOOH, undergoes selective conversion to MeOH (a) or non-selective conversion to HCOOH. HCOOH (b) and CO_2 (c) are formed by the consecutive over-oxidation of MeOH. Steps (B) and (C) are eliminated upon the addition of Cu^{2+} to the catalytic system[50]

Methyl hydroperoxide was found to be the primary product of the reaction which undergoes subsequent reaction(s) to consecutively form methanol, formic acid and carbon dioxide (figure 1.6). Methyl hydroperoxide was found to decompose to methanol without the presence of a catalyst, but at a much lower rate. It was shown that control of the product distribution could be achieved by the addition of extra-framework copper to the zeolite or homogeneous copper to the reaction medium. This increased the selectivity towards methanol by 'switching off' the transformation of methanol to formic acid.[49, 50, 54] A 2.5wt% Cu-

2.5wt% Fe/ZSM-5(30) catalyst achieved a selectivity of 93% to methanol without affecting the overall conversion of the reaction (0.7%). EPR studies found that Cu^{2+} scavenged ·OH radicals which have been shown to play a role in oxidation of methanol to HCOOH and CO_2.[49, 50]

This heterogeneous catalysis system displays high stability and efficiently converts methane to methanol using an environmentally favourable oxidant and solvent. However, it has not proved to be an economically viable process. This is because the cost associated with the oxidant, H_2O_2, is too great in comparison to the value of the product, methanol. A suitable alternative oxidant is required for the reaction. Molecular oxygen is the ideal candidate as it is inexpensive, readily available and environmentally friendly.

1.5 Catalysis Using Gold and Gold-Palladium Nanoparticles

Gold was long regarded as a poorly active catalyst, largely due to the chemical inertness its bulk form. This perception changed in the 1980's following publication of two papers in which supported gold nanoparticles were shown to display high levels of catalytic activity. Gold was shown to be a superior catalyst for the hydrochlorination of ethyne to vinyl chloride by Hutchings,[55] while Haruta demonstrated the effective ability of the nanoparticles to catalyse the low temperature oxidation of CO.[56] Gold nanoparticles have since been found to be highly active and selective catalysts for a variety of reactions.[57-59] The crucial factors in determining the activity of gold nanoparticles are generally considered to be small particle size (smaller particles are preferred due to their larger number of surface sites) and the identity of the support material (which can effect nanoparticle structure and stability).

The usefulness of gold as a catalyst has been further extended through investigation into the effect of adding a second metal component to form bimetallic nanoparticles. The addition of palladium in particular has been found to have an enhancing effect on the activity gold nanoparticles, as a synergistic

effect exists between these two metals for several substrates.[60-63] This is considered to be the result of an electronic effect. In the following sections the importance of gold and gold-palladium as oxidation catalysts is illustrated through the discussion of a selection of reactions for which they have been shown to be effective catalysts. Particular attention is given to reactions that are considered to be relevant to this project.

1.5.1 CO Oxidation

The oxidation of CO to CO_2 is industrially important for both automotive emission control and fuel cell applications. Haruta's work demonstrated the exceptional ability of gold nanoparticles to oxidise CO at low temperature using α-Fe_2O_3[56] as a support, and later also showed Au/TiO_2[64] to be an effective catalyst. Since then a variety of supporting materials have been successfully used for this reaction[65, 66] with Lahr and Ceyer reporting that this reaction can be carried out at -203 °C using a Au/Ni surface.[67] Despite extensive study, the nature of the active site and mechanism by which this reaction occurs are still unclear.[57, 68, 69] This is likely due to the fact that catalysts prepared by precipitation methods (the method of choice for this reaction[70, 71]) display a great deal of variation in the size and morphology of gold particles, and as such a number of different active sites and mechanisms may be involved in this reaction.

The choice of catalyst preparation method has been shown to have a significant effect on catalyst activity as different methods produce different particle size distributions. Small gold particle sizes (< 10 nm in diameter) are generally considered to be essential for effective CO oxidation catalysts. Lopez *et al.* analysed data collected from a number of papers published on this topic and concluded that particle size was the most significant factor in determining catalyst activity (figure 1.7).[65] This is due to the fact that smaller particles have a greater availability of low -coordination gold atoms. Support interactions were found to have a lesser effect on catalyst activity.

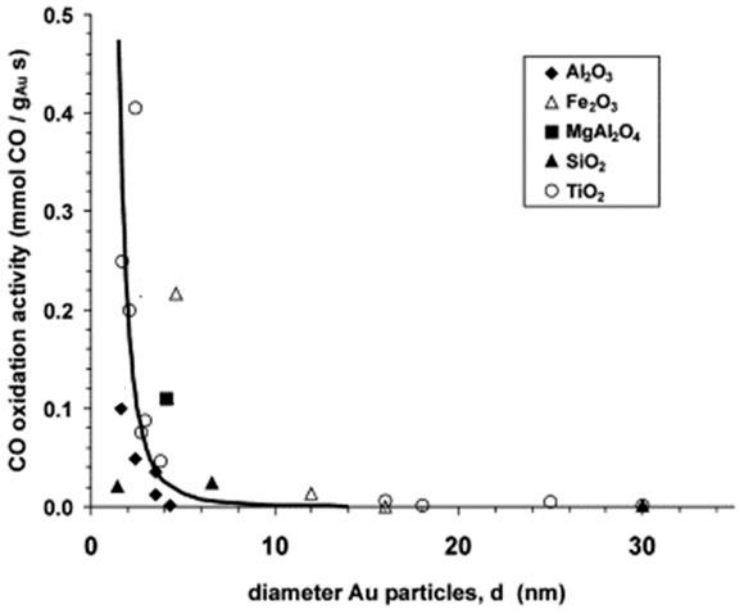

Figure 1.7 Correlation between average gold particle diameter and activity for CO oxidation at 273 K over various gold based catalysts. Compiled by Lopez *at al.*[65]

1.5.2 Synthesis of Hydrogen Peroxide

Currently H_2O_2 is produced on an industrial scale by the indirect anthraquinone process which was developed in 1939.[72, 73] This involves the hydrogenation of alkyl anthraquinone to produce a diol using a nickel or palladium catalyst. This is followed by the oxidation of the diol to regenerate the anthraquinone and produce H_2O_2. This process is only economically viable on a large scale, and so entails the hazardous storage and transportation of concentrated H_2O_2 solutions.[74] As such a green, direct process that could be carried out on a smaller scale would be preferable, particularly if high rates were achieved when using non-explosive conditions.

The direct synthesis of H_2O_2 through the combination of hydrogen and oxygen is a simple concept, but there are several intrinsic problems associated with it (figure 1.8).[62] One of the principal problems is the formation of water through either combustion or hydrogenation reactions. In addition H_2O_2 is an unstable molecule that will undergo decomposition to form water. All of these complications are difficult to avoid, as catalysts active for the direct synthesis of

H_2O_2 will also tend to catalyse these undesirable reactions. Furthermore, the mixing of high pressure H_2 and O_2 is inherently hazardous. Therefore only low concentrations of H_2 can be safely employed, thus limiting H_2O_2 yield.

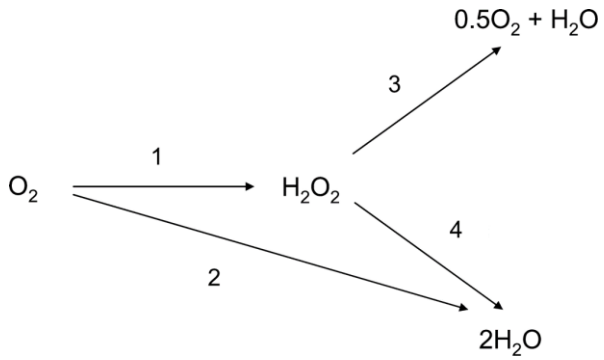

Figure 1.8 Reaction scheme for the direct synthesis of H_2O_2; synthesis (1), combustion (2), hydrogenation (3) and decomposition (4).[62]

The activity of Pd catalysts for the direct synthesis of H_2O_2 was first reported in a patent filed in 1914, and for many years thereafter research in this area focused on the use of Pd catalysts.[75] Pd catalysts were found to be active for this reaction, but they require the addition of halides and acids in order to attain high reaction rates and selectivity.[62, 74] This is undesirable as the presence of these additives makes the final H_2O_2 solution unsuitable for certain chemical processes.

The first reported use of gold to catalyse the direct synthesis of H_2O_2 was by Hutchings *et al.* (using a Au/Al_2O_3 catalyst)[76, 77] and subsequently by Haruta[78] and Ishihara.[79] The crucial advance in this area was the discovery that a synergistic effect exists between Au and Pd for the synthesis of H_2O_2. It was observed that Au-Pd alloys prepared by wet impregnation and supported on a range of materials are significantly more active than their monometallic counterparts.[62] Bimetallic Au-Pd catalysts display a lower H_2 conversion but enhanced selectivity to H_2O_2 compared with Pd catalysts, resulting in an overall increased rate of H_2O_2 synthesis (table 1.1).

Table 1.1 Activity of supported Pd, Au, Au-Pd catalysts for the synthesis of H_2O_2. [62]

Catalyst	Rate (mol H_2O_2 kg_{cat}^{-1} h^{-1})	H_2 Conversion (%)	H_2O_2 Selectivity (%)
5% Au/TiO_2	7	nd	nd
5% Pd/TiO_2	31	29	21
2.5% Au- 2.5% Pd/TiO_2	64	21	70
2.5% Au- 2.5% Pd/C	110	41	80

Conditions; 5% H_2/CO_2 and 25% O_2/CO_2, 1:2 H_2/O_2 at 3.7 MPa, 5.6 g CH_3OH, 2.9 g, 0.01 g catalyst and 1200 rpm. nd = not detected

Further investigations found that a calcination step in the catalyst preparation procedure was required to ensure catalyst stability.[62] Un-calcined catalysts lost approx. 90% of their metal content in their first use. The calcination step stabilised the catalysts for a number of uses, and also resulted in the formation of core-shell morphology for Au-Pd alloys supported by oxide materials. The homogeneous alloys present prior to calcination were found to be more active, but the need for catalyst stability necessitated the calcination step.

An investigation into the effect of pre-treating supporting materials with acid before catalyst preparation was conducted.[80] This investigation was prompted by the observation that higher H_2O_2 yields were achieved using catalysts with acidic supporting materials. It was found that pre-treatment of carbon with 2% HNO_3 prior to use as a support resulted in the suppression of the hydrogenation reaction pathway. Using a 2.5wt% Au- 2.5wt% Pd catalyst with a HNO_3 pre-treated carbon support a selectivity of >98% to H_2O_2 was achieved with a productivity of 160 mol kg_{cat}^{-1} h^{-1} without the use of any halide or acid additives.

The use of the sol-immobilisation method to prepare supported Au-Pd nanoparticles was also investigated by Hutchings *et al*.[81-83] It was found that although the sol-immobilised catalysts were very active for H_2O_2 synthesis they were also very active for the hydrogenation reaction, which resulted in poor selectivity (table 1.2). The difference in activity of these catalysts compared to those prepared by wet impregnation is believed to be caused by the smaller particle size and reduced oxidation state of Pd displayed by sol-immobilisation catalysts.

Table 1.2 H_2O_2 productivity and hydrogenation for Au-Pd/C prepared by sol-immobilisation and impregnation (Au: Pd = 1: 1 weight ratio) [82]

Catalyst	H_2O_2 Productivity	H_2O_2 Hydrogenation
	Mol H_2O_2 kg^{-1} (cat) h^{-1}	%
1wt% Au-Pd/C (Sol-im)	128	18
1wt% Au-Pd/C (Impreg.)	60	7

1.5.3 Oxidation of the Primary C-H Bonds in Toluene

In the modern chemical industry the selective oxidation of the primary C-H bonds is of significant importance to the exploitation of raw materials. Currently the industrial process of producing benzaldehyde involves the chlorination of toluene, and benzoic acid production uses acetic acid as a solvent making these processes environmentally unfavourable. As such the development of a heterogeneous catalyst for the oxidation of toluene has been the source of much study, as this reaction has been shown to produce benzyl alcohol, benzaldehyde and benzoic acid (figure 1.9). The use of catalysts based on copper and manganese,[84] cobalt[85], and chromium[86] have been investigated. These catalysts however proved to be ineffective, with conversions of <20% being observed in all cases.

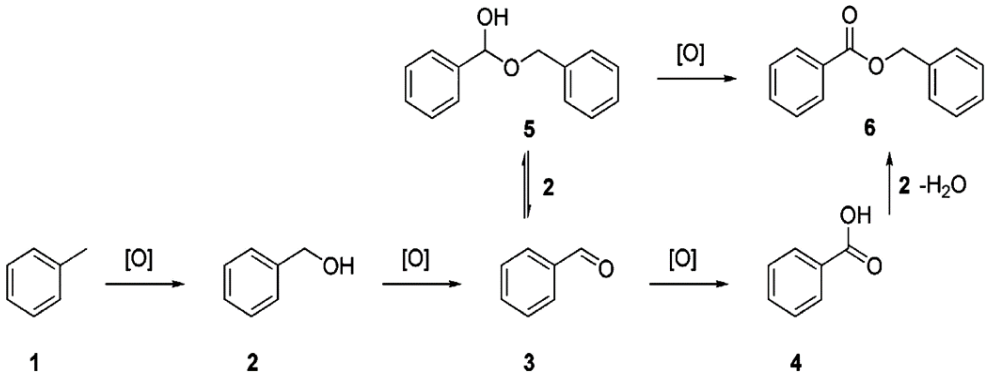

Figure 1.9 Oxidation of toluene (1) leading to benzyl alcohol (2), benzaldehyde (3), benzoic acid (4), hemiacetyl (5), and benzylbenzoate (6) [61]

In 2011 Hutchings *et al.* demonstrated the effective ability of alloyed Au-Pd nanoparticles to oxidise the primary C-H bonds of toluene under solvent-free conditions using molecular oxygen at 160 °C.[61] The activity of catalysts prepared by impregnation was initially investigated, but minimal activity was displayed. Subsequently catalysts prepared by sol-immobilisation (which produces smaller particles with a narrower size distribution) were tested, and were found to display far greater activity. A synergistic effect was observed for Au-Pd catalysts. When prepared by sol-immobilisation with a carbon support the gold monometallic catalyst achieved a conversion of 0.2% and the palladium 1.6%, whilst the catalyst prepared with a 1:2 molar ratio of Au: Pd converted 5.3% of the initial toluene.

Conversions as high as 94% with no production of CO_2 were achieved using a bimetallic catalyst over long reaction times. TiO_2 was also investigated as a support material but it was found to produce catalysts less than half as active as those prepared with a carbon support. Imaging of the both catalysts using high angle annular dark field (HAADF) STEM showed that mean particle size was not significantly affected by the choice of supporting material. TiO_2 supported nanoparticles were found to have a mean particle size of 3.9 nm while 3.7 nm was the mean for carbon supported nanoparticles. X-ray photoelectron spectroscopy of the two catalysts found that their surface composition was also similar with the Pd: Au ratio of the TiO_2 and carbon supported nanoparticles being 2.1 and 2.2 respectively.

However, the two catalysts did exhibit a key difference relating to the morphology of the nanoparticles.[61, 87] On TiO_2 the nanoparticles interact with the crystalline support such that an extended flat interface between the support and the metal is formed. Smaller particles on TiO_2 were found to be highly faceted and were mostly displayed a cub-octahedral or singly twinned morphology while larger particles tended to be multiply twinned. As a result both the (111) and (200) planes of the smaller particles were observed to be exposed while for larger particles the only the (111) plane was preferentially exposed. By contrast due to the reduced ability of the Au-Pd nanoparticles to wet the activated carbon support the carbon supported nanoparticles were observed to be rounder in

shape. Far less cub-octahedral or single or doubly twined particles were observed for the carbon catalyst. Instead the particles tended to display icosahedral and decahedral morphologies which exhibit (111) facets terminations.

As such it was hypothesised that the difference in activity between these two was the result of differing particle morphology. Two possible explanations have been suggested. Firstly, that the reduced number of low coordination sites present in the Au-Pd/TiO_2 (where the nanoparticles are flatter and more faceted) compared to the Au-Pd/C catalyst was the cause of the reduced activity of the TiO_2 supported nanoparticles. The second possibility suggested was that the lower activity of the Au-Pd/TiO_2 was the result of a reduced number of (111) terminated facets present in the catalyst. This work is considered to be of particular significance to this thesis as it was used as a proof of concept for the original work carried out on using supported Au-Pd nanoparticles to oxidise methane by Hutchings *et al.*[39]

Since then Hutchings *et al.* have reported the oxidation of toluene under milder conditions (80 °C) using TBHP (*tert*-butyl hydroperoxide) as an oxidant with Au-Pd/TiO_2.[88] In addition, investigations carried out into the nature of the reaction mechanism have found that surface-bound, oxygen-centred radicals play a role in this reaction.

1.5.4 Methane Oxidation

It was previously shown that supported Au-Pd nanoparticles are catalytically active for the oxidation of alcohols with H_2O_2 as oxidant,[63, 89] the activation of the primary C-H bond of toluene with TBHP and molecular oxygen,[61, 88] and the direct synthesis of H_2O_2.[80, 90] Each of these reactions was shown to proceed through the formation of a hydroperoxy intermediate. As such it was considered that supported Au-Pd nanoparticles may also be effective for the oxidation of methane, as it is known that methane can be oxidised using H_2O_2 as a source of oxygen.[35, 91] This led to an investigation into using supported Au-Pd nanoparticles as a catalyst for methane oxidation with H_2O_2 as an oxidant. It was

found that when carried out at low temperature (50 °C) with a 5wt% Au-Pd/TiO_2 catalyst prepared by impregnation this reaction gives a high selectivity for the formation of methanol (49%) although at low productivity (0.28 $mol_{products}\, kg_{cat}^{-1}\, h^{-1}$).[39]

As part of the same study EPR experiments were carried out in order to better understand the nature of the reaction pathway by determining which radical species are present during the reaction. During this study methyl and hydroxyl radicals were observed. Furthermore, although not observed, it was inferred that hydroperoxy radicals are also formed during these reactions as methyl hydroperoxide is the primary product formed. It is believed that this product is formed through the reaction of methyl and hydroperoxide radicals which are bound to the surface of the catalyst and so were not detected by the EPR studies. From this information it was concluded that these reactions occur by a radical mechanism. A time-on-line study showed that methyl hydroperoxide was the primary reaction product formed. The other reaction products, methanol, formic acid and carbon dioxide, are formed consecutively.[39, 60] Formaldehyde monohydrate ($CH_2(OH)_2$) was also detected but as the ^{1}H-NMR signal of this molecule is obscured by that of the solvent, water, it could not be detected routinely.

As the 5wt% Au-Pd/TiO_2 catalyst prepared by impregnation had already been shown to be an effective catalyst for synthesis of H_2O_2[62] it was reasoned that hydroperoxy species could be generated *in situ* from gaseous H_2 and O_2 to oxidise methane. A reaction was carried out under a mixture of methane, H_2 and O_2 diluted with N_2. This resulted in a three-fold increase in activity compared to a reaction where an amount of pre-formed H_2O_2 (equivalent to the theoretical maximum amount that could be produced by the gas mixture) was added.[39] In addition the *in situ* reaction also displayed improved methanol selectivity (68%). This approach has the added benefit of avoiding the cost associated with utilising pre-formed H_2O_2.

Initially Au-Pd nanoparticles supported on TiO_2 prepared by sol-immobilisation were tested for this reaction, but they showed reduced activity

compared to the same catalyst prepared by impregnation. [39] This was found to be caused by the higher rate of H_2O_2 decomposition associated with Au-Pd nanoparticles prepared by sol-immobilisation, which resulted in lower oxidant availability for methane oxidation in this system. Similarly increasing the metal loading of the impregnation catalyst from 1 to 5wt% resulted in only a slight increase in activity and a concurrent drop in TOF from 6.85 to 0.77 h^{-1}. Again this was reasoned to be caused by a reduction in oxidant availability. Upon increasing the metal loading the rate of H_2O_2 decomposition increased, thus hindering the methane oxidation reaction.

Varying the metal composition of the 5wt% Au-Pd/TiO_2 catalyst prepared by impregnation showed that, as observed for other substrates,[61-63] a synergistic effect exists between the Au and Pd.[60] An equivalent monometallic gold catalyst displayed lower activity but consumed less H_2O_2. Increasing Pd content corresponded to an increase in H_2O_2 consumption and methanol selectivity. The ideal ratio was found to be a 1 to 1 weight ratio of Au: Pd. At this ratio the bimetallic catalyst displayed improved methanol selectivity compared to the monometallic gold catalyst and reduced oxidant decomposition compared to the Pd catalyst.

Several different support materials for the Au-Pd nanoparticles were trialled with the observed order of activity being TiO_2 > γ-Al_2O_3 > C > SiO_2 > CeO_2.[60] The catalyst prepared using TiO_2 displayed more than twice the activity displayed by that prepared using CeO_2. The carbon and SiO_2 catalysts produced only methanol and carbon dioxide and displayed the highest rates of H_2O_2 decomposition. As such it is likely that methyl hydroperoxide was not observed as a product because it was easily decomposed by these catalysts. The γ-Al_2O_3 catalyst consumed less H_2O_2 than the TiO_2 catalyst even though these catalysts were found to have similar surface areas and crystallite sizes. It has been confirmed that TiO_2 itself is not active for this reaction[39], and as such it was concluded that the superior activity of the TiO_2 catalyst was related to the ability of TiO_2 to form hydroperoxy species and stabilise reactive oxygen species.[88, 92] These results demonstrate the importance of the effect of the supporting material on this reaction.

1.5.5 Catalysis Using Unsupported Gold Nanoparticles

Since ancient times colloidal gold has been used in the manufacture of coloured glass with the earliest known example being the Lycurgus cup, a Roman glass cage cup which dates from the 4th century. The tiny amounts of colloidal gold present in the glass produce a dichroic effect such that the glass appears to be red when lit from behind and green when lit from the front. The earliest record of a metal colloid being produced by the chemical reduction of a metal salt is from 1875 by Faraday, who reduced $HAuCl_4$ with phosphorous to form a colloidal gold sol.[93]

Today colloidal metal nanoparticles are regularly used as a component of heterogeneous catalysts as these methods allow the size and shape nanoparticles to be controlled.[94] Metal colloids can also be formed by physical methods (which involve subdividing bulk metals), electrochemical synthesis, and thermal decomposition.[94] Additionally the solvated metal atom dispersion method (SMAD) can be used to produce highly dispersed metallic catalysts.[95] This method involves forming weakly ligand stabilised metal atoms. This is achieved by evaporating the metal and trapping it in a cold solvent. As the solvated metal atoms are thermally unstable when they are warmed nucleation takes place such that particles form. An advantage of this method is that no waste products are produced. Once prepared the nanoparticles can be isolated as solid materials and redispersed in a solvent. In this section the focus shall be on colloids that are prepared by the chemical reduction of metal salt precursors.

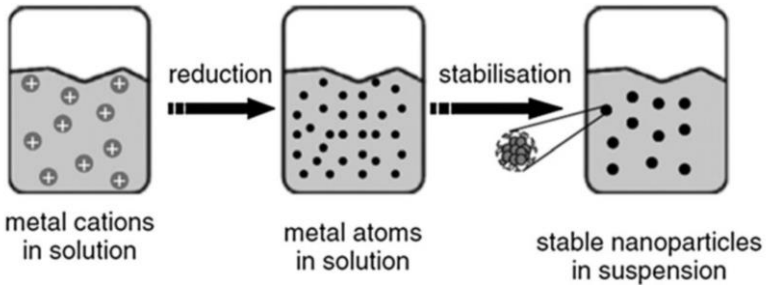

Figure 1.10 Generation of colloidal metal nanoparticles through the reduction of metal salt precursors.[94]

The inherent kinetic and thermodynamic instability of 'naked' metal nanoparticles necessitates the use of a stabilising agent in the synthesis of metal colloids (figure 1.10). The stabiliser prevents the metal particles from aggregating, thus controlling the size of the nanoparticles formed. Stabilisation of the nanoparticles may be electrostatic, steric, or a combination of both, depending on the choice of stabiliser. For example, steric stabilisation may be provided by linear polymers such as poly vinyl alcohol (PVA) and poly(*N*-vinyl-2-pyrrolidone) (PVP) that absorb onto the surface of the nanoparticles. Furthermore, studies published on metal nanoparticles prepared using a stabilising ligand have shown that the size of nanoparticles formed can be controlled by varying the ratio of metal to stabiliser used during preparation.[96-98] Increasing the amount of stabiliser used in preparation of the nanoparticles relative to the amount of metal produces smaller nanoparticles and *vice versa*. For example Miyake and Teranishi have reported that by varying the PVA to Pd ratio used to prepare Pd nanoparticles average particle size could be varied from 17 to 20 Å.[99]

It is generally believed that perimeter interfaces between gold nanoparticles and the support play a vital role in the markedly high catalytic activity of supported gold nanoparticles.[66, 100] Therefore, after colloidal gold nanoparticles are prepared they are typically supported on another material before use as a heterogeneous catalyst. This sol-immobilisation method is an effective method for preparing supported metal nanoparticles.[82, 87, 101]

The nano-sized gold colloids themselves display interesting optical properties. They are intensely coloured due to the surface plasmon resonance phenomenon, with the particular colour of the colloid depending on the size and shape of the nanoparticles and the dielectric constant of the surrounding medium (figure 1.11). Recently there have been reports of gold nanoparticles exhibiting catalytic activity without the presence of a support.[102] This would imply, in contrast to the widely held belief, that the gold nanoparticles are intrinsically active for these reactions. Some examples of such cases are illustrated below.

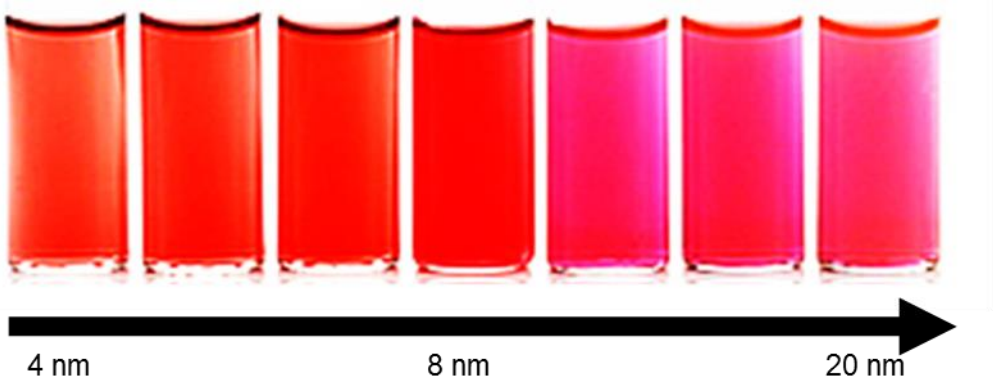

Figure 1.11 Gold colloids with various particle sizes.[101]

The activity of polymer stabilised colloidal gold nanoparticles for the aerobic oxidation of benzylic alcohols was demonstrated by Tsukunda *et al.*[103-105] PVP stabilised nanoparticles were prepared by the reduction of an aqueous solution of $HAuCl_4$ and PVP with $NaBH_4$. In order to investigate the effect of particle size, the colloidal nanoparticles were treated with Na_2SO_3, which caused particle growth. Similarly to systems using supported gold nanoparticles, they found that catalyst activity was dependant on particle size. Nanoparticles with a diameter greater than 5 nm were found to be inactive for the oxidation of *p*-hyrdoxybenzyl, with activity increasing rapidly with further reduction of particle size.

The identity of stabilising ligand was also found to have a significant effect on catalytic activity. PVP-stabilised gold nanoparticles were observed to display enhanced activity compared with those stabilised by poly(allylamine) (PAA). X-ray absorption near edge absorption measurements (XANES) and fourier transform infrared spectroscopy (FTIR) of absorbed CO on the PVP-stabilised nanoparticles showed the nanoparticles to be negatively charged by electron donation from the PVP. It was concluded that this enhanced the activity of the PVP-stabilised nanoparticles increased negative charge on the gold nanoparticles increases their activity for aerobic oxidation.

De Vos *et al.* used a similar preparation procedure to produce PVA-stabilised colloidal gold nanoparticles for the aerobic oxidation of 1,2-diols.[106, 107] TEM analysis showed the nanoparticles to have a narrow particle size distribution

(60% were between 4 and 6 nm in diameter) typical of particles prepared by reducing $HAuCl_4$ with $NaBH_4$. Complete chemoselectivity to the desired product, the corresponding α-hydroxycarboxylates, was achieved for the oxidation of 1,2-diols of various chain lengths (1,2-propanediol, 1,2-octanediol and 1,2-hexanediol). Interestingly the turnover frequency observed (850 h^{-1}) is comparable to that of the same reaction catalysed by carbon supported gold nanoparticles indicating that, in this case, supporting the nanoparticles does not affect their activity. However, supporting the nanoparticles would be expected to enhance the stability of the nanoparticles by preventing agglomeration. It also allows facile re-use of the catalyst as a supported catalyst is more easily separated from than products than colloidal nanoparticles.

The effect of aging and reuse on the activity of the unsupported nanoparticles was investigated by the same group. It was found that significant levels of activity (>50%) were maintained after extended time periods (24 days). One of the primary difficulties associated with unsupported nanoparticle systems is the issue of separating the nanoparticles from the reaction products for re-use. De Vos *et al.* addressed this issue, and showed that nanofiltration could be carried out with a poly(dimethlsiloxane) membrane allowing 99% of the gold to be recovered. Using this method they demonstrated that 60% of the initial activity could be retained after three consecutive reactions. This illustrated the fact that inherently, unsupported gold nanoparticles are re-usable, but that re-usability tends to be hindered by stability and separation issues.

The effect of the type of stabiliser used to prepare unsupported gold nanoparticles on their activity for the oxidation of glycerol was investigated by Prati *et al.*[108, 109] Again, it was observed that catalytic activity increased with decreasing particle size. The stability of gold nanoparticles prepared with PVA was compared with that of gold nanoparticles prepared with an electrostatic stabiliser, tetrakishydroxypropylphosphonium chloride (THPC). It was found that the bulky steric stabiliser, PVA, was more effective at preventing agglomeration over long time periods. As such the PVA-stabilised nanoparticles retained their activity for longer periods. The PVA-stabilised particles, however, were found to be roughly three times less active than those prepared with THPC, highlighting

the importance of stabiliser selection. This was explained in terms of the bulky PVA molecule causing steric congestion and thereby limiting the accessibility of the substrate to the active site.

Another example of the activity of gold nanoparticles in the absence of a support is the work of Rossi *et al.* who investigated the activity of gold nanoparticles for glucose oxidation.[110-112] This work was of particular interest to the study of the intrinsic activity of gold nanoparticles as it was conducted without the presence of a support or an added stabiliser. The gold particles were prepared in the presence of glucose which acted as both reactant and as a stabilising agent negating the need for any additional stabiliser. It was found that the initial rates of glucose oxidation were similar for reactions catalysed by the naked gold nanoparticles and those catalysed by Au/C (figure 1.12). However as the reaction continued the naked gold nanoparticles agglomerated forming an inactive solution after about 400 s whereas the supported nanoparticles maintained their activity for longer, which allowed total glucose conversion to be achieved. These results demonstrate that the unsupported gold nanoparticles can be equally as active as their supported counterparts, but that their inherent disadvantage is their instability.

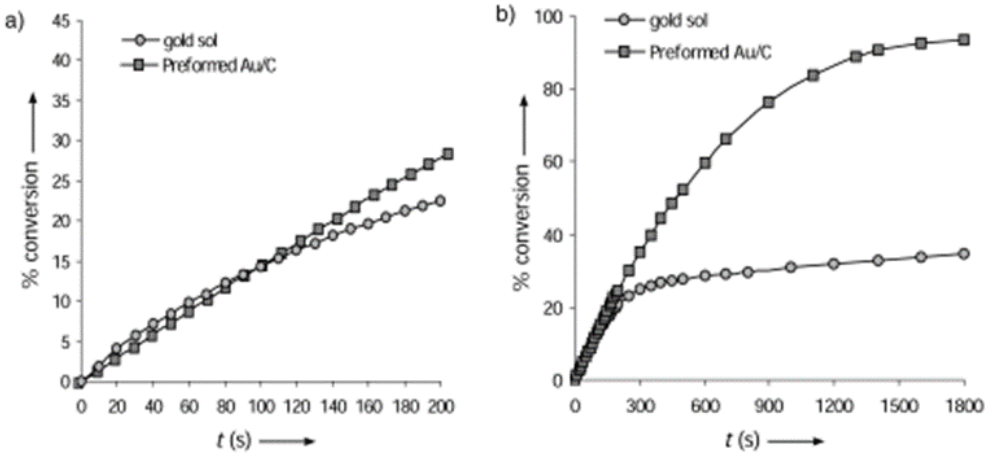

Figure 1.12a) Initial rate of glucose oxidation with naked and supported gold particles b) Rate of glucose oxidation with 'naked' and supported gold particles [112]

In the same study the effect of particle size was investigated. Particles of diameters ranging between 3-6 nm were produced by varying the concentration of the gold precursor employed in the preparation. Again, it was shown that smaller particles displayed higher activity, with the observed catalytic activity being inversely proportional to particle diameter.

It is clear from these reports on the activity of unsupported gold nanoparticles that a supporting material is not an essential catalyst component for several gold catalysed reactions. These results indicate that further investigation into the activity of unsupported gold based nanoparticles is required. This research will improve the understanding of both the intrinsic catalytic activity of the nanoparticles themselves as well as the effect and function of the support material.

1.6 Thesis Aims

The aims of this thesis are outlined below.

1. Au-Pd nanoparticles supported on TiO_2 have been shown to be effective catalysts for the oxidation of methane with H_2O_2. In this work the intrinsic activity of the Au-Pd nanoparticles for methane oxidation and the role of the support in this system will be explored. This will be achieved by investigating the activity of unsupported, colloidal Au-Pd nanoparticles and comparing this colloidal system with that of the supported nanoparticles. The basis for any difference in activity observed between these systems will also be examined.

2. Once the differences and similarities between the colloidal and supported Au-Pd nanoparticle systems have been established, a more in depth study will be carried out in order to determine the extent of the Au-Pd nanoparticles intrinsic activity for methane oxidation with H_2O_2 and the factors affecting it. This will include investigations into the effects of altering parameters associated with the preparation of the unsupported Au-Pd nanoparticles and the effects of various reaction parameters on the system.

3. The fifth chapter in this thesis will focus on investigating the use of methyl hydroperoxide in combination with H_2O_2 to activate methane without the presence of a metal catalyst. This first stage of this investigation will be to establish a method of producing methyl hydroperoxide and to this end a variety of copper catalysts will be prepared and tested. The second step in the investigation will be to optimise the reaction conditions and to confirm that the system is activating methane through the use of isotopically labelled methane.

1.7 References

1. What is Natural Gas?, http://naturalgas.org/overview/background/, Accessed 03/12/14.
2. What is the volume of world natural gas reserves?, http://www.eia.gov/tools/faqs/faq.cfm?id=52&t=8, Accessed 03/12/14.
3. Introduction to Shale Gas, http://shalegas-europe.eu/shale-gas-explained/introduction-to-shale-gas/, Accessed 03/12/14.
4. A. Caballero and P. J. Perez, *Chem. Soc. Rev.*, 2013, 42, 8809-8820.
5. S. J. Blanksby and G. B. Ellison, *Acc. Chem. Res.*, 2003, 36, 255-263.
6. B. Michalkiewicz, *Appl. Catal., A*, 2006, 307, 270-274.
7. LNG for transport, http://www.shell.com/global/future-energy/natural-gas/natural-gas-transport.html, Accessed 03/12/14.
8. C. Hammond, S. Conrad and I. Hermans, *ChemSusChem*, 2012, 5, 1668-1686.
9. M. Merkx, D. A. Kopp, M. H. Sazinsky, J. L. Blazyk, J. Muller and S. J. Lippard, *Angew. Chem. Int. Ed.*, 2001, 40, 2782-2807.
10. A. A. Shteinman, *Russ. Chem. Bull.*, 2001, 50, 1795-1810.
11. K. Yoshizawa and T. Yumura, *J. Inorg. Biochem.*, 2003, 96, 257-257.
12. K. Yoshizawa, *Acc. Chem. Res.*, 2006, 39, 375-382.
13. J. Colby, D. I. Stirling and H. Dalton, *Biochem. J.*, 1977, 165, 395-402.
14. S. I. Chan and S. S. F. Yu, *Acc. Chem. Res.*, 2008, 41, 969-979.
15. R. L. Lieberman and A. C. Rosenzweig, *Nature*, 2005, 434, 177-182.
16. P. Basu, B. Katterle, K. K. Andersson and H. Dalton, *Biochem. J.*, 2003, 369, 417-427.
17. L. A. Levchenko, A. P. Sadkov, N. V. Lariontseva, E. M. Koldasheva, A. K. Shilova and A. E. Shilov, *Dokl. Biochem. Biophys.*, 2001, 377, 123-124.
18. S. G. Lee, J. H. Goo, H. G. Kim, J. I. Oh, Y. M. Kim and S. W. Kim, *Biotechnol. Lett.*, 2004, 26, 947-950.
19. J. H. Lunsford, *Catal. Today*, 2000, 63, 165-174.
20. J. B. Hansen and P. E. Højlund Nielsen, in *Handbook of Heterogeneous Catalysis*, Wiley-VCH Verlag GmbH & Co. KGaA, 2008, DOI: 10.1002/9783527610044.hetcat0148.
21. G. C. Chinchen, K. Mansfield and M. S. Spencer, *Chemtech*, 1990, 20, 692-699.
22. K. Otsuka and Y. Wang, *Appl. Catal., A*, 2001, 222, 145-161.
23. J. S. J. Hargreaves, G. J. Hutchings and R. W. Joyner, *Nature*, 1990, 348, 428-429.
24. B. Michalkiewicz, *Appl. Catal., A*, 2004, 277, 147-153.
25. Y. Wang and K. Otsuka, *J. Chem. Soc., Chem. Commun.*, 1994, DOI: 10.1039/C39940002209, 2209-2210.
26. F. Goldshlen, A. A. Shteinman, A. E. Shilov and V. V. Eskova, *Russ. J. Phys. Chem*, 1972, 46, 785-&.
27. R. A. Periana, O. Mirinov, D. J. Taube and S. Gamble, *Chem. Commun.*, 2002, DOI: 10.1039/B205366G, 2376-2377.
28. R. A. Periana, D. J. Taube, S. Gamble, H. Taube, T. Satoh and H. Fujii, *Science*, 1998, 280, 560-564.

29. R. A. Periana, D. J. Taube, E. R. Evitt, D. G. Löffler, P. R. Wentrcek, G. Voss and T. Masuda, *Science*, 1993, 259, 340-343.
30. S. Mukhopadhyay and A. T. Bell, *J. Mol. Catal. A: Chem.*, 2004, 211, 59-65.
31. S. Mukhopadhyay and A. T. Bell, *Adv. Synth. Catal.*, 2004, 346, 913-916.
32. G. R. Williams, S. T. Kolaczkowski and P. Plucinski, *Catal. Today*, 2003, 81, 631-640.
33. B. Michalkiewicz, K. Kalucki and J. G. Sosnicki, *J. Catal.*, 2003, 215, 14-19.
34. C. J. Jones, D. Taube, V. R. Ziatdinov, R. A. Periana, R. J. Nielsen, J. Oxgaard and W. A. Goddard, *Angew. Chem. Int. Ed.*, 2004, 43, 4626-4629.
35. Q. Yuan, W. Deng, Q. Zhang and Y. Wang, *Adv. Synth. Catal.*, 2007, 349, 1199-1209.
36. R. Palkovits, C. von Malotki, M. Baumgarten, K. Muellen, C. Baltes, M. Antonietti, P. Kuhn, J. Weber, A. Thomas and F. Schueth, *ChemSusChem*, 2010, 3, 277-282.
37. R. Palkovits, M. Antonietti, P. Kuhn, A. Thomas and F. Schuth, *Angew. Chem. Int. Ed.*, 2009, 48, 6909-6912.
38. M. Lin and A. Sen, *J. Am. Chem. Soc.*, 1992, 114, 7307-7308.
39. M. H. Ab Rahim, M. M. Forde, R. L. Jenkins, C. Hammond, Q. He, N. Dimitratos, J. A. Lopez-Sanchez, A. F. Carley, S. H. Taylor, D. J. Willock, D. M. Murphy, C. J. Kiely and G. J. Hutchings, *Angew. Chem. Int. Ed.*, 2013, 52, 1280-1284.
40. R. Raja and P. Ratnasamy, *Appl. Catal., A*, 1997, 158, L7-L15.
41. A. B. Sorokin, E. V. Kudrik, L. X. Alvarez, P. Afanasiev, J. M. M. Millet and D. Bouchu, *Catal. Today*, 2010, 157, 149-154.
42. A. B. Sorokin, E. V. Kudrik and D. Bouchu, *Chem. Comm.*, 2008, DOI: 10.1039/B804405H, 2562-2564.
43. M. M. Forde, B. C. Grazia, R. Armstrong, R. L. Jenkins, M. H. A. Rahim, A. F. Carley, N. Dimitratos, J. A. Lopez-Sanchez, S. H. Taylor, N. B. McKeown and G. J. Hutchings, *J. Catal.*, 2012, 290, 177-185.
44. S. M. Auerbach, K. A. Currado and P. K. Dutta, *Handbook of Zeolites Science and Technology*, Marcel Dekker Inc, New York, 2003.
45. J. Čejka and H. v. Bekkum, 2005, vol. 157.
46. R. J. Argauer and G. R. Landolt, Google Patents, 1972.
47. C. H. Baerlocher, L. B. McCusker and D. H. Olson, *Atlas of Zeolite Framework Types*, Elsevier, 2007.
48. Y. Zheng, X. Li and P. K. Dutta, *Sensors* 2012, 12, 5170-5194.
49. C. Hammond, R. L. Jenkins, N. Dimitratos, J. A. Lopez-Sanchez, M. H. ab Rahim, M. M. Forde, A. Thetford, D. M. Murphy, H. Hagen, E. E. Stangland, J. M. Moulijn, S. H. Taylor, D. J. Willock and G. J. Hutchings, *Chem. Eur. J.*, 2012, 18, 15735-15745.
50. C. Hammond, M. M. Forde, M. H. Ab Rahim, A. Thetford, Q. He, R. L. Jenkins, N. Dimitratos, J. A. Lopez-Sanchez, N. F. Dummer, D. M. Murphy, A. F. Carley, S. H. Taylor, D. J. Willock, E. E. Stangland, J. Kang, H. Hagen, C. J. Kiely and G. J. Hutchings, *Angew. Chem. Int. Ed.*, 2012, 51, 5129-5133.
51. A. K. M. L. Rahman, M. Kumashiro and T. Ishihara, *Catal. Comm.*, 2011, 12, 1198-1200.
52. P. Kubanek, B. Wichterlova and Z. Sobalik, *J. Catal.*, 2002, 211, 109-118.
53. I. Yuranov, D. A. Bulushev, A. Renken and L. Kiwi-Minsker, *J. Catal.*, 2004, 227, 138-147.

54. M. R. Lin, T. Hogan and A. Sen, *J. Am. Chem. Soc.*, 1997, 119, 6048-6053.
55. G. J. Hutchings, *J. Catal.*, 1985, 96, 292-295.
56. M. Haruta, T. Kobayashi, H. Sano and N. Yamada, *Chem. Lett.*, 1987, DOI: 10.1246/cl.1987.405, 405-408.
57. A. S. K. Hashmi and G. J. Hutchings, *Angew. Chem. Int. Ed.*, 2006, 45, 7896-7936.
58. A. Corma and H. Garcia, *Chem. Soc. Rev.*, 2008, 37, 2096-2126.
59. C. Della Pina, E. Falletta, L. Prati and M. Rossi, *Chem. Soc. Rev.*, 2008, 37, 2077-2095.
60. M. Ab Rahim, M. M. Forde, C. Hammond, R. L. Jenkins, N. Dimitratos, J. A. Lopez-Sanchez, A. F. Carley, S. H. Taylor, D. J. Willock and G. J. Hutchings, *Top. Catal.*, 2013, 56, 1843-1857.
61. L. Kesavan, R. Tiruvalam, M. H. Ab Rahim, M. I. bin Saiman, D. I. Enache, R. L. Jenkins, N. Dimitratos, J. A. Lopez-Sanchez, S. H. Taylor, D. W. Knight, C. J. Kiely and G. J. Hutchings, *Science*, 2011, 331, 195-199.
62. J. K. Edwards and G. J. Hutchings, *Angew. Chem. Int. Ed.*, 2008, 47, 9192-9198.
63. D. I. Enache, J. K. Edwards, P. Landon, B. Solsona-Espriu, A. F. Carley, A. A. Herzing, M. Watanabe, C. J. Kiely, D. W. Knight and G. J. Hutchings, *Science*, 2006, 311, 362-365.
64. M. Haruta, N. Yamada, T. Kobayashi and S. Iijima, *J. Catal.*, 1989, 115, 301-309.
65. N. Lopez, T. V. W. Janssens, B. S. Clausen, Y. Xu, M. Mavrikakis, T. Bligaard and J. K. Norskov, *J. Catal.*, 2004, 223, 232-235.
66. A. Haruta, *Chem. Rec.*, 2003, 3, 75-87.
67. D. L. Lahr and S. T. Ceyer, *J. Am. Chem. Soc.*, 2006, 128, 1800-1801.
68. C. K. Costello, J. H. Yang, H. Y. Law, Y. Wang, J. N. Lin, L. D. Marks, M. C. Kung and H. H. Kung, *Appl. Catal., A*, 2003, 243, 15-24.
69. G. C. Bond and D. T. Thompson, *Gold Bull.*, 2000, 33, 41-51.
70. F. Moreau, G. C. Bond and A. O. Taylor, *J. Catal.*, 2005, 231, 105-114.
71. R. Zanella, L. Delannoy and C. Louis, *Appl. Catal., A*, 2005, 291, 62-72.
72. US 2369912, 1945.
73. *Du Pont Pat.,* US 2657980, 1939.
74. J. M. Campos-Martin, G. Blanco-Brieva and J. L. Fierro, *Angew. Chem. Int. Ed.*, 2006, 45, 6962-6984.
75. *Henkel & Cie Gmbh Pat.,* US 1108752, 1914.
76. P. Landon, P. J. Collier, A. J. Papworth, C. J. Kiely and G. J. Hutchings, *Chem. Commun.*, 2002, DOI: 10.1039/b205248m, 2058-2059.
77. P. Landon, P. J. Collier, A. F. Carley, D. Chadwick, A. J. Papworth, A. Burrows, C. J. Kiely and G. J. Hutchings, *Phys. Chem. Chem. Phys.*, 2003, 5, 1917-1923.
78. M. Okumura, Y. Kitagawa, K. Yamagcuhi, T. Akita, S. Tsubota and M. Haruta, *Chem. Lett.*, 2003, 32, 822-823.
79. T. Ishihara, Y. Ohura, S. Yoshida, Y. Hata, H. Nishiguchi and Y. Takita, *Appl. Catal., A*, 2005, 291, 215-221.
80. J. K. Edwards, B. Solsona, E. N. N, A. F. Carley, A. A. Herzing, C. J. Kiely and G. J. Hutchings, *Science*, 2009, 323, 1037-1041.

81. J. Pritchard, L. Kesavan, M. Piccinini, Q. He, R. Tiruvalam, N. Dimitratos, J. A. Lopez-Sanchez, A. F. Carley, J. K. Edwards, C. J. Kiely and G. J. Hutchings, *Langmuir*, 2010, 26, 16568-16577.
82. J. A. Lopez-Sanchez, N. Dimitratos, P. Miedziak, E. Ntainjua, J. K. Edwards, D. Morgan, A. F. Carley, R. Tiruvalam, C. J. Kiely and G. J. Hutchings, *Phys. Chem. Chem. Phys.*, 2008, 10, 1921-1930.
83. J. A. Lopez-Sanchez, N. Dimitratos, N. Glanville, L. Kesavan, C. Hammond, J. K. Edwards, A. F. Carley, C. J. Kiely and G. J. Hutchings, *Appl. Catal., A*, 2011, 391, 400-406.
84. X. Li, J. Xu, L. Zhou, F. Wang, J. Gao, C. Chen, J. B. Ning and H. Ma, *Catal. Lett.*, 2006, 110, 149-154.
85. R. L. Brutchey, I. J. Drake, A. T. Bell and T. D. Tilley, *Chem. Comm.*, 2005, DOI: 10.1039/B506426K, 3736-3738.
86. A. Singh and T. Selvam, *J. Mol. Catal. A: Chem.*, 1996, 113, 489-497.
87. G. J. Hutchings and C. J. Kiely, *Acc. Chem. Res.*, 2013, 46, 1759-1772.
88. M. I. bin Saiman, G. L. Brett, R. Tiruvalam, M. M. Forde, K. Sharples, A. Thetford, R. L. Jenkins, N. Dimitratos, J. A. Lopez-Sanchez, D. M. Murphy, D. Bethell, D. J. Willock, S. H. Taylor, D. W. Knight, C. J. Kiely and G. J. Hutchings, *Angew. Chem. Int. Ed.*, 2012, 51, 5981-5985.
89. N. Dimitratos, J. A. Lopez-Sanchez, D. Morgan, A. F. Carley, R. Tiruvalam, C. J. Kiely, D. Bethell and G. J. Hutchings, *Phys. Chem. Chem. Phys.*, 2009, 11, 5142-5153.
90. J. C. Pritchard, Q. He, E. N. Ntainjua, M. Piccinini, J. K. Edwards, A. A. Herzing, A. F. Carley, J. A. Moulijn, C. J. Kiely and G. J. Hutchings, *Green Chem.*, 2010, 12, 915-921.
91. G. B. Shul'pin, T. Sooknoi, V. B. Romakh, G. Suss-Fink and L. S. Shul'pina, *Tetrahedron Lett.*, 2006, 47, 3071-3075.
92. F. Bonino, A. Damin, G. Ricchiardi, M. Ricci, G. Spano, R. D'Aloisio, A. Zecchina, C. Lamberti, C. Prestipino and S. Bordiga, *J. Phys. Chem. B*, 2004, 108, 3573-3583.
93. M. Faraday, *Philos. Trans. R. Soc. London*, 1857, 147, 154-153.
94. C. J. Jia and F. Schuth, *Phys. Chem. Chem. Phys.*, 2011, 13, 2457-2487.
95. K. J. Klabunde, Y. X. Li and B. J. Tan, *Chemistry of Materials*, 1991, 3, 30-39.
96. T. Teranishi and M. Miyake, *Chem. Mater.*, 1998, 10, 594-600.
97. O. Masala and R. Seshadri, *Annu. Rev. Mater. Res.*, 2004, 34, 41-81.
98. X. Junyang, Hua, H., Jiang, Z., Ma, Y., Huang, H., *Langmuir*, 2012, 28, 6736-6741.
99. T. Teranishi and M. Miyake, *Chemistry of Materials*, 1998, 10, 594-600.
100. M. Haruta, *Faraday Discuss.*, 2011, 152, 11-32.
101. L. Prati and A. Villa, *Acc. Chem. Res.*, 2014, 47, 855-863.
102. Y. Mikami, A. Dhakshinamoorthy, M. Alvaro and H. Garcia, *Catal. Sci. Tech.*, 2013, 3, 58-69.
103. H. Tsunoyama, H. Sakurai, Y. Negishi and T. Tsukuda, *J. Am. Chem. Soc.*, 2005, 127, 9374-9375.
104. H. Tsunoyama, T. Tsukuda and H. Sakurai, *Chem. Lett.*, 2007, 36, 212-213.
105. H. Tsunoyama, N. Ichikuni, H. Sakurai and T. Tsukuda, *J. Am. Chem. Soc.*, 2009, 131, 7086-7093.
106. P. G. N. Mertens, I. F. J. Vankelecom, P. A. Jacobs and D. E. De Vos, *Gold Bull.*, 2005, 38, 157-162.

107. P. G. N. Mertens, M. Bulut, L. E. M. Gevers, I. F. J. Vankelecom, P. A. Jacobs and D. E. De Vos, *Catal. Lett.*, 2005, 102, 57-61.
108. A. Villa, D. Wang, D. S. Su and L. Prati, *Chemcatchem*, 2009, 1, 510-514.
109. L. Prati, P. Spontoni and A. Gaiassi, *Top. Catal.*, 2009, 52, 288-296.
110. M. Comotti, C. Della Pina, E. Falletta and M. Rossi, *Adv. Synth. Catal.*, 2006, 348, 313-316.
111. P. Beltrame, M. Comotti, C. Della Pina and M. Rossi, *Appl. Catal., A*, 2006, 297, 1-7.
112. M. Comotti, C. Della Pina, R. Matarrese and M. Rossi, *Angew. Chem., Int. Ed.*, 2004, 43, 5812-5815.

Experimental Procedures 2

2.1 Introduction

In this chapter the methods and procedures by which catalyst preparation, testing and characterisation over the course of this work are described.

2.2 Materials

The following materials were used throughout the course of this project.

Materials used for catalyst preparation;

- Aurochloric acid, $HAuCl_4.xH_2O$ (99.999%, *Sigma Aldrich*)
- Palladium chloride($PdCl_2$, *Johnson Matthey*)
- Polyvinylpyrrolidone, PVP(molecular weights 3.5 kDa, 10 kDa, 40 kDa, 53 kDa, 360 kDa, 1300 kDa, *Sigma Aldrich*)
- Polyvinyl alcohol, PVA (*Sigma Aldrich*)
- Sodium Borohydride, $NaBH_4$(*Sigma Aldrich*)
- Titanium Dioxide,TiO_2 (P25, *Degussa*)
- Silicon Carbide, SiC (400 nm mesh, *Sigma Aldrich*)
- Copper nitratetrihydrate, $CuNO_3.3H_2O$ (99% *Sigma Aldrich*)
- Copper sulphatepentahydrate, $CuSO_4.5H_2O$ (≥98% *Sigma Aldrich*)
- Copper chloride, $CuCl_2$(99.999% *Sigma Aldrich*)

- Copper acetate, $Cu(CO_2CH_3)_2$(98%, *Sigma Aldrich*)
- Urea, $CO(NH_2)_2$(*Sigma Aldrich*)
- Sodium Hydroxide, NaOH (*Sigma Aldrich*)
- Acetic Acid, CH_3COOH (*Sigma Aldrich*)
- Ethanol, C_2H_5OH (*Sigma Aldrich*)
- Citric Acid, $C_6H_8O_7$(*Sigma Aldrich*)
- Nitric Acid, HNO_3(*Sigma Aldrich*)
- ZSM-5 (SiO_2 : Al_2O_3molar ratio= 30 *Zeolyst*)
- Copper Acetylacetonate, $Cu(acac)_2$ (98%, *Sigma Aldrich*)

Materials for catalyst testing;

- Methane, CH_4 (99.999%, *BOC gases*)
- ^{13}C methane, $^{13}CH_4$, (research grade, *BOC gases*)
- Nitrogen, N_2 (99.999%, *BOC gases*)
- Hydrogen peroxide (50% wt in H_2O, *Sigma Aldrich*)
- Sodium chloride, NaCl (*Sigma Aldrich*)
- Methanol, CH_3OH (HPLC grade *Sigma Aldrich*)
- Deuterium oxide, D_2O (99.9 atom % D *Sigma Aldrich)*

2.3 Definitions

2.3.1 % Oxygenate Selectivity

The selectivity towards oxygenated products is expressed as a percentage of the total products produced.

$$\frac{\text{Moles } (CH_3OH+CH_3OOH+HCOOH) \text{ formed}}{\text{Moles } (CH_3OH+CH_3OOH+HCOOH+CO_2) \text{ formed}} \times 100$$

2.3.2 Catalyst Productivity

Catalyst productivity if calculated as the number of moles of products formed per kilogram of catalyst per hour.

$$\text{Productivity} = \text{moles}_{(\text{products})}\ \text{kg}^{-1}{}_{(\text{catalyst})}\ \text{h}^{-1}$$

2.3.3 Turnover Frequency (TOF)

The turnover frequency is calculated as the number of moles of products formed per moles of metal in the catalyst per hour.

$$\text{TOF} = \text{moles}_{(\text{products})}\ \text{moles}^{-1}{}_{(\text{metal in catalyst})}\ \text{h}^{-1}$$

2.4 Catalyst Preparation

2.4.1 Preparation of Colloids

Au, Pd and bimetallic Au-Pd polyvinylpyrrolidone (PVP) stabilised colloids were prepared by the chemical reduction of metal salt precursors. This method involves mixing a reducing agent hydrogen, alcohol, hydrazine or in this case, sodium borohydride with of the metal salt precursor(s) and a stabilising agent.[1] The stabilising agent may be a ligand, polymer or surfactant whose role is to prevent particle agglomeration. In this way the formation of well dispersed metal nanoparticles is ensured and particle size is controlled. The final size and morphology of the prepared nanoparticles is determined by a combination of factors such as type of stabiliser, precursor and reducing agent employed as well as their concentrations and the solvent and temperature in which the reduction takes place.

An aqueous solution of concentration 1.94×10^{-4} M of the metal precursors ($HAuCl_4$ and $PdCl_2$) was prepared. The molar ratio of gold to palladium used was 1:1 unless otherwise stated. A typical preparation would involve pipetting 1.287 ml of an 11.5 mg/ml solution of $HAuCl_4$ and 1.273 ml of a 6.1 mg/ml solution of $PdCl_2$ (acidified with HCl) into 800 ml of deionised water. 276 mg of PVP (typically with a molecular weight of 10 kDa) was dissolved in 10 ml of water to produce a 1 wt% solution. 1 ml of the PVP solution was then pipetted into the solution of the metal chloride salts to produce a solution with a PVP to metal weight ratio of 1.2:1. After 2-3 minutes of stirring 1 ml of freshly prepared 0.1 M

$NaBH_4$ solution was added such that the molar ratio of $NaBH_4$ to metal was 5:1. This produced a dark brown colloid which was stirred for 30 min to ensure that all the metal present was reduced.

If a more concentrated colloid was required this was achieved by using a rotary evaporator with a 90 °C water bath under continuous vacuum. The original solution was always prepared using the same concentration of the metal precursor(s) as variations in this concentration during the formation of the nanoparticles can have an effect on the size and shape of the nanoparticles formed. Therefore when a more concentrated colloid was required water was removed from the colloid by rotary evaporator post-synthesis of the nanoparticles to reduce potential variation in the size and shape of the nanoparticles formed. The standard colloid metal concentration used throughout this work was 7.57×10^{-4} M. The colloids were prepared at a metal concentration of 1.94×10^{-4} M to ensure that the preparation method was comparable to that used in previously published reports.[2-4] However, due to the issues surrounding reproducibility detailed in chapter 4 section 4.2 the higher metal concentration (7.57×10^{-4} M) was typically used. During the preparation of monometallic palladium colloids care was taken to prevent re-oxidation by preparing and storing the colloid under nitrogen.

2.4.2 Preparation of Supported Nanoparticles by Sol-immobilisation Method

The sol-immobilisation method for the preparation of supported metal nanoparticles involves the preparation of metal nanoparticles in the presence of a stabilising agent (as described above) followed by their immobilisation on a support material. Typically the metal particles absorb on to the support surface when the support is mixed with the colloidal solution. The identity of the stabiliser molecule, the surface area of the support material and its isoelectric point can all effect the kinetics of absorption.[5, 6]

Supported catalysts were prepared by the same method as the unsupported nanoparticles with the following additional steps. After the colloid had been

stirred for 30 min the support material was added to the colloid, the amount depended on the desired metal loading. The solution was then acidified to pH 1 using sulphuric acid. The solution became colourless over 60 min of stirring as the nanoparticles were adsorbed on to the support. The catalyst was then filtered, washed thoroughly with distilled water (2 L) and left to dry in an oven at 110 °C overnight.[2]

2.4.3 Preparation of Copper Catalysts

In this study CuO was prepared using three different methods i.e. modified sol-gel, precipitation and quick precipitation. Each preparation method is described below.

2.4.3.1 Modified sol-gel method

The standard sol-gel method involves the synthesis of a colloidal solution (sol) which acts as a precursor for the formation a gel. The precursor is typically produced by the hydrolysis of an organic alkoxide and gelation then occurs as a result of condensation of the partially hydrolysed species.[7] Wan *et al.* have reported that nano-sized NiO can be prepared from nickel nitrate using, what is termed, a modified sol-gel method.[8] In this method the dispersive precursor is prepared through the coordination of a multidentate ligand (citric acid) and a metal ion. The role of the citric acid is to prevent agglomeration through steric effects. The ligand is then removed by thermal decomposition so that only the metal nanoparticles remain. In the same study it was found that the following factors have a significant effect on the surface area of the final NiO; the pH of the solution, the ratio of nickel nitrate to citric acid and the heating rate and temperature used for the calcination of the precursor. In this study the same method (described below) was used to prepare CuO.

A concentrated copper nitrate solution (3.044 g of $Cu(NO_3).3H_2O$ in 5 ml) was added dropwise to a beaker of citric acid solution (2.421 g in 5 ml) with stirring. The prepared solution was composed of a 1:1 molar ratio of copper to citric acid. This was acidified to pH 1 using several drops of nitric acid.[8] The resultant transparent solution was heated to 70 ^{0}C with stirring. This slow evaporation of

the solution was continued until such time as a viscous residue was produced (typically 30 min). The residue was then dried at 110 °C for 16 hr during which a gel precursor developed. This precursor was then calcined at 300 °C in static air.

2.4.3.2 Quick precipitation method

A quick precipitation method for the formation of CuO nanoparticles has previously been reported by Wang *et al.*[9] This method produced highly disperse CuO nanoparticles of about 6 nm with a narrow size distribution using copper acetate as a precursor. It was shown that the morphology of the nanoparticles could be controlled by varying the reaction temperature and through the addition of glacial acetic acid which prevents hydrolysis of the copper acetate solution. Adding glacial acetic acid and carrying out the reaction at 100 °C was found to produce spherical particles ranging in size between 5-7 nm. These conditions were replicated for the preparation used for this study which is described in full below.

1 ml glacial acetic acid was added to 300 ml of 0.1 M copper acetate solution in a round-bottomed flask fitted with a condenser.[9] The solution was heated to 100 °C with stirring at which point 0.8 g NaOH was added. This reduced the pH of the solution to 6-7 immediately causing a black precipitate to be formed. The solution was cooled to room temperature before being centrifuged in order to collect the precipitate. The precipitate was then washed with 1 L water and 1 L ethanol and finally dried at room temperature.

2.4.3.3 Precipitation method

Copper compounds of various morphologies and compositions may be prepared from the homogeneous precipitation of copper salts in solution in the presence of urea. Kratohvil and Matijević have previously investigated the effects of varying the identity and concentration of the copper precursor and the concentration of urea on the resultant copper compounds using this method.[10] The report of this study details the conditions required to produce various particle morphologies and compositions. Six sets of these conditions were chosen for investigation. As such as part of this study the precipitation method was used

to produce six different copper catalyst (as described below). The particular sets of conditions used are shown in table 2.1 including the particle morphologies observed for each set of conditions by Kratohvil and Matijević.[10]

A copper precursor (copper chloride, copper sulphate or copper nitrate) was precipitated with urea by refluxing in 300 ml water at 100 °C for 16 hr in a 500 ml round-bottomed flask.[10] The copper precursor, its concentration and the concentration of urea employed were varied depending on which catalyst was being prepared (see table 2.1). The precipitate obtained was separated from the solvent by filtration. It was then washed with water (2 L) and dried at 110 ^{0}C for 16 hr. The catalyst was then calcined in static air at 350 ^{0}C.

Table 2.1 Copper precursors, their concentrations and the concentration of urea used to prepared various copper catalyst by co-precipitation.

Copper Precursor	Particle Morphology	Concentration of Copper Precursor (M)	Concentration of Urea (M)
$CuSO_4$	Needles	1.5×10^{-2}	5×10^{-1}
$CuSO_4$	Platelets	1.2×10^{-3}	3×10^{-1}
$Cu(NO_3)_2$	Spheres	1.5×10^{-2}	2×10^{-1}
$Cu(NO_3)_2$	Platelets	3.0×10^{-2}	1×10^{-1}
$CuCl_2$	Bipyramids	8.0×10^{-3}	2×10^{-1}
$CuCl_2$	Spheres	3.0×10^{-2}	3×10^{-1}

2.4.4 Preparation of Cu/ZSM-5 by Solid State Ion Exchange

Solid state ion exchange in a simple but effective method of modifying zeolites. It involves intimately mixing the starting zeolite with a finely dispersed powder of a compound of the ion to be exchanged in to the zeolite. The mixture is then heat treated at high temperature.[11] 1.25wt% Cu/ZSM-5(30) was prepared by solid state ion exchange during this study. It has previously been reported that Fe/ZSM-5, Cu-Fe/ZSM-5 and Cu/ZSM-5 prepared using this method are active for the oxidation of CH_4 with H_2O_2.[3, 12] Commercial ZSM-5 has been shown also been shown to be active for this reaction due to trace Fe impurities. Addition of Cu to commercial ZSM-5 has been shown to improve the selectivity of the catalyst to

CH_3OH and CH_3OOH as it switchs off the over-oxidation of CH_3OH to HCOOH. This is due to the ability of Cu to scavenge $^{\bullet}OH$ radicals.

The first step in this preparation was the high temperature activation of the zeolite support. Typically 0.5 g NH_4-ZSM-5 (SiO_2/Al_2O_3 molar ratio = 30) was heated under flowing air in a furnace to 550 ºC for 3 hr. Next 2 g of 1.25% Cu/ZSM-5(30) was prepared by manually grinding 0.1 g copper acetylacetonate together with 1.975 g of the activated zeolite support for 30 min. The mixture was then calcined at 550ºC for 3 hr.

2.5 Catalyst Testing

Catalyst testing was carried out in 50 ml stainless steel Parr autoclave reactors containing a Teflon liner (working volume 35 ml). Each reactor was connected to a separate gas burette to facilitate gas mixing (figure 2.1). Reactor heating was generally controlled by a pre-set programme using the software associated with the reactor.

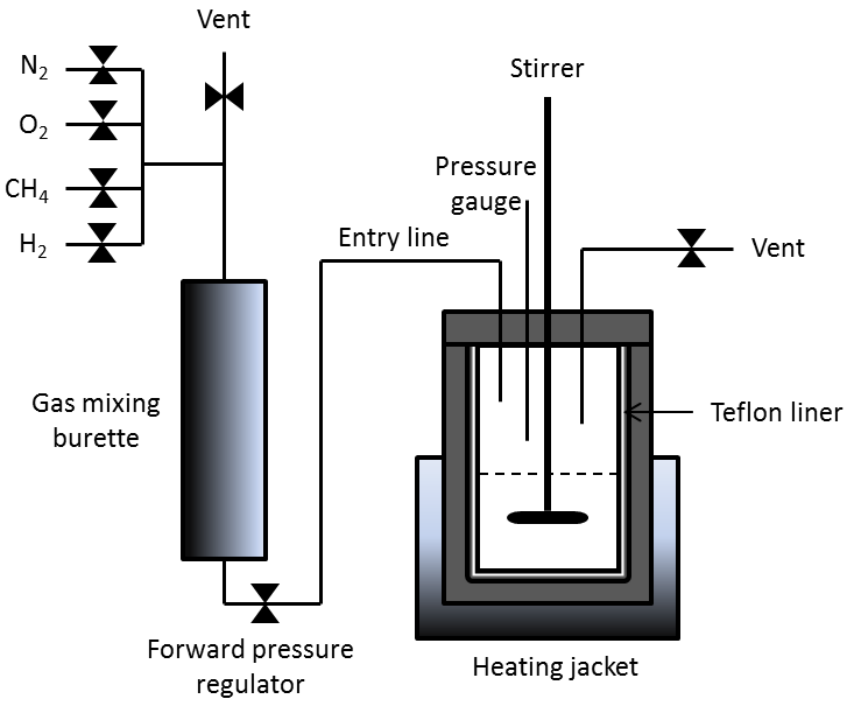

Figure 2.1 Schematic representation of autoclave reactor.

In a typical experiment 10 ml of colloid ([metal] = 7.57×10^{-4} M) or 10 ml of water plus the desired amount of supported catalyst were placed in the reactor with a measured amount of H_2O_2 (50 wt%).The reactor was then sealed and purged three times with methane before being pressurised to 30 bar with methane and heated to 50 °C When isotopically labelled experiments were carried out the ^{13}C methane was added directly into the reactor to prevent contamination of the gas burettes. Once the reactor had reached the set temperature stirring at 1500 rpm was initiated. At the end of the reaction (typically 30 min) heating and stirring was stopped and the reactor vessel was cooled to below 10 °C using an ice bath to minimise loss of volatile products. The reaction gas was collected for analysis using a gas sample bag. In the case of reactions catalysed by supported nanoparticles the reaction mixture was filtered before analysis. When colloidal nanoparticles were used the reaction mixture was centrifuged briefly to remove any solids which would interfere with NMR analysis of the liquid products.

2.6 Analysis of Products

2.6.1 ^{1}H-Nuclear Magnetic Resonance Spectroscopy (NMR)

Nuclear Magnetic Resonance Spectroscopy is a powerful analytical tool which exploits the magnetic properties of certain nuclei. When an atom contains an uneven number of protons and/or neutrons (e.g. ^{1}H, ^{13}C, ^{15}N) it has a non-zero nuclear spin which creates a magnetic moment. When a magnetic field is applied to these nuclei the magnetic moments can align parallel (low energy state) or anti-parallel (high energy state) to applied magnetic field.[13] Radio waves can be used to cause nuclei to resonate between the two energy states. This resonance frequency is dependent on the surrounding chemical environment of the nucleus and so this information can be used to identify molecules in a sample. ^{1}H-NMR can also be used for quantitative analysis as the integration of the signal a compound produces is proportional to the number of proton responsible for that signal.

^{1}H-NMR (500 MHz Bruker spectrometer) was used to identify liquid phase reaction products. A solvent suppression program was performed in order to minimize the signal arising from the solvent (water). Typically, 0.7 ml of sample and 0.1 ml of D_2O (for lock) were placed in an NMR tube with an internal standard for analysis at room temperature. This internal standard consisted of 1% TMS in $CDCl_3$ contained in a sealed capillary tube. It was calibrated against known methanol standards and used to quantify all observed liquid products. Examples of calibration curves of TMS inserts are shown in figure 2.2. A typical spectrum from a methane oxidation reaction is shown in figure 2.3 and peak assignments are listed in table 2.2 (only the peak used in quantification is reported).

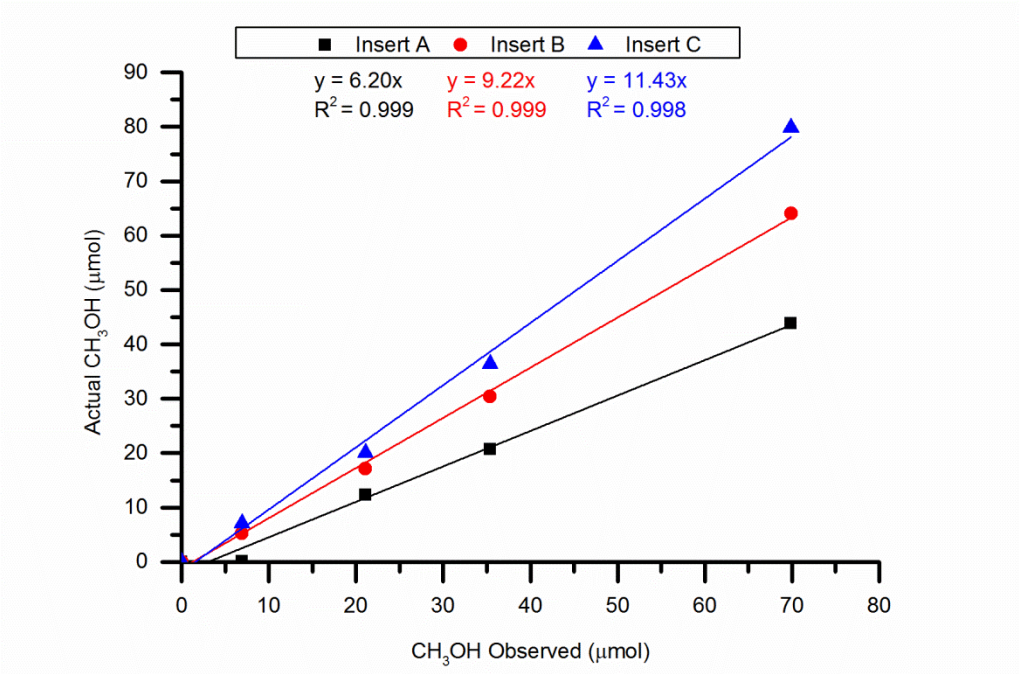

Figure 2.2 Calibration factors for three TMS NMR inserts

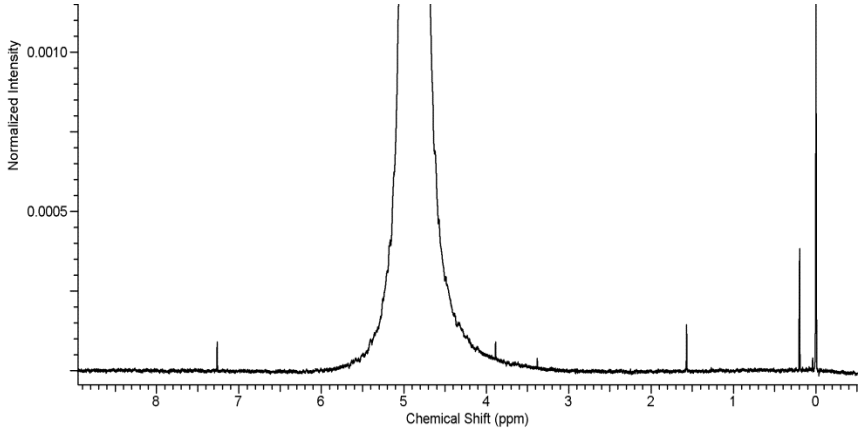

Figure 2.3 ^{1}H-NMR spectrum of reaction liquid following standard methane oxidation reaction catalysed by Au-Pd nanoparticles.

Table 2.2 Assignments of ^{1}H-NMR signals observed during the course of this work. In the case of reaction products only the peak used for quantification is reported.

Species	Chemical Shift/Multiplicity
Tetramethylsilane ($Si(CH_3)_4$, standard)	δ 0.0 ppm, s
Methane dissolved in water (CH_4)	δ 0.2 ppm, s
H_2O in $CDCl_3$	δ 1.55 ppm, s
Acetone ($(CH_3)_2CO$ contaminant)	δ 2.05 ppm, s
Acetic acid (CH_3COOH, contaminant)	δ 2.1 ppm, s
Methanol (CH_3OH)	δ 3.35 ppm, s
Methyl Hydroperoxide (CH_3OOH)	δ 3.89 ppm, s
Water (H_2O, solvent)	δ 4.8 ppm, s
Formaldehyde monohydrate ($CH_2(OH)_2$, generally obscured by H_2O)	δ 4.89 ppm, s
$CHCl_3$ in $CDCl_3$	δ 7.25 ppm, s
Formic Acid (HCOOH)	δ 8.2 ppm, s

2.6.2 Gas Chromatography(GC)

The only gas phase product of the reactions was CO_2 which was analysed by GC using a Varian 450-GC and a FID detector. The GC unit was equipped with a CP-SiL5CB column (50 m, 0.33 mm diameter, He carrier gas) and a methaniser.

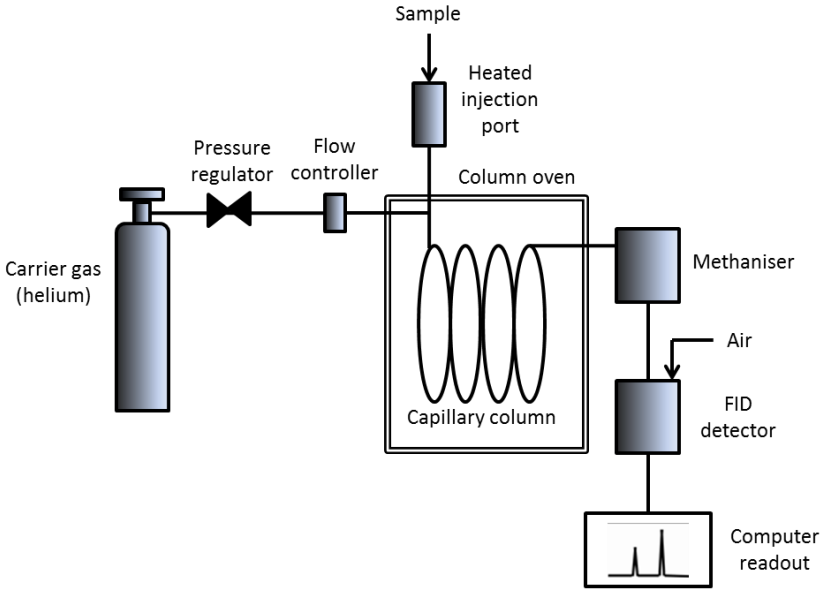

Figure 2.4 Schematic of gas chromatography setup.

Gas chromatography is used to analyse organic compounds which can be vaporised and are thermally stable enough not to decompose at the temperatures employed for analysis. Analysis begins by injecting the sample into a heated injection port where the sample is vaporised (unless it is already a gas).[14] An inert gas, typically helium, carries the vaporised sample through the chromatographic column. The inert gas is referred to as the mobile phase and the column as the stationary phase. The separation of the analytes is based upon their relative affinities for the stationary phase which consists of a microscopic liquid layer of varying polarity on an inert solid coating the inside of a metal tube. The varying interactions of the individual constituents of the sample with the column causes each of them to be eluted at a different time. This is referred to as the retention time of an analyte and is characteristic for different compounds.

Once separated and eluted from the column the various compounds in the sample are detected in this case by a Flame Ionisation Detector (FID). As the sample leaves the column it is mixed with hydrogen and air and passed through a flame. The burning of organic compounds produces ions and electrons. The resulting current is detected by two oppositely charged plates and is proportional to the concentration of organic compounds in the gas stream allowing the sample to be quantitatively analysed.

As CO_2 detectability is low for FID detectors a methanizer unit was used to convert CO_2 to methane after separation on the column but before reaching the detector. This unit consists of a nickel and cobalt catalyst which reduces the column effluent with hydrogen. The GC used in this work was also equipped with a TCD (Thermal Conductivity Detector) but this detector was not used for this project as it is not sensitive enough to detect the low concentrations of CO_2 that were produced.

2.6.3 Hydrogen Peroxide determination by titration

The amount of H_2O_2 remaining at the end of each reaction was quantified by titrating a portion of the reaction mixture against acidified $Ce(SO_4)$ solution of known concentration using ferroin as indicator.

2.7 Catalyst Characterisation

2.7.1 Ultraviolet-visible Spectroscopy (UV-vis)

UV-vis spectroscopy concerns the molecular absorption of electromagnetic radiation in the ultraviolet and visible spectral regions (190 nm to 800 nm).[15] When exposed to electromagnetic radiation in this range certain atomic and molecular species can absorb it causing them to undergo an electronic excitation from the ground state to a higher energy state. The specific difference in energy between the two states can be calculated based on the frequency of the electromagnetic radiation observed (equation 2.1).

$$\Delta E = h\upsilon$$

Equation 2.1

Where;
E = Energy, J
h = Planck's constant (6.63×10^{-34} J s)
υ = the frequency of the incident radiation, s^{-1}

These energy states are discreet and are affected by the surrounding electronic environment such that the wavelength of the absorbed photon can be used to identify the species which absorbed it. The energies associated with transitions between different arrangements of valence electrons falls within the UV-vis region of the electromagnetic spectrum. In addition concentration of the absorbing species can be determined using the Beer-Lambert Law (equation 2.2) which states that the concentration of the absorbing species is proportional to the absorbance.

$$A = \varepsilon[c]l$$

Equation 2.2

Where;
A = absorbance, dimensionless
ε= molar extinction coefficient, M^{-1} cm^{-1}
$[c]$ = concentration, M
l = path length of sample cell, cm

UV-vis spectra of colloidal gold nanoparticles display a feature of particular interest. In the visible region an intense absorption band is observed, this is the result of a phenomenon known as surface plasmon resonance. Surface Plasmon resonance occurs when the wavelength of radiation hitting metal nanoparticles is greater than the size of the particles. Under these conditions the coherent excitation of all free conduction band electrons results in a collective in-phase oscillation. As particle size increases the resonance band narrows as scattering length increases.[16]

All UV-vis spectra were recorded on a Jasco V-570 UV/VIS/NIR spectrophotometer over a range of 200 – 700 nm at a data interval of 1 nm. Samples were placed in quartz cuvettes for analysis which were carried out at room temperature.

2.7.2 Microwave Plasma Atomic Emission Spectroscopy (MP-AES)

When a molecule is subjected to radiation of an energy that matches that of the difference between two energy levels an electronic transition occurs from a low energy ground state to a higher energy transition state. Whereas other techniques (e.g. UV-vis spectroscopy) analyse the energy absorbed by the molecule, atomic emission spectroscopy concerns the energy emitted by a molecule as it relaxes back to the ground state. As such the wavelength of radiation emitted is characteristic to the element that emitted it. The concentration of the element in the sample can also be determined as the intensity of the emitted radiation is proportional to the number of atoms of the element present in the sample.

Various atomic emission sources such as flame, arc, spark and plasma sources may be used to produce atomic emission spectra. In this work a microwave plasma source was utilised. Plasma sources provide many advantages over flame emission spectroscopy including lower susceptibility to chemical interferences due to the higher operating temperatures and good emission spectra can be produced for most elements using the same excitation conditions.[14]

The amount of copper leeched from Cu/ZSM-5 and various copper oxide catalysts during a standard reaction was quantified using the MP-AES technique. Analysis was carried out at a wavelength of 324.8 nm on an Agilent 4100 spectrometer equipped with a nitrogen plasma source

2.7.3 Infra-red Spectroscopy (IR)

Infrared spectroscopy is a widely used vibrational spectroscopic technique. It exploits the fact molecules possess discrete levels of vibrational energy. These vibrations can be excited by photons; if the frequency of a vibrational mode is matched by the incident IR radiation the molecule will undergo a transition to a higher energy state.[15] As the bond vibrational modes are associated with characteristic vibrational frequencies they can be identified by analysing the wavelengths of IR radiation that have been absorbed. Using this technique the

bond lengths and force constraints of a molecule can be determined. In catalysis its most common use is the study of adsorbed species. Not all molecular vibrational modes are observed by IR spectroscopy. For a particular vibrational mode in a molecule to be detected by IR the vibration must result in a change in dipole moment.

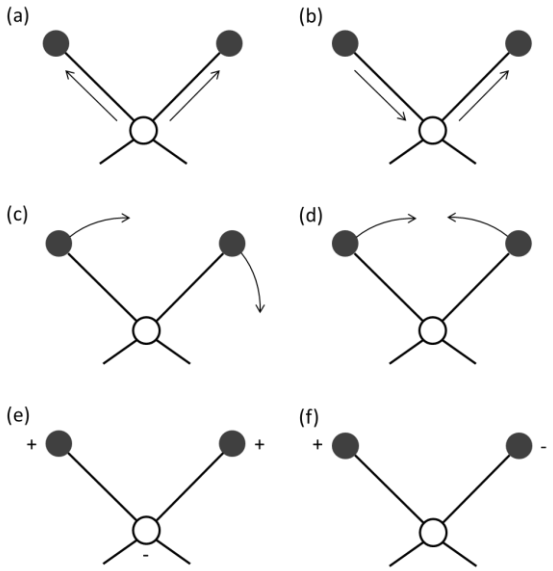

Figure 2.5 Molecular stretching vibrations; (a) symmetric and (b) asymmetric. Molecular bending vibrations (c) in plane rocking, (d) in-plane scissoring, (e) out of plane wagging and (f) out of plane twisting.

Diffuse reflectance infrared Fourier transform spectroscopy (DRIFTS) allows loose powder samples to be analysed eliminating the need to prepare the wafer typically required for transmission infrared spectroscopy. During this study DRIFT spectroscopy was utilised to determine the way in which the stabiliser molecule, PVP, was chemisorbed onto the surface of gold-palladium nanoparticles that had been prepared by the sol method. This analysis was carried out on a Bruker Tensor 27 spectrometer over a range of 4000- 1500 cm^{-1} and with a total of 4000 scans preformed for each sample. Colloidal samples were prepared for analysis by mixing 10 µL of sample with 0.3 g of KBr powder and drying overnight at 110 °C. This sample preparation method and peak assignments were based on the work of Huang *et al.*[17]

2.7.4 Powder X-Ray Diffraction (XRD)

XRD provides information on the bulk crystallographic phases in a sample and can also be used to estimate crystallite size. The technique is based on the elastic scattering of X-ray photons by atoms in the sample. X-rays are the type of electromagnetic radiation used as they have sufficient energy to penetrate solids and also have wavelengths in the angstrom range.[15] When scattered, monochromatic X-rays are in phase they interfere constructively producing a diffraction pattern. This pattern allows the lattice spacings between crystal planes to be calculated using Bragg's equation (Equation 2.3). The crystalline phases present in the sample can be identified through comparison of the collected diffraction pattern with a database of diffraction patterns. The primary limitation of this technique is that the sample must have sufficient long range lattice order (typically 5 nm or above) in order for peaks to be observed.

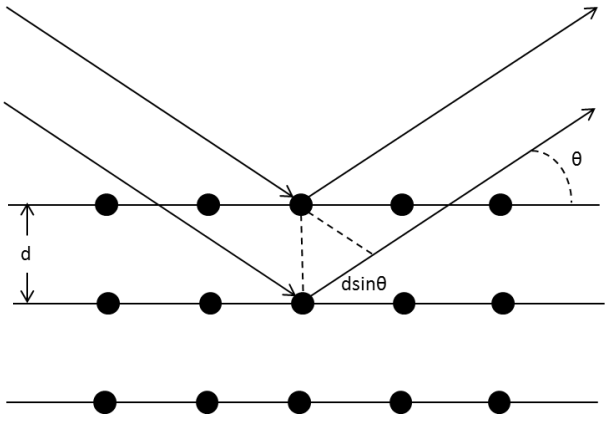

Figure 2.6 In phase x-rays scattered in an ordered lattice resulting in constructive interference.

$$n\lambda = 2d\sin\theta$$

Equation 2.3

Where
λ= wavelength of X-rays, Å
d = distance between lattice planes, Å
θ = scattering angle (angle between incoming X-rays and the normal to the reflecting plane), degrees
n = order of reflection (an integer)

The Scherrer equation (equation 2.4) can be used to relate particle size to line width. This is possible because peak broadening occurs for crystallite sizes less than 100 nm as a result of incomplete destructive interference by out of phase X-rays.

$$< L >= \frac{K\lambda}{\beta \cos\theta}$$

Equation 2.4

Where
$<L>$= dimension of the particle in the direction perpendicular to the reflecting plane, Å
λ= X-ray wavelength, Å
β= line broadening at half the maximum intensity, radians
θ= angle between beam and normal on the reflecting plane, degrees
K= a constant, dimensionless

In this work XRD was used to identify the crystal phases of copper catalysts prepared by different methods. Powder X-ray Diffraction analysis was carried out using a PANalytical MPD diffractometer with a $CuK_{\alpha 1}$ x-ray radiation source (λ = 0.154098 nm) at ambient temperature. Samples were typically scanned in the range of 10-70 degrees at settings of 40 kV and 40 mA. Samples were ground by hand before being mounted on silicon wafers for analysis. Crystal structures were assigned to diffractograms using ICDD (International Centre for Diffraction Data) software.

2.7.5 X-Ray Photoelectron Spectroscopy (XPS)

An atom in the sample will absorb photons of energy causing core or valence electrons to be ejected with a specific kinetic energy that is proportional to its binding energy. This is known as the photoelectric effect. XPS is a technique based on the photoelectric effect which is frequently used to characterise catalysts. It can provide information on the elemental composition of a sample, the oxidation states of the elements present and, less frequently, the dispersion of one phase over another. During analysis a sample is irradiated with a single wavelength of x-ray radiation causing core or valence electrons to be ejected with a specific kinetic energy, E_k by the photoelectric effect. The frequency of the

excitation energy is kept constant and the work function of the spectrometer (the energy required to eject an electron from the Fermi level into a vacuum) is known. As such by measuring the kinetic energy of the ejected electrons the binding energy of the photoelectron, which is characteristic to the element that emitted it, can be determined using equation 2.5.

$$E_k = hv - E_b - \varphi$$

Equation 2.5

Where
E_k = kinetic energy of ejected photoelectron, J
h = Planck's constant (6.63×10^{-34} J s)
v = frequency of excitation energy, s^{-1}
E_b = binding energy of the photoelectron, J
ϕ= work function of the spectrometer, J

As photoelectrons have a limited escape depth (1-12 nm) XPS is a surface specific technique. Binding energies are not only element specific but also increase with increasing oxidation state as electrons become more tightly bound. As such small changes in the binding energies of core electrons allow for the determination of oxidation states of surface atoms.[15]

XPS was utilised to identify the oxidation states present in both the copper catalysts and the gold-palladium colloids prepared during this study. A Kratos Axis Ultra DLD system was used to collect XPS spectra using monochromatic Al Kα X-ray source operating at 144 W. Colloidal samples were pipetted on to clean glass slides and the supporting solvent removed by the pumping system of the spectrometer sample fast-entry lock. The covering of sample was sufficient such that no underlying glass signal was observed.

Data was collected with pass energies of 160 eV for survey spectra, and 40 eV for the high resolution scans. The system was operated in the Hybrid mode, using a combination of magnetic immersion and electrostatic lenses and acquired over an area approximately 300×700 μm^2. A magnetically confined charge compensation system was used to minimize charging of the sample surface, and all spectra were taken with a 90 ° take off angle. A base pressure of $\sim 1 \times 10^{-9}$ Torr was maintained during collection of the spectra. Binding energies are calibrated to the intense C(1s) signal at 285 eV.

2.7.6 Electron Microscopy (TEM and SEM)

The resolving power of a microscope is limited by the wavelength of its incidence beam. As such nano-sized objects cannot be imaged with an optical microscope as the wavelength of the incident beam is bigger than that of the objects we wish to observe. The wavelength of electrons is less than one angstrom so far greater resolution can be achieved using electron microscopes compared to light microscopes.[15] As such electron microscopy can be used to easily determine the size, orientation and morphology of particles in a sample. In addition it can also provide information on the nature of the atoms present and how they are structured within the particles. When an electron beam interacts with a sample several different detectable signals are produced (figure 2.7). The type of signal that is analysed depends on which type of electron microscopy is being utilised.

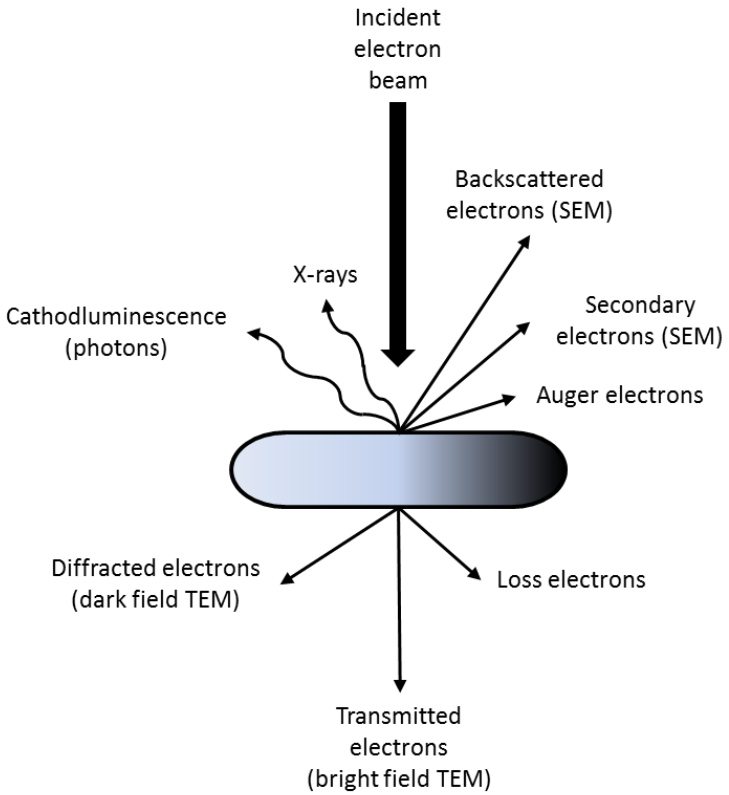

Figure 2.7 Interaction between the incident electron beam and a sample

Transmission electron microscopy (TEM) is the type most commonly used to analyse supported metal particles. It analyses the electrons which have passed (or been transmitted) through a sample. The incident electron beam is one of high energy and intensity that is emitted by a cathode. When the beam emerges from the sample it produces a 2-D projection of the sample as beam attenuation depends on sample density and thickness. The projection is then magnified by the objective lens to produce a "bright field" image. TEM microscope can also be used to analyse the electrons which are diffracted upon passing through the sample. Images collected using this technique are referred to as dark field images and can be particularly useful in detecting supported particles as crystalline particles are emphasized.

Scanning electron microscopy involves scanning across the surface of a sample with a narrow electron beam in a raster-pattern. Images are produced by mapping detected signals from either secondary or back scattered electrons as a function of the position of the incident electron beam.[15] Images generated from the secondary electrons only provide information about the sample surface as that is where they originate. Higher energy backscattered electron can be used to obtain information on sample composition as they are expelled from deeper regions of the sample. As such heavier elements will appear brighter in these images. Contrast in images produced from secondary electrons is caused by orientation.

TEM analysis was carried out on supported and unsupported gold-palladium catalysts in order to determine particle size distribution, particle morphology and the arrangement of gold and palladium atoms within the particles Analysis was carried out at Lehigh University. Samples of supported catalysts, Au-Pd/TiO_2, were prepared for analysis by dry dispersion of the catalyst powder onto a holey carbon TEM grid. To analyse the colloidal particles a drop of the colloid was deposited, and then allowed to evaporate, onto a 300-mesh copper TEM grid covered with an ultrathin continuous C film. Bright-field TEM imaging experiments were carried out using a 200 kV JEOL 2000FX transmission electron microscope equipped with an Oxford Instruments XEDS system.

SEM analysis was performed using Carl Zeiss SMT EVO series electron microscope. Samples of copper oxide catalysts were prepared for analysis by adhering them to aluminium stubs using carbon conductive tape. Thus the morphology of copper catalyst particles was determined.

2.7.7 Brunauer Emmett Teller (BET) Isotherm Analysis

The Brunauer – Emmett – Teller theory is a model for the multilayer physical adsorption of gases onto solid surfaces. It is the basis of an analytical technique used to measure the specific surface area and pore size of solid samples. The first step in this technique involves degassing a dry sample before cooling to 77 K. The sample is then exposed to an inert gas (typically nitrogen) some of which will adsorb onto the surface of the sample. An adsorption isotherm is the relationship between the amount of gas adsorbed onto the surface and the pressure of the gas.[18]

$$\frac{\mathrm{p}}{v(p_0 - p)} = \frac{1}{v_m c} + \frac{c-1}{v_m c}\frac{p}{p_0}$$

Equation 2.6

Where
p = pressure, Pa
p_0= saturation pressure of the gas, Pa
v = volume, m^3
v_m= volume of gas required to form unimolecular adsorbed layer, m^3
c = BET constant, dimensionless

Using the BET equation (equation 2.6) it can be deduced that for a plot of $p/v(p_0\text{-}p)$ against (p/p_0) the intercept will equal $1/v_m$ and the slope will be equal to $c\text{-}1/v_m c$. From this the volume of gas required to form a complete unimolecular adsorbed layer on the sample can be calculated. As the size and number of the molecules of the absorbing gas in known this allows the surface area of the sample to be determined.

BET analysis was carried out at 77 K on a Micrometrics Gemini 2360 surface area analyser. All samples of approx. 0.1 g were degassed prior to analysis for 1 hour at 120 ºC for 45 min. Adsorptions isotherms were analysed using BET

methods. Using this technique the specific surface areas of various copper catalysts were determined.

2.8 References

1. C. J. Jia and F. Schuth, *Phys. Chem. Chem. Phys.*, 2011, 13, 2457-2487.
2. J. A. Lopez-Sanchez, N. Dimitratos, P. Miedziak, E. Ntainjua, J. K. Edwards, D. Morgan, A. F. Carley, R. Tiruvalam, C. J. Kiely and G. J. Hutchings, *Phys. Chem. Chem. Phys.*, 2008, 10, 1921-1930.
3. C. Hammond, M. M. Forde, M. H. Ab Rahim, A. Thetford, Q. He, R. L. Jenkins, N. Dimitratos, J. A. Lopez-Sanchez, N. F. Dummer, D. M. Murphy, A. F. Carley, S. H. Taylor, D. J. Willock, E. E. Stangland, J. Kang, H. Hagen, C. J. Kiely and G. J. Hutchings, *Angew. Chem. Int. Ed.*, 2012, 51, 5129-5133.
4. G. J. Hutchings and C. J. Kiely, *Acc. Chem. Res.*, 2013, 46, 1759-1772.
5. A. Villa, D. Wang, G. M. Veith, F. Vindigni and L. Prati, *Catal. Sci. Technol.*, 2013, 3, 3036-3041.
6. F. Porta, L. Prati, M. Rossi, S. Coluccia and G. Martra, *Catal. Today*, 2000, 61, 165-172.
7. D. A. Ward and E. I. Ho, *Ind. Eng. Chem. Res.*, 1995, 34, 421-433.
8. Y. H. Wu, Y.; Wu, T.; Chen, T.; Weng, W.; Wan, H. , *Mater. Lett.*, 2007, 61, 3174-3178., 61, 3174-3178.
9. J. Zhu, D. C. Li, X. H.; Yang, L. Lu and X. Wang, *Mater. Lett.*, 2004, 58, 3324-3327.
10. S. K. Matijević and S. Kratohvil, *J. Mater. Res.*, 1991, 6, 766-777.
11. E. G. Derouane, F. Lemos, C. Naccache and F. R. Ribeiro, *Zeolite Microporous Solids: Synthesis, Structure, and Reactivity*, Springer, 1992.
12. C. Hammond, R. L. Jenkins, N. Dimitratos, J. A. Lopez-Sanchez, M. H. ab Rahim, M. M. Forde, A. Thetford, D. M. Murphy, H. Hagen, E. E. Stangland, J. M. Moulijn, S. H. Taylor, D. J. Willock and G. J. Hutchings, *Chem. Eur. J.*, 2012, 18, 15735-15745.
13. A. K. Brisdon, *Inorganic Spectroscopic Methods*, Oxford Science Publications, 1998.
14. F. J. H. D. A Skoog, S. R Crouch, *Principles of Instrumental Analysis*, Thmson Brooks/Cole, 6th Edition edn., 2007.
15. J. W. Niemantsverdriet, *Spectroscopy in Catalysis*, Wiley -VCH, 2000.
16. G. Cao, *Nanostructures & Nanomaterials; Synthesis, Properties & Applications*, Imperial College Press, 2007.
17. X. Junyang, Hua, H., Jiang, Z., Ma, Y., Huang, H., *Langmuir*, 2012, 28, 6736-6741.
18. P. H. E. S. Brunauer, E. Teller, Edward, *J. Am. Chem. Soc.*, 1938, 60 309–319.

3 *Comparison of Supported and Unsupported Au-Pd Nanoparticles for the Selective Oxidation of Methane*

3.1 Introduction

It is speculated that the interfaces between supported Au nanoparticles and the surface of the support play an essential role in the markedly high catalytic activity of supported Au nanoparticles.[1] Previous studies have already shown that it is not necessary to support gold nanoparticles for them to be catalytically active for several gold catalysed reactions such as CO oxidation,[2] alcohol oxidation,[3, 4] selective hydrogenations[5] and glucose oxidation.[6] However although unsupported gold nanoparticles display similar initial catalytic activity to their supported counterparts supporting the nanoparticles greatly improves their stability. In addition supported nanoparticles allow for far easier re-use and separation from the reaction products compared with unsupported nanoparticles. For example the work carried out by Rossi *et al.* on the oxidation of glucose found that unsupported gold nanoparticles showed similar activity levels to that of Au/C over short reaction times.[6] However, the supported gold nanoparticles maintained their activity for long enough to achieve total glucose conversion whereas the colloidal gold coagulated into larger particles forming an inactive solution.

Au-Pd nanoparticles supported on TiO_2 have previously been found to be effective catalysts for the low temperature liquid phase oxidation of CH_4 using H_2O_2 as an oxidant (reaction scheme shown in figure 3.1).[7]

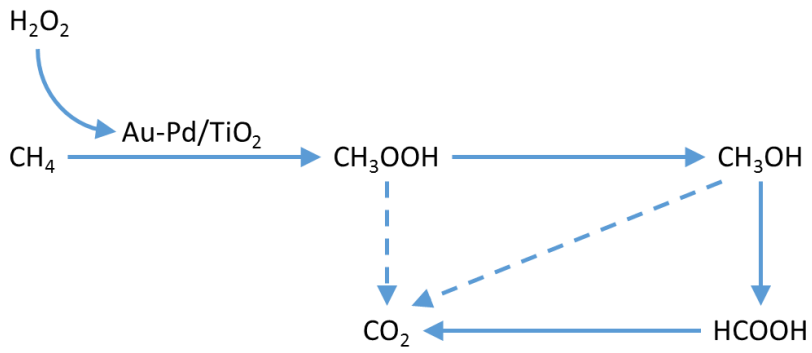

Figure 3.1 Reaction pathway for the oxidation of CH_4 with H_2O_2 by Au-Pd/TiO_2.

It is already known that the choice of support can have a significant effect on the outcome of this reaction.[8] For example Au-Pd nanoparticles supported on TiO_2 were found to be twice as active as those supported on CeO_2. Here the activity of unsupported Au-Pd nanoparticles for the same reaction is investigated. It is hoped that this research would aid the understanding of both the intrinsic catalytic activity of the Au-Pd nanoparticles and the role the support plays in this reaction. The main focus at the outset of this work was on comparing the activity of colloidal Au-Pd nanoparticles stabilised in water by PVP with Au-Pd nanoparticles which had been prepared in the same manner but which had then been supported on TiO_2.

The aim of this chapter is to compare, in detail, these two catalytic systems for the oxidation of CH_4. This includes comparing their catalytic activity, reaction pathways and re-usability. In order to better understand the unsupported Au-Pd system, the colloidal Au-Pd nanoparticles are fully characterised. The effect of the presence of the stabiliser molecule, PVP, in solution in the unsupported Au-Pd nanoparticle system is also examined. The basis for the difference in activity between these systems is identified and explored through a series of experiments in section 3.4.

3.2 Preliminary Investigations using Unsupported Au-Pd nanoparticles for Methane Oxidation

We have recently reported that Au-Pd nanoparticles supported on TiO_2 prepared by a wet impregnation method are active for the oxidation of CH_4 at 50 °C using H_2O_2 as the oxidant.[7] This method involves preparing a solution of $HAuCl_4$ and $PdCl_2$ whose concentration is governed by the porosity of the chosen support. The solution and the support are then combined to form a smooth paste which is subsequently dried and calcined. This calcination step ensures that surface Pd is fully oxidised to Pd^0. The composition of the Au-Pd nanoparticles after calcination is dependent on the identity of the support. Carbon supported Au-Pd nanoparticles tend to be random alloys while core-shell particles, with a Au-core and Pd-shell, tend to form on oxide supports. When using this preparation method a wide variety of supported nano-structure are formed. The Au-Pd/TiO_2 displays a bimodal particle size distribution.[9] Most particles fall in the 5- 20 nm size range. Smaller particles tend to contain more palladium than gold with diameters mostly ranging from 1-2 nm although sub-nanometer particles are also present. Larger gold rich particles are also formed with diameters as high as 20 nm.[9] A trimodal particle size distribution has been reported for Au-Pd nanoparticles supported on activated carbon.[10] The smallest nanoparticles range in size from 2-5 nm, while intermediate nanoparticles vary between 10-40 nm. Small numbers of partilces >100 nm have also been detected

The sol-immobilisation method is an alternative method used for the preparation of supported Au-Pd nanoparticles. In contrast to the impregnation method Au-Pd nanoparticles prepared by sol immobilisation have a much narrower particle size distribution with 3 nm being the average diameter of the particles when they are initially formed as an aqueous colloid by the method described in chapter 2, section 2.4.1.[9, 11] This preparation method affords much greater control over particle size than the impregnation method through the use of a stabilising ligand which regulates particle growth. Additionally this method

generates particles of more uniform composition producing more particles that are homogeneous Au-Pd alloys although the smaller particles tend to be gold rich.[12] The majority of colloidal Au-Pd nanoparticles exhibit either icosahedral or decahedral morphology. Their morphology may then change upon being supported with the final morphology being dependant on the supporting material utilised. For example when the Au-Pd nanoparticles are supported on TiO_2 the majority of particles are cube-octahedral in character whereas when supported on carbon particle morphology remains similar to that of the colloid.[12]

In previous work on CH_4 oxidation using H_2O_2 as an oxidant Au-Pd nanoparticles supported on TiO_2 prepared by sol-immobilisation were found to be less effective catalysts for CH_4 oxidation compared to 1wt% Au-Pd/TiO_2 prepared by impregnation. Extremely low amounts of liquid phase product were detected for reactions catalysed by sol-immobilised Au-Pd/TiO_2 and the ratio of H_2O_2 decomposed to products produced per reaction was extremely high (table 3.1).[7] It was concluded that the reason for the difference in activity between the two preparation methods was due to the difference in the rate of H_2O_2 decomposition for the two catalysts. Supported Au-Pd nanoparticles prepared by sol-immobilisation have been shown to be highly active for both the synthesis and decomposition of H_2O_2.[13] However Au-Pd/TiO_2 prepared by impregnation is considered the more effective catalyst for H_2O_2 synthesis as it displays a lower rate of H_2O_2 decomposition. In the CH_4 oxidation reactions this leads to the reduced oxidant availability for the sol-immobilised catalyst system resulting in reduced activity (0.003% conversion) compared to the impregnation catalyst (0.02% conversion).

Table 3.1 Effect of preparation method on the catalytic activity of $AuPd/TiO_2$ for the liquid phase oxidation of CH_4 with H_2O_2 under mild conditions. This data is from reference 8.

Catalyst	Product amount (μmol)				Oxy. sel. (%)	TOF (h^{-1})	Prod. (mol kg^{-1} h^{-1})	H_2O_2 / Products
	CH_3OH	CH_3OOH	HCOOH	CO_2				
$AuPd/TiO_2$ (Impreg)	0.30	1.82	2.43	0.36	85	6.9	0.5	429
$AuPd/TiO_2$ (sol. Im.)	0.60	0.00	0.00	0.41	59	2.8	0.07	4940
TiO_2	0.00	0.00	trace	0.00	-	-	-	-

Conditions; 5000 μmol H_2O_2, 50 ^{0}C, total volume 10 ml, 30 bar CH_4, 30 min, 1500 rpm
Catalyst; 10 mg, 1 wt % metal, Au :Pd = 1:1 nomial molar ratio

As the sol-immobilisation preparation technique can be used to prepare either supported or unsupported nanoparticles it allows for a direct comparison between nanoparticles of similar size and composition with and without the presence of a supporting material. In previous studies on CH_4 oxidation using supported Au-Pd nanoparticles, TiO_2 was chosen as the support. It has been shown that TiO_2 alone shows no activity for CH_4 oxidation under typical reaction conditions and in the absence of Au-Pd nanoparticles minimal decomposition of H_2O_2 occurs (Table 3.1). For these reasons it was selected as the support material used for comparison with the unsupported Au-Pd nanoparticles. A systematic series of experiments have been carried out using colloidal nanoparticles to investigate the intrinsic activity of the Au-Pd nanoparticles for CH_4 oxidation.

3.2.1 Choice of Stabilising Ligand

During the preparation of colloidal Au-Pd nanoparticles by the sol method the effect of the polymer stabiliser is an important factor. Polyvinyl alcohol (PVA) is a polymer commonly used for this purpose. It is possible to remove PVA from a supported catalyst surface by reflux, this can often be advantageous when investigating the activity of supported nanoparticles.[14] In this case however as the nanoparticles are being used in their colloidal form this was not a requirement. It was essential that the stabiliser molecule used for this work was stable under the reaction conditions employed as unlike the procedure for

preparing supported catalysts no washing or reflux step was possible to remove the stabiliser either from solution or from the catalyst surface. As shown in table 3.2, when particles stabilised with PVA were used to carry out blank reactions in the absence of CH_4 0.43 μmol HCOOH was detected in the liquid phase and 2.47 μmol CO_2 was detected in the gas phase. These products are believed to originate from impurities in the PVA. PVA is manufactured by the polymerisation of vinyl acetate which is followed by partial hydrolysis.[15] Impurities may result from the manufacturing process including CH_3OH. It is believed that the products detected from the Au-Pd Colloid (PVA) reaction carried out under N_2 originate from these impurities. The results of a reaction carried out with PVA alone under N_2 corroborates this hypothesis. Both CH_3OH (0.07 μmol) and HCOOH (0.47 μmol) were detected in the liquid phase while CO_2 was also detected in the gas phase (1.64 μmol). It was considered undesirable, analytically, to utilise a stabiliser for this study whose impurities generated similar products to those generated by the catalyst being investigated.

Table 3.2 Blank reactions carried out to investigate the stability of polymer stabilising ligands under reaction conditions.

Catalyst	Product amount (μmol)				Oxy. sel. (%)	TOF (h^{-1})	Prod. (mol kg^{-1} h^{-1})	H_2O_2 / Products
	CH_3OH	CH_3OOH	HCOOH	CO_2				
AuPd Colloid - PVA	0.00	0.00	0.43	2.47	15	0.77	0.8	235
AuPd Colloid - PVP	0.00	0.00	0.00	2.17	-	0.57	0.6	295
PVA	0.07	0.00	0.47	1.64	22	-	0.8	118
PVP	0.00	0.00	0.00	1.70	-	-	0.7	147

Conditions: 1000 μmol H_2O_2, 50 ^{0}C, total volume 10 ml, 30 bar N_2, 30 min, 1500 rpm, 7.57 μmol metal per reaction. Colloid; PVP/PVA: metal = 1.2:1, Au:Pd = 1:1 molar ratio, [metal] = 7.57×10^{-4} M

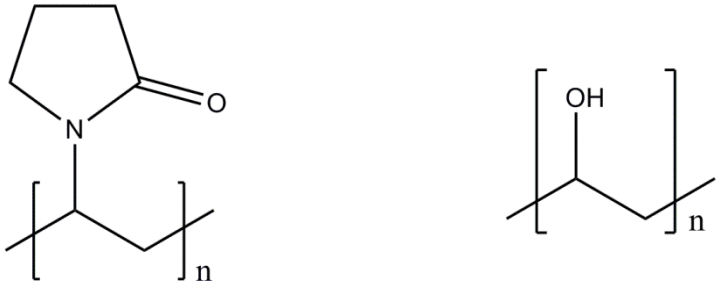

Figure 3.2 Polymers used as stabilising molecules in the preparation of colloidal nanoparticles by the sol method. (a) Polyvinly pyrrolidone, PVP (b) Polyvinyl alcohol, PVA

It was considered undesirable analytically to utilise a stabiliser for this study whose impurities generated similar products to those generated by the catalyst being investigated. Polyvinyl pyrrolidone (PVP) was then considered as a possible alternative as a stabiliser ligand (see figure 3.2 for structure). Similar blank reactions were carried out with PVP stabilised nanoparticles as had been carried out with those stabilised using PVA. In this case no oxygenated products were observed without the presence of CH_4 (table 3.2) for either the PVP only or the PVP Au-Pd colloid reaction. CO_2 was detected in the gas phase of both reactions; 2.17 and 1.70 μmol respectively. As the amount of CO_2 detected is comparable for the two reactions the CO_2 is considered to originate from impurities in the PVP. However less products were detected compared with the PVA reactions and significantly no oxygenated products were detected as such PVP was used as the stabilising ligand in the preparation of colloidal nanoparticles for the duration of this study.

PVP is a non-ionic polymer which, as a bulky molecule, provides the Au-Pd nanoparticles with steric stabilisation. Tsukuda *et al.* have shown that PVP stabilised Au nanoparticles are negatively charged by electron donation from the PVP.[4] For this reason the chemisoption of the PVP to the nanoparticle is stronger than that of the long chain alcohol, PVA. As such it may be expected that smaller particles are formed when PVP in utilised as a stabiliser instead of PVA. However, no significant difference in particle size was observed in this study. The average particle size of PVP and PVA stabilised nanoparticles was found to be 3.0 nm and

2.8 nm respectively. These particle sizes were determined by analysis of TEM images of the nanoparticles (section 3.3.3). PVA of average molecular weight 89-98 kDa was employed in this study while the standard size of PVP used is 10 kDa. In section 4.4.5 it is shown that varying the molecular weight of PVP used to prepare the colloidal nanoparticles between 3.5 and 360 kDa does not significantly affect the activity of the Au-Pd nanoparticles. As such the difference in size between PVA and PVP alone is unlikely to significantly affect the activity of the Au-Pd nanoparticles.

3.2.2 Comparison of Catalytic Activity of Supported and Unsupported Au- Pd Nanoparticles for Methane Oxidation

Once it was established that PVP was stable under reaction conditions, reactions were carried out using PVP stabilised Au-Pd colloidal nanoparticles in the presence of CH_4. An aqueous Au-Pd colloid was prepared by the sol method (described in chapter 2, section 2.4.1) using a PVP to metal ratio of 1.2 by weight and a metal to $NaBH_4$ molar ratio of 5. It was prepared such that the final metal concentration (after the rotary evaporator step) was 7.57×10^{-4} M. This colloid was then used to carry out CH_4 oxidation reactions in the Parr autoclave reactor (for full experimental details see chapter 2). Standard reaction procedure involved charging the reactor with 57 µL of 50wt% H_2O_2 (1000 µmol) and 10 ml of the aqueous colloid. The reactor was then pressurised to 30 bar with CH_4 and heated to 50 °C. When the reactor had reached 50 °C stirring automatically commenced for 30 min. A similar reaction catalysed by Au-Pd/TiO_2 (prepared by immobilising the PVP stabilised colloids) was carried out for comparative purposes. The same reaction conditions were used for this reaction with sufficient mass (115 mg) of 1wt% Au-Pd/TiO_2 placed in the reactor so that the reaction vessel contained an equivalent amount of metal (7.57 µmol) for each reaction. The results of these reactions, shown in table 3.3, show that the unsupported nanoparticles display enhanced catalytic activity under these conditions compared to the TiO_2 supported nanoparticles.

Table 3.3 Comparison of the catalytic activity of supported and unsupported Au-Pd nanoparticles for the liquid phase oxidation of CH_4 with H_2O_2 under mild conditions.

Catalyst	Product amount (μmol)				Oxy. sel. (%)	TOF (h^{-1})	Prod. (mol kg^{-1} h^{-1})	H_2O_2 / Products
	CH_3OH	CH_3OOH	HCOOH	CO_2				
AuPd Colloid	3.19	9.76	7.04	3.09	86	5.36	35.3	36
$AuPd/TiO_2$	0.43	0.00	0.00	1.23	26	0.11	0.03	575

Conditions; 1000 μmol H_2O_2, 50 ^{0}C, total volume 10 ml, 30 bar N_2, 30 min, 1500 rpm, 7.57 μmol metal per reaction.
Colloid; 10 kDa PVP, PVP: metal = 1.2: 1, Au: Pd = 1: 1 molar ratio, [metal] = 7.57×10^{-4} M
Supported catalyst; 1wt% metal, PVP: metal = 1.2:1, Au: Pd = 1: 1 molar ratio, 115 mg

The colloidal system produced 16.8 μmol of total products with an oxygenate selectivity of 93%, whereas the supported Au-Pd nanoparticles produced only 1.66 μmol of product with an oxygenate selectivity of 26%. The productivity and turnover frequency of these systems were calculated for comparative purposes. The productivity over 30 min of the colloidal system is 29.4 mol kg^{-1}_{cat} h^{-1} compared to 0.03 mol kg^{-1}_{cat} h^{-1} when the same amount of metal is supported on TiO_2. The productivity of each catalyst is calculated as the moles of products produced by the catalyst per kilogram of catalyst per hour. As such the difference in these two figures is partly due to the difference in the amount of products produced by the two system but mostly due to the extremely low mass of catalyst used in the colloidal reaction. The productivity value for the colloidal system compares favourably to that of both methane monooxygenase (5.1 mol kg^{-1}_{cat} h^{-1})[16] and Fe-Cu/ZSM-5 (16.5 mol kg^{-1}_{cat} h^{-1}).[17]

Because of the large difference in the catalyst mass employed by these two systems it is useful to also compare their turnover frequencies (TOFs) as this value is calculated based on moles of metal in the reactor and not the mass of the catalyst. The TOF of the colloidal system was calculated to be 5.36 h^{-1} while the TOF of the supported catalyst system was 0.11 h^{-1}. These fascinating results show that not only are the Au-Pd nanoparticles able to selectively oxidise CH_4 using H_2O_2 as an oxidant when unsupported but that they are more effective catalysts for this reaction without the TiO_2 support. In addition the colloidal system has a

higher selectivity to the desired oxygenated products. It is clear from these results that the presence a of metal- support interface is not required for this reaction. The primary advantage of utilising a colloidal system is the increase in available nanoparticle surface area however this is unlikely to be the sole cause of the 48 fold difference in the amount of products produced by the colloidal and supported catalyst systems.

Furthermore the H_2O_2 usage for the colloidal system is more efficient than the supported system. When the nanoparticles are supported on TiO_2 the ratio of H_2O_2 consumed to products produced is 575 under these conditions whereas the unsupported nanoparticles consume 36 moles of H_2O_2 for every mole of products produced. This is an important factor to consider in CH_4 oxidation reactions where H_2O_2 is used as an oxidant because of the high cost associated with H_2O_2. Colloidal Au-Pd nanoparticles immobilised on TiO_2 have already been found to be highly active for the direct synthesis of H_2O_2. This demonstrates the ability of the colloidal nanoparticles to generate hydroperoxy species. However the catalyst is not considered to be effective for this reaction as it is also very active for H_2O_2 decomposition. As the unsupported nanoparticles decompose significantly less H_2O_2 than the Au-Pd/TiO_2 the Au-Pd colloids may be particularly suited to carry out methane oxidation reactions with *in situ* generation of H_2O_2.

These results show that supporting the nanoparticles has a significant effect on their behaviour as a catalyst for the oxidation of CH_4. Similar activity levels have also been observed when utilising various support materials (section 3.4.3). Evidently the role of the support has not yet been fully determined. Investigating the cause of this effect will is the focus of the investigations reported in this chapter.

3.2.3 Monometallic Colloids

Monometallic Au and Pd colloids were prepared by the sol method and used to carry out CH_4 oxidation reactions under standard conditions (table 3.4). The monometallic colloids were also found to be active for the oxidation of CH_4. The Au colloid was shown to have markedly reduced activity (TOF =0.72 h^{-1})

compared to the bimetallic Au-Pd colloid (TOF = 5.4 h^{-1}) as well as poor oxygenate selectivity (47%). The Pd colloidal system conversely was found to be effective for oxidising CH_4. It achieved a similar TOF to the bimetallic system (4.5 h^{-1}) as well as displaying a similar product distribution (the oxygenate selectivity for both systems >85%).

Table 3.4 Comparison of the catalytic activity of monometallic Au and Pd , and bimetallic Au-Pd colloidal nanoparticles for the liquid phase oxidation of CH_4 with H_2O_2 under mild conditions.

Catalyst	Product amount (μmol)				Oxy. sel. (%)	TOF (h^{-1})	Prod. (mol kg^{-1} h^{-1})	H_2O_2 / Products
	CH_3OH	CH_3OOH	HCOOH	CO_2				
AuPd Colloid	3.19	9.76	7.04	3.09	86	5.4	35	36
Au + Pd Colloids	2.86	7.00	0.29	0.96	91	2.9	19	51
Au Colloid	0.71	0.57	0.00	1.44	47	0.72	3.7	351
Pd Colloid	5.57	7.43	3.00	1.04	94	4.5	42	567

Conditions; 1000 μmol H_2O_2, 50 °C, 30 bar CH_4, 30 min, total volume 10 ml, 1500 rpm, 7.57 μmol metal per reaction.
Colloid; 10 kDa PVP, Au: Pd = 1:1 molar ratio, PVP: metal = 1.2:1 molar ratio, [metal] = 7.57×10^{-4} M

The notable difference between the Pd and bimetallic systems is their H_2O_2 usage. The monometallic colloid system showed over 15 times higher consumption of H_2O_2 when compared to the bimetallic system. It has previously been established in literature on the direct synthesis of H_2O_2 using supported catalysts that Pd-only catalysts display high rates of H_2O_2 degradation by decomposition and over hydrogenation. The addition of Au to these catalysts minimises the degradation of H_2O_2 improving selectivity.[18, 19] A similar effect is observed here with the addition of Au to Pd resulting in far more effective use of H_2O_2 in the bimetallic colloidal system compared to either of the monometallic systems. These results are in keeping with previously reported work on Au and Pd supported on TiO_2 for CH_4 oxidation with H_2O_2.[8] The Hutchings group has previously found that the monometallic Au/TiO_2 catalyst also has reduced activity for CH_4 oxidation compared to the supported bimetallic catalyst and that

Pd/TiO_2 consumes more H_2O_2 than $AuPd/TiO_2$ under the same reaction conditions.

In order to investigate whether there is a synergistic effect between Au and Pd when using bimetallic Au-Pd colloid for CH_4 oxidation a reaction was carried out using a mixture of monometallic colloids with the same total metal concentration. It was found that the mixed system produced around half the total products produced by the bimetallic nanoparticles although it did display high oxygenate selectivity of 91%. This is likely due to the fact that the greater portion of the products are generated by the more active Pd colloid which also display a high oxygenate selectivity (94%). This observation confirms that a synergistic effect exists between Au and Pd for this reaction. This result is in keeping with the synergistic effects of Au-Pd alloys that have previously been observed for other substrates.[12, 20]

3.2.4 Homogeneous reactions

In order to compare the colloidal system to an equivalent homogeneous system, reactions were carried out using aqueous solutions of the metal precursors ($HAuCl_4$ and $PdCl_2$) used for preparation of the colloidal nanoparticles. The precursor materials were first dissolved in dilute HCl before being diluted to the required concentrations. In order to give an accurate comparison to the colloidal system the concentrations of the metal precursor solutions tested corresponded to the calculated number of surface sites present in a standard colloid reaction. It was reasoned that this concentration would give a more meaningful comparison than simply matching the total metal concentration of a standard colloidal reaction.

In order to calculate the number of surface sites present in a standard colloid reaction the number of gold particles in a nanoparticle was calculated from the mean particle diameter using equation 3.1.[21] It was assumed that the nanoparticles follow the Mackay model for icosahedral gold particles (equation 3.2).[22, 23] Using this model it can be determined that a nanoparticle of diameter 2.6 nm will contain 309 atoms. These atoms are arranged into 4 shells with the

outermost shell containing 162 atoms. Given that the average diameter of an unsupported Au-Pd nanoparticle prepared by the sol method is 3.0 nm (determined by TEM see section 3.3.3) it was assumed that the ratio of surface metal atoms to total metal atoms in the colloidal system is 0.52.

$$d^3 = 0.0342n$$

Equation 3.1[21]

$$n = \frac{10}{3}K^3 - 5K^2 - \frac{11}{3}K - 1$$

Equation 3.2[22]

d = nanoparticle diameter
n = no. of atoms in a Mackay icosahedron
K = no. of shells in a Mackay icosahedron

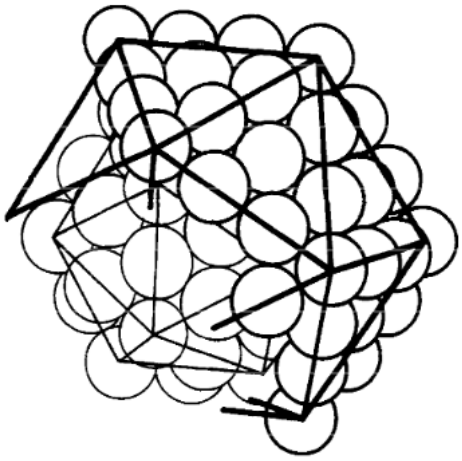

Figure 3.3 Shell structure of a closed-shell 55-atom icosahedron with a portion of the next shell based on the Mackay model. Reproduced from reference 19.

CH_4 oxidation reactions were carried out using aqueous solutions of $HAuCl_4$, $PdCl_2$ and $HAuCl_4$ and $PdCl_2$ in a 1: 1 molar ratio at concentrations of 3.96×10^{-4} M (figure 3.4). $PdCl_2$ produced 1.86 μmol of total products which is markedly lower than the amount of total products produced by the Au-Pd colloid (16.8 μmol) although the selectivity to oxygenated products for this reaction was reasonably high (87%). The total products produced by the $HAuCl_4$ reaction (3.08 μmol) was greater than that of the $PdCl_2$ but still much lower than the colloid and the product distribution was shifted towards carbon dioxide so that the oxygenate

selectivity was reduced to 71%. None of the three homogeneous systems investigated produced HCOOH and all of them showed less effective H_2O_2 usage than the colloid system. The $PdCl_2$ system in particular showed poor H_2O_2 usage which was expected due to the high rate of H_2O_2 degradation typically displayed by Pd only catalysts. [18]

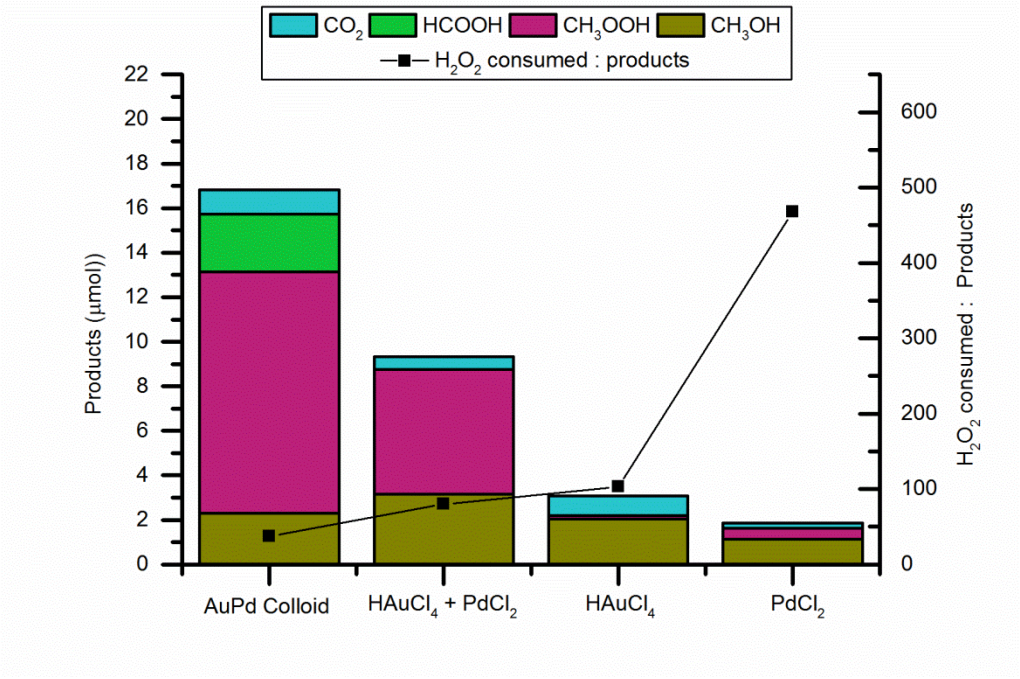

Figure 3.4 Comparison of the catalytic activity of colloidal Au-Pd nanoparticles, $HAuCl_4$ and $PdCl_2$ for the liquid phase oxidation of CH_4 with H_2O_2 under mild conditions.

Conditions; 1000 µmol H_2O_2, 50 ^{0}C, total volume 10 ml, 30 bar CH_4, 30 min, 1500 rpm.
Colloid; 10 kDa PVP, PVP :metal = 1.2:1, Au: Pd = 1:1 molar ratio, [metal] = 7.57×10^{-4} M
Homogeneous metal solutions; [metal] = 3.96×10^{-4} M

Combining the Au and Pd precursors in a 1: 1 ratio showed some synergistic effect as was found to be the case with the Au-Pd alloyed colloidal nanoparticles. The total amount of products produced by the bimetallic homogeneous reaction was 9.32 µmol compared to 3.08 µmol and 1.86 µmol for the $HAuCl_4$ and $PdCl_2$ respectively and has oxygenate selectivity (94%) was similar to that of the colloidal system (93%). However this is not believed to be the result of any synergistic effect taking place between the homogeneous Au and Pd but rather that alloyed particles are being formed during the reaction. At the end of the

reaction the liquid was found to be colourless when it had originally been a clear light yellow and some precipitate had also formed.

In an effort to confirm the formation of metal particles during the reaction UV-vis analysis was carried out on the solutions post reaction (figure 3.5).

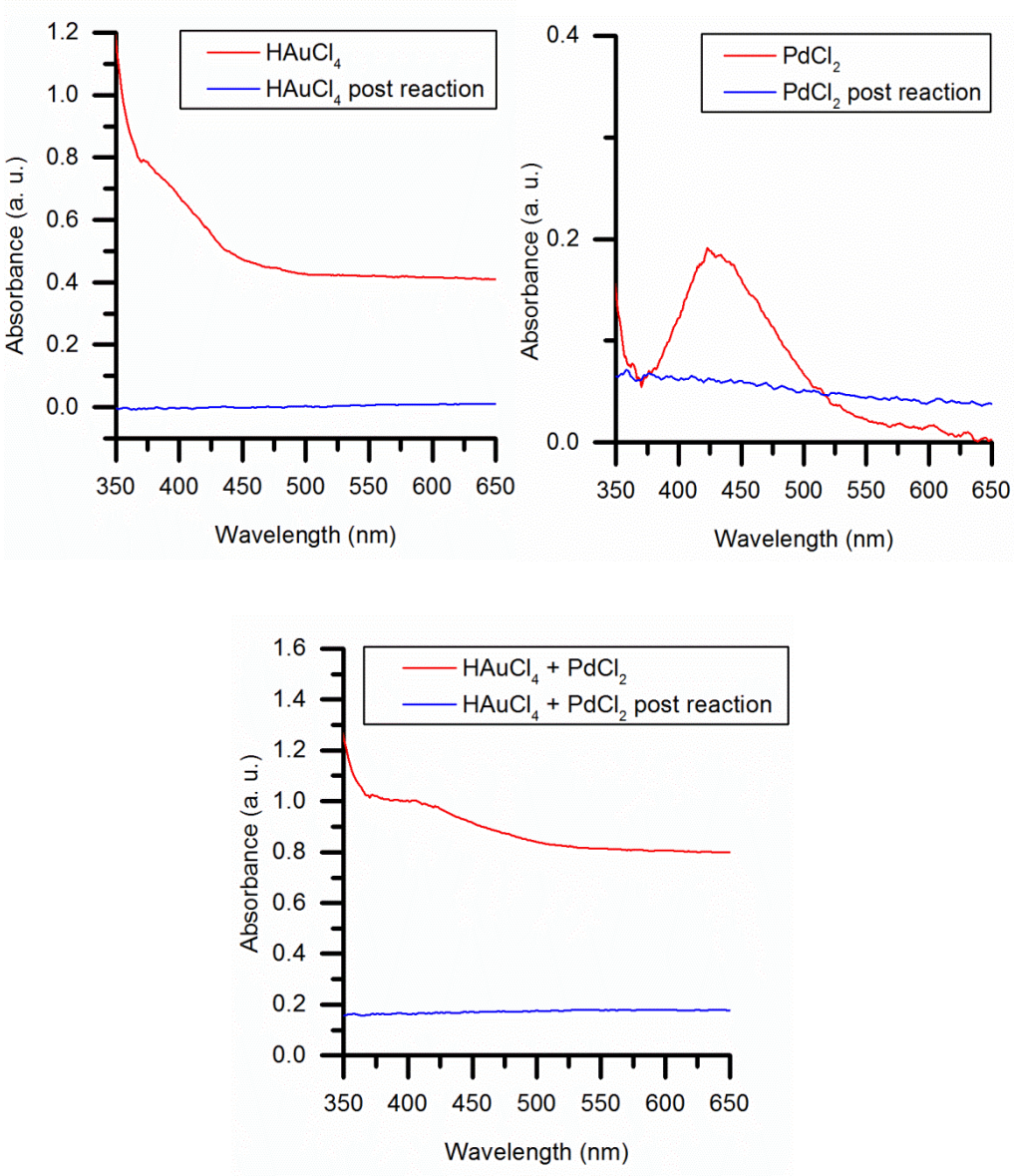

Figure 3.5 UV-vis spectra of $HAuCl_4$, $PdCl_2$ and a mixture of $HAuCl_4$ and $PdCl_2$ before and after use for CH_4 oxidation reactions. [total metal] = 3.96×10^{-4} M

The idea behind this analysis was that had metal particles formed during the homogeneous gold reaction the surface plasmon resonance band characteristic of gold nanoparticles would be observed.[24] However without the presence of a stabiliser molecule the precipitated metal was not suspended in solution. As such it sank to the bottom of the cuvette used for the UV-vis analysis so that it was not possible to determine directly if gold nanoparticles had been formed. Nevertheless it was determined that the Au and Pd had precipitated out of solution by the end of the reaction. Comparing the UV-vis spectrum of the aqueous metal chloride solutions before and after reaction showed a reduction in the absorbance after reaction over all wavelengths employed compared to the reference (water). It is therefore considered that the synergistic effect observed between the Au and Pd in the homogeneous reaction is the result of the alloying of these metals during the reaction and not a synergistic effect between the Au and Pd in solution.

A CH_4 oxidation reaction was carried out with 20 times the amount of $HAuCl_4$ and $PdCl_2$ used for the reactions shown in figure 3.4. The purpose of this reaction was to produce a greater amount the precipitate in order to facilitate its characterisation. SEM imaging of the precipitate was carried out. The SEM images shown in figure 3.6 show spherical metal particles of average size 0.2 μm. These images confirm that the metal precipitates out of solution during the CH_4 oxidation reaction carried out using $PdCl_2$ and $HAuCl_4$.

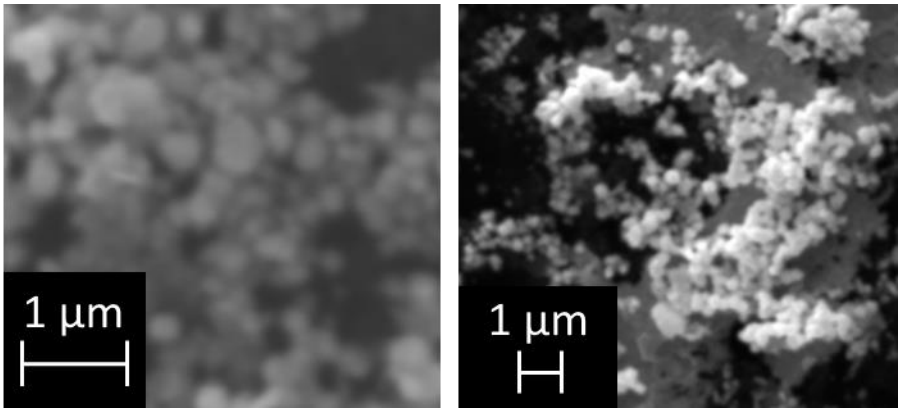

Figure 3.6 SEM images of precipitate formed during a CH_4 oxidation reaction carried out with $HAuCl_4$ and $PdCl_2$. (79.3 ×10^{-4} M total metal, 1:1 molar ratio Au: Pd)

3.2.5 Investigating the Role of PVP

After observing that the unsupported Au-Pd nanoparticles exhibited significantly enhanced activity for the oxidation of CH_4 compared to those supported on TiO_2 various possible reasons for the differences in activity were considered. One possibility was that the stabilising ligand, PVP, used in the preparation of the nanoparticles could be contributing to the reaction products. In order to eliminate this possibility a colloid reaction was carried out using isotopically labelled CH_4 so that the any products that did not originate from CH_4 could be identified. The reaction was carried out using standard conditions described in chapter 2, section 2.5 with the only alternation being that a portion of $^{12}CH_4$ was replaced with $^{13}CH_4$.

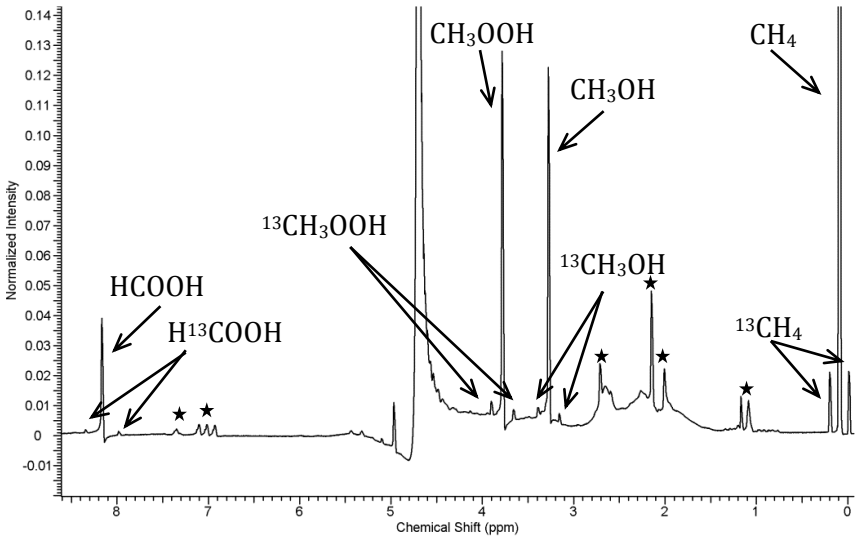

Figure 3.7 ^{1}H-NMR spectrum showing ^{12}C and ^{13}C oxygenated products of a CH_4 oxidation reaction where a portion of $^{12}CH_4$ was replaced with $^{13}CH_4$.

★ = peaks originating form contaminants (δ = 2.1 ppm and δ = 2.15 ppm correspond to acetic acid and acetone)
δ = 4.86 ppm corresponds to formaldhyde monohydrate ($CH_2(OH)_2$) which cannot be detected rountinely by 500 Hz NMR spectrometer as the signal is obscured by the H_2O peak.

NMR analysis for this reaction was carried out on a 600 Hz NMR spectrometer as greater sensitivity was required to accurately quantify the

amount of ^{13}C products. It was found by integrating the ^{13}C satellite peaks that the proportion of products observed containing the ^{13}C isotope matched the initial proportion of isotopically labelled CH_4 (figure 3.7). This confirmed that all the products detected were formed from the oxidation of CH_4 without any contribution from the oxidation of PVP.

All supported Au-Pd catalysts tested for comparative purposes were prepared using PVP by the sol method as was the case for the unsupported nanoparticles. Thermogravimetric analysis (TGA) of a sample of the 1wt% Au-Pd/TiO_2 prepared using PVP displayed a 1% weight loss when heating the sample from 120 to 380 °C (figure 3.8). This weight loss was attributed to the loss of the PVP stabiliser. As the catalyst is prepared with a metal to PVP ratio of 1:1.2 it appears the majority (if not all) of the PVP binds to the catalyst surface and is not removed during the washing step in catalyst preparation. However any PVP in solution is removed during the preparation of supported catalysts during the filtration and washing steps. The possibility that some PVP may be present in solution during the colloidal reactions and that it may in some way be enhancing the activity of the Au-Pd nanoparticles was considered.

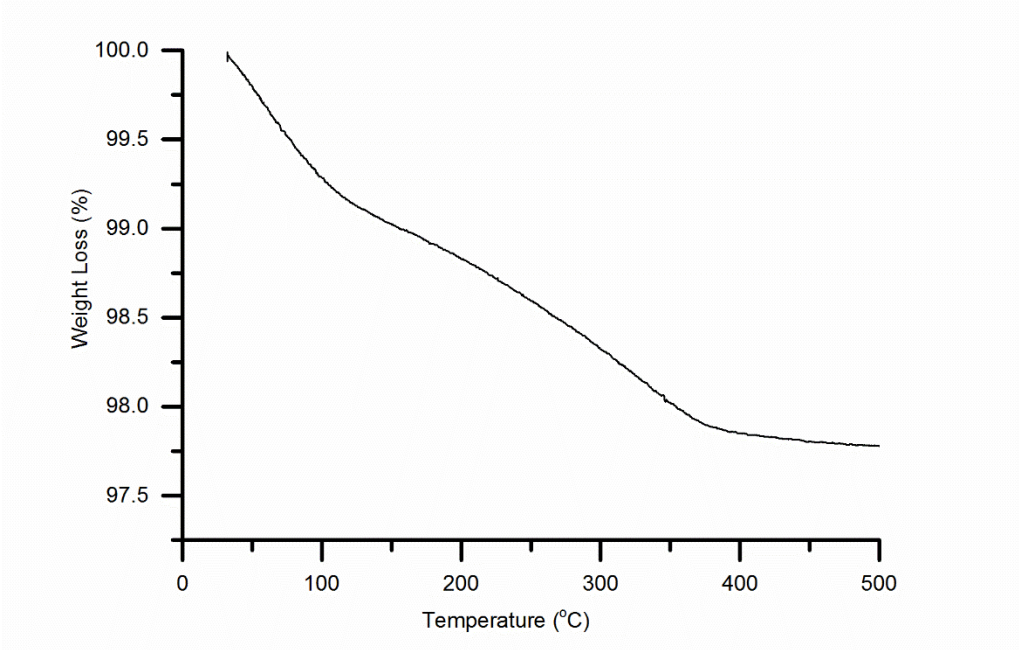

Figure 3.8 TGA analysis of 1wt % Au-Pd/TiO_2 prepared using PVP.

Catalyst; 1wt% metal, PVP: metal = 1.2:1, Au: Pd = 1: 1 molar ratio, 115 mg

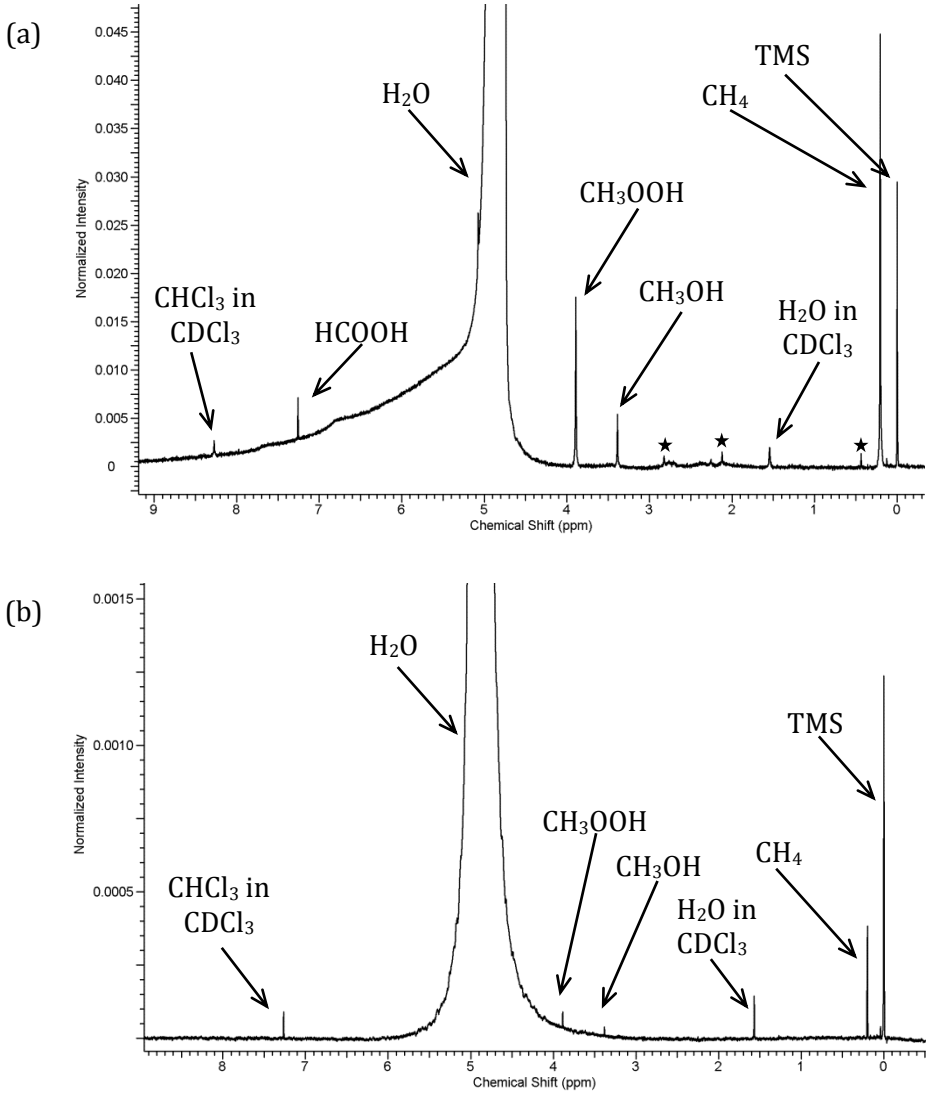

Figure 3.9 ^{1}H-NMR spectra showing the products of a CH_4 oxidation with (a) colloidal Au-Pd nanoparticles prepared using PVP showing an intense solubilised CH_4 peak (δ = 0.2 ppm) and (b) $AuPd/TiO_2$ where a less intense CH_4 peak can be observed.

★ = peaks originating form contaminants (δ = 2.1 ppm and δ = 2.15 ppm correspond to acetic acid and acetone)

During testing it became apparent that when PVP is present in solution it results in an increased amount of CH_4 being solubilised in the aqueous reaction liquid compared to a reaction where no PVP is present in solution. This was observed in the NMR analysis of the liquid products. It can clearly be seen when comparing the NMR spectra of the reaction liquids of CH_4 oxidation reactions

catalysed by colloidal Au-Pd nanoparticles with that of a reaction catalysed by Au-Pd/TiO_2. As can be seen in figure 3.9 the intensity of the CH_4 peak for the colloid reaction is much greater than that of the supported catalyst reaction.

This feature was observed whenever PVP was present in solution. Attempts at quantifying the difference in the amount of CH_4 solubilised in water under reaction conditions with and without the presence of PVP in solution were unsuccessful. This was largely due to the fact that the reaction liquid could not be analysed by NMR under reaction conditions i.e. under 30 bar CH_4. Quantifying the amount of CH_4 present in solution post reaction was not found to be meaningful as it was not possible to standardise the time between reaction and NMR analysis resulting in variable amounts of CH_4 degassing from the reaction liquid prior to analysis. This increase in solubility is likely to increase the concentration of CH_4 surrounding the Au-Pd particle as this is where the PVP is located which could lead to the observed increase in the amount of products being produced. In order to investigate this effect further, reactions were carried using Au-Pd nanoparticles supported on TiO_2 with and without additional PVP being added in to the reactor (table 3.5).

Table 3.5 Comparison of the catalytic activity of Au-Pd colloidal nanoparticles, Au – Pd / TiO_2 and Au – Pd / TiO_2 with additional PVP in solution for the liquid phase oxidation of CH_4 with H_2O_2 under mild conditions.

Catalyst	Product amount (μmol)				Oxy. sel. (%)	TOF (h^{-1})	Prod. (mol kg^{-1} h^{-1})	H_2O_2 / Products
	CH_3OH	CH_3OOH	HCOOH	CO_2				
AuPd Colloid	3.19	9.76	7.04	3.09	86	5.4	35	36
AuPd/TiO_2	0.43	0.00	0.00	1.23	26	0.1	0.03	575
AuPd/TiO_2 + PVP	0.86	0.43	0.00	1.51	46	0.7	0.2	326

Conditions; 1000 μmol H_2O_2, 50 ^{0}C, total volume 10 ml, 30 bar N_2, 30 min, 1500 rpm, 7.57 μmol metal per reaction.
Colloid; 10 kDa PVP, PVP :metal = 1.2:1, Au:Pd = 1 :1 molar ratio, [metal] = 7.57×10^{-4} M
Supported catalyst; 1wt% metal, PVP :metal = 1.2:1, Au :Pd = 1: 1 molar ratio, 115 mg

Sufficient PVP was added into the reactor so that the concentration matched that of a standard colloid reaction. The amount of products produced by the

supported catalyst increased from 1.66 μmol to 2.8 μmol when PVP was added to the reactor and the selectivity to oxygenated products increased from 26% to 46%. The increase in catalytic activity of AuPd/TiO_2 in the presence of PVP is considered to be significant however it is still markedly reduced compared to that of the unsupported nanoparticles. Thus it can be concluded that although the presence of PVP in solution improved the catalytic activity of the Au- Pd nanoparticles by increasing the solubility of the CH_4 (particularly in the area surrounding the nanoparticles) it is not solely responsible for the difference in activity observed between the supported and unsupported nanoparticles.

It is interesting that in this system PVP enhances the catalytic activity of Au-Pd nanoparticles as it has previously been reported that removing the stabilising ligand from the surface of metal nanoparticles can improve their activity. Somorjai *et al.* have shown that various stabilising ligands, including PVP, can be partially removed from the surface of Pt nanoparticles by UV-ozone treatment thereby improving their activity for CO oxidation.[25, 26] It is believed that some portion of the stabilising ligand layer blocks the reactive sites so that the partial removal of the stabilising ligands results in an increase in catalytic turnover rate. A similar observation was made by Prati *et al.* who reported that PVA reduced the activity of unsupported gold nanoparticles for the oxidation of glycerol through steric congestion of the active sites.[27] The increase in catalytic activity of Au-Pd/TiO_2 for CH_4 oxidation observed upon the addition of PVP to the reaction implies that in this system the stabilising ligand does not block reactive sites but is in fact increasing the concentration of the substrate in the area surrounding the catalyst surface.

3.2.6 Time on Line Study

CH_4 oxidation reactions catalysed by colloidal Au-Pd nanoparticles were carried out over various lengths of time up to 240 min in order to determine the reaction pathway. This included a reaction which was halted after 0 min (i.e. when the reactor had reached 50 °C) to determine what, if any, products were generated during the 10 min heat up step of the reaction procedure. The standard reaction conditions were altered slightly for this study to allow for the

increased amount of H_2O_2 decomposition expected over longer time lengths. For all reactions in the time on line study the amount of H_2O_2 added to the reactor was 5000 µmol as opposed to the typical 1000 µmol.

The temporal selectivity towards reaction products as well as the total amount of products produced by these reactions is shown in figure 3.10.

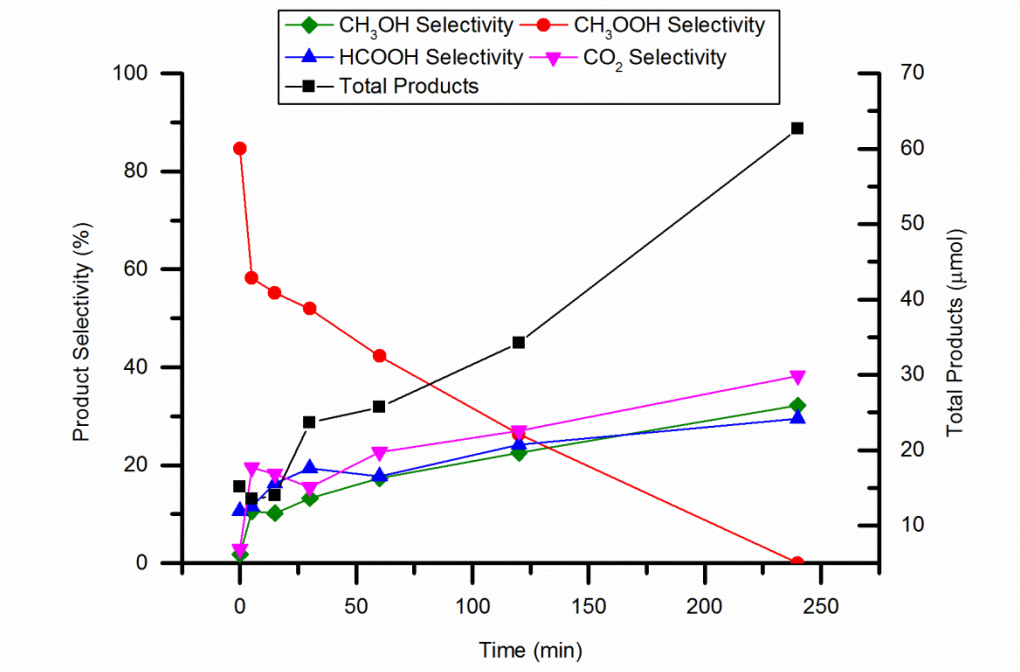

Figure 3.10 Time- on- line plot of CH_4 oxidation with H_2O_2 catalysed by colloidal Au-Pd nanoparticles.

Conditions; 5000 µmol H_2O_2, 50 °C, 30 bar CH_4, total volume 10 ml, 1500 rpm, 7.57 µmol metal per reaction.
Colloid; 10 kDa PVP, PVP :metal = 1.2:1, Au:Pd = 1 :1 molar ratio, [metal] = 7.57×10^{-4} M

The figure shows that as the reaction proceeds the total amount of reaction products generated increases with time. The selectivity to methyl hyroperoxide is high for short time lengths but drops as the reaction proceeds. This indicates that it is the primary product of this reaction as is the case for reactions catalysed by Au-Pd/TiO_2.[7] It is interesting to note that methyl hydroperoxide has also been reported to be the primary reaction product for CH_4 oxidation reactions with H_2O_2 which are catalysed by Fe and Cu zeolites indicating that the reaction proceeds through the same intermediates for each of these systems.[28] As time

goes on the CH_3OOH undergoes subsequent reactions to form the secondary products CH_3OH and HCOOH. This is indicated by the drop in selectivity to methyl hydroperoxide over time as the selectivity to the secondary products increases. Complete oxidation of these secondary products results in the formation of CO_2. This over-oxidation causes the oxygenate selectivity to decrease from 94% after 30 min to 61% after 240 min. From this data it can be determined that the reaction pathway for CH_4 oxidation reactions catalysed by unsupported Au- Pd nanoparticles is the same as that for reactions catalysed by supported Au- Pd

3.3 Catalyst Characterisation

Several characterisation techniques were utilised to analyse the colloidal Au, Pd and bimetallic Au-Pd nanoparticles prepared by sol- immobilisation. The aim of this was to investigate the nature of the nanoparticles prepared (particle size distribution, oxidation state etc.) and to identify any notable differences with the supported nanoparticles.

3.3.1 UV-vis Spectroscopy

UV-Vis spectroscopy, shown in figure 3.11, was used to provide an indication on whether the colloidal particles formed were indeed bimetallic in nature and not simply a mixture of Au and Pd particles.

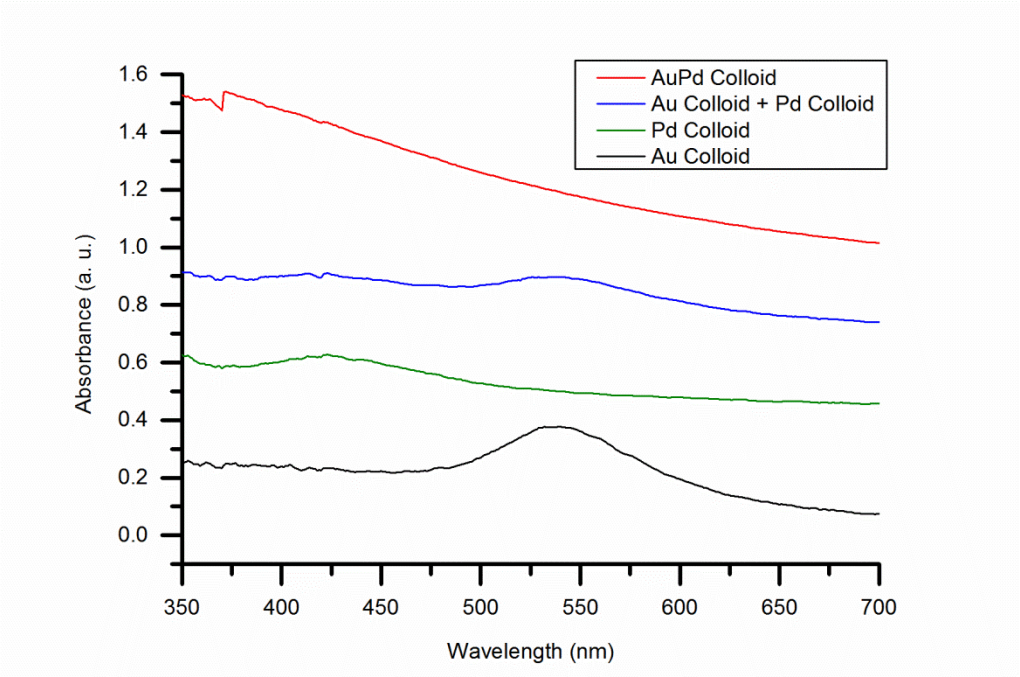

Figure 3.11 UV-vis spectra of monometallic Au and Pd colloids, a mixture of Au and Pd colloids and a bimetallic Au- Pd colloid.

Colloids; 10 kDa PVP, PVP: metal = 1.2:1 molar ratio, [metal] = 7.57×10^{-4} M
Bimetallic colloid and mixture of monometallic colloids; Au: Pd = 1:1 molar ratio

A UV-vis spectrum for pure gold nanoparticles will display an intense absorption band caused by surface plasmon resonance (discussed in chapter 2).[24, 29] This broad plasmon band was observed for the monometallic Au colloid between 500-550 nm. A less intense plasmon band was also observed in the UV-vis spectrum of a 1: 1 molar mixture of monometallic Au and Pd colloids. The disappearance of this plasmon band during analysis of the Au- Pd colloid indicates that the nanoparticles are bimetallic in nature. However it cannot be concluded from this result that all the nanoparticles present are bimetallic in nature. A more detailed structural analysis, such as that provided by high angle annular dark filed (HAADF) STEM, would be necessary to determine the actual proportion of bimetallic and monometallic nanoparticles. Previously reported analysis of Au-Pd/TiO_2 prepared by sol-immobilisation has shown the supported nanoparticles are also alloyed bimetallic particles.[12, 20] No plasmon band was observed during the analysis of the monometallic Pd colloid. This was to be

expected as the surface plasmon resonance peak for Pd nanoparticles < 10 nm in size is below 250 nm.[29]

3.3.2 XPS

XPS analysis was carried out on samples of the Au, Pd and bimetallic Au-Pd colloids in order to determine the oxidation state(s) of the metals present on the surfaces of the samples. In order to carry out the analysis samples of the colloids were pipetted on to clean glass slides and dried by the pumping system of the spectrometer sample fast-entry lock. The covering of sample was sufficient such that no underlying glass signal was observed. The spectra were analysed using Casa XPS software and the binding energies were calibrated to the intense C(1s) signal at 285 eV.

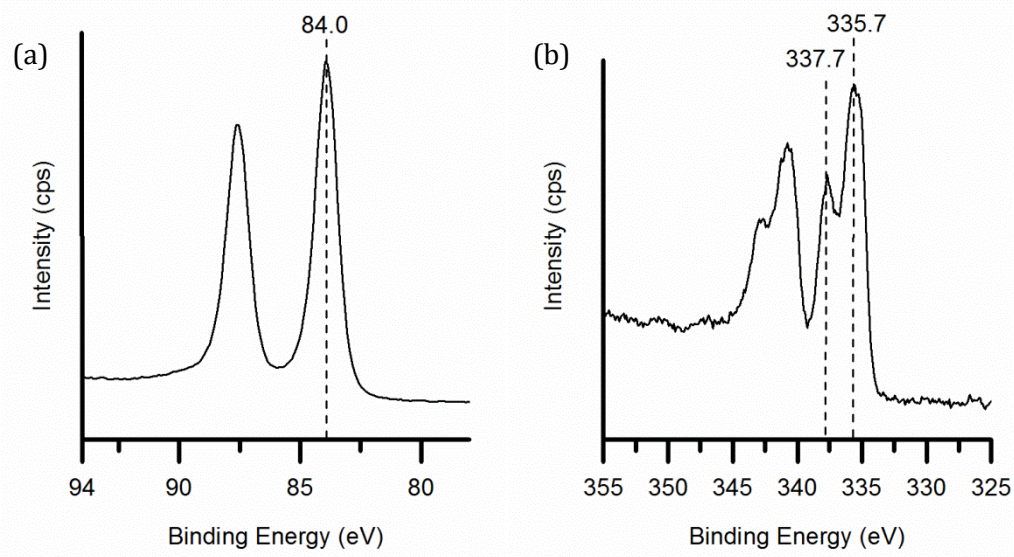

Figure 3.12 XPS spectra; (a) Au(4f) for Au Colloid and (b) Pd(3d) for Pd Colloid
Colloids; 10 kDa PVP, PVP: metal = 1.2:1 molar ratio, [metal] = 7.57×10^{-4} M

The XPS spectrum of the monometallic gold colloid is displayed in figure 3.12(a). From this spectrum the binding energy of the electron emitted from the Au(4f) orbital was measured as 84.0 eV. 84.0 eV is the value given in the literature for the XPS signal of the Au(4f) orbital of Au^0.[30] Therefore the metallic oxidation state of Au is present in this colloidal sample. No other signals

corresponding to other oxidation states of Au were observed in the spectrum. Additionally the Au(4f) peak is symmetrical implying that this peak is not making any other signals. As such it was concluded that the Au in the monometallic Au nanoparticles is completely metallic in nature.

XPS analysis of a sample of the monometallic Pd colloid produced the spectrum shown in 3.12(b). In this spectrum signals corresponding to two distinct Pd oxidation states were observed. The accepted binding energy of the Pd(3d) orbital of metallic Pd is 335.1 eV which is comparable to that of a Pd(3d) signal observed in the colloidal sample, 335.7 eV.[30] The second signal observed for Pd(3d) is at binding energy 337.7 eV which is similar to 338.0 eV, the literature value for the Pd(3d) signal of Pd^{2+}.[30] This analysis signifies that the colloidal Pd nanoparticles are comprised of both Pd^{0} and Pd^{2+}. This is in keeping with the observed tendency of the monometallic Pd colloid to re- oxidise over time. At no point in this work was the re-oxidation of the Au or Au- Pd colloids observed whereas if the Pd colloid was left open to air it would, within the space of a few hours, become clear and light brown/yellow in colour where it had previously been opaque and dark brown. Addition of reducing agent at this point would cause it to again become opaque and dark brown as the nanoparticles reformed. For this reason the monometallic Pd colloid was always prepared and stored under N_2.

XPS spectra of a sample of the bimetallic Au-Pd colloid are shown in figure 3.13.

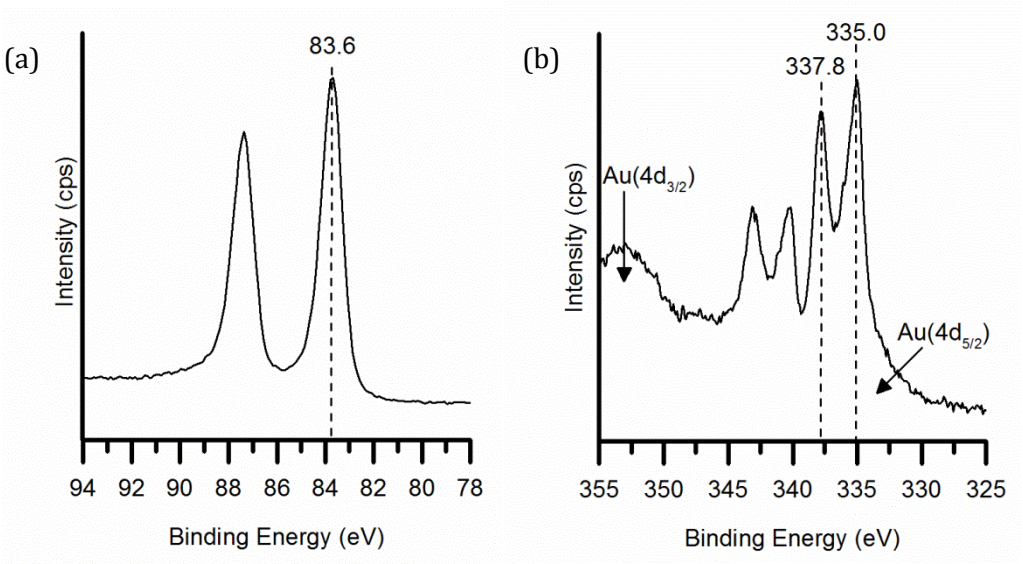

Figure 3.13 XPS spectra; (a) Au(4f) for AuPd Colloid and (b) Pd(3d)/Au(4d) for AuPd Colloid

Colloid; 10 kDa PVP, Au: Pd = 1:1 molar ratio, PVP: metal = 1.2:1, [metal] = 7.57×10^{-4} M

As in the analysis of the monometallic Au colloid, the analysis of the bimetallic Au-Pd colloid showed no signals that corresponded to any other oxidation state of Au except that of the metallic oxidation state. The binding energy of the Au(4f) was measured as 83.6 eV while the accepted value for the Au(4f) signal of metallic Au is 84.0 eV. The signals of two oxidation states of Pd were again detected in this sample. The signals at 337.8 and 335.0 eV were designated as the Pd(3d) orbitals of Pd^{2+} and Pd^{0} respectively (literature values Pd^{0} 335.1 eV and Pd^{2+} 338.0 eV). The binding energies are shifted slightly compared to the accepted literature values indicating possible electron transfer between the metal.

3.3.3 TEM

Samples of the Au-Pd colloid and the supported catalyst were characterised by TEM to determine the particle size distribution (figure 3.14).

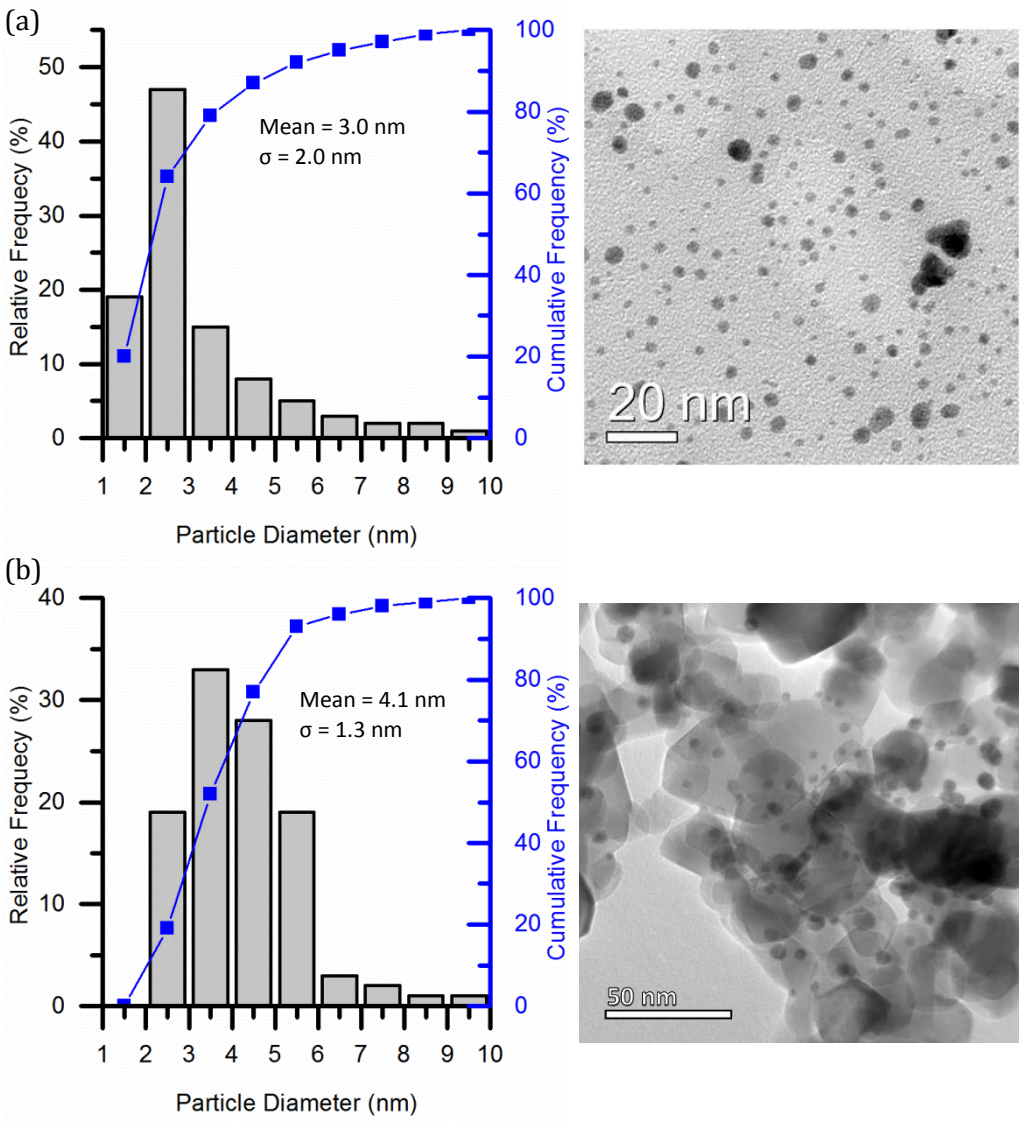

Figure 3.14 TEM images and particle size distribution of (a) colloidal and (b) TiO_2 supported Au-Pd nanoparticles prepared by sol-immobilisation using PVP the stabiliser.

Both the supported and unsupported nanoparticles were found to have a narrow, mono-modal particle size distribution typical of nanoparticles prepared by the sol method.[12, 20] The Au-Pd colloidal nanoparticles were observed to have a mean particle size of 3.0 ± 2.0 nm whereas the supported bimetallic nanoparticles were shown to have a slightly larger mean particle size of 4.1 ± 1.3 nm. This slight increase in particle diameter is not believed to be the result of particle agglomeration. The morphology of the Au-Pd nanoparticles changes slightly upon being supported causing an increase in particle diameter. Colloidal Au-Pd

nanoparticles prepared with PVA were have previously been reported to also have a mean particle size of 3 nm but with particles ranging in size from 1-5 nm whereas the PVP stabilised nanoparticles were observed to have a wider particle size range, 1-10 nm.[31] The PVA stabilised nanoparticles were observed to have an icosahedral morphology whereas once supported on TiO_2 they adopt a cube-octahedral shape.[12] Similar morphologies were observed for both the supported and unsupported Au-Pd nanoparticles prepared using PVP as those previously reported for PVA stabilised Au-Pd nanoparticles.

3.3.4 IR Spectroscopy

Infrared spectroscopic analysis was carried out on a standard Au-Pd colloid prepared using PVP as the stabiliser ligand by the sol method (figure 3.15).

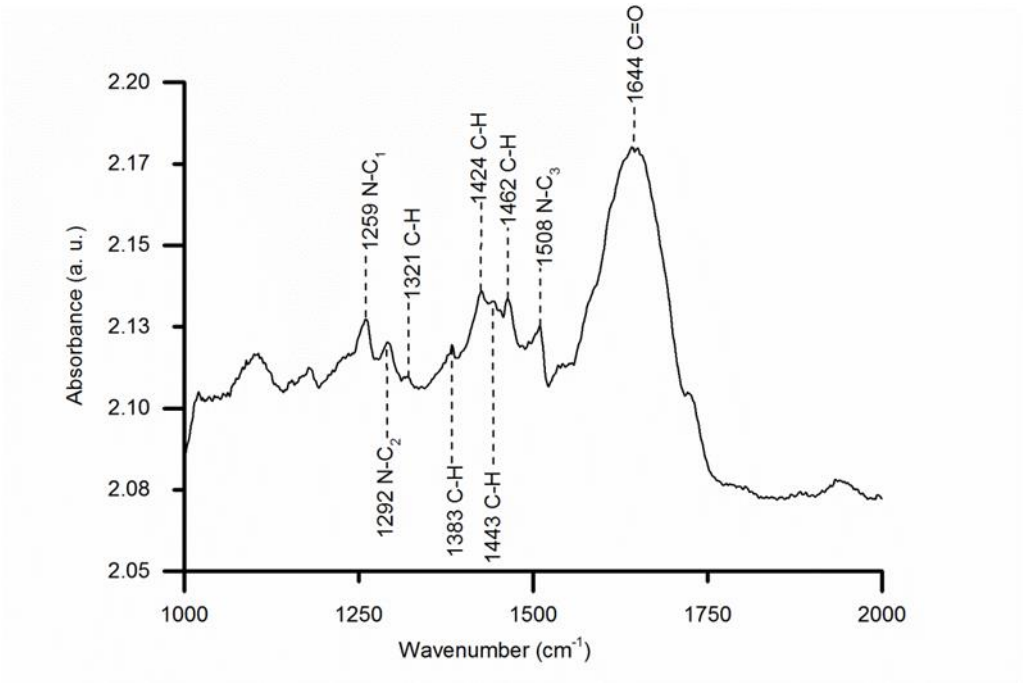

Figure 3.15 Infrared spectrum of colloidal Au-Pd nanoparticle prepared using PVP as a stabilising ligand

Colloid; 10 kDa PVP, Au: Pd = 1:1 molar ratio, PVP: metal = 1.2:1, [metal] = 7.57×10^{-4} M

The aim of this analysis was to determine the nature of the interaction between the PVP molecules and the metal nanoparticle surface. It has been

reported by Huang *et al.* that when Pd nanoparticles are prepared using PVP as a stabiliser the interaction between the PVP molecules and the Pd surface varies depending on the size of the nanoparticles prepared.[32] The size of metal nanoparticles can be controlled during preparation by adjusting the ratio of PVP to metal.[33] Greater amounts of PVP have been found to generate smaller nanoparticles and in this case the PVP molecules chemisorb onto the surface the atom with their O atoms. When larger Pd nanoparticles are prepared with fewer PVP molecules both the O and N atom of the PVP molecule will chemisorb onto the nanoparticle surface.

The infrared spectrum of the Au-Pd colloid sample displays peaks at wavenumbers similar to the peaks in an infrared spectrum of PVP dissolved in water (table 3.6).

Table 3.6 Peak assignments for infrared spectrum of and aqueous solution of PVP and PVP chemisorbed on Au-Pd nanoparticles. Peak assignments and vibrational modes of PVP are based on those reported in reference 26.

Vibrational modes	Wavenumber (cm^{-1})	
	PVP	Au-Pd Colloid
N-C stretch of CH_2 (N-C_1)	1277	1259
N-C stretch of CH_2 (N-C_2)	1292	1292
C-H_2 wag	1321	1321
C-H bend	1384	1383
C-H_2 scissor	1424	1424
C-H_2 scissor	1442	1443
C-H_2 scissor	1464	1462
N-C stretch of N-C=O (N-C_3)	1499	1508
C=O stretch	1659	1643

Colloid; 10 kDa PVP, Au: Pd = 1:1 molar ratio, PVP: metal = 1.2:1, [metal] = 7.57×10^{-4} M

The most notable difference is the red shift of the C=O stretch vibrational band by 16 cm^{-1} when the PVP is chemisorbed on to the Au-Pd nanoparticles. This indicates that the C=O bond has been weakened upon chemisorption on to

the metal surface. From this data that it can be concluded that when Au-Pd nanoparticles are prepared by the sol method with a PVP to metal ratio of 1.2 the PVP molecules absorb on to the metal nanoparticles through their O atom and that the structure of the stabilising molecules remains intact (figure 3.16). Were the PVP molecules also chemisorbed through the N atom you would expect the N-C stretch vibrational bands of N-C=O and N-C-C (N-C_3 and N-C_2) to disappear. This is in line with the results reported by Huang *et al.* that showed that when Pd nanoparticles are <7 nm in size only the O atom of the PVP.[32] Based on these results it is likely that the absorption mode of PVP onto the monometallic colloidal Pd nanoparticles prepared as part of this study is the same as that for the bimetallic Au-Pd nanoparticles i.e it occurs through the chemisorption of the O atom of PVP. However, it's possible that the binding of PVP to the monometallic Au nanoparticles occurs through a different absorption mode. It has been reported that for PVP stabilised monometallic Au nanoparticles are negatively charged through electron donation from the PVP stabilisers molecules.[4] This has not been reported to be the case for Pd nanoparticles. Therefore the binding strength of the PVP to the metallic nanoparticles is likely to follow the trend of Au>Au-Pd>Pd.

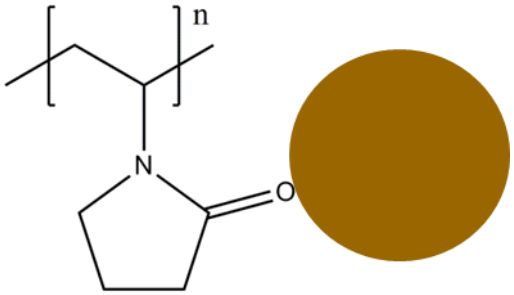

Figure 3.16 PVP molecule chemisorbed with its O atom on the surface of an Au-Pd nanoparticle.

3.4 Investigations into the Difference in Activity between Colloidal Au-Pd Nanoparticles and Au-Pd/TiO_2

Thus far it has been shown that the colloidal Au-Pd nanoparticles are active for CH_4 oxidation without the presence of a supporting material. Furthermore it has been found the unsupported Au-Pd nanoparticles display enhanced activity for CH_4 oxidation with H_2O_2 compared to Au-Pd nanoparticles supported on TiO_2 and the product distribution of the colloidal system favours the primary oxygenated products to a greater extent than the supported catalyst. The TiO_2 support material without the presence of any metal nanoparticles is inactive in this system. It has also been confirmed that the breakdown of the stabiliser, PVP, is not the source of the increased amount of products detected from the colloidal system compared to the amount detected from the supported catalyst system. Characterisation carried out on the Au-Pd nanoparticles show that the supported and unsupported nanoparticles are similar in both size and composition. The investigations reported in this section were carried out with the aim of better understanding the cause of the difference in activity between the supported and unsupported nanoparticles.

3.4.1 Comparison of H_2O_2 Consumption in the Supported and Unsupported Systems

To further investigate the differences between the Au-Pd colloid and the Au-Pd/TiO_2 (sol-immobilisation) systems reactions were carried out with a different set of conditions. This set of conditions matched those used in previous work carried out using supported metal catalysts for CH_4 oxidation reactions.[7, 8, 17] The difference is a reduction in the concentration of metal in the reactor from 7.57×10^{-4} M to 0.89×10^{-4} M, all other reaction parameters are the same as for the standard set of reaction conditions. These reactions were carried out as it was thought that the altered conditions might improve the H_2O_2 usage in the supported system. Reducing the amount of metal in the reactor would be

expected to reduce the rate of H_2O_2 decomposition. Previously reported work on CH_4 oxidation using Au-Pd/TiO_2(impreg.) prepared by the impregnation method have found that reducing the metal loading of the catalyst increases its TOF as the rate of H_2O_2 decomposition drops leading to improved oxidant availability.[7] The results of the reactions carried out using the Au-Pd colloid and Au-Pd/TiO_2 (sol-im.) using the altered reaction conditions are shown in table 3.7.

Table 3.7 Comparison of the catalytic activity of supported and unsupported Au-Pd nanoparticles for the liquid phase oxidation of CH_4 with H_2O_2 under mild conditions.

Catalyst	Product amount (μmol)				Oxy. sel. (%)	TOF (h^{-1})	Prod. (mol kg^{-1} h^{-1})	H_2O_2 / Products
	CH_3OH	CH_3OOH	HCOOH	CO_2				
AuPd Colloid	5.86	7.14	5.14	1.30	93	43.7	228	18
AuPd/TiO_2 (Sol-im.)	1.00	0.00	0.00	0.43	70	3.21	0.20	642

Conditions; 1000 μmol H_2O_2, 50 ^{0}C, total volume 10 ml, 30 bar CH_4, 30 min, 1500 rpm, 0.89 μmol metal per reaction.
Colloid; 10 kDa PVP, PVP: metal = 1.2: 1, Au: Pd = 1: 1 molar ratio, [metal] = 0.89×10^{-4} M
Supported catalyst; 1wt% metal, PVP: metal = 1.2:1, Au: Pd = 1: 1 molar ratio, 28 mg

Again the colloidal system shows enhanced activity over the supported catalyst system as was previously observed under standard conditions. In fact although the activity of the supported catalyst has improved under these conditions the difference in activity between the two systems is even more pronounced than under standard conditions. The total amount of products produced by the colloidal system is 19.44 μmol giving a particularly high TOF (as a result of the very low amount of metal used in the reaction) of 43.7 h^{-1}. By contrast the supported catalyst generated 1.43 μmol of products and as was noted in previous reactions exhibits poor H_2O_2 usage with the ratio of H_2O_2 consumed by the reaction to products produced being 642.

Despite the exceptionally high TOF achieved by the colloidal system under these conditions for reasons concerning reproducibility (discussed in chapter 4 section 4.2) these reaction conditions were not employed as standard reaction conditions for other reactions in this study. The main point of interest illustrated

from the results of these reactions relates to the difference in the amount of H_2O_2 remaining at the end of the reactions for each system (table 3.8) when of equivalent amounts of metal and support material are employed.

Table 3.8 Comparison of H_2O_2 consumption in CH_4 oxidation reactions catalysed by TiO_2, unsupported Au-Pd nanoparticles and Au-Pd nanoparticles supported on TiO_2.

Catalyst	Metal per reaction (μmol)	H_2O_2 Consumed (%)	TOF (h^{-1})	Oxygenated Products (μmol)
TiO_2	-	18	0.00	0.00
AuPd Colloid	0.89	35	43.7	18.14
AuPd/TiO_2	0.89	92	3.21	1.00
AuPd Colloid	7.57	80	35.3	19.99
AuPd/TiO_2	7.57	95	0.03	0.43

Conditions; 1000 μmol H_2O_2, 50 ^{0}C, total volume 10ml, 30 bar CH_4, 30 min, 1500 rpm,.
Colloid; 10 kDa PVP, PVP: metal = 1.2: 1, Au: Pd = 1: 1 molar ratio, [metal] = 0.89×10^{-4} M
Supported catalyst; 1wt% metal, PVP: metal = 1.2:1, Au: Pd = 1: 1 molar ratio, 28 mg TiO_2: 28 mg

Under standard reaction conditions 80% of the H_2O_2 added to the reactor will be consumed by the colloidal system whereas for the supported catalyst system 95% will be consumed. This difference is more pronounced under the altered reaction conditions where less metal is present in the reactor. Under these conditions the H_2O_2 consumption of the Au-Pd colloid reaction drops to 35% but the Au-Pd/TiO_2 reaction still consumes over 90% of the H_2O_2. If TiO_2 alone is added to a reaction without the presence of any metal nanoparticles 18% of the initial H_2O_2 will be consumed. It is remarkable that under the altered reaction conditions the combined amount of H_2O_2 degraded by the unsupported Au-Pd nanoparticles and the TiO_2 support is less than the amount of H_2O_2 decomposed by the Au-Pd/TiO_2

This observation is the key to understanding the difference in activities between these two systems. It implies that the supported Au-Pd nanoparticles have an intrinsically higher rate of H_2O_2 decomposition compared to that of the colloidal nanoparticles. Despite this increased rate of H_2O_2 decomposition much

lower total product amounts are observed for the supported Au-Pd nanoparticle catalysts indicating that TiO_2 supported Au-Pd nanoparticles can readily decompose H_2O_2, but are not as effective at promoting the reaction between H_2O_2 and CH_4 to produce primary oxygenates as the unsupported Au-Pd particles. There are two possible explanations for this; either the radicals generated from the H_2O_2 decomposition are being quenched in the supported system resulting in poor H_2O_2 usage or the rate of H_2O_2 decomposition in the supported system is so much faster than the rate of CH_4 oxidation that there is very little oxidant available to react with CH_4. Either case would result in less products being formed compared to the colloidal system

3.4.2 Addition of Support to AuPd Colloid Reaction

In order to discover the cause of the difference in activity between the Au-Pd colloid and $AuPd/TiO_2$ it had to be considered that the support material, TiO_2, itself was in some way hindering the activity of the Au-Pd nanoparticles. One possible explanation for this could be that the TiO_2 is acting as a quenching medium for the active radicals generated during the reaction. The oxidation of CH_4 with H_2O_2 when catalysed by Au-Pd nanoparticles is known to occur via a radical mechanism.[7] Catalyst testing has shown that the supported system displays less efficient H_2O_2 usage than colloidal system. If the TiO_2 was scavenging the hydroperoxy or hydroxyl radicals this would explain the poor H_2O_2 usage and low activity observed for reactions catalysed with $Au-Pd/TiO_2$ despite being an efficient system for the breakdown of H_2O_2. In contrast, the colloidal Au-Pd nanoparticles decompose the H_2O_2 at a much slower rate, but the radicals generated are not quenched in this system so the oxidation of CH_4 is much more effect.

In order to investigate this possibility, reactions were carried with Au-Pd colloids where various amounts of the TiO_2 support (2-28 mg) were added to the reaction. The results of these reactions are shown in figure 3.17.

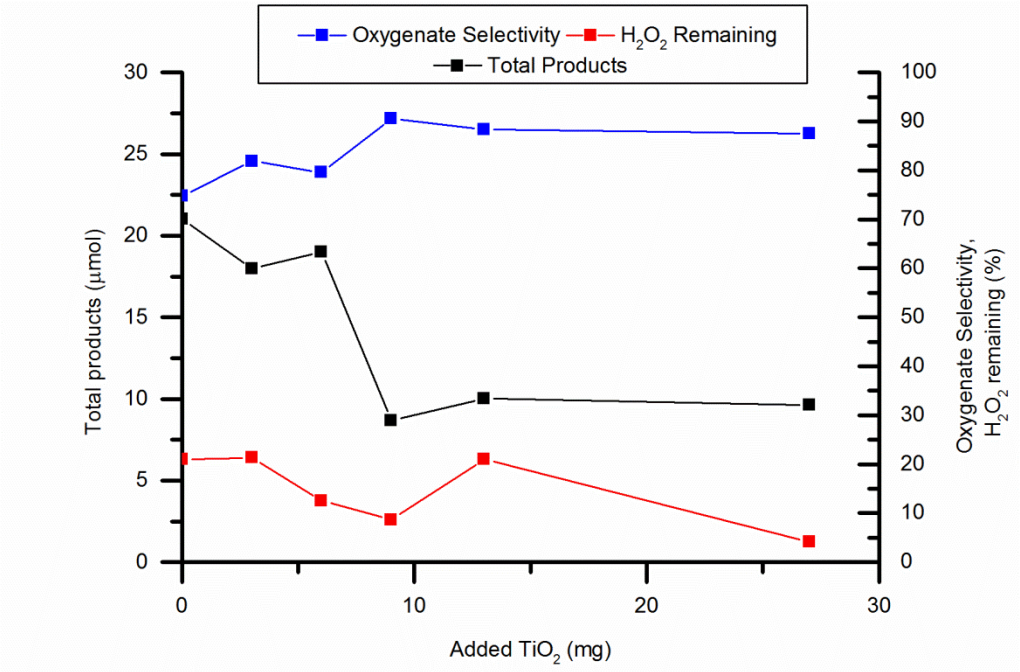

Figure 3.17 CH_4 oxidation reactions carried out with H_2O_2 and colloidal Au-Pd nanoparticles where various amounts TiO_2 were added to the reactor.

Conditions; 1000 µmol H_2O_2, 50 °C, 30 bar CH_4, total volume 10 ml, 1500 rpm, 7.57 µmol metal per reaction.
Colloid; 10 kDa PVP, Au: Pd = 1:1 molar ratio, PVP: metal = 1.2:1, [metal] = 7.57×10^{-4} M

An appreciable decrease in the total products generated was observed as the amount of TiO_2 added to the reaction was increased. Adding ≥9 mg of TiO_2 results in a particularly significant drop in activity. Adding 9 mg of TiO_2 results in less than half the total products being produced compared to a reaction where no TiO_2 is added. It is interesting to note that the amount of H_2O_2 remaining at the end of each reaction doesn't vary greatly.

These results confirm that the TiO_2 support material hinders the CH_4 oxidation reaction. It should be noted that at the end of the reactions where TiO_2 was added the TiO_2 was noticeably darker in colour. This suggests that some of the metal nanoparticles become supported over the course of the reaction. As

such it is not certain whether the drop in catalytic activity observed upon adding TiO_2 to the reactions was caused by the TiO_2 itself or the result of the formation of a metal- support interface in the reactor. As this interface forms the PVP stabiliser molecules may also absorb on to the support. This was considered as a possible explanation for the reduction in catalytic activity upon supporting the colloidal nanoparticle as once supported the PVP could possibly limit the access of the substrate to the active site. This hypothesis was discounted as it has been reported that Au-Pd/TiO_2 prepared by sol-immobilisation using PVA where the PVA was removed by reflux in water prior to testing (TOF = 2.79 h^{-1})[7] displays similar activity for the oxidation of CH_4 by PVP stabilised Au-Pd/TiO_2 (TOF = 3.21 h^{-1}). Furthermore it was shown in this study that adding additional PVP into a CH_4 oxidation reaction catalysed by Au-Pd/TiO_2 (PVP stabilised) enhanced the activity of the catalyst (section 3.2.5).

As the reaction proceeds through a radical mechanism it may be that the TiO_2 is acting as a radical scavenger and so hinders the utilisation of H_2O_2 towards producing oxygenated products. Alternatively it may be that the nature of the metal- support interface in some way increases the rate of H_2O_2 decomposition compared to the unsupported system so that the oxidant is destroyed before having the opportunity to take part in the oxidation of CH_4. Further experiments were carried out in order to examine these two possible explanations for the difference in activity between the supported and unsupported nanoparticle systems.

3.4.3 Support Trials

Once it was established that supporting the Au-Pd nanoparticles on TiO_2 reduced their activity for CH_4 oxidation compared to the unsupported system it was hypothesised that this effect could be avoided through the use of an alternative support material. If the TiO_2 is hindering catalytic activity by quenching the radicals generated by the reaction then the only requirement to prevent this reduction in activity is to identify a support material which does not act as a radical quencher. Doing so would create a catalytic system with the advantages of the supported system (facile separation of catalyst from products

and increased catalyst stability) while maintaining the enhanced activity and high oxygenate selectivity of the colloidal system.

With this aim in mind several Au-Pd catalysts were prepared using a variety of support materials (C, SiC, CeO_2, Al_2O_3, MgO). CH_4 oxidation reactions were carried out using these catalysts, the results of which are shown in table 3.9. Standard reaction conditions were altered slightly for these reactions to match those employed for the testing of supported Au-Pd catalysts in references 10 and 22. These conditions differ from the standard reactions conditions in two ways. Firstly the amount of H_2O_2 added to the reactor is 5000 μmol instead of 1000 μmol and the mass of catalyst used is 28 mg rather than 115 mg. The reason for this is the Au-Pd/TiO_2 catalyst preforms better under these conditions (TOF = 2.8 h^{-1} compared to 0.11 h^{-1} under standard conditions), likely due to the increase in oxidant availability as the lowering the amount of metal in the reaction reducing the rate of decomposition. Using these conditions also allows for more accurate comparison with previous work on CH_4 oxidation using supported Au-Pd nanoparticles and Fe-Cu/ZSM-5.[7, 8, 17] All of the supported catalyst tested under these conditions destroyed over 90% of the H_2O_2 present in the reactor and produced less than 3 μmol of products. The best activity was displayed by the AuPd/C catalyst which achieved a TOF of 4.6 h^{-1} although its oxygenate selectivity was poor at 35%. The results of the AuPd/SiC system are notable for their particularly high selectivity to CH_3OOH, 98%. Under the same conditions the colloidal system has a TOF of 72 h^{-1} and exhibits an oxygenate selectivity of 93%.

Table 3.9 Effect of support material on the catalytic activity of supported Au-Pd nanoparticles for the oxidation of CH_4 using H_2O_2 as oxidant.

Catalyst	Product amount (µmol)				Oxy. sel. (%)	TOF (h^{-1})	Prod. (mol kg^{-1} h^{-1})	H_2O_2 / Products
	CH_3OH	CH_3OOH	HCOOH	CO_2				
AuPd Colloid	12.57	14.86	2.43	2.18	93	72	377	14
$AuPd/TiO_2$	0.60	0.00	0.00	0.41	59	2.8	0.1	4635
AuPd/C	0.71	0.00	0.00	1.35	35	4.6	0.1	2330
AuPd/SiC	1.86	0.00	0.00	0.04	98	4.3	0.1	2608
$AuPd/CeO_2$	1.29	0.00	0.00	0.64	67	4.3	0.1	2529
$AuPd/Al_2O_3$	1.43	0.00	0.00	0.45	76	4.2	0.1	2644
AuPd/MgO	1.00	0.00	0.00	0.89	53	4.3	0.1	2617

Conditions; 5000 µmol H_2O_2, 50 ^{0}C, total volume 10ml, 30 bar CH_4, 30 min, 1500 rpm, 0.89 µmol metal per reaction.
Supported catalyst; 1wt% metal, PVP: metal = 1.2:1, Au: Pd = 1: 1 molar ratio, 28 mg

It is apparent from these results that regardless of the support material employed supporting Au-Pd nanoparticles results in a reduction in catalytic activity. It is interesting to note that for every support material trialled the >90% of the initial H_2O_2 was consumed during the reaction resulting in a high ratio of H_2O_2 consumed to products produced for all the supported systems. It is unlikely that all of these varied materials are behaving as radical quenchers as it was previously speculated that the TiO_2 was acting. A more likely explanation is that the drop in activity observed upon supporting the Au-Pd nanoparticles is caused by the nature of the metal- support interface as opposed to the support material itself. The rate of H_2O_2 decomposition increases in conjunction with the observed drop in activity when the Au-Pd nanoparticles are supported suggesting that the metal-support interface causes the rate of H_2O_2 decomposition to increase relative to that of the unsupported system thus causing the significant drop in catalytic activity.

To confirm that the support materials themselves were not the cause of the increased rate of H_2O_2 decomposition displayed by the supported nanoparticles compared to the colloidal nanoparticles, three of the support materials (TiO_2, C

and SiC) were used to carry out CH_4 oxidation reactions using the same conditions as those used for the reactions in table 3.9. The results of these reactions are shown in table 3.10 In each instance the combined H_2O_2 decomposition of the unsupported nanoparticles (8% of the initial H_2O_2) and the support material is less than that of the nanoparticles supported on the same material. For example SiC decomposes 2% of the initial H_2O_2 over the course of the reaction compared with 99% when Au-Pd/SiC is utilised as a catalyst. Similar results were given by both TiO_2 and C. These results corroborate the theory that it is the nature of the metal- support interface, as opposed to the support material itself that is responsible for the high rate of H_2O_2 decomposition displayed by the supported Au-Pd nanoparticles.

Table 3.10 Comparison of H_2O_2 consumption in CH_4 oxidation reactions catalysed by TiO_2, C, SiC, supported Au-Pd nanoparticles and colloidal Au-Pd nanoparticles.

Catalyst	H_2O_2 Consumed (%)	Oxygenated Products (μmol)
AuPd Colloid	8	32.04
TiO_2	7	0.00
AuPd/TiO_2	93	0.60
C	90	0.00
AuPd/C	96	0.71
SiC	2	0.00
AuPd/SiC	99	1.86

Conditions; 5000 μmol H_2O_2, 50 ^{0}C, total volume 10ml, 30 bar CH_4, 30 min, 1500 rpm, 0.89 μmol metal per reaction.
Supported catalyst; 1wt% metal, PVP: metal = 1.2:1, Au: Pd = 1: 1 molar ratio, 28 mg

3.4.4 H_2O_2 Decomposition Studies

It has been confirmed that the combined amount of H_2O_2 decomposed by the unsupported Au-Pd nanoparticles and by the TiO_2 was less than the total H_2O_2 decomposed by the supported Au-Pd/TiO_2 system. At this stage it was considered important to investigate the differences in how the H_2O_2 decomposed in the supported and unsupported systems. With this in mind reactions were carried out to establish H_2O_2 decomposition profiles for the both systems. Time- on- line

plots for CH_4 oxidation reactions under standard conditions with either colloidal Au-Pd or Au-Pd/TiO_2 are shown in figures 3.18 and 3.19 respectively. The amount of H_2O_2 remaining in the reactor after each time period is included in these graphs illustrating the major difference in the H_2O_2 decomposition profiles of these systems.

At the start of each reaction, in both cases, a considerable amount of H_2O_2 has already decomposed. This decomposition has occurred in the 10 min heat up step required to bring the reactor to temperature. The oxidant, catalyst and CH_4 are already present in the reactor during this step although stirring does not commence until the reactor is at 50 °C. At this time in the colloidal system 26% of the H_2O_2 had been consumed and 15.1 μmol of products have been generated. It would seem that stirring is not a requirement for CH_4 oxidation to take place for the colloidal system which is reasonable as the PVP increases the solubility of the CH_4 and the nanoparticles are suspended in solution so that the catalyst and the substrate are already in contact before stirring is initialised. The system is not mass transfer limited even without stirring. From this point on the amount of H_2O_2 remaining in the reactor gradually decreases over time as the amount of products produced increases. The product distribution for the colloidal system continuously favours the oxygenated products throughout the reaction time with the oxygenate selectivity always reaming stable above 80%.

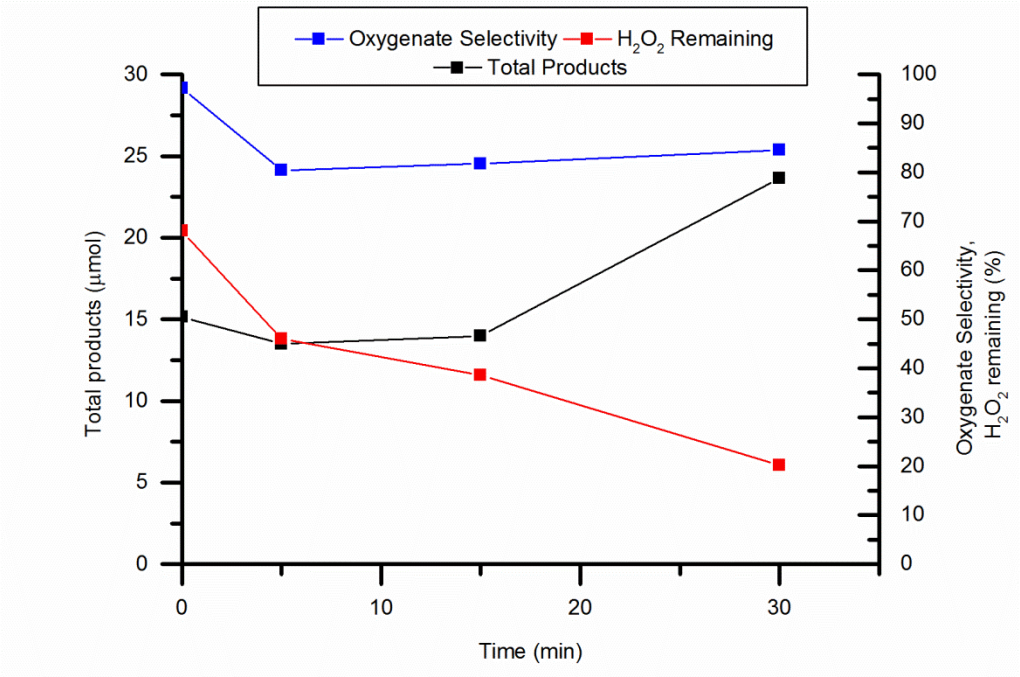

Figure 3.18 Time- on- line plot of H_2O_2 decomposition and products produced during CH_4 oxidation with H_2O_2 in the presence of colloidal Au- Pd nanoparticles.

Conditions; 1000 µmol H_2O_2, 50 °C, 30 bar CH_4, total volume 10 ml, 1500 rpm, 7.57 µmol metal per reaction.
Colloid; 10 kDa PVP, PVP :metal = 1.2:1, Au:Pd = 1 :1 molar ratio, [metal] = 7.57×10^{-4} M

As was observed in the colloidal system a substantial amount of H_2O_2 decomposition occurs in the supported catalyst reactions before stirring has begun. However in this case almost all of the H_2O_2 (90%) has been consumed before any stirring has occurred and unlike the Au-Pd colloid reaction very little CH_4 oxidation has occurred at this stage. Less than 0.2 µmol of products have been generated and this is entirely composed of CO_2. It is only after the stirring has started that oxygenated products begin to be produced. The amount of products formed and the oxygenate selectivity increase gradually over the course of the reaction from this point on.

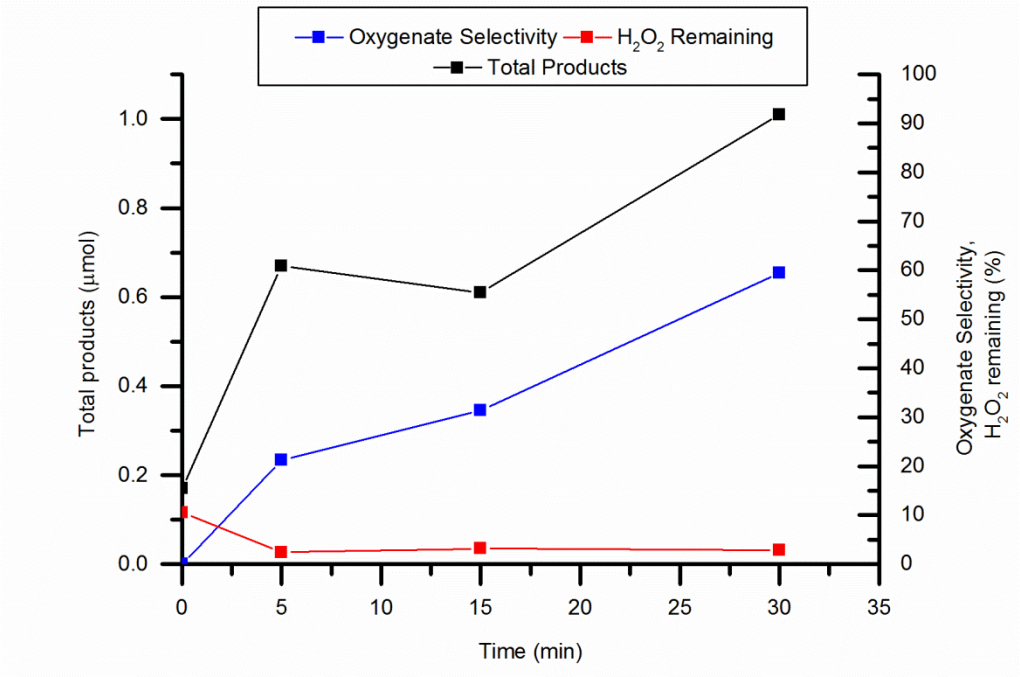

Figure 3.19 Time- on- line plot of H_2O_2 decomposition and products produced during CH_4 oxidation with H_2O_2 in the presence of Au-Pd/TiO_2.

Conditions; 1000 µmol H_2O_2, 50 ^{0}C, total volume 10 ml, 30 bar CH_4, 30 min, 1500 rpm
Catalyst; 28 mg, 1 wt % metal, Au: Pd = 1:1 molar

This data illustrates two main points about the difference in H_2O_2 decomposition in the two systems. Firstly that H_2O_2 degradation occurs far more gradually in the colloidal system then in reactions where supported nanoparticles are used. And secondly there is a considerable difference between the amounts of H_2O_2 present at the start of a reaction for each of these systems. As the results of reactions where different support materials were trialled show similar levels of overall H_2O_2 consumption and activity to the Au-Pd/TiO_2 catalysed reactions it is reasonable to assume that the H_2O_2 decomposition profiles of all the supported catalysts trialled are comparable. At this stage the root cause of the difference in activity between the supported and unsupported nanoparticles would appear to be the vast difference in oxidant availability between the two systems.

3.4.5 Reactions with Equal Initial H_2O_2

It the hydrogen peroxide decomposition studies described in the previous section it was found that at the start of the reactions (i.e. when the reactor has reached 50 °C and stirring begins) 26% of the hydrogen peroxide in the colloidal system and 90% of the hydrogen peroxide in the supported system has already decomposed. In light of these results it was considered possible that the difference in the amount of H_2O_2 present in the reactor at the start of the reactions for these systems could be the sole cause of the difference in their catalytic activity. In order to rule out this possibility it was necessary to carry out reactions with both the supported and unsupported nanoparticles where the reaction conditions were altered to ensure the initial H_2O_2 concentration was the same for each system. The first set of these reactions were carried out at room temperature (20 °C) so that there was no heat up step involved in the reaction procedure (Table 3.11). Under these conditions the reaction catalysed by Au-Pd/TiO_2 produced no oxygenated products, only CO_2, giving a TOF of only 0.8 h^{-1}. Whereas the colloidal system achieved a TOF of 1.9 h^{-1} and displayed a selectivity of 95% to oxygenated products. In addition the H_2O_2 usage for the colloidal system was over 70 times more efficient compared to that of the supported catalyst.

Table 3.11 Comparison of supported and unsupported Au-Pd nanoparticles for the selective oxidation of CH_4 at 20 °C.

Catalyst	Product amount (μmol)				Oxy. sel. (%)	TOF (h^{-1})	Prod. (mol kg^{-1} h^{-1})	H_2O_2 / Products
	CH_3OH	CH_3OOH	HCOOH	CO_2				
AuPd Colloid	0.61	6.26	0.00	0.40	95	1.9	13	29
AuPd/TiO_2	0.00	0.00	0.00	0.38	0.0	0.8	0.0	2202

Conditions; 1000 μmol H_2O_2, 20 ^{0}C, total volume 10ml, 30 bar CH_4, 30 min, 1500 rpm, 7.57 μmol metal per reaction.
Colloid; 10 kDa PVP, PVP: metal = 1.2: 1, Au: Pd = 1: 1 molar ratio, [metal] = 7.57×10^{-4} M
Supported catalyst; 1wt% metal, PVP: metal = 1.2:1, Au: Pd = 1: 1 molar ratio, 115 mg

Additional reactions were carried out at 50 °C to investigate the catalytic activity of these two systems when the same initial amount of oxidant is present for both

systems. In this case the H_2O_2 was not added into the reactor until the system had reached 50° C (table 3.12). Therefore there was no opportunity for H_2O_2 degradation before stirring was started. Again the supported catalyst system generated only a small amount CO_2 with no other products and consumed all of the H_2O_2 present. It is possible in this case that adding the H_2O_2 when the reactor had already reached 50 °C caused an increase in the rate of its decomposition. Yet again the colloidal nanoparticles outperform their supported equivalent. Under these conditions a TOF of $12h^{-1}$ was achieved and the ratio of H_2O_2 consumed to products was particularly low, 18. The oxygenate selectivity for this reaction is fairly high at 87% although the distribution of products is notable shifted towards HCOOH.

Table 3.12 Comparison of supported and unsupported Au-Pd nanoparticles for the selective oxidation of CH_4 at 50 °C where the oxidant H_2O_2 has not been added until the reactor reached 50 °C.

Catalyst	Product amount (μmol)				Oxy. sel. (%)	TOF (h^{-1})	Prod. (mol kg^{-1} h^{-1})	H_2O_2 / Products
	CH_3OH	CH_3OOH	HCOOH	CO_2				
AuPd Colloid	6.20	5.14	28.36	5.71	87	12	79	18
$AuPd/TiO_2$	0.00	0.00	0.00	0.69	0.0	1.6	0.0	1448

Conditions; 1000 μmol H_2O_2, 50 ^{0}C, total volume 10 ml, 30 bar CH_4, 30 min, 1500 rpm, 7.57 μmol metal per reaction.
Colloid; 10 kDa PVP, PVP: metal = 1.2: 1, Au: Pd = 1: 1 molar ratio, [metal] = 7.57×10^{-4} M
Supported catalyst; 1wt% metal, PVP: metal = 1.2:1, Au: Pd = 1: 1 molar ratio, 115 mg

It is clear that these results rule out the possibility that the reduced activity of $AuPd/TiO_2$ compared to the AuPd colloid is caused by the difference in the initial H_2O_2 of the two systems. The colloidal system has been shown to be more active even when the reaction conditions are altered to ensure the same amount of H_2O_2 is present at the start of the reaction for both systems. It can therefore be concluded that the difference in catalytic activity observed between the supported and unsupported Au-Pd nanoparticles under standard reaction conditions is the result of their differing rates of H_2O_2 decomposition. The fast rate of H_2O_2 decomposition in reactions catalysed by $Au\text{-}Pd/TiO_2$ limits the oxidant availability for CH_4 oxidation while in the colloidal system the rate of

H_2O_2 decomposition is more closely matched to the rate of CH_4 oxidation. Similar activities and overall H_2O_2 decomposition were observed when various different support materials were used implying that it is the support- metal that interface, as opposed to the support material itself, that causes the increase in the rate of H_2O_2 decomposition compared to the colloidal system

3.5 Investigation into the Stability of Au-Pd Colloids

So for it has been shown that not only do the unsupported Au-Pd nanoparticles show enhanced catalytic activity for CH_4 oxidation with H_2O_2 compared to supported Au-Pd nanoparticles but also significantly increased oxygenate selectivity as well as improved H_2O_2 usage. However reusability is also an important factor in evaluating catalysts. Au-Pd/TiO_2 has been reported to be reusable for CH_4 oxidation reactions.[8] There is an appreciable drop in activity after the first use but for subsequent uses both the activity and oxygenate selectivity remain stable. However the reusability of the colloidal nanoparticles is limited as it has been observed over the course of this work that Au-Pd colloids prepared with a metal concentration of 7.57×10^{-4} M tend to collapse during a standard CH_4 oxidation reaction.

Visual inspection of the Au-Pd colloid post reaction shows that by the end of the reaction much of the metal originally present in colloidal form has precipitated out of solution. A dark residue can generally be seen coating the reaction vessel after reaction. In addition centrifuging the reaction mixture successfully separates the solid material from the aqueous solution whereas prior to reaction this is not possible. In order to determine whether this precipitate was catalytically active for CH_4 oxidation the precipitate formed during three separate standard reactions was collected by centrifuging the reaction liquid. The precipitate was then washed and re-dispersed in water and used to carry out a reaction. No liquid phase products were detected from this reaction and only 0.64 μmol of CO_2 was produced. 92% of the initial H_2O_2 was consumed during the reaction. Blank reactions (without the presence of a

catalyst) using the same conditions display <5% peroxide decomposition it can therefore be concluded that the precipitate is very active for the decomposition of hydrogen peroxide. In this section the reusability of the colloidal Au-Pd nanoparticles is investigated as well as the cause of their instability under reactions conditions including characterisation of the colloid post reaction.

3.5.1 Characterisation of Au-Pd Colloids Post-Reaction

Visual inspection of the Au-Pd colloid post- reaction has indicated that the metal nanoparticles destabilise during the course of the reaction causing the metal to precipitate out of solution. It is clear that the colloid is collapsing during the reaction so in order to better understand the way in which the colloid is altered over the course of the reaction samples of the colloidal Au-Pd nanoparticles were characterised by UV-vis spectroscopy and TEM post reaction.

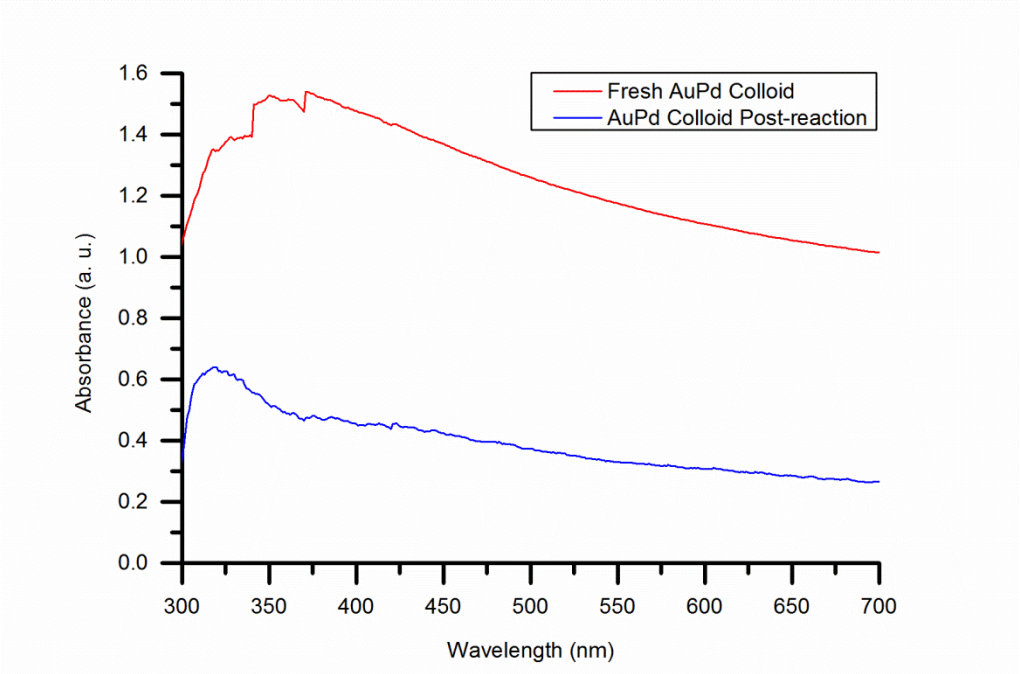

Figure 3.20 UV-vis spectra of Au-Pd colloid before and after being used to catalyse a CH_4 oxidation reaction with H_2O_2.

Conditions; 1000 µmol H_2O_2, 50 °C, 30 bar CH_4, total volume 10 ml, 1500 rpm, 7.57 µmol metal per reaction.
Colloid; 10 kDa PVP, PVP :metal = 1.2:1, Au:Pd = 1 :1 molar ratio, [metal] = 7.57×10^{-4} M

Uv-vis spectroscopy showed a reduction in absorption across all wavelengths employed in analysis compared to the reference, water (figure 3.20). This is in keeping with the observation that colloid is collapsing. TEM analysis showed an increase in average particle size during the reaction from 3 to 40.7 nm (figure 3.21). The TEM images show that particle clusters, some even larger than 100 nm are formed during the reaction. This suggests that the metal nanoparticles are forming large agglomerates which are precipitating out of solution. These results indicate that the stabiliser ligand is in some way being affected by the reaction conditions allowing the nanoparticles to agglomerate and the colloid to destabilise.

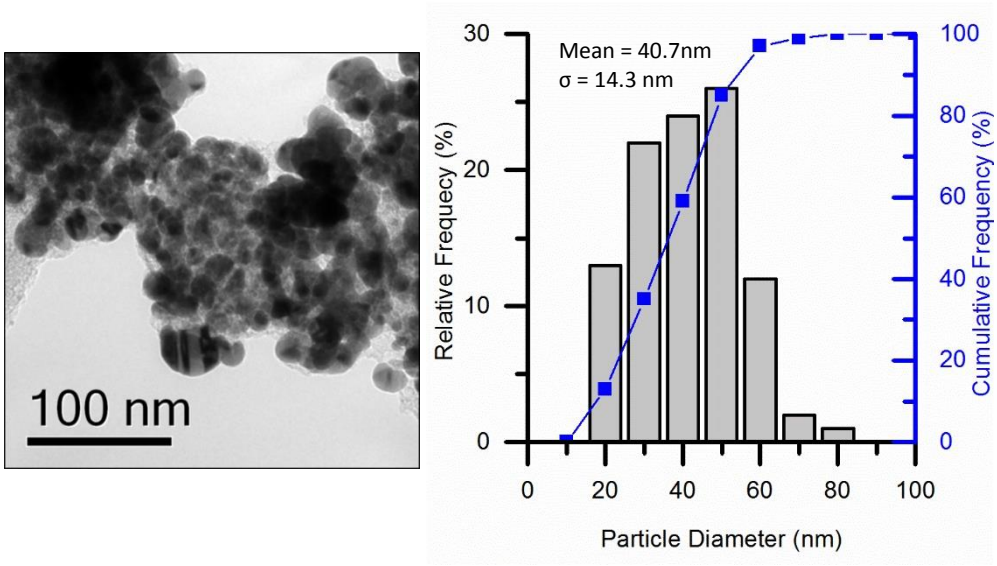

Figure 3.21 TEM image and particle size distribution of Au-Pd colloid after use as catalyst for CH_4 oxidation reaction with H_2O_2.

Conditions; 1000 µmol H_2O_2, 50 °C, 30 bar CH_4, total volume 10 ml, 1500 rpm, 7.57 µmol metal per reaction.
Colloid; 10 kDa PVP, PVP :metal = 1.2:1, Au:Pd = 1 :1 molar ratio, [metal] = 7.57×10^{-4} M

3.5.2 Identification of Factors Causing Instability of Au-Pd Colloids

The Au-Pd colloids have been observed to be stable at room temperature and pressure but destabilise over the course of a standard reaction. It can be inferred

that some aspect of the reaction conditions employed interfere with the stabilising action of the PVP ligand leading to the collapse of the colloid. In order to establish which factors in the standard reaction conditions are causing this a series of trials were carried out. The first set of these trials involved subjecting samples of Au-Pd colloid to 30 min of stirring at various speeds. The UV-vis spectra of the samples after being subjected to stirring are shown in figure 3.22. There is some reduction observed in the absorbance of the higher wavelengths utilised but overall there is little change in the UV-vis spectra post- stirring. This result confirms that stirring alone does not cause the colloid to collapse.

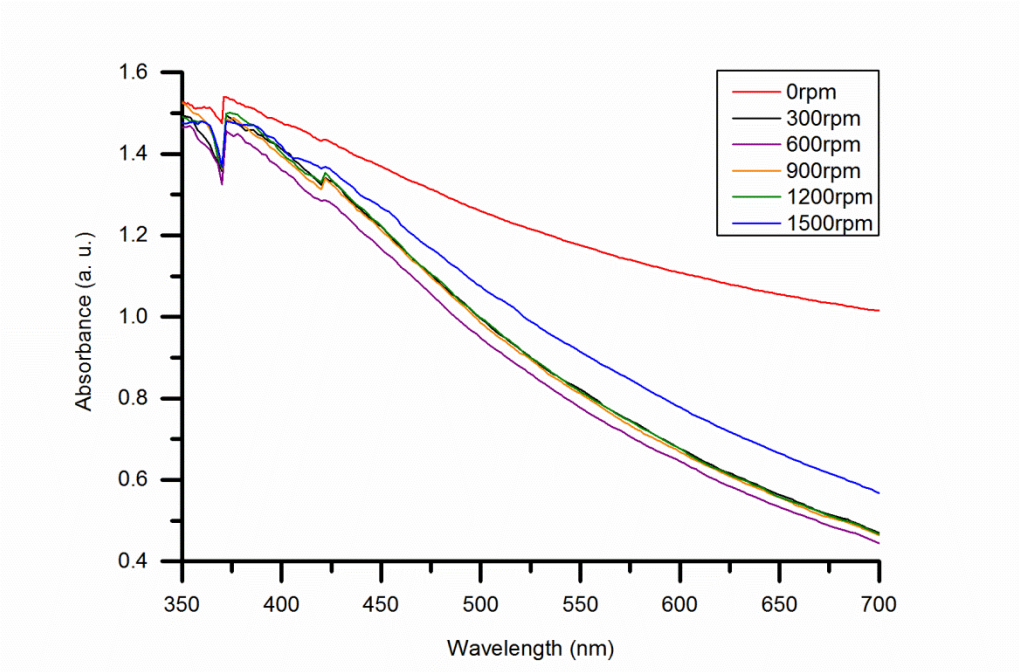

Figure 3.22 UV-vis spectra of Au-Pd colloid before and after being stirred at different rate in an autoclave reactor for 30min under room temperature and pressure.

Conditions; 30 min, total volume 10 ml
Colloid; 10 kDa PVP, PVP :metal = 1.2:1, Au:Pd = 1 :1 molar ratio, [metal] = 7.57×10^{-4} M

Trials were then carried out where H_2O_2 was added to the colloid before stirring (table 3.13).

Table 3.13 Testing of Au-Pd colloid stability under various conditions.

Stirring Speed (rpm)	H_2O_2 (μmol)	Pressure (bar)	Gas	Collapse
300	0.00	1.01	Air	No
600	0.00	1.01	Air	No
900	0.00	1.01	Air	No
1200	0.00	1.01	Air	No
1500	0.00	1.01	Air	No
1500	1000	1.01	Air	Yes
300	1000	1.01	Air	No
300	1000	10.0	CH_4	Yes
0.00	0.00	30.	CH_4	Yes
0.0	0.00	10.0	CH_4	Yes
0.0	0.00	5.0	CH_4	Yes
0.0	0.00	30.0	N_2	No
0.0	0.00	1.01	CH_4	No

Conditions; 30 min, total volume 10 ml
Colloid; 10 kDa PVP, PVP :metal = 1.2:1, Au:Pd = 1 :1 molar ratio, [metal] = 7.57×10^{-4} M

It was found that stirring the colloid at 1500 rpm, (standard reaction stirring speed) with 1000 μmol H_2O_2 caused the colloid to collapse although if the stirring speed was reduced to 300 rpm the colloid remained stable. Further testing showed that pressurising the reactor containing the colloid and 1000 μmol H_2O_2 with 10 bar CH_4 caused the system to destabilise. In fact it was found that if the reactor vessel was pressurised with as little as 5 bar of CH_4 for 30 min without any stirring or H_2O_2 the colloid would collapse. This was not found to be the case when the system was pressurised with 30 bar of N_2. From these results it can be concluded that although the combination of stirring and H_2O_2 causes the colloid to destabilise the primary reason for collapse is the substrate, CH_4. It was shown in section 3.2.5 that PVP increases the solubility of CH_4 in water. This result suggests that as the CH_4 enters the PVP shell surrounding the nanoparticles that it interferes with the stabilising action of the PVP allowing the nanoparticles to agglomerate and thus causing the colloid to collapse. It was found that bubbling

CH_4 through a sample of the Au-Pd colloid did not cause collapse however adding H_2O_2 to this set up did not result in the formation of any liquid phase products even for long reaction times (16 h). Therefore it is not possible to generate products from this system without employing CH_4 pressures which cause the colloid to collapse.

It was hypothesised that using higher molecular weights of PVP in the colloid preparation might increase the stability of the system. Colloids prepared with a PVP molecular weight of up to 360 kDa were tested and were observed to destabilise under standard reaction conditions (for catalytic activity results see chapter 4 section 4.4.6). PVP with molecular weights >360 kDa are available as such it is possible that increased stability may be achieved by further increasing the molecular weight of PVP beyond 360 kDa. The focus of this work, however, was to examine the intrinsic activity of the Au-Pd nanoparticles for CH_4 oxidation as such further investigations into the effect of PVP molecular weight on colloid stability were not carried out.

It should be noted that when testing colloids of lower metal concentrations a higher stability was observed. Centrifuging of the reaction liquid did not appear to remove all of the metal present in solution as some of the brown colour of the colloid was retained although the liquid was no longer entirely opaque. In fact it was discerned that CH_4 oxidation continued in the reaction liquid after removal from the reactor when the colloid did not fully destabilise as it was not possible to entirely separate the catalyst from the reaction liquid by centrifuge. This lead to reproducibility issues when using colloids with low metal concentrations as products continued to be generated prior to NMR analysis. These results are discussed in full in chapter 4 section 4.2.

3.5.3 Reuse Reactions

It has been established that the Au-Pd colloids collapse under pressures as low as 5 bar of CH_4 limiting their reusability. This not however imply that the nanoparticles themselves are not reusable only that the colloid is destabilised during reaction. It was considered desirable to evaluate the intrinsic reusability

of the Au-Pd nanoparticles. This was achieved by reducing the reaction time from 30 to 10 min to prevent the colloid destabilising. It was not possible to carry out a typical reuse procedure where two consecutive reactions are carried out and a sample is taken for analysis in between as sampling would alter of the colloidal system would alter the metal concentration. Instead the first reaction was carried out over a 10 min interval using standard reaction conditions. The second reaction was carried out as the first except after the initial 10 min interval sufficient H_2O_2 was added to restore the original H_2O_2 concentration (based on the amount of H_2O_2 consumed by the first reaction) and the reactor was re-pressurised with CH_4 to run another reaction immediately after.

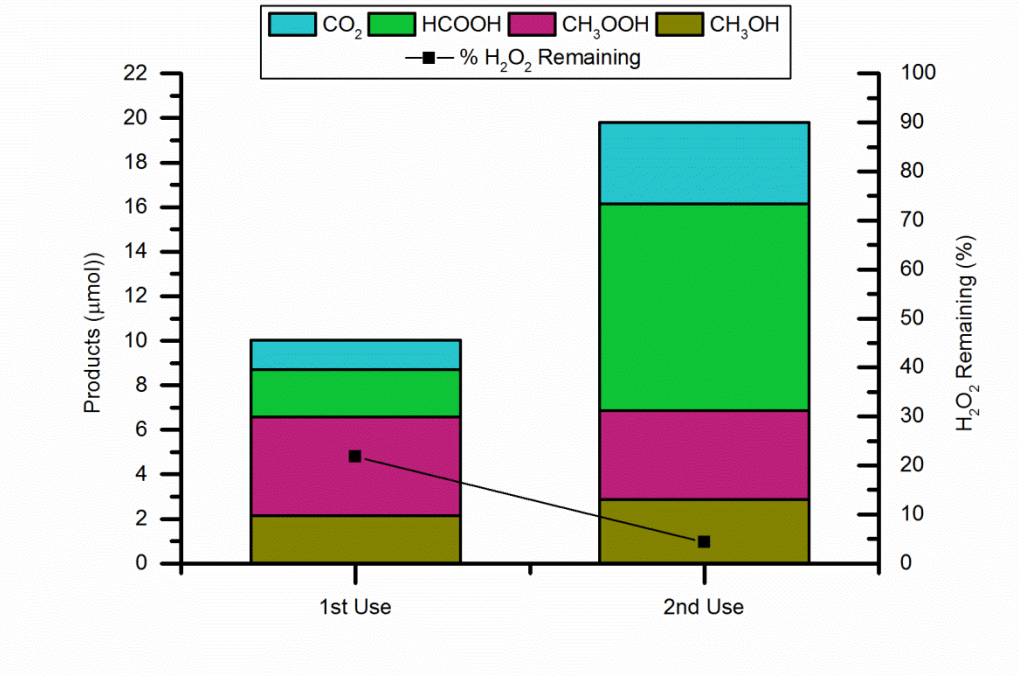

Figure 3.23 Reuse of Au-Pd colloid for CH_4 oxidation reaction with H_2O_2 as oxidant.
Conditions; 1000 µmol H_2O_2, 50 °C, 30 bar CH_4, total volume 10 ml, 1500 rpm, 7.57 µmol metal per reaction.
Colloid; 10 kDa PVP, PVP :metal = 1.2:1, Au:Pd = 1 :1 molar ratio, [metal] = 7.57×10^{-4} M

In this was way it was possible to compare the products generated by 1 ×10 min reaction and 2 ×10 min reactions without affecting the metal concentration of the system (figure 3.23). The results show that twice the amount of total products are produced after 2 x 10 min reactions then after the first 10 min

reaction indicating that the TOF (7.94 h^{-1} for 1×10 min reaction, 7.84 h^{-1} for 2×10 min reaction) of the colloidal nanoparticles is maintained over multiple reactions.

3.6 Conclusions

CH_4 oxidation reactions have been carried out with H_2O_2 and colloidal Au-Pd nanoparticles prepared using PVP as a stabilising ligand. These reactions were found to proceed via the same reaction pathway as CH_4 oxidation reactions catalysed using Au-Pd/TiO_2. In both systems CH_3OOH is produced as the primary product which undergoes subsequent transformation to form CH_3OH and HCOOH before complete oxidation to CO_2. Monometallic Au and Pd colloids were shown to be less effect for this reaction compared to the bimetallic Au-Pd colloid. This demonstrates that there is a synergistic effect between the Au and Pd in the colloidal system which is also observed when the nanoparticles are supported.

Despite these similarities, the Au-Pd nanoparticles in the absence of a supporting material display greatly enhanced activity for CH_4 oxidation with H_2O_2 compared to their supported counterpart under identical reaction conditions. Supporting the Au-Pd nanoparticles on TiO_2 results in a tenfold drop in the amount of products generated under standard reaction conditions and a drop in selectivity to desired oxygenated products from 86% to 26%. In addition the utilisation of H_2O_2 in the colloidal system is significantly more efficient than reactions with supported Au-Pd nanoparticles.

It has been established that the difference in activity between these two systems is due to the vast difference in their rates of H_2O_2 decomposition. In reactions catalysed by supported Au-Pd nanoparticles the oxidant is consumed at such a fast rate that very little is available to take part in the oxidation of CH_4. By contrast the rate of H_2O_2 decomposition in the colloidal system is more closely matched to the rate of CH_4 oxidation ensuring that oxidant usage is more effective and more oxygenated products are formed. Au-Pd nanoparticles supported on a range of supporting materials have been found to generate similar amounts of products while consuming similar amounts of H_2O_2 to Au-Pd/TiO_2. It can therefore be concluded that the formation of a support-metal interface and not

the support material itself is responsible for the increased rate of H_2O_2 decomposition when Au-Pd nanoparticles are supported.

Overall this work has demonstrated that in the case of CH_4 oxidation with H_2O_2 the intrinsic catalytic activity of Au-Pd nanoparticles for CH_4 oxidation with H_2O_2 is hindered by supporting them. The colloidal system is unlikely to be suitable for carrying out CH_4 oxidation on an industrial scale due to issues which limit the reusability of the Au-Pd colloid. Firstly separation of the nanoparticles from the oxygenated products is more difficult when using colloidal Au-Pd nanoparticles compared to a supported catalyst. In addition low pressures of CH_4 have been found to cause the colloid to destabilise. However the aim of this work was to investigate the inherent activity of the Au-Pd nanoparticles and the role of the support in the reaction and this has been achieved. It has been demonstrated that this system is an example of a support hindering a reaction. It is hoped that these results will help inform future catalytic design for both CH_4 oxidation and H_2O_2 synthesis.

3.7 References

1. A. Haruta, *Chem. Rec.*, 2003, 3, 75-87.
2. Peter Kracke, Terry Haas, Howard Saltsburg and M. Flytzani-Stephanopoulos, *J. Phys. Chem. C*, 2010, 114, 16401-16407.
3. H. Tsunoyama, H. Sakurai, Y. Negishi and T. Tsukuda, *J. Am. Chem. Soc.*, 2005, 127, 9374-9375.
4. H. Tsunoyama, N. Ichikuni, H. Sakurai and T. Tsukuda, *J. Am. Chem. Soc.*, 2009, 131, 7086-7093.
5. I. Biondi, G. Laurenczy and P. J. Dyson, *Inorg. Chem.*, 2011, 50, 8038-8045.
6. M. Comotti, C. Della Pina, R. Matarrese and M. Rossi, *Angew. Chem., Int. Ed.*, 2004, 43, 5812-5815.
7. M. H. Ab Rahim, M. M. Forde, R. L. Jenkins, C. Hammond, Q. He, N. Dimitratos, J. A. Lopez-Sanchez, A. F. Carley, S. H. Taylor, D. J. Willock, D. M. Murphy, C. J. Kiely and G. J. Hutchings, *Angew. Chem. Int. Ed.*, 2013, 52, 1280-1284.
8. M. Ab Rahim, M. M. Forde, C. Hammond, R. L. Jenkins, N. Dimitratos, J. A. Lopez-Sanchez, A. F. Carley, S. H. Taylor, D. J. Willock and G. J. Hutchings, *Top. Catal.*, 2013, 56, 1843-1857.
9. J. K. Edwards, B. E. Solsona, P. Landon, A. F. Carley, A. Herzing, C. J. Kiely and G. J. Hutchings, *J. Catal.*, 2005, 236, 69-79.
10. A. A. Herzing, M. Watanabe, J. K. Edwards, M. Conte, Z. R. Tang, G. J. Hutchings and C. J. Kiely, *Faraday Discuss.*, 2008, 138, 337-351.

11. N. Dimitratos, J. A. Lopez-Sanchez, D. Morgan, A. F. Carley, R. Tiruvalam, C. J. Kiely, D. Bethell and G. J. Hutchings, *Phys. Chem. Chem. Phys.*, 2009, 11, 5142-5153.
12. L. Kesavan, R. Tiruvalam, M. H. Ab Rahim, M. I. bin Saiman, D. I. Enache, R. L. Jenkins, N. Dimitratos, J. A. Lopez-Sanchez, S. H. Taylor, D. W. Knight, C. J. Kiely and G. J. Hutchings, *Science*, 2011, 331, 195-199.
13. J. Pritchard, L. Kesavan, M. Piccinini, Q. A. He, R. Tiruvalam, N. Dimitratos, J. A. Lopez-Sanchez, A. F. Carley, J. K. Edwards, C. J. Kiely and G. J. Hutchings, *Langmuir*, 2010, 26, 16568-16577.
14. J. A. Lopez-Sanchez, N. Dimitratos, C. Hammond, G. L. Brett, L. Kesavan, S. White, P. Miedziak, R. Tiruvalam, R. L. Jenkins, A. F. Carley, D. Knight, C. J. Kiely and G. J. Hutchings, *Nature Chemistry*, 2011, 3, 551-556.
15. M. Egginger, M. Irimia-Vladu, R. Schwodiauer, A. Tanda, I. Frischauf, S. Bauer and N. S. Sariciftci, *Advanced Materials*, 2008, 20, 1018-+.
16. J. Colby, D. I. Stirling and H. Dalton, *Biochem. J.*, 1977, 165, 395-402.
17. C. Hammond, M. M. Forde, M. H. Ab Rahim, A. Thetford, Q. He, R. L. Jenkins, N. Dimitratos, J. A. Lopez-Sanchez, N. F. Dummer, D. M. Murphy, A. F. Carley, S. H. Taylor, D. J. Willock, E. E. Stangland, J. Kang, H. Hagen, C. J. Kiely and G. J. Hutchings, *Angew. Chem. Int. Ed.*, 2012, 51, 5129-5133.
18. D. P. Dissanayake and J. H. Lunsford, *J. Catal.*, 2003, 214, 113-120.
19. N. N. Edwin, J. K. Edwards, A. F. Carley, J. A. Lopez-Sanchez, J. A. Moulijn, A. A. Herzing, C. J. Kiely and G. J. Hutchings, *Green Chem.*, 2008, 10, 1162-1169.
20. J. A. Lopez-Sanchez, N. Dimitratos, P. Miedziak, E. Ntainjua, J. K. Edwards, D. Morgan, A. F. Carley, R. Tiruvalam, C. J. Kiely and G. J. Hutchings, *Phys. Chem. Chem. Phys.*, 2008, 10, 1921-1930.
21. M. B. Cortie and E. v. d. Lingen, *Mater. Lett.*, 2002, 26, 1-14.
22. A. L. Mackay, *Acta Crystallogr.*, 1962, 15, 916-&.
23. T. P. Martin, *Phys. Rep.*, 1996, 273, 199-241.
24. S. Link and M. A. Ei-Sayed, *Annu. Rev. Phys. Chem.*, 2003, 54, 331-366.
25. J. Y. Park, C. Aliaga, J. R. Renzas, H. Lee and G. A. Somorjai, *Catal. Lett.*, 2009, 129, 1-6.
26. C. Aliaga, J. Y. Park, Y. Yamada, H. S. Lee, C.-K. Tsung, P. Yang and G. A. Somorjai, *J. Phys. Chem. C*, 2009, 113, 6150-6155.
27. A. Villa, D. Wang, D. S. Su and L. Prati, *Chemcatchem*, 2009, 1, 510-514.
28. C. Hammond, R. L. Jenkins, N. Dimitratos, J. A. Lopez-Sanchez, M. H. ab Rahim, M. M. Forde, A. Thetford, D. M. Murphy, H. Hagen, E. E. Stangland, J. M. Moulijn, S. H. Taylor, D. J. Willock and G. J. Hutchings, *Chemistry-a European Journal*, 2012, 18, 15735-15745.
29. J. A. Creighton and D. G. Eadon, *J. Chem. Soc., Faraday Trans.*, 1991, 87, 3881-3891.
30. J. F. Moulder, *Handbook of X-ray Photoelectron Spectroscopy: A Reference Book of Standard Spectra for Identification and Interpretation of XPS Data*, Physical Electronics, 1995.
31. G. J. Hutchings and C. J. Kiely, *Acc. Chem. Res.*, 2013, 46, 1759-1772.
32. X. Junyang, Hua, H., Jiang, Z., Ma, Y., Huang, H., *Langmuir*, 2012, 28, 6736-6741.
33. T. Teranishi and M. Miyake, *Chem. Mater.*, 1998, 10, 594-600.

4 Further Investigations into the Use of Au-Pd Colloidal Nanoparticles as Catalysts for Methane Oxidation

4

4.1 Introduction

In the previous chapter the activity of unsupported Au-Pd colloidal nanoparticles was compared with that of supported Au-Pd nanoparticles for the oxidation of CH_4 with H_2O_2. It was established that colloidal Au-Pd nanoparticles can carry out this challenging reaction under mild conditions and in fact perform better as catalysts for CH_4 oxidation without the presence of a support. Unsupported gold nanoparticles have previously been found to be active for a variety of typical Au catalysed reactions[1, 2] however there are a limited number of reports of nanoparticles being more catalytically active without the presence of a supporting material. This prompted further investigations to be carried out into the optimisation of the colloidal system for CH_4 oxidation. The aim of this chapter is investigate the intrinsic catalytic activity of the Au-Pd nanoparticles for CH_4 oxidation and the factors affecting it.

Firstly the reproducibility and standard error for these reactions is established. Then the effect on the system of varying several different reaction parameters is investigated. From these investigations a set of optimised reaction conditions is identified. The colloidal Au-Pd nanoparticles are tested under these optimised reaction condition in order to test the limit of the systems capability

for CH_4 oxidation. In section 4.4 the results of studies on the influence of various parameters relating to the preparation of the Au-Pd nanoparticles are reported such as the effect of altering the ratio of Au to Pd and use of PVP of different molecular weights. The effect of varying the ratio of PVP to metal is also examined. It has been previously reported in the literature on metal nanoparticles that changing the ratio of stabilising ligand to metal used during preparation of metal nanoparticles alters the size of the nanoparticles.[3-5] It is known that particle size is generally a significant factor in determining the activity of gold nanoparticles[6-9] so it would be useful to determine its effect on this system. In addition it was found in chapter 3 that the presence of PVP enhances the activity of the colloidal Au-Pd nanoparticles by increasing the solubility of CH_4 in solution which is particularly interesting given that there have been previous reports of PVP hindering catalytic activity of metal nanoparticles by blocking reactive sites.[9-11] For these reasons the effect of PVP: metal was considered to be of particular interest and so was subject to a more in-depth examination than the other preparation parameters investigated.

4.2 Reproducibility and Standard Errors

The reproducibility of CH_4 oxidation reactions with H_2O_2 colloidal Au-Pd nanoparticles was investigated in order to determine the standard error for reactions using this system. This was achieved by carrying out several reactions under identical conditions with samples of Au-Pd nanoparticles from the same batch. The results of these reactions are shown in table 4.1.

Table 4.1 Reproducibility of CH_4 oxidation reactions with H_2O_2 catalysed by the same batch of colloidal Au-Pd nanoparticles.

Reaction no.	Total Products (μmol)	Oxy. sel. (%)	H_2O_2 Remaining (%)
1	16.72	92	30
2	16.80	94	37
3	17.25	93	33
Average	16.93	93	33
Stand. dev.	0.29	1.0	3.5

Conditions; 1000 μmol H_2O_2, 50 °C, 30 bar CH_4, 30 min, total volume 10 ml, 1500 rpm, 7.57 μmol metal per reaction.
Colloid; 10 kDa PVP, Au: Pd = 1:1 molar ratio, PVP: metal = 1.2:1 molar ratio, [metal] = 7.57×10^{-4} M

From these results the standard deviation on the amount of products produced was calculated to be ±0.29 μmol while the standard deviation on oxygenate selectivity was ±1.0% and ±3.5% on the percentage of initial H_2O_2 remaining at the end of the reaction. As such the standard error for reactions where the same batch of colloid is being used is 2% on the total amount of products produced, 1% on selectivity towards oxygenates and 11% on the percentage of the initial H_2O_2 remaining.

The variation in activity observed between batches of colloidal nanoparticles prepared using the exact same procedure was also quantified (table 4.2). The variation observed between these reactions is significantly greater than the variation displayed between reactions using the same batch of nanoparticles. For this reason all studies reported in this work where a reaction parameter is being investigated (as opposed to a parameter associated with catalyst preparation) the same batch of colloid is used for all reaction. Between different batches of Au-Pd colloidal nanoparticles the standard error on the amount of products generated was found to be 15% while the standard error on oxygenate selectivity and the percentage initial H_2O_2 remaining was found to be 10 and 34% respectively. This variation is likely to be the result of particle growth occurring as the colloids age which has previously been observed for gold colloids.[9] As such when reporting the investigations into the effect of varying elements of the Au-Pd

colloid preparation procedure the values reported for a standard colloid are from a colloid of the same age as the other colloids tested in the study.

Table 4.2 Reproducibility of CH_4 oxidation reactions with H_2O_2 catalysed by the different batches of colloidal Au-Pd nanoparticles.

Colloid no.	Total Products (μmol)	Oxy. sel. (%)	H_2O_2 Remaining (%)
1	26.23	92	30
2	21.02	75	21
3	23.08	78	12
4	23.65	85	20
5	16.93	93	31
Average	22.18	84	23
Stand. dev.	3.48	8	8

Conditions; 1000 μmol H_2O_2, 50 °C, 30 bar CH_4, 30 min, total volume 10 ml, 1500 rpm, 7.57 μmol metal per reaction.
Colloid; 10 kDa PVP, Au: Pd = 1:1 molar ratio, PVP: metal = 1.2:1 molar ratio, [metal] = 7.57×10^{-4} M

During the course of this work the possibility of using a lower metal concentration (1.89×10^{-4} M) as the standard reaction metal concentration was considered. Using 1.89×10^{-4} M as opposed to 7.57×10^{-4} M as the standard metal concentration would eliminate the need for a rotary evaporator step in the procedure for the preparation of the colloidal nanoparticles. In addition as this colloid produced > 20 μmol of products under standard conditions, which is comparable to a typical colloid, reducing the metal concentration dramatically increases the TOF of the system (5.6 h^{-1} for a typical colloid, 21 h^{-1} for reduced metal concentration colloid). The effect of temperature on this lower metal concentration system was investigated (figure 4.1).

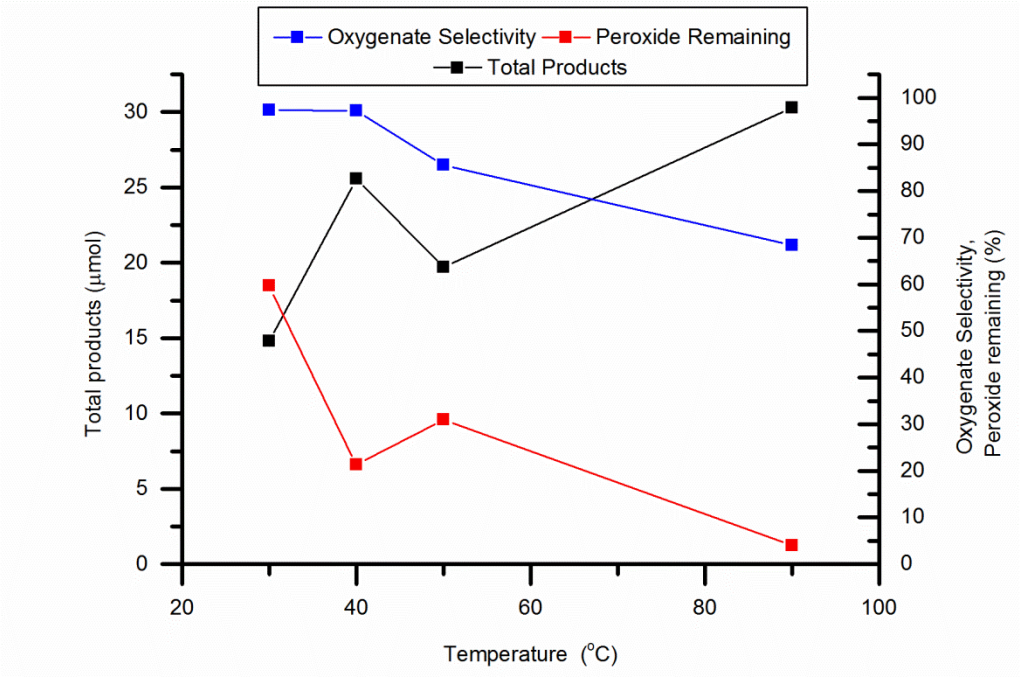

Figure 4.1 CH_4 oxidation reactions carried out at various temperatures using H_2O_2 and a Au-Pd colloid of metal concentration 1.89×10^{-4} M.

Conditions; 1000 µmol H_2O_2, 50 °C, 30 bar CH_4, 30 min, total volume 10 ml, 1500 rpm, 1.89 µmol metal per reaction.
Colloid; 10 kDa PVP, Au: Pd = 1:1 molar ratio, PVP: metal = 1.2:1 molar ratio, [metal] = 1.89×10^{-4} M

Increasing the reaction temperature from 30 to 90 °C resulted in an increase in the total amount of products generated from 14.81 to 30.30 µmol with a concurrent decrease in oxygenate selectivity from 97 to 68%. The increase in reaction temperature also resulted in a decrease in the amount of H_2O_2 remaining at the end of the reaction (from 60% at 30 °C to 4% µmol at 90 °C). These results are in keeping with the study of the effect of reaction temperature on CH4 oxidation catalysed by the 7.57×10^{-4} M Au-Pd colloid (section 4.2.3). However a greater level of irregularity was observed in catalytic activity for the reactions carried out with the colloid of reduced metal concentration.

The cause of the irregularity in these results was investigated. One explanation considered was that there may be variation in the metal concentration between aliquots of the Au-Pd colloid. To investigate this possibility the concentrating of Au in three samples of the same colloid was

quantified by ICP-AES (inductively coupled plasma atomic emission spectroscopy). Each sample was analysed to duplicate. The results of this analysis are shown in table 4.3. Minimal variation in Au concentration was detected between the aliquots. As such variation in metal concentration between samples was eliminated as the possible cause of the irregularity in catalytic activity displayed by the 1.89×10^{-4} M Au-Pd colloid.

Table 4.3 ICP-AES analysis of three aliquots of a Au-Pd Colloid

Sample no.	Au conc. (mg/L)	
	Analysis 1	Analysis 2
1	9.26	8.52
2	9.98	9.33
3	9.52	9.70

Colloid; 10 kDa PVP, Au: Pd = 1:1 molar ratio, PVP: metal = 1.2:1 molar ratio, [metal] = 1.89×10^{-4} M

The irregularity in observed catalytic activity for the 1.89×10^{-4} M Au-Pd colloid was investigated further and it was found that at this reduced metal concentration the Au-Pd colloid was less prone to collapse. It was noted that post-reaction the reaction liquid retained the colour of the original colloid and less dark residue was observed in the reaction vessel at the end of the reaction compared to reactions carried out with a colloid prepared with the standard metal concentration. As such it was not possible to completely separate the metal nanoparticles from the reaction liquid by centrifugation, this was only possible when the colloid collapsed. Therefore while the reaction liquid was awaiting analysis it still contained Au-Pd nanoparticles, H_2O_2 and a significant amount of CH_4 due to the increased CH_4 solubility caused by the presence of the PVP stabiliser. It was considered possible that CH_4 oxidation was continuing after the liquid had been removed from the reactor and prior to analysis. To investigate this possibility a sample of reaction liquid was analysed by NMR at a known time and then analysed two hours later and the results were compared, see table 4.4.

Table 4.4 Comparison of results of ^{1}H NMR analysis of the same reaction liquid of a CH_4 oxidation reaction carried out using H_2O_2 and an Au-Pd colloid of metal concentration 1.89×10^{-4} M carried out immediately after reaction and 2 hours later.

Time (min)	CH_3OH (μmol)	CH_3OOH (μmol)	Total Products (μmol)
0	0.43	1.71	2.14
120	1.14	2.00	3.14

Colloid; 10 kDa PVP, Au: Pd = 1:1 molar ratio, PVP: metal = 1.2:1 molar ratio, [metal] = 1.89×10^{-4} M

As the amount of all three oxygenated products present in the sample increased over the two hour period this confirms that for reactions catalysed by Au-Pd colloids of metal concentration 1.89×10^{-4} M CH_4 oxidation continues after removal of the reaction liquid from the reactor because the colloids are more stable. As it was not possible to routinely ensure a fixed amount of time elapsed between reaction and analysis a higher metal concentration (7.57×10^{-4} M) was employed as the standard colloid metal concentration throughout this work.

4.3 Optimisation of Reaction Parameters

In this section the results of systematic investigations into the effect of reaction conditions on the catalytic activity of the Au-Pd colloids (typically 7.57×10^{-4} M) are reported. This comprises of studies on the effect of CH_4 pressure, initial H_2O_2 concentration, reaction temperature and reactor stirring speed. The value of each parameter under which the system preforms best is determined from each of these studies and is then combined to produce a set of optimised conditions. The Au-Pd colloid system is tested under these optimised conditions and compared to the results of a reaction carried out under standard conditions.

4.3.1 Effect of Oxidant Concentration

The results of reactions which were carried out using Au-Pd colloidal nanoparticles where the initial concentration of the oxidant, H_2O_2, was varied are shown in figure 4.2.

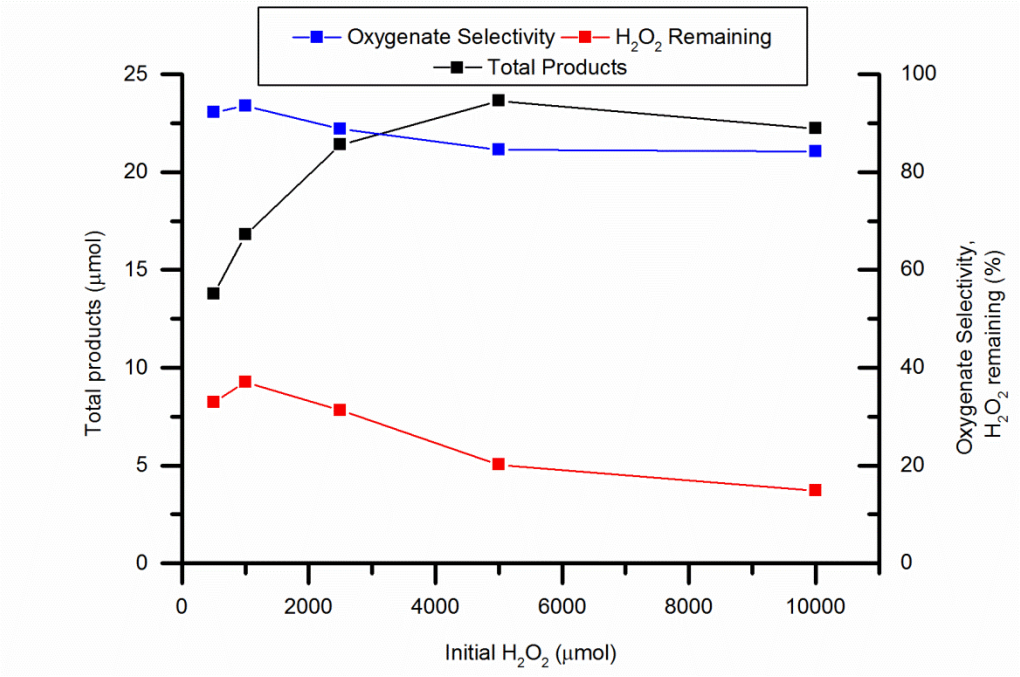

Figure 4.2 CH_4 oxidation reactions carried out using colloidal Au-Pd nanoparticles and various initial concentrations of H_2O_2.

Conditions; 50 °C, 30 bar CH_4, 30 min, total volume 10 ml, 1500 rpm, 7.57 µmol metal per reaction.
Colloid; 10 kDa PVP, Au: Pd = 1:1 molar ratio, PVP: metal = 1.2:1 molar ratio, [metal] = 7.57×10^{-4} M

As initial H_2O_2 concentration is increased oxygenate selectivity remains high (>85%) while the percentage of H_2O_2 remaining decreases from 35 to 18% across the concentrations investigated. In agreement with previous studies[12] it was found that higher initial concentrations of H_2O_2 resulted in an increase in the total amount of products produced. Increasing the initial H_2O_2 concentrations from 500 to 5000 µmol corresponded to an increase of roughly 10 µmol in the amount of products generated. Further increasing the H_2O_2 concentration did not result in any more products being produced. It was found that that increasing the initial

H_2O_2 concentration reduced the efficiency of H_2O_2 usage. The ratio of H_2O_2 consumed to products produced increased from 24 to 383 when the amount of initial H_2O_2 was increased from 500 µmol to 10,000 µmol.

4.3.2 Effect of CH_4 Pressure

A series of CH_4 oxidation reactions were carried out using colloidal Au-Pd nanoparticles where different pressures of CH_4 between 10 and 50 bar were employed for each reaction. The results of these reactions are shown in figure 4.3.

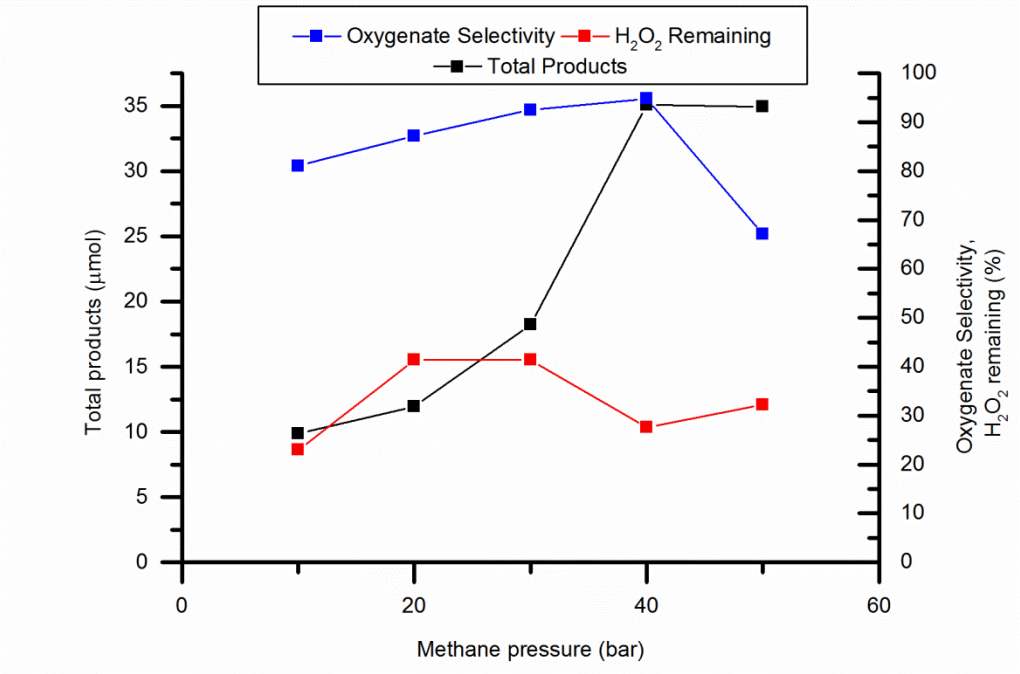

Figure 4.3 CH_4 oxidation reactions carried out using colloidal Au-Pd nanoparticles and H_2O_2 under various pressures of CH_4.

Conditions; 1000 µmol H_2O_2, 50 °C, 30 min, total volume 10 ml, 1500 rpm, 7.57 µmol metal per reaction.
Colloid; 10 kDa PVP, Au: Pd = 1:1 molar ratio, PVP: metal = 1.2:1 molar ratio, [metal] = 7.57×10^{-4} M

From these results it was found that increasing the CH_4 pressure in this system from 10 to 40 bar results in a dramatic increase from 9.86 to 35.10 µmol in the total amount of products formed. This is due to the increase in the

solubility of methane in water that results from increasing methane pressure e.g. increasing the partial pressure of methane from 1 to 50 bar increases the solubility of methane in pure water from 7.6×10^{-4} mol kg^{-1} to $4.215\times^{-2}$ mol kg^{-1} at 60 °C.[13] Oxygenate selectivity was also improved by roughly 11% by increasing the CH_4 pressure from 10 to 40 bar. This observation is consistent with previous observations that higher CH_4 pressure, and therefore greater solubility of CH_4 in water,[14] results in less over-oxidation of the primary products to CO_2.[15, 16] Increasing the CH_4 pressure from 40 to 50 bar does not result in any increase in the amount of products produced but causes a considerable and unexpected shift in product distribution to CO_2. This is not observed in the supported system.[17] As it was found in chapter 3, section 3.5 that CH_4 causes the Au-Pd colloid to collapse and the resulting precipitate is inactive for CH_4 oxidation it is possible that this drop in selectivity is the related to an increase in instability as the CH_4 pressure is increased. If a greater amount of metal precipitates earlier in the reaction this would lead to the colloid becoming inactive during the reaction such that over-oxidation continues without further formation of primary products thus causing a shift in product distribution to CO_2. Overall H_2O_2 decomposition remained constant within experimental error for the duration of the study such that H_2O_2 utilisation is greatly improved at higher pressures.

4.3.3 Effect of Reaction Temperature

In order to investigate the effect of temperature on the Au-Pd colloidal system a series of reactions were carried out at various temperatures ranging from 5 to 90 °C (figure 4.4). An increase in the amount of total products generated by the system from 4.5 to 28.5 μmol was observed upon raising the reaction temperature from 5 to 90 °C. However this increase in reaction temperature also caused a substantial drop in the selectivity of the system to the desired oxygenated products from 87% at 5 °C to only 40% at 90 °C. This is caused by the increased rate of over-oxidation of the other reaction products to CO_2 which has been previously observed in CH_4 oxidation reactions when reaction temperature is increased.[17] Increasing the reaction temperature also

resulted in an increased rate of H_2O_2 decomposition with no residual H_2O_2 being detected at temperatures above 70 °C after 30 min.

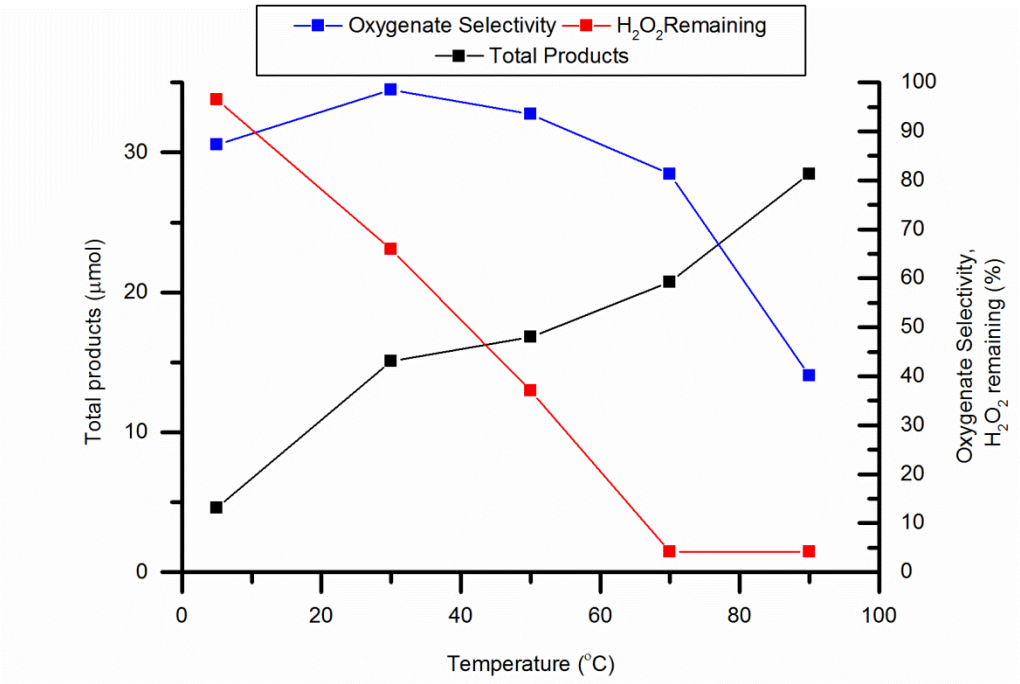

Figure 4.4 CH_4 oxidation reactions carried out at various temperatures using colloidal Au-Pd nanoparticles and H_2O_2.

Conditions; 1000 µmol H_2O_2, 30 bar CH_4, 30 min, total volume 10 ml, 1500 rpm, 7.57 µmol metal per reaction.
Colloid; 10 kDa PVP, Au: Pd = 1:1 molar ratio, PVP: metal = 1.2:1 molar ratio, [metal] = 7.57×10^{-4} M

4.3.4 *Effect of Stirring Rate*

Figure 4.5 shows the results of CH_4 oxidation reactions carried out with colloidal Au-Pd nanoparticles where a range of different stirring speeds were employed. An increase in the rate of H_2O_2 decomposition was observed as the stirring speed was increased from 250 to 1500 rpm. Nearly 40% of the initial H_2O_2 remained at the end of the 30 min reaction when the stirring speed was set to 250 rpm whereas only 10% remained at the end of the reaction which was stirred at a speed of 1500 rpm. Increasing the stirring speed from 250 to 500 rpm caused a moderate drop in the amount of products produced (27 to 20 µmol). No significant change in the amount of products produced was observed upon

subsequent increase of stirring speed. No clear trend was observed for the effect of stirring speed on oxygenate selectivity which varied between 76 to 90% over the course of the study. These results imply that the reaction is not mass transport limited.

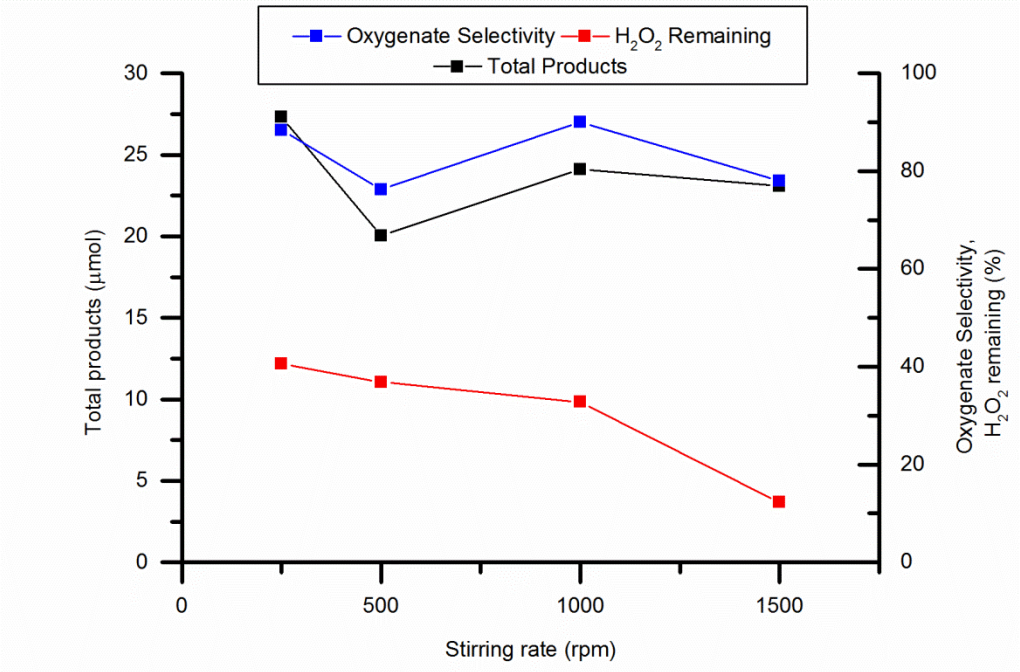

Figure 4.5 CH_4 oxidation reactions carried out using colloidal Au-Pd nanoparticles and H_2O_2 where the system was subjected to various stirring speeds.

Conditions; 1000 µmol H_2O_2, 50 °C, 30 bar CH_4, 30 min, total volume 10 ml, 7.57 µmol metal per reaction.
Colloid; 10 kDa PVP, Au: Pd = 1:1 molar ratio, PVP: metal = 1.2:1 molar ratio, [metal] = 7.57×10^{-4} M

4.3.5 Optimised Reaction Conditions

Once the optimum value for each reaction parameter was determined a reaction was carried out using a standard Au-Pd colloid where these conditions were combined in order to enhance the activity of the nanoparticles. The aim of this experiment was to maximise the activity of the Au-Pd nanoparticles while maintaining high selectivity to the desired oxygenated products and low hydrogen peroxide consumption. In this way the extent/limit of the catalysts ability to oxidise methane with hydrogen peroxide was investigated. The

optimum reaction conditions determined from this investigation were found to be; initial H_2O_2 = 5000 μmol, reaction temperature = 60 °C, CH_4 pressure = 40 bar and stirring speed = 1000 rpm. Table 4.5 shows the results of this reaction compared with a reaction carried out under previously used standard conditions.

Table 4.5 Comparison of standard and optimised reaction conditions for CH_4 oxidation with H_2O_2 and colloidal Au-Pd nanoparticles.

Conditions	Product amount (μmol)				Oxy. sel. (%)	TOF (h^{-1})	Prod. (mol kg^{-1} h^{-1})	H_2O_2 / Products
	CH_3OH	CH_3OOH	HCOOH	CO_2				
Standard	3.19	9.76	7.04	3.09	86	5.4	35	36
Optimised	11.00	13.86	9.57	8.11	81	11	74	110

Standard Conditions; 1000 μmol H_2O_2, 50 °C, 30 bar CH_4, 30 min, total volume 10 ml, 1500 rpm, 7.57 μmol metal per reaction.
Optimised Conditions; 5000 μmol H_2O_2, 60 °C, 40 bar CH_4, 30 min, total volume 10 ml, 1000 rpm, 7.57 μmol metal per reaction.
Colloid; 10 kDa PVP, Au: Pd = 1:1 molar ratio, PVP: metal = 1.2:1 molar ratio, [metal] = 7.57×10^{-4} M

These results show that under optimised conditions, the colloidal Au-Pd particles can produce 42.5 μmol of products while maintaining a high selectivity to oxygenated products of 81% as compared to 16.8 μmol of products under the initial standard conditions. This procedure of optimizing the individual reaction parameters resulted in the colloidal system achieving a TOF of 11.2 h^{-1}, over double the TOF under standard conditions. However oxidant usage was found to be less efficient under the optimised conditions with the ratio of H_2O_2 consumed to products produced increasing from 36 to 110 compared to a reaction carried out under standard conditions. This is in line with the results from the study on the effect of initial H_2O_2 concentration where it was found that increasing the initial H_2O_2 concentration reduces the efficiency of H_2O_2 usage.

4.4 Effect of Catalyst Preparation

In order to better understand the Au-Pd colloid system the effect on catalytic activity of altering various parameters involved in the preparation of colloidal Au-Pd nanoparticles was investigated. In this section the results of CH_4 oxidation

reactions with H_2O_2 are reported for various Au-Pd colloids which were prepared by the sol method but each with a specific variation to the standard procedure described in chapter 2, section 2.4.1. In this way the effect of several catalyst preparation variables was determined. The effect of varying the ratio of stabilising ligand, PVP, to metal is dealt with it in detail in the next section, 4.5.

4.4.1 Investigation into the Effect of Au: Pd

A series of colloids were prepared with different Au: Pd molar ratios. The results of CH_4 oxidation reactions carried out under standard conditions using these colloids are displayed in figure 4.6

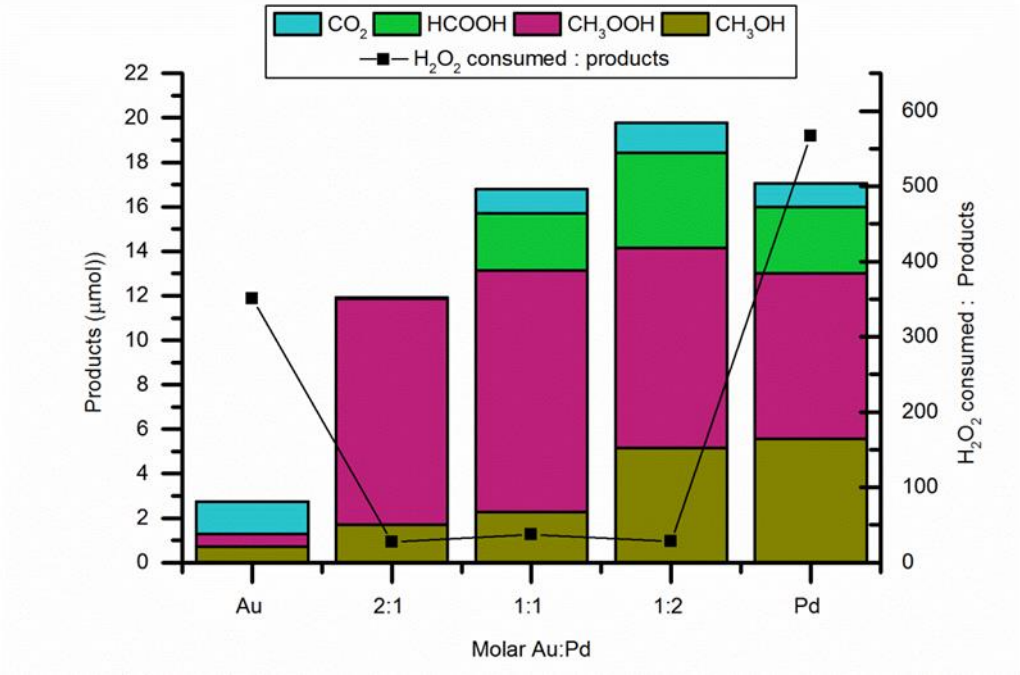

Figure 4.6 Effect of Au: Pd molar ratio on catalytic activity of Au-Pd colloid for CH_4 oxidation reactions with H_2O_2.

Conditions; 1000 µmol H_2O_2, 50 °C, 30 bar CH_4, 30 min, total volume 10 ml, 1500 rpm, 7.57 µmol metal per reaction.
Colloid; 10 kDa PVP, PVP: metal = 1.2:1 molar ratio, [metal] = 7.57×10^{-4} M

As previously discussed in chapter 3 the monometallic Au and Pd colloids exhibited significantly higher H_2O_2 usage when compared to their bimetallic counterparts. The ratio of H_2O_2 consumed to products generated decreases

dramatically from 570 for the monometallic Pd colloid to 40 for the bimetallic Au-Pd colloid prepared with equimolar amounts of Au and Pd. This shows that, as previously reported, the addition of Au to the Pd nanoparticles is essential to reduce the rate of H_2O_2 decomposition and improve the usage of activated H_2O_2.[18, 19] The reaction carried out with the Au-Pd colloid prepared with a 1:2 molar ratio of Au: Pd generated the most products in the study. However when compared with the standard colloid with a 1:1 molar ratio of Au: Pd the product distribution is sifted towards formic acid (22% for 1:2 Au: Pd compared with 15% for 1:1 Au: Pd).

It has previously been reported that varying the Au to Pd ratio of bimetallic nanoparticles can affect the structure of the nanoparticle. Prati *et al*. have reported that when preparing Au-Pd nanoparticles by a two-step method (first $HAuCl_4$ is reduced with $NaBH_4$ then $PdCl_2$ is reduced with hydrogen) varying the Au: Pd ratio has limited effect on particle size but significant variation is observed in particle morphology.[20] Well alloyed nanoparticles were found to have large (111) surface areas and Au rich nanoparticles tended to be multiply twinned with exposed (111) and (100) surfaces. The Pd rich particles by contrast tended to be irregular in shape and not multiply twinned.

In this study it was found that Pd-rich colloids produce a greater amount of products while maintaining a high selectivity towards oxygenated products. Whereas Au-rich colloids display improved selectivity towards the desired oxygenated products CH_3OH and CH_3OOH but generate less total products per reaction. It was also noted that the addition of Au to the Pd colloid that monometallic enhanced the stability of the colloid. Pd colloids were notably less stable than both the bimetallic and monometallic Au colloids. Monometallic Pd colloids were observed to re-oxidise within the a few hours after preparation unless prepared and stored under N_2 whereas neither the bimetallic nor Au colloids were observed to re-oxidise at any point during the course of this work.

4.4.2 Core-shell Colloids

Typical preparation procedure for the Au-Pd colloids involves simultaneous reduction of the Au and Pd chloride precursors in order to form alloyed metal nanoparticles. Core-shell bimetallic nanoparticles can also be prepared by the sol method by first reducing the core metal and then subsequent reduction of the shell metal so that one metal (the shell) coats the outside of the other (the core).[21, 22] Using this method nanoparticles of one method are formed first and then act as nucleation seeds for the deposition of the second metal. For example to prepare a Pd(Au) (Pd shell with an Au core) colloid an aqueous solution of PVP and $HAuCl_4$ is prepared with the same amounts of $HAuCl_4$ and PVP used in a typical colloid preparation. Half the standard total amount of $NaBH_4$ is then added to reduce the gold. After 30 min of stirring $PdCl_2$ is added in the same quantity that is used in a standard preparation and the Pd is reduced with an amount of $NaBH_4$ equal to that used to reduce the Au. In this way the second metal uses the first to nucleate and two separate layers of metal are formed.

By this method both Au(Pd) and Pd(Au) colloidal nanoparticles were prepared. In order to determine their particle size distributions TEM analysis was carried out at Lehigh University on samples of both of these colloids. Representative TEM images and particle size distribution of the Pd(Au) colloid is shown in figure 4.7 and the same is shown in figure 4.8 of the Au(Pd) colloid.

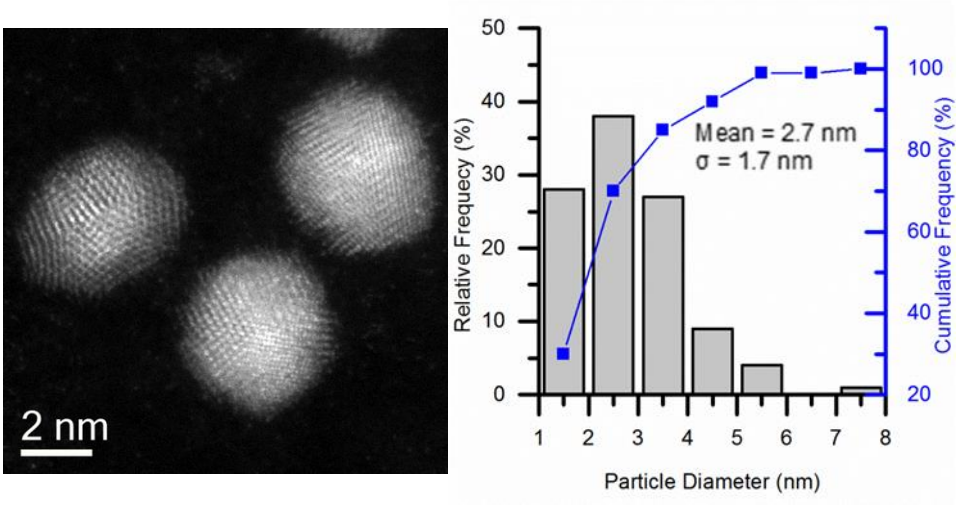

Figure 4.7 TEM images and particle size distribution of Pd(Au) colloidal nanoparticles.

Colloid; 10 kDa PVP, Au :Pd = 1: 1,PVP: metal = 1.2:1 molar ratio, [metal] = 7.57×10^{-4} M

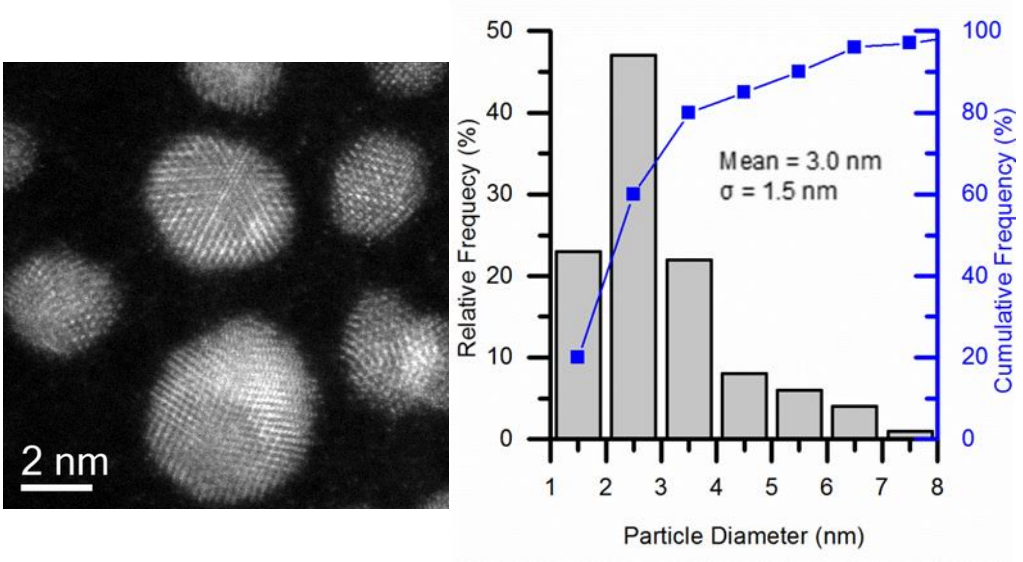

Figure 4.8 TEM images and particle size distribution of Au(Pd) colloidal nanoparticles.

Colloid; 10kDa PVP, Au :Pd = 1: 1,PVP: metal = 1.2:1 molar ratio, [metal] = 7.57×10^{-4} M

Both colloids were found to have a narrow particle size distribution which is typical for nanoparticles prepared by the sol method. The average particle diameter of the Pd(Au) colloid was found to be 2.7 nm while the Au(Pd) colloid

displayed an average particle size of 3.0 nm. These average particle sizes are comparable to that of the standard colloid prepared with alloyed Au-Pd nanoparticles, 3.0 nm. In addition to the particle size distribution the composition of a selection of nanoparticles was also analysed. High angle annular dark field (HAADF) STEM imaging was used to study the elemental segregation of the Au and Pd components within the colloidal nanoparticles. This was achieved through examination of the atomic mass (z-) contrast which is inherent to HAADF imaging. As HAADF images are formed from the incoherently scattered electrons they are sensitive to variations in the number of atoms in the sample hence the z-contrast. It was found that in both the Au(Pd) and Pd(Au) samples in addition to the core-shell nanoparticles a significant proportion of nanoparticles were homogeneous alloys. A smaller number of particles were identified as half and half Au-Pd hetero-junctions. This was not observed in previous studies of core-shell Au-Pd nanoparticles prepared by sol-immobilisation.[21-23] Those studies, however, used PVA to stabilise the nanoparticles where in this study PVP was used. The binding of PVP to the nanoparticle is stronger than that of PVA which illustrated by the fact that PVA can be easily refluxed off a catalyst surface.[24] This stronger binding of PVP to the metal nanoparticles is the result of electron donation from to PVP to the metal nanoparticles. These TEM results would suggest that PVP interferes with the nucleation of the second metal such that core-shell nanoparticles are not reliably formed. To understand the reason for this the mechanism of formation of the nanoparticles would need to be investigated. In situ TEM could be used to observe the shape, size and number of the formed nanoparticles and/or in situ x-ray absorption near edge spectroscopy (XANES) could provide information on the oxidation state of the particulate metals.

CH_4 oxidation reactions were carried out with H_2O_2 using both of the colloids prepared by the core-shell method and the results were compared to that of a standard Au-Pd colloid (figure 4.9).

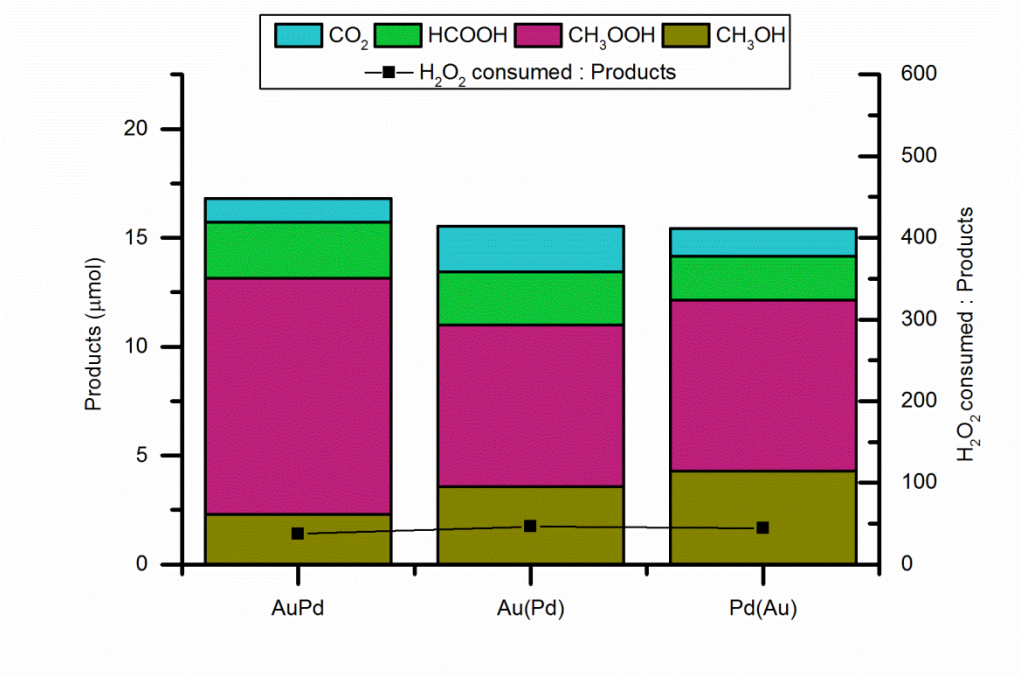

Figure 4.9 Comparison of the catalytic activity of alloyed and core-shell Au-Pd nanoparticles for the oxidation of CH_4 with H_2O_2

Conditions; 1000 µmol H_2O_2, 50 °C, 30 bar CH_4, 30 min, total volume 10 ml, 1500 rpm, 7.57 µmol metal per reaction.
Colloid; 10 kDa PVP, Au :Pd = 1: 1,PVP: metal = 1.2:1 molar ratio, [metal] = 7.57×10^{-4} M

The results of all three reactions were comparable in terms of total amount of products produced, product distribution and H_2O_2 usage. All three colloids produced roughly 16 µmol of products and displayed an oxygenate selectivity of over 80%. The ratio of H_2O_2 consumed to products produced was below 50 for the each of the three reactions. Taking into consideration the variation in activity observed between batches of colloid (discussed in section 4.2) it is clear that preparing the metal nanoparticles by the core-shell procedure has minimal effect on the activity of the final colloid. This is likely caused by the fact that a significant proportion of the nanoparticles present in the colloidal samples are not core-shell.

4.4.3 Effect of Metal Concentration

An investigation into the effect of metal concentration on the results of CH_4 oxidation reactions with H_2O_2 using colloidal Au-Pd nanoparticles was carried out (figure 4.10).

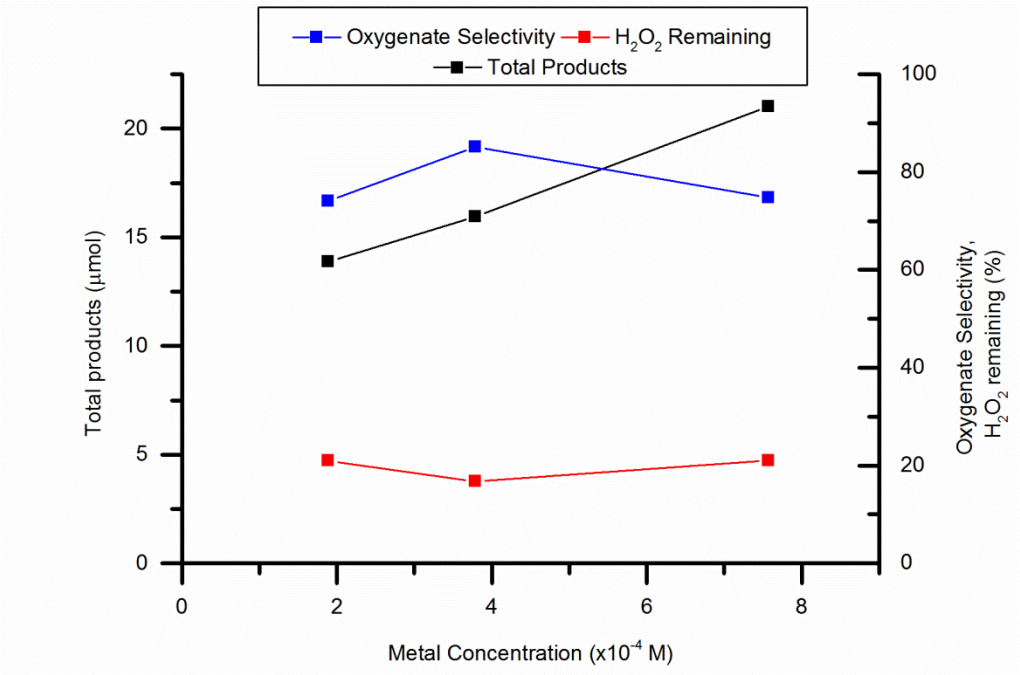

Figure 4.10 CH_4 oxidation reactions carried out with H_2O_2 and Au-Pd colloids of various metal concentrations

Conditions; 1000 µmol H_2O_2, 50 °C, 30 bar CH_4, 30 min, total volume 10 ml, 1500 rpm. Colloid; 10 kDa PVP, Au: Pd = 1:1 molar ratio, PVP: metal = 1.2:1 molar ratio.

Samples of a typical Au-Pd colloid ([metal] = 7.57×10^{-4} M) were diluted to 3.79×10^{-4} M and 1.89×10^{-4} M and were used to carry out CH_4 oxidation reactions. It was considered preferable to dilute a standard colloid rather than prepare new colloids with different metal concentrations to avoid any possible effects that altering the metal concentration during nanoparticle preparation might have on particle size or composition. The results of the reactions carried out with the dilute colloids are shown in figure 4.10. As shown in the graph changing the metal concentration in the reactor has minimal effect on both H_2O_2 consumption and on the selectivity towards oxygenated products. The amount of total

products produced however appears to increase linearly with metal concentration. The reaction with a metal concentration of 1.89×10^{-4} M produced 18 μmol of products. This figure increased to 23 μmol of products when the metal concentration was increased to 7.57×10^{-4} M.

These results are contrary to the results reported on CH_4 oxidation with H_2O_2 using Au-Pd/TiO_2 prepared by impregnation.[15] In that work it was found that the total amount of products generated did not increase linearly with metal concentration. In fact increasing the metal loading on the TiO_2 from 1wt% to 5wt% caused a drop in TOF from 6.85 h-1 to 0.77 h-1. This was shown to be caused by an increase in H_2O_2 consumption caused by the increase in the amount of metal in the reactor. This is not the case in the colloidal system as H_2O_2 consumption remains stable regardless of the change in metal concentration. As such in the colloidal system the TOF actually increases from 5.5 h^{-1} to 14 h^{-1} when the metal concentration is dropped from 7.57×10^{-4} M to 1.89×10^{-4} M.

4.4.4 Effect of Chloride

In the previous section the effect of metal concentration on the activity of Au-Pd colloids for CH_4 oxidation was investigated. As the colloidal metal nanoparticles are prepared using chloride metal precursors changing the metal concentration by diluting a Au-Pd colloid will also cause a change in the chloride concentration. As such it was necessary to also investigate the effect of chloride concentration on the activity of the colloidal nanoparticles to ensure that any change in activity caused by the diluting the colloid was indeed the result of the change in metal and not chloride concentration. With this aim in mind reactions were carried out with a standard Au-Pd colloid where various amounts of NaCl were added to the reactor (figure 4.11).

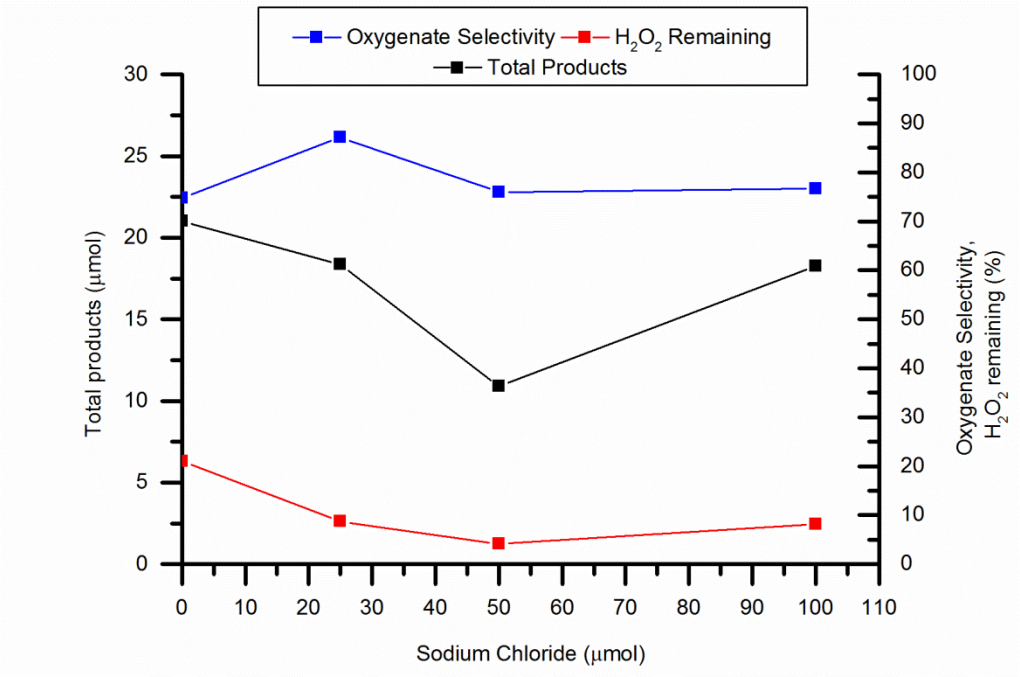

Figure 4.11 CH_4 oxidation reactions carried out with H_2O_2 and Au-Pd colloidal nanoparticles where various amounts of NaCl were added to the reactor.

Conditions; 1000 µmol H_2O_2, 50 °C, 30 bar CH_4, 30 min, total volume 10 ml, 1500 rpm, 7.57 µmol metal per reaction.
Colloid; 10 kDa PVP, Au: Pd = 1:1 molar ratio, PVP: metal = 1.2:1 molar ratio, [metal] = 7.57×10^{-4} M

The pH of the Au-Pd colloid was measured before and after addition of 100 µmol of NaCl, it was found to vary from 2.20 to 2.01 when the NaCl was added. H_2O_2 consumption and selectivity to oxygenated products remained stable throughout the investigation. It was hypothesised that Cl may stabilise the H_2O_2 during reaction as this effect of Cl is well documented in the literature.[25] However, this was not found to be the case in this study as the variation observed in the percentage of H_2O_2 remaining was minimal (4 -8%). Only a slight variation in oxygenate selectivity was observed (75-87%). This result indicates that the addition of NaCl to the reactor does not have a significant effect on colloid stability. An increase in colloid instability would have resulted in more rapid agglomeration of Au-Pd nanoparticles hindering the further generation of products. As over-oxidation of the already formed products continues without the generation of more products the products distribution would shift towards

CO_2. As this is not observed in this study it can be concluded that colloid stability has not been effected by the addition of NaCl. No clear trend was observed for the total amount of products generated as chloride concentration increased. Reactions carried out with 0, 25 and 100 μmol of NaCl added to the reactor produced similar amount of products while the reaction carried out with 50 μmol of added NaCl produced roughly half the amounts of products formed by the other reactions. Overall it is clear that increasing the chloride concentration in this system does not have a beneficial effect on the activity of the Au-Pd nanoparticles. From these results it can be concluded that the increase in the amount of products produced upon increasing the metal concentration for this system (section 4.4.3) is not the caused by the concurrent increase in chloride concentration.

4.4.5 Effect of PVP Molecular Weight

Three Au-Pd colloids were prepared by the sol method, as described in chapter 2, with the standard metal concentration of 7.57 ×10-4 M using various molecular weights of PVP (3.5, 40 and 360 kDa).

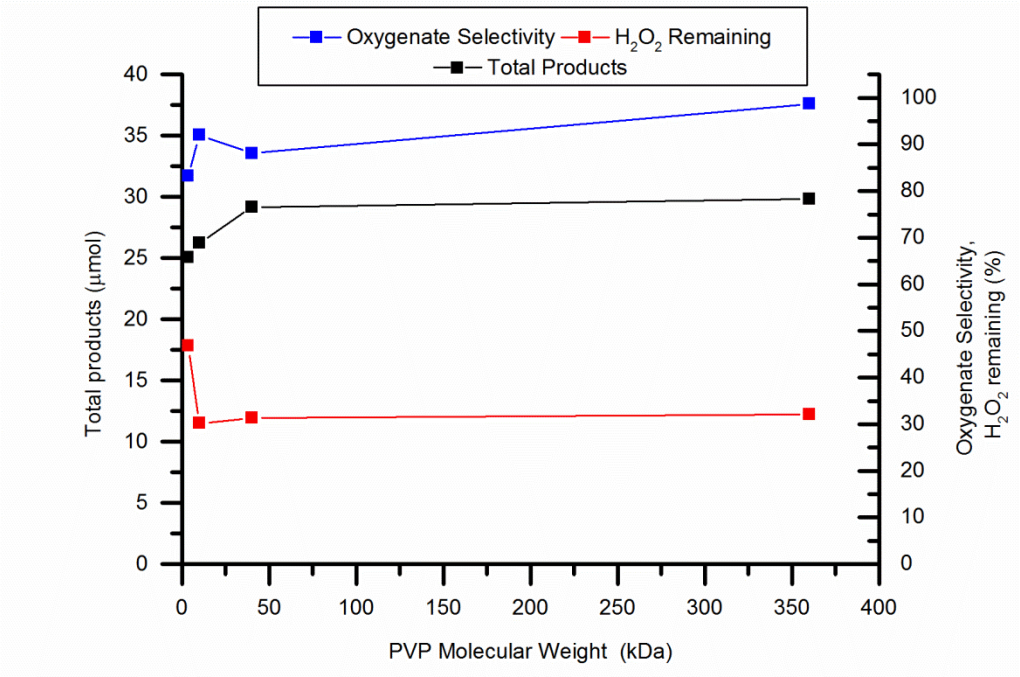

Figure 4.12 Effect of PVP molecular weight on catalytic activity of Au-Pd colloidal nanoparticles for the oxidation of CH_4 with H_2O_2.

Conditions; 5000 µmol H_2O_2, 50 °C, 30 bar CH_4, 30 min, total volume 10 ml, 1500 rpm, 7.57 µmol metal per reaction.
Colloid; Au: Pd = 1:1 molar ratio, PVP: metal = 1.2:1 molar ratio, [metal] = 7.57×10^{-4} M

CH_4 oxidation reactions were carried out under standard conditions using these colloids and H_2O_2 as the oxidant (figure 4.12). The results of these reactions were compared with a reaction catalysed with an Au-Pd colloid prepared with PVP of molecular weight 10 kDa, the typical PVP size used throughout this work. The results of these reactions are shown in figure 4.12. A slight increase in the amount of products produced was observed as PVP molecular weight was increased. Increasing the PVP size from 3.5 to 40 kDa results in an increase in total products of 10 µmol however increasing the PVP size from 40 to 360 kDa only produced an extra 2 µmol of products. Oxygenate selectivity is also favourably affected by the increase in molecular weight of the stabilising ligand. Although again it is only a very moderate improvement from 85 to 98% considering the PVP size is increasing by two orders of magnitude from 3.5 to 360 kDa. H_2O_2 consumption is unaffected by changes in PVP size from 10 to 360

kDa although the 3.5 kDa colloid consumed 20% less oxidant than the other colloids tested.

Overall these results show that varying the PVP molecular weight used for colloid preparation has only a modest effect on the activity of the colloidal nanoparticles for CH_4 oxidation. It was noted in chapter 3 that a colloid prepared with 360 kDa PVP had slightly increased stability compared to the standard colloid (10 kDa PVP) i.e. the 360 kDa PVP colloid did not collapse under 5 bar CH_4. It is therefore possible that the improvement in activity observed with increased PVP size may be brought about by enhanced stability as more oxygenated products are likely to be produced if particle agglomeration is reduced.

4.5 Effect of PVP: metal

Studies published on metal nanoparticles prepared using a stabilising ligand have shown that the size of nanoparticles formed can be controlled by varying the ratio of metal to stabiliser during preparation.[3, 4, 26] In order to investigate the effect of particle size on the Au-Pd colloidal system the PVP to metal weight ratio was manipulated so that colloids with differing average nanoparticle sizes were produced. Au-Pd colloids were prepared with PVP to metal ratios of 0.05, 0.1, 5, 10 and 20 and compared to a standard Au-Pd colloid with a PVP to metal ratio of 1.2. Varying the PVP to metal weight ratio can also affect the stability and shielding of the metal nanoparticles. Increasing the amount of stabiliser used to prepare colloidal nanoparticles relative to the amount of metal employed is likely to increase the stability of the final colloid and *vice versa*. However it has been reported that when steric stabilisers, such as PVP, are employed in colloid preparation catalytic activity can be negatively affected due to steric hindrance of the active sites.[9, 27] Therefore increasing the amount of PVP relative the amount of metal used to prepare the colloid could result in a drop in activity. However in the system under investigation PVP has been shown to increase the solubility of methane in water thus promoting the reaction it is therefore possible that in this

case increasing the PVP: metal ratio may improve the activity of the system by increasing the amount of methane that can access the metal surface.

All colloids prepared with various ratios of PVP to metal were analysed by TEM to quantify the variations in particle size. Further characterisation was carried out by UV-vis spectroscopy and XPS on the colloids with PVP to metal ratios of 0.005, 0.1 and 20 with the aim of identifying any disparity with the standard Au-Pd colloid in terms of nanoparticle composition. CH_4 oxidation reactions were carried out using the various colloids with the aim of investigating the effect of particle size on catalyst activity.

4.5.1 Characterisation of Au-Pd Nanoparticles with Various PVP: Metal by TEM

TEM analysis of the colloidal Au-Pd nanoparticles confirmed that varying the ratio of PVP to metal in the preparation of the colloidal nanoparticles altered the size of nanoparticles generated (figure 4.14). It was found that reducing the amount of stabilising ligand employed resulted in an increase in nanoparticle size and *vice versa* (figure 4.13).

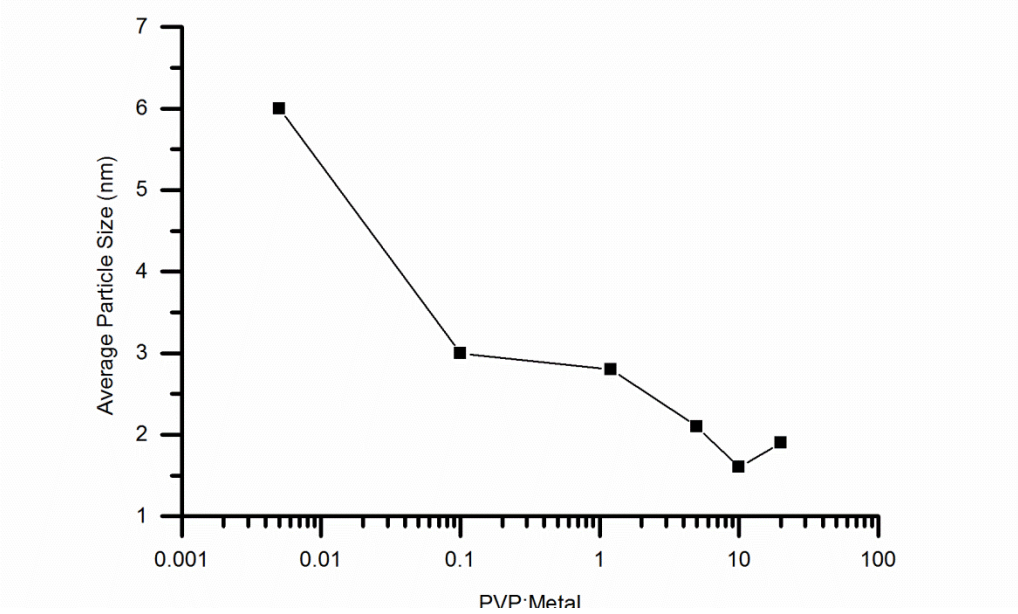

Figure 4.13 Effect of PVP: metal weight ratio on particle size of Au-Pd nanoparticles prepared by the sol method.

(a)

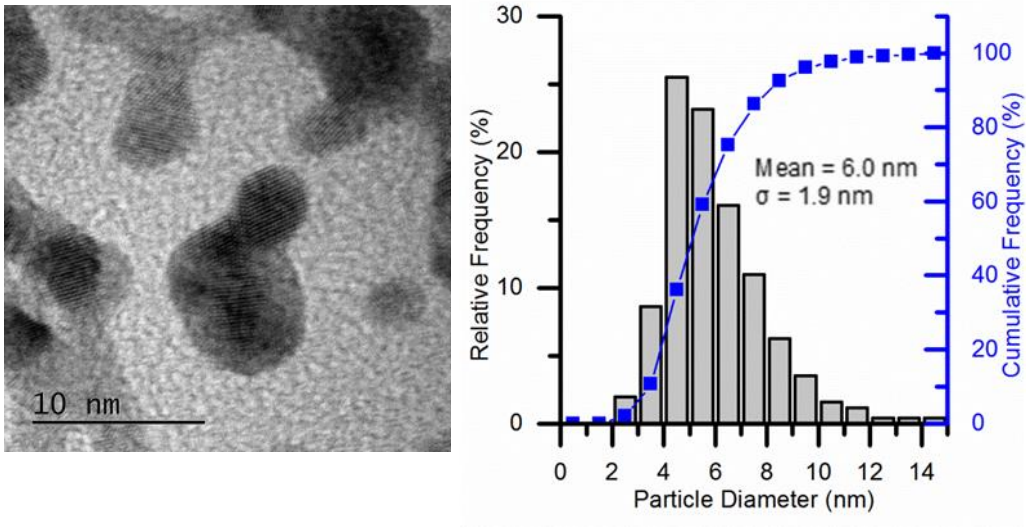
10 nm
Mean = 6.0 nm
σ = 1.9 nm
Relative Frequency (%)
Cumulative Frequency (%)
Particle Diameter (nm)

(b)

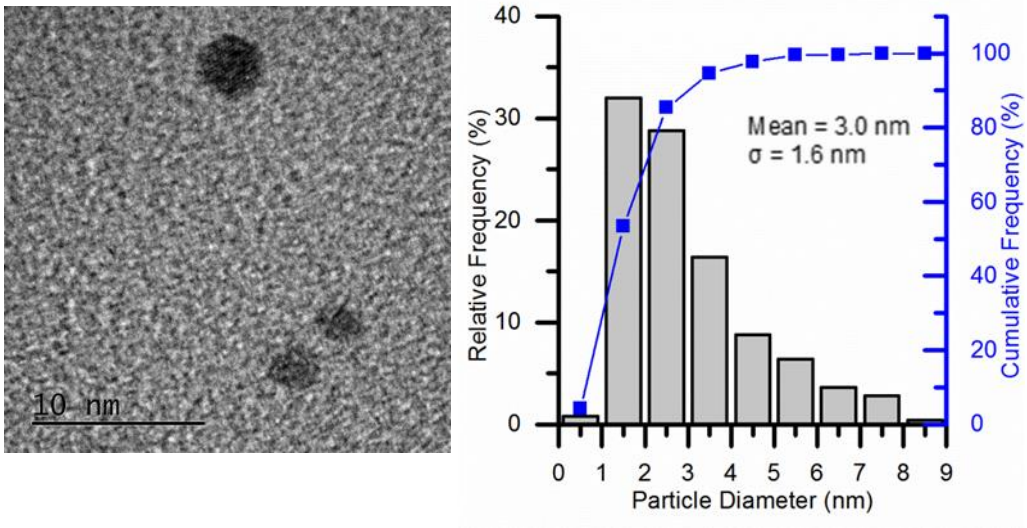
10 nm
Mean = 3.0 nm
σ = 1.6 nm
Relative Frequency (%)
Cumulative Frequency (%)
Particle Diameter (nm)

(c)

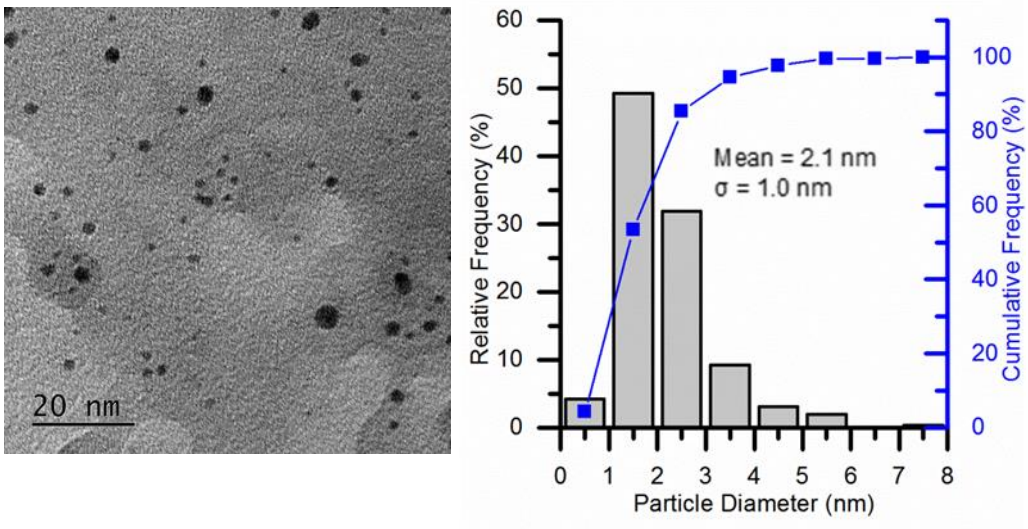
20 nm
Mean = 2.1 nm
σ = 1.0 nm
Relative Frequency (%)
Cumulative Frequency (%)
Particle Diameter (nm)

(d)

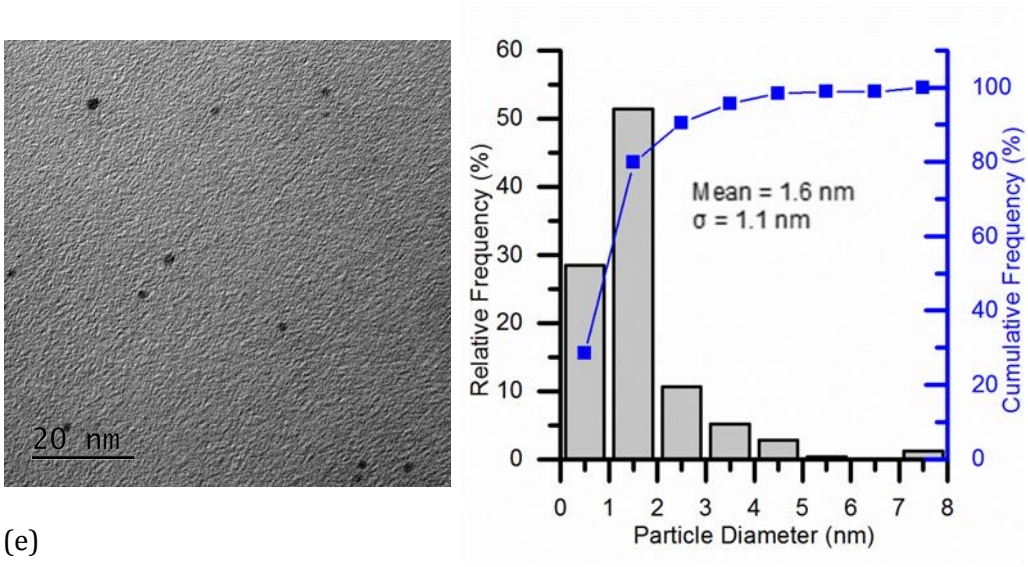

(e)

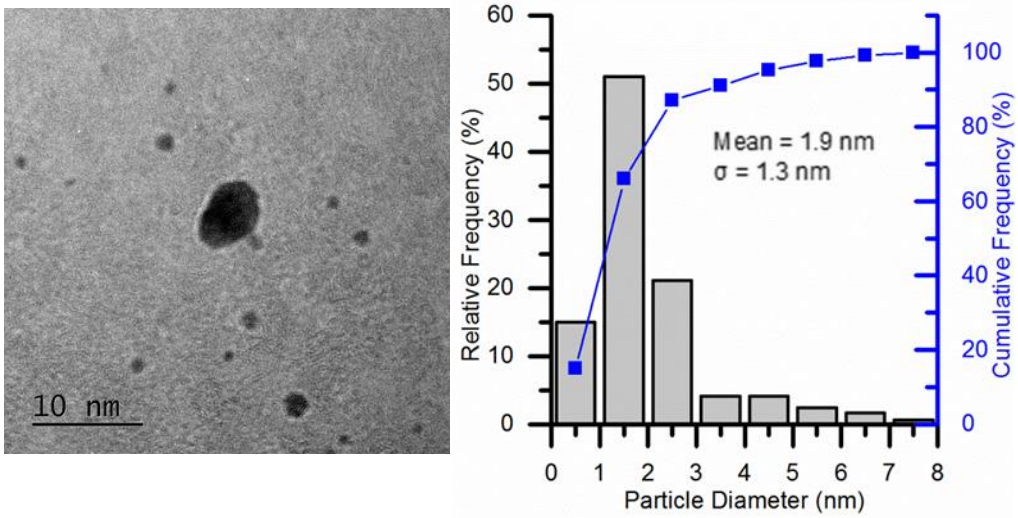

Figure 4.14 TEM images and particle size distributions for colloidal nanoparticles prepared with various weight ratios of PVP: metal; (a) 0.005, (b) 0.1,(c) 5, (d) 10, (e) 20.

Colloid; 10 kDa PVP, Au: Pd = 1:1 molar ratio, molar ratio, [metal] = 7.57×10^{-4} M

This trend is in line with literature reports on the preparation of metal nanoparticles with a stabilising ligand.[3, 4, 26] Nanoparticles with an average diameter of 6.0 nm were formed when a colloid was prepared with a PVP: metal of 0.005 whereas using a PVP: metal ratio of 20 created nanoparticles with an average diameter of 1.9 nm. All samples of colloidal nanoparticles analysed displayed a narrow, mono-modal particle size distribution as is to be expected

when preparing nanoparticles by the sol method.[7, 21] Although nanoparticles prepared with a PVP-metal ratio of 0.005 had a slightly wider particle size distribution compared to the other colloids with particles ranging in size from 2 to 14 nm when a particle size range of < 9 nm was observed for the other Au-Pd colloids.

4.5.2 Characterisation of Au-Pd Nanoparticles with Various PVP: Metal by XPS

XPS analysis was carried out on colloids prepared with PVP: metal ratios of 0.005, 0.1 and 20 (figure 4.15).

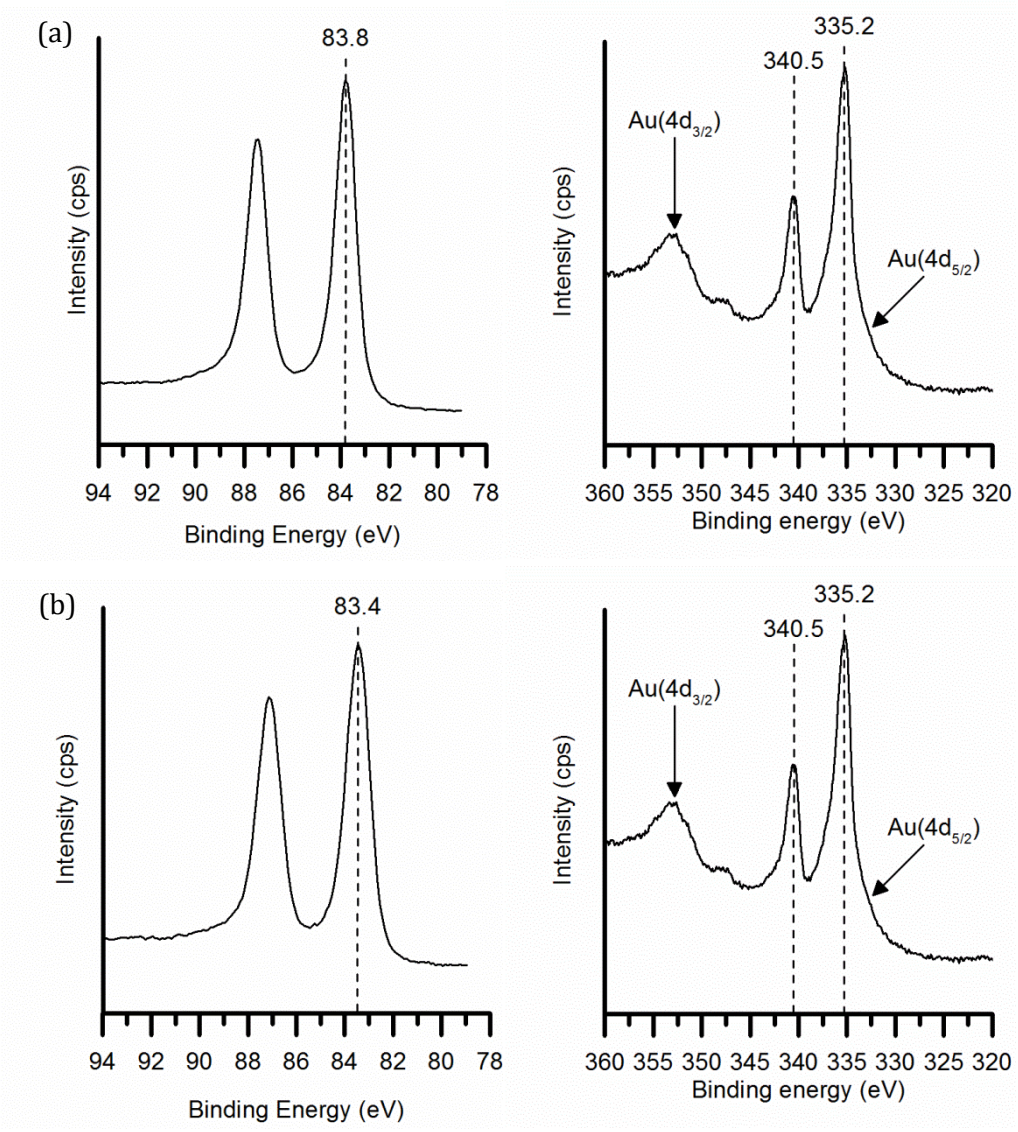

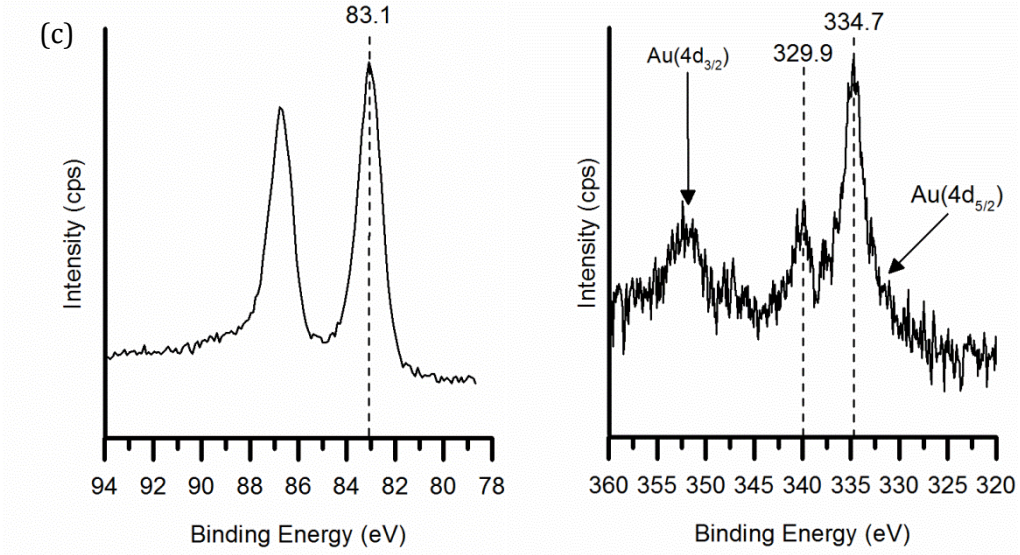

Figure 4.15 Au(4f) and Pd(3d)/Au(4d) XPS spectra of samples of Au-Pd colloids prepared using PVP: metal of weight ratios (a) 0.005, (b) 0.1 and (c) 20.

Colloid; 10 kDa PVP, Au: Pd = 1:1 molar ratio, [metal] = 7.57×10^{-4} M.

All Au-Pd colloid samples analysed showed that both the Au and the Pd are in the metallic oxidation state. This is in agreement with the XPS analysis carried out on the standard Au-Pd colloid prepared with a PVP: metal of 1.2. Furthermore these sample show interaction between the Au and Pd as observed in the standard colloid. Electron transfer between the metals is indicated by the shift in binding energies compared to the monometallic colloid samples analysed in chapter 3. The Au(4f) is shifted from 84.0 eV to ~83.4 eV and the Pd(3d) peak is shifted from 335.7 eV to ~335.0 eV. The presence of the elements sodium, chloride and boron were also observed during the analysis of all colloid samples. These elements originate from the chloride metal precursors and reducing agent, $NaBH_4$ used in the preparation of the nanoparticles (see chapter 2, section 2.4.1 for full preparation procedure). It was noted that the XPS spectrum of the Au-Pd colloid prepared with a PVP: metal of 20 was particularly noisy; this is likely caused by the high level of PVP present on the surface of the metal.

4.5.3 Characterisation of Au-Pd Nanoparticles with Various PVP to Metal Ratios by UV-vis Spectroscopy

Au-Pd colloids prepared with PVP: metal ratios of 0.005, 0.1 and 20 were analysed using UV-vis spectroscopy. The spectra generated (figure 4.16) confirmed that, like the Au-Pd colloid with a PVP: metal of 1.2, the nanoparticles formed using these PVP: metal of 0.005, 0.1 and 20 are composed of alloyed Au and Pd.

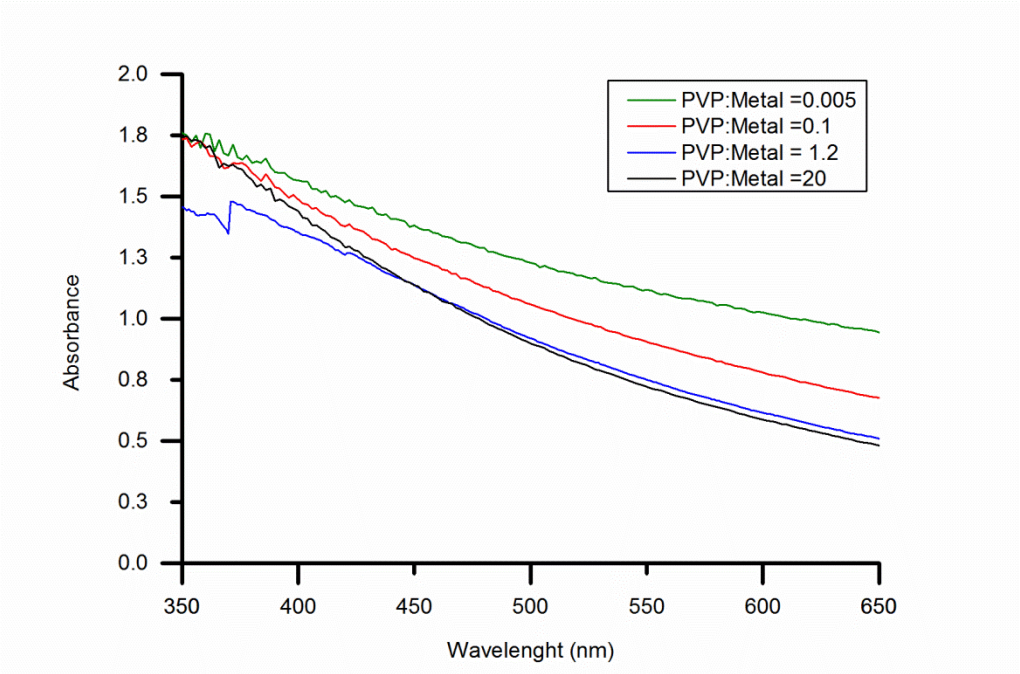

Figure 4.16 UV-vis spectra of samples of Au-Pd colloids prepared using various PVP: metal weight ratios.

Colloid; 10 kDa PVP, Au: Pd = 1:1 molar ratio, [metal] = 7.57×10^{-4} M.

This was determined based on the observed absence of a plasmon band in the 500 to 550 nm region.[28, 29] The presence of a plasmon band in this region would have indicated the presence of monometallic Au nanoparticles this is not however observed when Au is alloyed to Pd (for further details see chapter 3 section 3.3.1). Overall there is very little difference in the UV-vis spectra of the four colloids indicating that particle size is the only changing factor.

4.5.4 CH_4 Oxidation Reactions Using Colloidal Au-Pd Nanoparticles with Various PVP: Metal

CH_4 oxidation reactions were carried out using the colloidal Au-Pd nanoparticles prepared with PVP: metal of 0.005, 0.1, 5, 10 and 20. Problems were encountered in the analysis of the NMR spectra of reactions using colloids with PVP: metal ≥5. The higher levels of stabiliser molecules in solution increased the amount of noise in the spectra and also caused peaks in the spectra to broaden. These issues created uncertainty in the reliability of the analysis of these spectra and so are not reported. The results of CH_4 oxidation reactions carried out with H_2O_2 and Au-Pd colloids with PVP: metal ratios of 0.005, 0.1 and 1.2 are shown in table 4.6.

Table 4.6 Comparison of catalytic activity of Au-Pd colloids prepared with various PVP: metal weight ratios for the oxidation of CH_4 with H_2O_2.

PVP : Metal	Product amount (μmol)				Oxy. sel. (%)	TOF (h^{-1})	Prod. (mol kg^{-1} h^{-1})	H_2O_2 / Products
	CH_3OH	CH_3OOH	HCOOH	CO_2				
1.2	3.19	9.76	7.04	3.09	86	5.4	35	36
0.1	0.00	0.00	0.00	1.22	0.0	0.3	2.1	698
0.005	0.00	0.00	0.00	1.08	0.0	0.3	1.9	772

Conditions; 1000 μmol H_2O_2, 50 °C, 30 bar CH_4, 30 min, total volume 10 ml, 1500 rpm 7.57 μmol metal per reaction.
Colloid; 10 kDa PVP, Au: Pd = 1:1 molar ratio, molar ratio, [metal] = 7.57×10^{-4} M.

Rather surprisingly neither the 0.005 nor the 0.1 PVP: metal ratio colloid produced any oxygenated products, only small amounts of CO_2. H_2O_2 consumption for both of these reactions was comparable to reaction catalysed using an Au-Pd colloid using the standard PVP: metal. There are several possible reasons for this remarkable drop in catalytic activity. The first being the increased particle size of these colloids compared to the standard colloid. This may be a factor in the reaction catalysed by the colloid with a PVP: metal of 0.005 as the average particle size in this system is 6.0 nm compared to 2.8 nm for the standard colloid (although the particle size distribution still contains smaller particles). However the difference in average particle size between the 0.1 PVP: metal colloid and the standard colloid in minimal, 3.0 nm compared to 2.8 nm, so

it is unlikely that this could cause such a significant drop in activity. Another possibility is that the reduced concentration of PVP is inhibiting activity compared to the standard Au-Pd nanoparticles. The presence of PVP in solution has already been shown (in chapter 3, section 3.2.5) to be beneficial to the catalytic activity of the Au-Pd nanoparticles by increasing the concentration of the substrate CH_4 at the metal surface. However the addition of PVP to a reaction catalysed by supported Au-Pd nanoparticles has only a moderate effect on the outcome of the reaction. The final possibility is that reducing the amount of PVP present during the reaction has a negative impact on the stability of the Au-Pd colloid. If the nanoparticles are more prone to agglomeration during reaction then the catalytic activity of the Au-Pd nanoparticles may be diminished.

4.5.5 CH_4 Oxidation Reactions Using Supported Au-Pd Nanoparticles with Various PVP: Metal

In order to determine whether the extreme drop in activity of the Au-Pd nanoparticles observed in the previous section when the ratio of PVP: metal was reduced was related to a concomitant increase in instability portions of the same colloids were supported on TiO_2 and tested for CH_4 oxidation. It was found that nanoparticles prepared with PVP: metal ≤5 could not be supported on TiO_2 using the standard sol- immobilisation procedure. It would appear that high amounts of PVP interfere with the nanoparticles adhering to the support material.

Attempts were made to also determine the particle size distribution of the nanoparticles prepared using a PVP: metal ratio of 0.005 and 0.1 after they had been supported on TiO_2. However TEM analysis reported in this section was carried out at Cardiff university whereas TEM analysis reported in chapter 3, section 3.3.3 and in section 4.4.2 of this chapter was carried out at Lehigh university on a more powerful microscope (for full details see chapter 2, section 2.7.6). Images collected at Cardiff University of supported Au-Pd nanoparticles were not of sufficiently high resolution to determine a meaningful average particle size. Poor resolution of images with lower magnification hindered the detection of larger particles biasing the calculated average particle size. However

based on the difference in mean particle size of the standard colloid (3 nm) and the standard supported catalyst (4.1 nm) it can be assumed that the mean particle sizes of the supported nanoparticles are similar to those of the corresponding colloids.

CH_4 oxidation reactions were carried out using Au-Pd nanoparticles which were prepared with PVP: metal of 0.005, 0.1 and 1.2 after being supported on TiO_2. The results of these reactions are shown in table 4.7.

Table 4.7 Comparison of catalytic activity of Au-Pd nanoparticles supported on TiO_2 prepared with various PVP: metal weight ratios for the oxidation of CH_4 with H_2O_2.

PVP : Metal	Product amount (μmol)				Oxy. sel. (%)	TOF (h^{-1})	Prod. (mol kg^{-1} h^{-1})	H_2O_2 / Products
	CH_3OH	CH_3OOH	HCOOH	CO_2				
1.2	0.60	0.00	0.00	0.41	59	2.8	1.8	4635
0.1	0.36	0.00	0.00	0.07	84	1.0	0.8	11176
0.005	1.70	0.00	0.00	0.54	76	5.0	3.9	2173

Conditions; 5000 μmol H_2O_2, 50 °C, 30 bar CH_4, 30 min, total volume 10 ml, 1500 rpm 0.89 μmol metal per reaction.
Catalyst; 28 mg, 1wt% Au-Pd/TiO_2, 10 kDa PVP, Au: Pd = 1:1 molar ratio.

Unlike their unsupported counterparts all three reactions catalysed by Au-Pd/TiO_2 produced oxygenated products. Similarly to the colloidal systems the H_2O_2 consumption was not significantly affected by the ratio of PVP: metal used to prepare the supported nanoparticles. All three reaction catalysed by supported Au-Pd nanoparticles consumed > 90% of the initial H_2O_2. Less than 2.5 μmol of products were generated by each supported catalyst tested. Overall the ratio of PVP to metal used to prepare Au-Pd/TiO_2 does not have a clear effect on the activity of the nanoparticles. This supports the theory that the extreme drop in activity observed when the ratio of PVP: metal used in the preparation of the unsupported colloidal nanoparticles is decreased from 1.2 to 0.1 is the result of an associated drop in the stability of the colloid.

The aim of this investigation was to determine the effect of particle size on the intrinsic activity of the Au-Pd nanoparticles for the oxidation of CH_4. As such further investigations into the effect of PVP: metal on colloid stability were not

carried out. However these results illustrate the need to stability as an important factor in future investigations of unsupported nanoparticle systems.

4.5.6 CH_4 Oxidation Reactions Using Colloidal Au-Pd Nanoparticles with Narrow Range of PVP: Metal

Investigations into varying the PVP: metal over a wide range have found that Au-Pd colloids prepared with very low PVP: metal (0.005 and 0.1) do not produce oxygenated products under standard reaction conditions. Whereas reactions carried out with Au-Pd colloids prepared with much higher PVP: metal (5, 10 and 20) could not be successfully analysed. As such this investigation provided limited information on the effect of PVP: metal on the catalytic activity of the colloidal system. Therefore investigations were carried out into the effect of PVP: metal over a much narrower range. Au-Pd colloids were prepared with PVP: metal of 0.6 and 2.4. Standard CH_4 oxidation reactions were carried out using these colloids and the results were compared with that of a standard colloid (figure 4.17). As the relationship between average particle size and PVP: metal is logarithmic (figure 4.13) only moderate variation in particle size is to be expected between these colloids. Consequently any variation in activity observed between these colloids is unlikely to be caused by any particle size effects but rather are a result of the different PVP concentrations. Some variation in the amount of products generated by each colloid was observed; 33 μmol for the 0.6 PVP: metal colloid, 26 μmol for the 1.2 PVP: metal colloid and 31 μmol for the 2.4 PVP: metal colloid. However these results are considered to be comparable as they lie within the 15% standard error calculated for reactions using different batches of colloid. The product distribution for each reaction was very similar with each reaction achieving >85% selectivity to oxygenated products. Varying PVP: metal across this range was found to have minimal effect on the efficiency of H_2O_2 usage. Overall, within this range, the ratio of stabilising ligand to metal used in the preparation of the Au-Pd colloid was not shown to have a significant influence on catalytic activity.

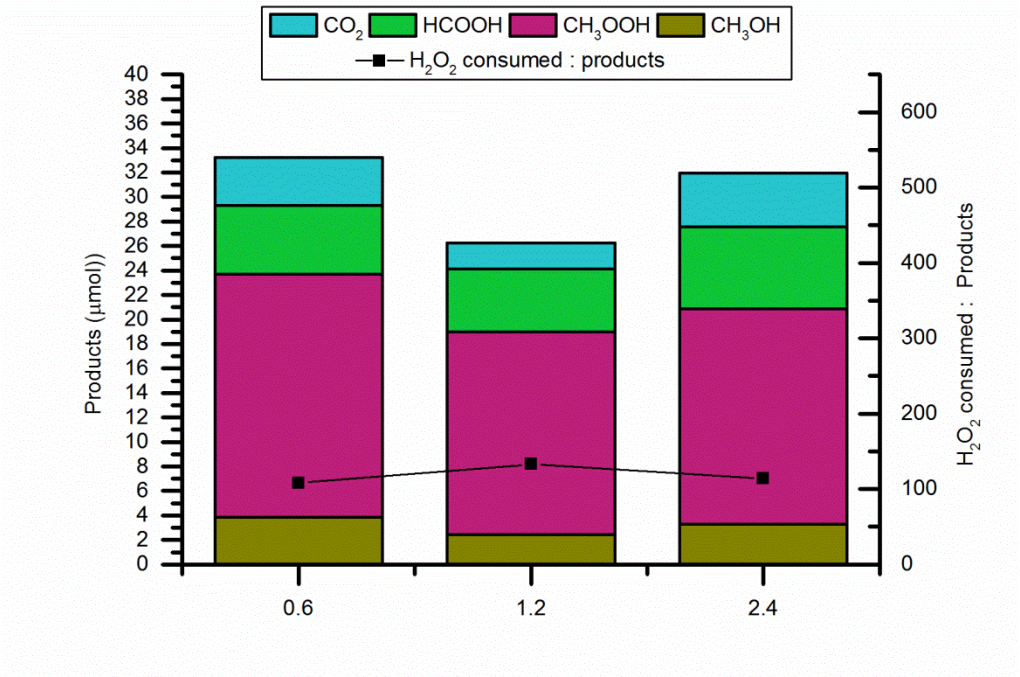

Figure 4.17 Effect of varying PVP: metal weight ratio from 0.6 to 2.4 on catalytic activity of colloidal Au-Pd nanoparticles for CH_4 oxidation with H_2O_2.

Conditions; 5000 µmol H_2O_2, 50 °C, 30 bar CH_4, 30 min, total volume 10 ml, 1500 rpm 7.57 µmol metal per reaction.
Colloid; 10 kD PVP, Au: Pd = 1:1 molar ratio, [metal] = 7.57×10^{-4} M

4.6 Conclusions

In this chapter the use of Au-Pd colloidal nanoparticles as a catalyst for the oxidation of CH_4 with H_2O_2 was investigated in detail. A set of optimised reaction conditions was identified by first optimising each individual reaction parameter and then combining the results. A reaction carried out based on the results of this procedure achieved a productivity of 74.4 mol kg^{-1}_{cat} h^{-1} demonstrating that the Au-Pd nanoparticles are intrinsically highly active for this reaction. This productivity value compares very favourably to methane monooxygenase (MMO)[30] which has a productivity of 5.1 mol kg^{-1}_{cat} h^{-1} and Fe-Cu/ZSM-5[12] systems which have a productivity of 16.5 mol kg^{-1}_{cat} h^{-1}.

Studies carried out on the effects of several preparation procedure parameters found that an equimolar ratio of Au: Pd was the most effective for

preparing Au-Pd nanoparticles as catalysts for CH_4 oxidation. Neither preparing the nanoparticles using the core-shell method nor varying the size of the stabilising ligand (PVP) used was found to have a significant effect on the activity of the nanoparticles. Increasing the metal concentration of the Au-Pd colloids resulted in an increase in the amount of products generated during a reaction but caused a concurrent drop in TOF. Systems with lower metal concentration were found to have significantly higher TOFs in contrast to reports on using Au-Pd/TiO_2 for CH_4 oxidation where the TOF of the reaction dropped with increasing metal loading as it caused an increase in H_2O_2 decomposition.[15]

To provide a meaningful comparison of two catalytic systems for the same reaction ideally selectivity should be compared at iso-conversion. As such in order to compare the oxygenate selectivity of the Au-Pd colloidal system with that of the previously published results for the 5wt% Au-Pd/TiO_2 (impreg.) catalyst CH_4 oxidation reactions were selected where the systems converted similar amounts of CH_4. As the Au-Pd colloidal nanoparticles display significantly enhanced activity compared to the 5wt% Au-Pd/TiO_2 (impreg.) catalyst the Au-Pd colloid reaction selected for comparison was both shorter and carried out at lower temperature (5 °C, 0.5 hr) than the 5wt% Au-Pd/TiO_2 (impreg.) reaction selected (50 °C, 2 hr). Under these conditions the conversion for the Au-Pd colloid system is 0.015% while the conversion of the 5wt% Au-Pd/TiO_2 (impreg.) reaction is 0.016%. R2 The oxygenate selectivity of these reactions is 87 and 37% for the colloidal and impregnation catalyst systems, respectively. Therefore at similar conversions the Au-Pd colloidal system is displays higher selectivity to the desired oxygenated products than the 5wt% Au-Pd/TiO_2 (impreg.) catalyst.

Investigations into the effect of PVP: metal found that the size of the Au-Pd nanoparticles could be controlled by manipulating this parameter. Conducting reactions with colloids prepared with greater amounts of PVP (PVP: metal of 5, 10 and 20) caused problems with the NMR analysis of the liquid phase products. Au-Pd colloids prepared with very low PVP: metal of 0.005 and 0.1 did not produce any oxygenated products when tested for CH_4 oxidation. Both the change in particle size and the effect of PVP on CH_4 solubility were ruled out as the primary cause of this dramatic drop in activity. As such the drop in activity of the

nanoparticles observed when the PVP: metal is reduced to ≤0.1 is likely due to the increased instability caused by the reduced PVP concentration. This theory is supported by the fact that Au-Pd nanoparticles prepared with PVP: metal of 0.005 and 0.1 produced oxygenated products when supported on TiO_2. It was found that varying the PVP: metal employed in Au-Pd nanoparticle preparation over more limited range (such that the effect of particle size would be minimal) did not have a significant effect on the catalytic activity of the nanoparticles.

Overall the colloidal Au-Pd nanoparticles have been found to be effective catalysts for CH_4 oxidation with H_2O_2 and a better understanding of the system has been attained through systematic investigation of various aspects of the system. It has been shown that the Au-Pd nanoparticles display a high level of intrinsic activity for this reaction however further exploration of the use of unsupported nanoparticles as catalysts will necessitate an investigation into the factors effecting colloid stability.

4.7 References

1. M. Comotti, C. Della Pina, R. Matarrese and M. Rossi, *Angew. Chem., Int. Ed.*, 2004, 43, 5812-5815.
2. Y. Mikami, A. Dhakshinamoorthy, M. Alvaro and H. Garcia, *Catal. Sci. Tech.*, 2013, 3, 58-69.
3. Y. W. Tan, X. H. Dai, Y. F. Li and D. B. Zhu, *J. Mater. Chem.*, 2003, 13, 1069-1075.
4. T. Teranishi and M. Miyake, *Chem. Mater.*, 1998, 10, 594-600.
5. O. Masala and R. Seshadri, *Annu. Rev. Mater. Res.*, 2004, 34, 41-81.
6. H. Tsunoyama, H. Sakurai, Y. Negishi and T. Tsukuda, *J. Am. Chem. Soc.*, 2005, 127, 9374-9375.
7. J. A. Lopez-Sanchez, N. Dimitratos, P. Miedziak, E. Ntainjua, J. K. Edwards, D. Morgan, A. F. Carley, R. Tiruvalam, C. J. Kiely and G. J. Hutchings, *Phys. Chem. Chem. Phys.*, 2008, 10, 1921-1930.
8. H. Tsunoyama, N. Ichikuni, H. Sakurai and T. Tsukuda, *J. Am. Chem. Soc.*, 2009, 131, 7086-7093.
9. A. Villa, D. Wang, D. S. Su and L. Prati, *Chemcatchem*, 2009, 1, 510-514.
10. C. Aliaga, J. Y. Park, Y. Yamada, H. S. Lee, C.-K. Tsung, P. Yang and G. A. Somorjai, *J. Phys. Chem. C*, 2009, 113, 6150-6155.
11. J. Y. Park, C. Aliaga, J. R. Renzas, H. Lee and G. A. Somorjai, *Catal. Lett.*, 2009, 129, 1-6.
12. C. Hammond, M. M. Forde, M. H. Ab Rahim, A. Thetford, Q. He, R. L. Jenkins, N. Dimitratos, J. A. Lopez-Sanchez, N. F. Dummer, D. M. Murphy,

A. F. Carley, S. H. Taylor, D. J. Willock, E. E. Stangland, J. Kang, H. Hagen, C. J. Kiely and G. J. Hutchings, *Angew. Chem. Int. Ed.*, 2012, 51, 5129-5133.
13. Z. Duan and S. Mao, *Geochimica et Cosmochimica Acta*, 2006, 70, 3369-3386.
14. J. Kiepe, S. Horstmann, K. Fischer and J. Gmehling, *Ind. Eng. Chem. Res.*, 2003, 42, 5392-5398.
15. M. H. Ab Rahim, M. M. Forde, R. L. Jenkins, C. Hammond, Q. He, N. Dimitratos, J. A. Lopez-Sanchez, A. F. Carley, S. H. Taylor, D. J. Willock, D. M. Murphy, C. J. Kiely and G. J. Hutchings, *Angew. Chem. Int. Ed.*, 2013, 52, 1280-1284.
16. C. Hammond, R. L. Jenkins, N. Dimitratos, J. A. Lopez-Sanchez, M. H. ab Rahim, M. M. Forde, A. Thetford, D. M. Murphy, H. Hagen, E. E. Stangland, J. M. Moulijn, S. H. Taylor, D. J. Willock and G. J. Hutchings, *Chem. Eur. J.*, 2012, 18, 15735-15745.
17. M. Ab Rahim, M. M. Forde, C. Hammond, R. L. Jenkins, N. Dimitratos, J. A. Lopez-Sanchez, A. F. Carley, S. H. Taylor, D. J. Willock and G. J. Hutchings, *Top. Catal.*, 2013, 56, 1843-1857.
18. D. P. Dissanayake and J. H. Lunsford, *J. Catal.*, 2003, 214, 113-120.
19. N. N. Edwin, J. K. Edwards, A. F. Carley, J. A. Lopez-Sanchez, J. A. Moulijn, A. A. Herzing, C. J. Kiely and G. J. Hutchings, *Green Chem.*, 2008, 10, 1162-1169.
20. D. Wang, A. Villa, F. Porta, L. Prati and D. Su, *The Journal of Physical Chemistry C*, 2008, 112, 8617-8622.
21. R. C. Tiruvalam, J. C. Pritchard, N. Dimitratos, J. A. Lopez-Sanchez, J. K. Edwards, A. F. Carley, G. J. Hutchings and C. J. Kiely, *Faraday Discuss.*, 2011, 152, 63-86.
22. V. Peneau, Q. He, G. Shaw, S. A. Kondrat, T. E. Davies, P. Miedziak, M. Forde, N. Dimitratos, C. J. Kiely and G. J. Hutchings, *Phys. Chem. Chem. Phys.*, 2013, 15, 10636-10644.
23. G. J. Hutchings and C. J. Kiely, *Acc. Chem. Res.*, 2013, 46, 1759-1772.
24. J. A. Lopez-Sanchez, N. Dimitratos, C. Hammond, G. L. Brett, L. Kesavan, S. White, P. Miedziak, R. Tiruvalam, R. L. Jenkins, A. F. Carley, D. Knight, C. J. Kiely and G. J. Hutchings, *Nature Chemistry*, 2011, 3, 551-556.
25. J. M. Campos-Martin, G. Blanco-Brieva and J. L. Fierro, *Angew. Chem. Int. Ed.*, 2006, 45, 6962-6984.
26. X. Junyang, Hua, H., Jiang, Z., Ma, Y., Huang, H., *Langmuir*, 2012, 28, 6736-6741.
27. L. Prati, P. Spontoni and A. Gaiassi, *Top. Catal.*, 2009, 52, 288-296.
28. J. A. Creighton and D. G. Eadon, *J. Chem. Soc., Faraday Trans.*, 1991, 87, 3881-3891.
29. S. Link and M. A. Ei-Sayed, *Annu. Rev. Phys. Chem.*, 2003, 54, 331-366.
30. J. Colby, D. I. Stirling and H. Dalton, *Biochem. J.*, 1977, 165, 395-402.

Activation of Methane by Methyl Hydroperoxide

5

5.1 Introduction

As discussed in previous sections the observed primary product of CH_4 oxidation with H_2O_2 is methyl hydroperoxide (CH_3OOH). In un-published work carried out by M. H. Ab Rahim within the Hutchings group it was observed that when the reaction liquid from a CH_4 oxidation reaction catalysed by CuO was separated from the catalyst by filtration and then used to carry out subsequent CH_4 oxidation reaction without any addition of a catalyst the amount of products in the reactor increased.[1] The product distribution of the initial CuO catalysed reaction strongly favoured CH_3OOH with small amounts of CH_3OH and CO_2 also produced (no HCOOH was detected). It was determined that the CH_3OOH was the cause of this effect as no significant copper leaching was detected in the reaction liquid and the presence of CH_3OH alone in the reactor will not generate further products.

These results suggested the possibility that CH_3OOH in combination with H_2O_2 could be used to activate CH_4 without the presence of a heterogeneous catalyst. The aim of this chapter is to explore this possibility. It is considered to be a three stage study; the first being the investigation of various possible copper catalysts for the production of CH_3OOH. Soluble copper species were excluded from this investigation due the requirement that the catalyst be easily separated from the reaction liquid so that the reaction liquid could then be used for a

subsequent reaction without the presence of a copper catalyst. The second stage of the investigation is the optimisation of the reaction using CH_3OOH for the activation of CH_4 and finally the chapter concludes with a preliminary investigation into the mechanism by which this reaction occurs.

5.2 Methyl Hydroperoxide Production by Methane Oxidation using Copper Oxide Catalysts

The synthesis of CH_3OOH reported in the literature involves the reaction of dimethyl sulfate with H_2O_2 followed by an extraction step using ether and fractionation.[2] This synthesis, in addition to being fairly complex and yielding only 5% CH_3OOH, is also hazardous.[3] So much so that there have been reports in the literature of explosions occurring during the procedure. As CH_3OOH is itself explosive and unstable it is not commercially available. As such CH_4 oxidation reactions were carried out to generate it for this study.

In the work carried out by M. H. Ab Rahim CuO and H_2O_2 were used to carry out a CH_4 oxidation reaction to produce the initial aqueous reaction mixture, comprising of CH_3OH and CH_3OOH, for use in a subsequent reaction.[1] Copper based catalysts had previously been reported in theoretical studies to be active for the oxidation of CH_4.[4] The presence of Cu^{2+} during CH_4 oxidation with H_2O_2 as part of a heterogeneous catalyst or in homogeneous form in the reaction medium has been shown to shut off the further oxidation of CH_3OH to HCOOH and reduce the production of CO_2 through radical quenching thus increasing selectivity to the desired oxygenate products (CH_3OOH and CH_3OH).[5-7] EPR studies have found that Cu^{2+} scavenges ·OH radicals which have been found to be responsible for the over-oxidation of CH_3OH to HCOOH.[6, 7]

A preliminary investigation was carried out into the use of CH_3OOH, produced from a CuO catalysed CH_4 oxidation reaction, to carry out a second CH_4 oxidation reaction in the absence of a solid catalyst. The aim of this experiment

was to establish whether similar results to those reported by M. H. Ab Rahim could be produced prior to further investigation into the production of CH_3OOH. A CuO catalyst was prepared by the modified sol-gel method (see chapter 2 section 2.4.3 for description) and used to carry out a standard CH_4 oxidation reaction. At the end of the reaction the CH_4 and any gas phase products were vented and the catalyst was separated from the reaction liquid by filtration. The reaction products and H_2O_2 present in the liquid were quantified as previously described before sufficient H_2O_2 and water were added to the liquid to give a total volume of 10 ml with 5000 μmol of H_2O_2. This mixture was then placed in a separate reactor and a standard CH_4 oxidation was carried without the further addition of a catalyst. The results of this reaction are shown in table 5.1. The amount of products present in the reactor increased by 414% from 4.00 to 16.55 μmol over a 30 min period. However CO_2 represented a considerable portion of the products present at the end of the reaction with only 65% of the total products detected being liquid phase, oxygenated products.

Table 5.1 CH_4 oxidation reaction carried out with CH_3OOH and H_2O_2 in the absence of a solid catalyst.

	Product amounts (μmol)					Increase (%)	Oxygenated Products (%)
	MeOH	MeOOH	HCOOH	CO_2	Total		
Initial*	2.86	1.14	0.00	-	4.00	-	100
Final	3.57	7.14	0.00	5.84	16.55	414	65

Conditions; 5000 μmol H_2O_2, 50 ^{0}C, total volume 10 ml, 30 bar CH_4, 30 min, 1500 rpm.
*Initial mixture formed through CH_4 oxidation with H_2O_2 and CuO prepared by modified sol-gel using the following conditions; 28 mg catalyst, 5000 μmol H_2O_2, 50 ^{0}C, total volume 10 ml, 30 bar CH_4, 30 min, 1500 rpm.

5.2.1 Effect of Copper Oxide Preparation Method on Catalytic Activity for Methane Oxidation

In order to study the activity of CH_3OOH it was first necessary to select a catalyst with which to carry out the initial CH_4 oxidation reaction to generate the CH_3OOH. In order for a catalyst to be selected for this purpose it must meet certain criteria. Namely that it reproducibly produce a substantial amount of CH_3OOH without significant levels of copper leeching occurring. Copper based

catalysts were selected for this purpose as the presence of copper in the catalyst in known to scavenge ·OH radicles which contribute to over-oxidation such that the selectivity to CH_3OOH and CH_3OH is increased when Cu is present.[6, 7] In order to identify such a catalyst three different methods for preparing Cu based catalysts were investigated. The method which produced the most effective catalyst was then selected for further study. The preparation parameter of this method were varied in order to produce catalysts with differing attributes. The aim of this study was to better understand the factors which affect the catalytic activity of Cu based catalysts for CH_4 oxidation. In particular, the effects of particle size, particle morphology and copper oxidation state were examined. It was considered that gaining a better understanding of these factors would facilitate the design of a catalyst that selectively produces CH_3OOH.

Cu catalysts were prepared using three different methods from the literature (described in full in chapter 2 section 2.4.3). The first, the precipitation method, involved precipitation of $CuCl_2$ with urea before refluxing with water, drying and calcination at 300 °C.[8] This method had been reported to produce copper compounds of various particle size, shape and composition depending on the copper precursor used, its concentration and the concentration of urea. In this instance the preparation conditions utilised were those reported to produce bipyramidal, atacamite ($CuCl_2.3Cu(OH)_2$) particles of 5 μm in size.

The modified sol-gel CuO catalyst was prepared by the slow evaporation of a solution of $Cu(NO_3)_2$ and citric acid at pH 1 until a viscous residue was formed. It was then dried such that a gel precursor developed. Finally it was calcined at 300 °C in order to remove the citric acid which acts as a stabiliser during the formation of the sol. This method was previously used by Wan *et al.* to produce nano-sized spherical NiO particles.[9] When the preparation was carried out at pH 1 it was found that the NiO particles formed had a particle size of 8.1 nm and a specific surface area of 105 $m^2\ g^{-1}$. Increasing the pH resulted in an increase in particle size and a concomitant reduction in surface area. In order to maximise the specific surface area of the catalyst in this study the preparation of CuO using this method was carried out at pH 1.

Finally, to prepare CuO by the quick-precipitation method a copper acetate solution was mixed with glacial acetic acid and heated to 100 °C. At this point NaOH was added to adjust the pH to 6-7. This resulted in the formation of a black precipitate which was collected by centrifugation and then dried. This quick precipitation method was selected for this investigation as it was reported to produce highly dispersed CuO nanoparticles with a narrow particle size distribution. The preparation of CuO by this method was described by Wang *et al.*[10] Using the same conditions as those employed in this study it was reported that spherical CuO particles were formed with a particle size range from 5-7 nm. XRD analysis of the same particles showed that the particle were composed of a single CuO phase with a monoclinic structure. It was also found that the morphology of the particles could be altered by varying the reaction conditions.

The results of CH_4 oxidation reactions carried out using these three Cu catalysts are shown figure 5.1. The CuO catalyst prepared by quick-precipitation displayed high selectivity towards CH_3OOH (65%) and efficient H_2O_2 usage. However the reaction generated less than 3 μmol of total products. The modified sol-gel catalyst generated a greater amount of products, 4.89 μmol, but the distribution of products formed by this reaction favoured CO_2 limiting CH_3OOH selectivity to only 13%. The precipitation Cu catalyst generated 2.14 μmol of CH_3OOH, the highest amount detected in this study. As such the precipitation method was selected as the preferred method by which to prepare Cu catalysts for the production of CH_3OOH for this study.

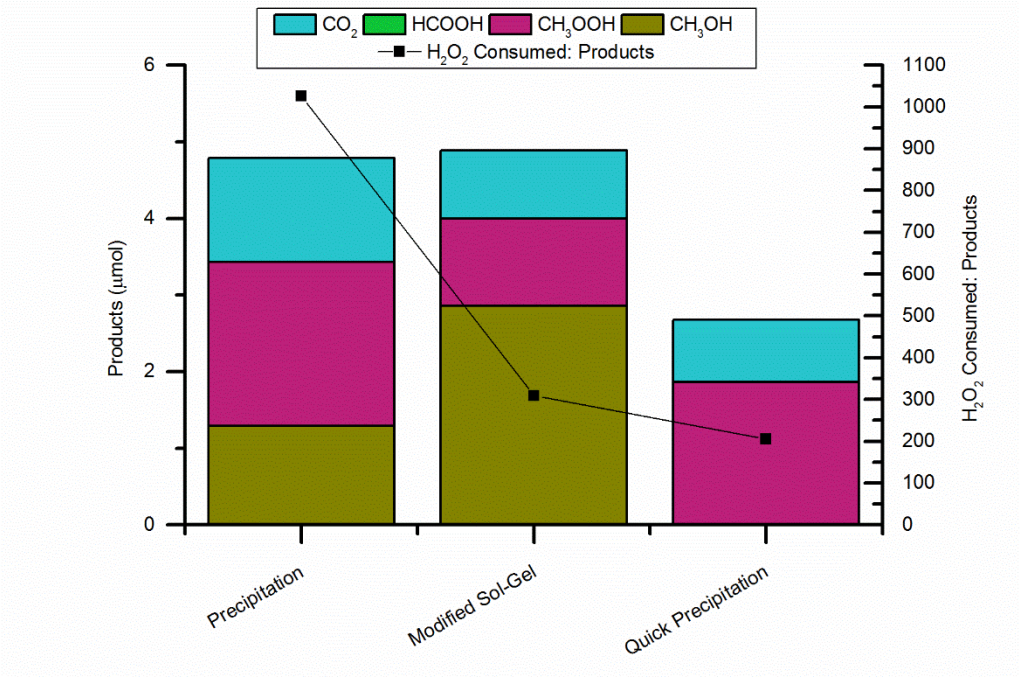

Figure 5.1 Comparison of activity of CuO prepared by various methods for CH_4 oxidation with H_2O_2.

Conditions; 28 mg catalyst, 5000 µmol H_2O_2, 50 ^{0}C, total volume 10 ml, 30 bar CH_4, 30 min, 1500 rpm.
Precipitation catalyst prepared with 8×10^{-3} M $CuCl_2$ and 2×10^{-1} M urea. See chapter two for full description of catalyst preparation methods.

Once it was established that a Cu catalyst prepared by precipitation using $CuCl_2$ and urea could generate more CH_3OOH than the CuO catalysts prepared by the quick precipitation or the modified sol-gel method it was determined that further investigation should be carried out into the preparation of Cu catalysts by precipitation. It has been reported that by varying the copper salt used as a precursor, its concentration and the concentration of urea used in the precipitation procedure the particle morphology and composition of the final Cu catalyst can be controlled.[8, 11, 12] In this way the effects of particle size, shape and Cu oxidation state were investigated.

With the aim of maximising the production of CH_3OOH, six different Cu catalysts were prepared by precipitation. Two were prepared using $CuSO_4$ as the Cu precursor. The concentrations of urea and $CuSO_4$ used corresponded to those used by S. Kratohvil and E. Matijević to produce particles of needle and platelet

type morphology.[8] Similarly $Cu(NO_3)_2$ was used to generate two more Cu catalysts. The concentrations of $Cu(NO_3)_2$ and urea used matched those used to generate platelet and spherical shaped particles in the same study. Finally, $CuCl_2$ was used to make two more catalysts, this time with concentrations that were expected to produce catalysts whose particle morphology was bipyramidal and spherical (according to the same study). Full details of these procedures including concentration of Cu precursors and urea are given in chapter 2. From this point on each catalyst prepared by precipitation shall be referred to by the Cu salt used as a precursor in its preparation and its particle morphology based on the paper by S. Kratohvil and E. Matijević.[8] It should be noted that in figure 5.1 the catalyst referred to as a precipitation catalyst is a $CuCl_2$ bipyramidal type Cu catalyst as this was the type of precipitation catalyst originally prepared by M. H. ab Rahim.[1]

Figure 5.2 shows the results of CH_4 oxidation reactions carried out with H_2O_2 and various Cu catalysts prepared by precipitation. The catalysts are identified in the graph by the type of Cu precursor used in their preparation and their particle morphology. The catalysts prepared using $CuSO_4$ as a precursor were found to be the most active for the oxidation of CH_4 with the needle shaped particles producing 19.32 μmol and the catalyst with platelet type particles producing 12.49 μmol of products. Both catalysts prepared with $CuSO_4$ achieved a selectivity of roughly 75% towards CH_3OOH such that the needles produced 14.57 μmol of CH_3OOH and the platelets produced 9.71 μmol. The catalysts prepared with $Cu(NO_3)_2$ generated the least amount of CH_3OOH with the spherical and platelet type particles producing 0.86 and 1.71 μmol of CH_3OOH respectively. Slightly more CH_3OOH was produced by the catalysts prepared with $CuCl_2$. The $CuCl_2$ prepared bipyramids generated 2.14 μmol of CH_3OOH while the spheres produced 2.86 μmol. Overall the Cu catalysts prepared using $CuSO_4$ showed the highest CH_3OOH productivities with the needle shaped particles producing the most CH_3OOH of all the catalysts tested.

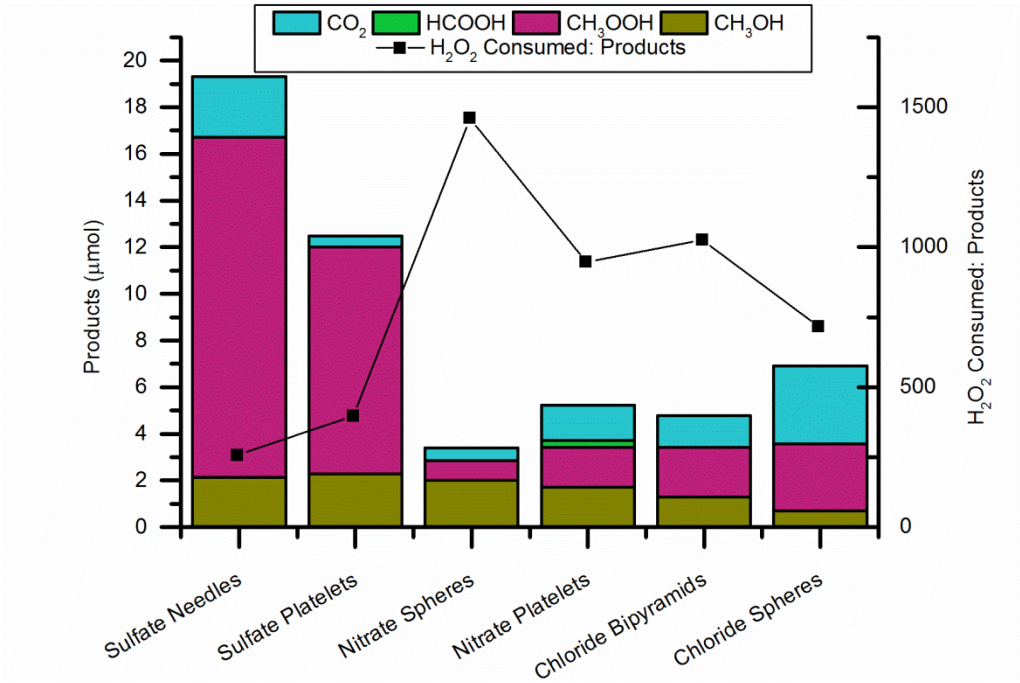

Figure 5.2 Comparison of activity of Cu catalysts prepared by precipitation using different Cu precursors and various concentration of Cu precursor and urea.

Conditions; 28 mg catalyst, 5000 µmol H_2O_2, 50 ^{0}C, total volume 10 ml, 30 bar CH_4, 30 min, 1500 rpm.
Sulfate needles; 1.5×10^{-2} M $CuSO_4$ and 5×10^{-1} M urea
Sulfate platelets; 1.2×10^{-3} M $CuSO_4$ and 3×10^{-1} M urea
Nitrate spheres; 1.5×10^{-2} M $Cu(NO_3)_2$ and 2×10^{-1} M urea
Nitrate platelets; 3×10^{-2} M $Cu(NO_3)_2$ and 1×10^{-1} M urea
Chloride bipyramids; 8×10^{-3} M $CuCl_2$ and 2×10^{-1} M urea
Chloride spheres; 3×10^{-2} M of $CuCl_2$ and 3×10^{-1} M of urea

5.2.2 MP-AES Analysis of Reactions Carried out Using Copper Catalysts Prepared by Precipitation

The aim of this investigation into Cu catalysts is to identify a catalyst which consistently produces a significant amount of CH_3OOH which can then go on to be used in a subsequent reaction. It is therefore an essential requirement that during the initial CH_4 oxidation reaction the chosen catalyst does not leach an amount of copper into solution great enough to contribute to the amount of products produced in the subsequent reaction. In order to investigate this possibility the reaction solutions from the CH_4 oxidation reactions carried out

with the six different Cu catalyst prepared by precipitation were analysed by MP-AES. The results of this analysis are shown in table 5.2.

Table 5.2 Results of MP-AES analysis carried out on reaction liquids of CH_4 oxidation reaction catalysed by various Cu catalysts prepared by precipitation.

Precursor	Theoretical morphology	Cu detected (mg/L)
$CuSO_4$	Needles	1.05
$CuSO_4$	Platelets	1.06
$Cu(NO_3)_2$	Spheres	0.54
$Cu(NO_3)_2$	Platelets	0.18
$CuCl_2$	Bipyramids	133
$CuCl_2$	Spheres	61.8

Conditions; 5000 μmol H_2O_2, 50 °C, , total volume 10 ml, 30 bar CH_4, 30 min, 28 mg catalyst
Sulfate needles; 1.5×10^{-2} M $CuSO_4$ and 5×10^{-1} M urea
Sulfate platelets; 1.2×10^{-3} M $CuSO_4$ and 3×10^{-1} M urea
Nitrate spheres; 1.5×10^{-2} M $Cu(NO_3)_2$ and 2×10^{-1} M urea
Nitrate platelets; 3×10^{-2} M $Cu(NO_3)_2$ and 1×10^{-1} M urea
Chloride bipyramids; 8×10^{-3} M $CuCl_2$ and 2×10^{-1} M urea
Chloride spheres; 3×10^{-2} M of $CuCl_2$ and 3×10^{-1} M of urea

The catalysts prepared using $CuCl_2$ were found to leach a considerable amount of copper into solution during reaction making them unsuitable for use in this work. Concentrations of 133 mg/L (for the bipyramids) and 61.8 mg/L (for the spheres) of Cu were detected which were the highest concentrations of Cu detected in this investigation. The catalysts prepared using $Cu(NO_3)_2$ displayed the lowest levels of copper leaching with concentrations of 0.54 and 0.18 mg/L of Cu being detected for the spheres and platelets respectively. A slightly greater degree of copper leaching was observed for the catalysts prepared using $CuSO_4$ with concentrations of just over 1 mg/L being detected in their reaction liquids.

To determine whether the levels of copper leaching observed for the Cu compounds prepared with $CuSO_4$ or $Cu(NO_3)_2$ were high enough to contribute to the formation of CH_4 oxidation products a homogeneous reaction was carried out under standard conditions. Sufficient $Cu(NO_3)_2$ to give a Cu concentration of 1 mg/L was added to the reactor. This reaction did not generate any liquid phase

products and only 0.38 μmol of CO_2. It can therefore be concluded that the levels of copper leaching observed for the Cu catalysts prepared with $CuSO_4$ or $Cu(NO_3)_2$ are not high enough to significantly affect the overall outcome of a standard CH_4 oxidation reaction.

5.2.3 Characterisation by SEM of Copper Catalysts Prepared by Precipitation

In order to confirm that the particle morphology of the Cu catalysts prepared by precipitation matched that of the morphologies previously reported, samples of each catalyst were examined using SEM.[8, 11, 12] From these images (figure 5.3) it was confirmed that the particle morphologies of the catalysts prepared using $CuSO_4$ matched those previously reported. The preparation where 1.5×10^{-2} M of $CuSO_4$ and 5×10^{-1} M of urea was used was found to produce needle shaped particles. Whereas the preparation that employed 1.2×10^{-3} M of $CuSO_4$ and 3×10^{-1} M of urea produced platelet like particles. It should be noted that the difference in morphology observed between the needle and platelet particles was less pronounced than that shown in the paper published by S. Kratohvil and E. Matijević.[8] In particular the difference in the length of the two types of particles is noticeably greater in that paper compared with that observed here.

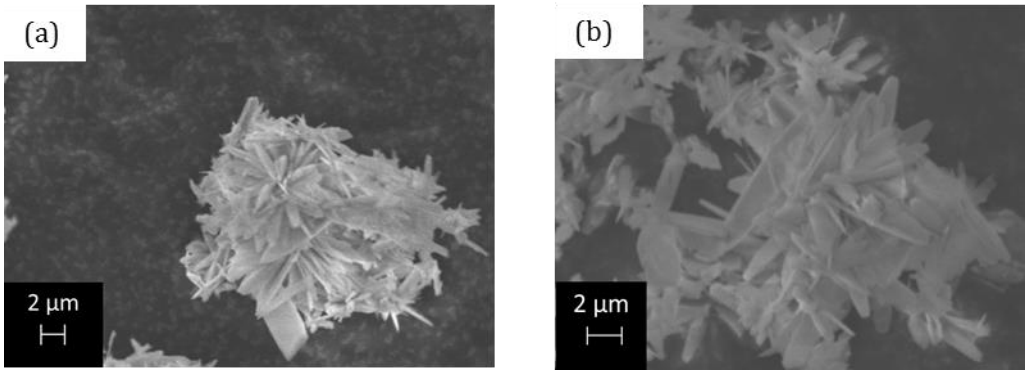

Figure 5.3 SEM images of Cu catalysts prepared by precipitation using $CuSO_4$.

(a) Sulfate needles; 1.5×10^{-2} M $CuSO_4$ and 5×10^{-1} M urea
(b) Sulfate platelets; 1.2×10^{-3} M $CuSO_4$ and 3×10^{-1} M urea

From the SEM images in figure 5.4 it was confirmed that $Cu(NO_3)_2$ had been successfully used to generate particles of two different morphologies. Preparing a Cu catalyst by precipitation of 1.5×10^{-2} M $Cu(NO_3)_2$ and 2×10^{-1} M urea produced spherical particles while a concentration of 3×10^{-2} M $Cu(NO_3)_2$ and 1×10^{-1} M of urea produced platelet particles. These results are in line with the morphologies previously reported.[8]

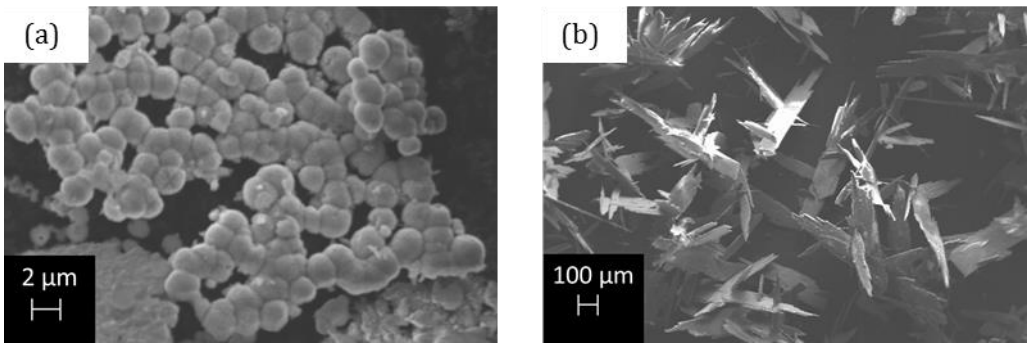

Figure 5.4 SEM images of Cu catalysts prepared by precipitation using $Cu(NO_3)_2$.
(a) Nitrate spheres; 1.5×10^{-2} M $Cu(NO_3)_2$ and 2×10^{-1} M urea
(b) Nitrate platelets; 3×10^{-2} M $Cu(NO_3)_2$ and 1×10^{-1} M urea

SEM analysis (figure 5.5) showed that when concentrations of 8×10^{-3} M of $CuCl_2$ and 2×10^{-1} M of urea were utilised to form a Cu catalyst by precipitation bipyramidal particles were formed. This was expected to be the case based on the work carried out by S. Kratohvil and E. Matijević.[8] According to the same paper spherical particles were produced using $CuCl_2$ as a precursor by changing the concentration of $CuCl_2$ used in the preparation to 3×10^{-2} M and the concentration of urea to 3×10^{-1} M. However when the same concentrations of precursor were used to carry out a precipitation in this work spherical particles were not formed. As shown in the SEM in figure 5.5 the particles have a bipyramidal, rather than a spherical, morphology similar to that of the other Cu catalyst prepared using $CuCl_2$. As such further characterisation was not carried out on this catalyst. In every other instance the particle morphology of the prepared Cu catalyst matched the morphology previously reported for the identical procedure.

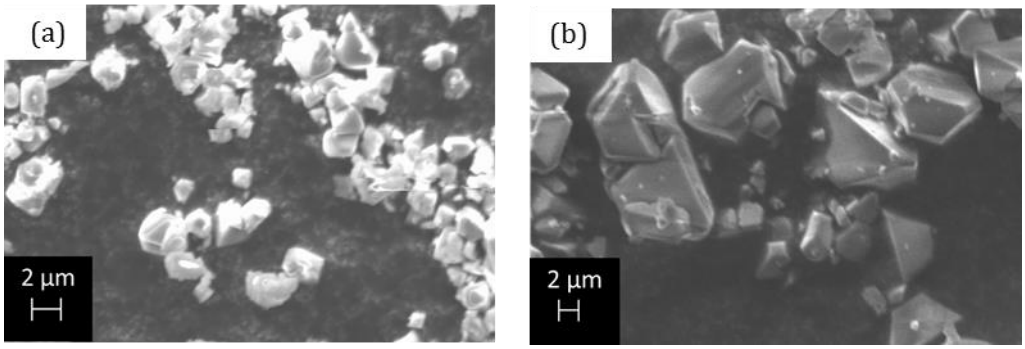

Figure 5.5 SEM images of Cu catalysts prepared by precipitation using $CuCl_2$.

(a) Chloride bipyramids; 8×10^{-3} M $CuCl_2$ and 2×10^{-1} M urea
(b) Chloride spheres; 3×10^{-2} M of $CuCl_2$ and 3×10^{-1} M of urea

5.2.4 Characterisation by XRD of Copper Compounds Prepared by Precipitation

The composition and structure, after calcination at 300 °C, of the Cu catalyst prepared by precipitation was determined through analysis of catalyst samples by x-ray diffraction. The ICDD (International Centre for Diffraction Data) database was used to assign crystal phases to the collected diffractograms. Figure 5.6 shows the x-ray diffraction pattern of both the needle and platelet type particles prepared using $CuSO_4$ while the 2θ values of the most intense peak are shown in table 5.3. In both cases the diffraction pattern was found to correspond to that of brochantite, $CuSO_4.3Cu(OH)_2$(ICDD file no. 13-398). This is in agreement with the results previously reported[8] for the needle type particles however the composition of the platelets was reported to correspond to posnjakite, $CuSO_4.3Cu(OH)_2.H_2O$. Posnjakite is a kinetic precursor of brochantite[13] and as such it's likely that posnajakite was formed initially but converted to brochantite.

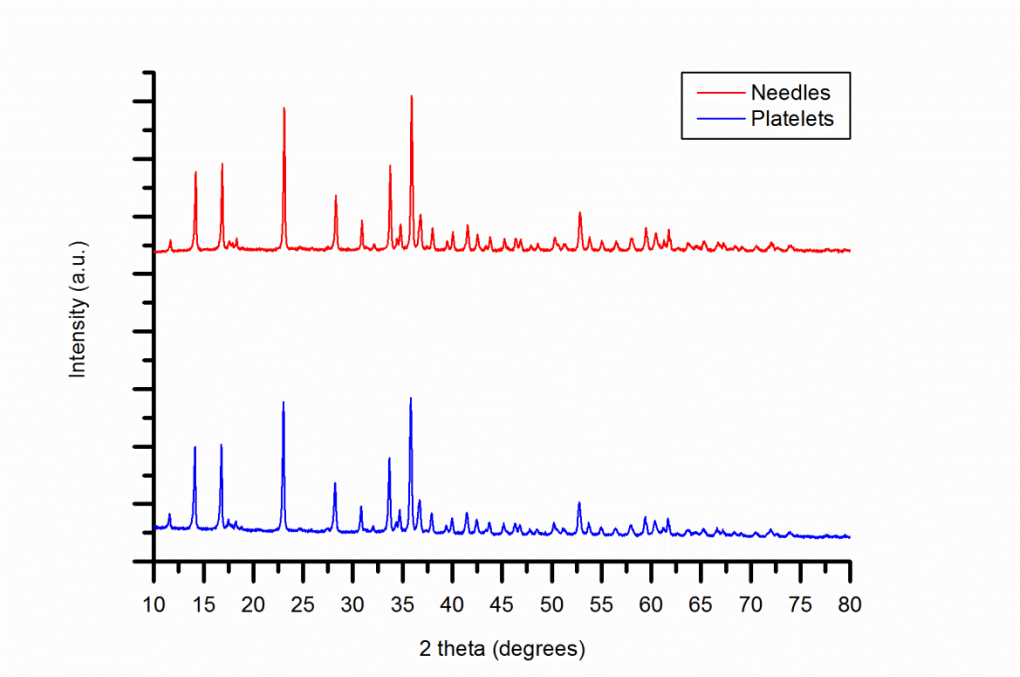

Figure 5.6 Powder X-ray diffraction patterns of Cu catalysts prepared by precipitation using $CuSO_4$ indicating that both catalysts are brochantite (ICDD file no. 13-398).

Sulfate needles; 1.5×10^{-2} M $CuSO_4$ and 5×10^{-1} M urea
Sulfate platelets; 1.2×10^{-3} M $CuSO_4$ and 3×10^{-1} M urea

Table 5.3 Powder X-ray diffraction pattern peaks of Cu catalysts prepared by precipitation using $CuSO_4$ indicating that both catalysts are brochantite (ICDD file no. 13-398).

Crystal plane			2θ (deg)		
h	k	l	Reference	Needles	Platelets
2	0	0	13.880	14.131	14.141
2	1	0	16.547	16.775	16.809
2	2	0	22.795	23.076	23.050
2	3	0	30.591	28.248	27.617
4	2	0	33.459	33.687	33.798
3	3	0	34.481	34.758	34.472
0	2	2	35.612	35.866	35.882
5	1	0	36.358	36.614	36.669
1	2	2	37.703	38.005	37.961
5	2	0	39.765	39.553	39.453
0	3	2	41.246	41.431	41.499
2	4	2	52.546	52.843	52.804
-8	0	2	59.196	59.439	59.442
-2	0	4	61.562	61.092	61.269

Sulfate needles; 1.5×10^{-2} M $CuSO_4$ and 5×10^{-1} M urea
Sulfate platelets; 1.2×10^{-3} M $CuSO_4$ and 3×10^{-1} M urea

Based on the x-ray diffraction patterns shown in figure 5.7 (peak list shown in table 5.4) both Cu catalysts prepared using $Cu(NO_3)_2$ were found to be tenorite, CuO (ICDD file no. 45-0937). The composition previously reported for the Cu catalysts prepared using the same concentrations of $Cu(NO_3)_2$ and urea was that of malachite, $Cu_2(OH)_2CO_3$.[8, 11] However the thermal decomposition of malachite to tenorite begins at 310 °C[14] and the catalyst was calcined at 350 °C as such the initial catalyst likely consisted of malachite.

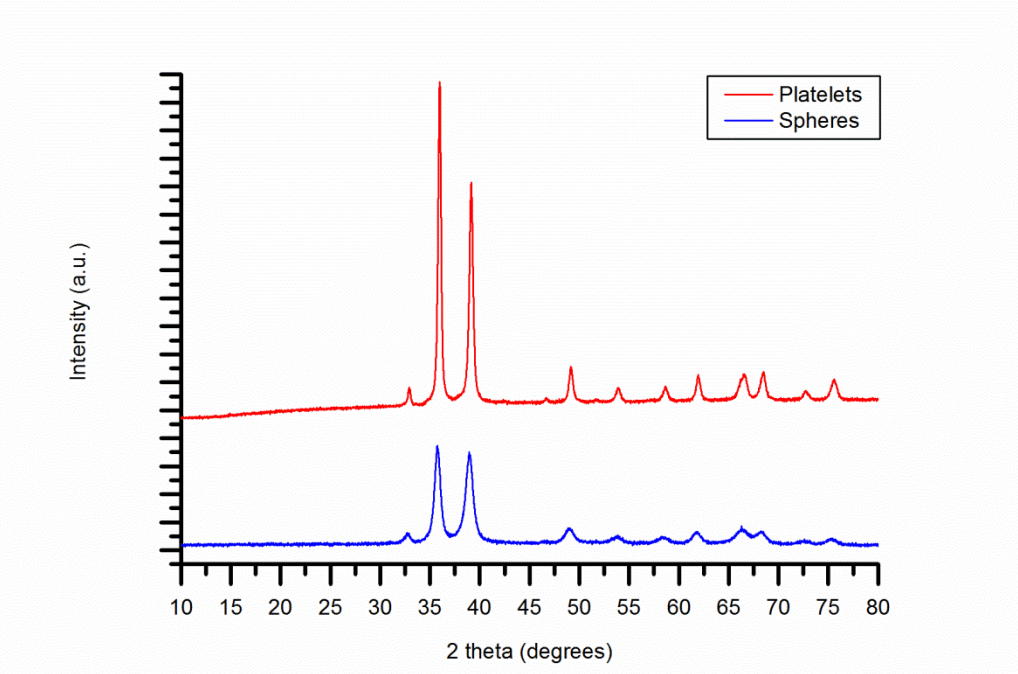

Figure 5.7 Powder X-ray diffraction patterns of Cu catalysts prepared by precipitation using $Cu(NO_3)_2$ indicating that both catalyst are tenorite (ICDD file no. 45-0937).

Nitrate spheres; 1.5×10^{-2} M $Cu(NO_3)_2$ and 2×10^{-1} M urea
Nitrate platelets; 3×10^{-2} M $Cu(NO_3)_2$ and 1×10^{-1} M urea

Table 5.4 Powder X-ray diffraction pattern peaks of Cu catalysts prepared by precipitation using $Cu(NO_3)_2$ indicating that both catalyst are tenorite (ICDD file no. 45-0937).

Crystal plane			2θ (deg)		
h	k	l	Reference	Platelets	Spheres
0	0	2	35.496	35.934	35.727
1	1	1	38.731	39.103	38.900
-2	0	2	48.727	49.115	48.953
-1	1	3	61.535	61.887	61.727
-3	1	1	66.250	66.415	66.255
-2	2	0	68.091	68.376	68.148
3	1	1	72.429	72.687	72.614
-2	2	2	75.227	75.498	75.263

Nitrate spheres; 1.5×10^{-2} M $Cu(NO_3)_2$ and 2×10^{-1} M urea
Nitrate platelets; 3×10^{-2} M $Cu(NO_3)_2$ and 1×10^{-1} M urea

The x-ray diffraction pattern of the bipyramidal particles prepared using $CuCl_2$ is shown in figure 5.8 and the 2θ positions of the mst intense peaks are shown in table 5.5. From this diffraction pattern it was determined that the particles consist of atacamite, $Cu_2Cl(OH)_3$ (ICDD file no. 19-389). This is in agreement with the composition reported by S. Kratohvil and E. Matijević for the Cu compound they prepared using the same precursor concentrations.[8]

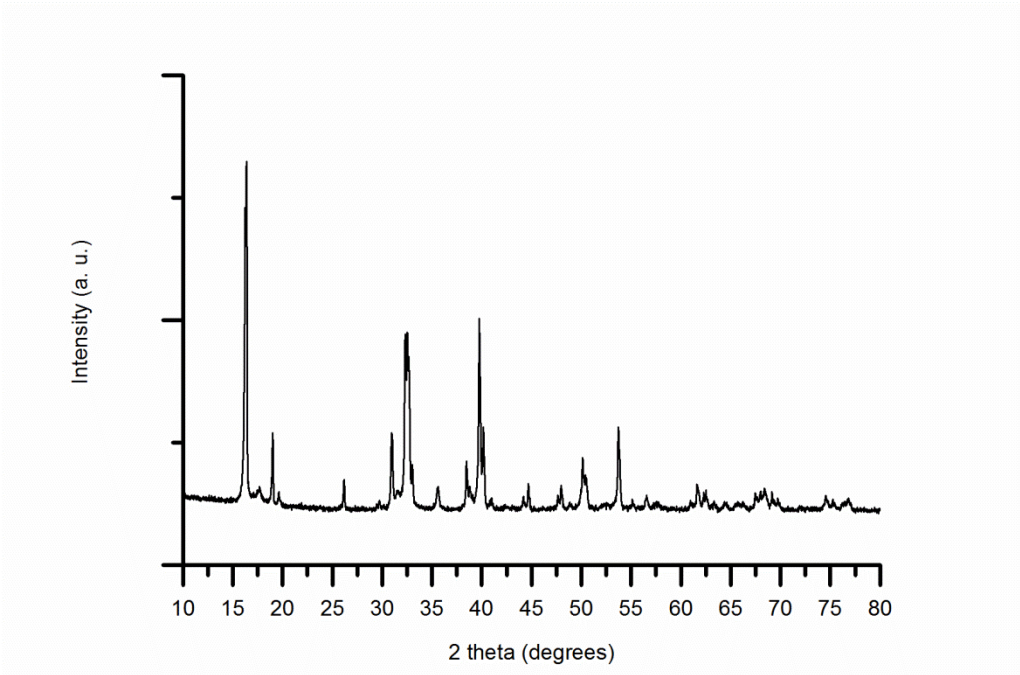

Figure 5.8 Powder X-ray diffraction pattern of Cu catalyst prepared by precipitation using $CuCl_2$ indicating that the prepared catalyst is atacamite (ICDD file no. 19-389)

Chloride bipyramids; 8×10^{-3} M $CuCl_2$ and 2×10^{-1} M urea

Table 5.5 Powder X-ray diffraction pattern of Cu catalyst prepared by precipitation using $CuCl_2$ indicating that the prepared catalyst is atacamite (ICDD file no. 19-389)

Crystal plane			2θ (deg)	
h	k	l	Reference	Sample
0	1	1	16.326	16.277
1	0	1	18.961	17.369
-1	2	1	30.941	30.942
-1	0	3	31.008	31.021
2	1	0	32.346	32.294
1	2	1	32.517	32.682
0	1	3	32.638	32.682
-2	0	2	32.772	32.765
0	2	2	32.997	33.000
2	0	2	38.467	38.550
-2	2	1	39.809	39.740
0	2	3	40.107	40.144
2	3	0	50.222	50.115

Chloride bipyramids; 8×10^{-3} M $CuCl_2$ and 2×10^{-1} M urea

From the most intense peaks of the XRD diffractograms of the Cu catalysts prepared by precipitation, crystallite size was estimated for each sample using the Scherrer equation. The results of these calculations are shown in table 5.6. and are compared with the average particle sizes of the samples as determined by analysis of the SEM images shown in section 5.2.3. There is a significant difference between the figures obtained from the Scherrer equation and those obtained from the analysis of the SEM images. XRD is a bulk technique therefore the values given by the Scherrer equation represent the average across the entire analysed sample whereas only a small sample is analysed in the SEM images. In addition larger particles are more clearly visible in the SEM images such that smaller particles are more likely to be neglected. These reasons are considered to be the cause of the substantial difference between the two sets of data. It can be ascertained from this data that the platelet type particles prepared from $Cu(NO_3)_2$ are clearly the largest particles of the samples analysed. The SEM data estimates them to be 643 times larger than the other particles analysed while the Scherrer equation determines them to be 1.57 times larger than the other particles. However, this catalyst displays similar activity for the oxidation of CH_4 with the spherical particles synthesised from $Cu(NO_3)_2$ which produced 3.39

μmol of reaction products and while the much larger platelet type particles produced 5.22 μmol. Therefore particle size does not appear to play a significant role in determining the activity of these Cu catalysts for CH_4 oxidation.

Table 5.6 Mean particle sizes and crystallite sizes of Cu catalysts prepared by precipitation as determined by analysis of SEM images and the Scherrer equation respectively.

Precursor	Theoretical Morphology	Mean Particle Size, SEM (μm)	Crystallite Size, Scherrer eq. (μm)	TOF (h^{-1})
$CuSO_4$	Needles	0.52	0.07	5.1
$CuSO_4$	Platelets	0.39	0.05	3.3
$Cu(NO_3)_2$	Spheres	0.19	0.03	0.9
$Cu(NO_3)_2$	Platelets	315	0.11	1.4
$CuCl_2$	Bipyramids	0.79	0.07	1.3

Sulfate needles; 1.5×10^{-2} M $CuSO_4$ and 5×10^{-1} M urea
Sulfate platelets; 1.2×10^{-3} M $CuSO_4$ and 3×10^{-1} M urea
Nitrate spheres; 1.5×10^{-2} M $Cu(NO_3)_2$ and 2×10^{-1} M urea
Nitrate platelets; 3×10^{-2} M $Cu(NO_3)_2$ and 1×10^{-1} M urea
Chloride bipyramids; 8×10^{-3} M $CuCl_2$ and 2×10^{-1} M urea
Chloride spheres; 3×10^{-2} M of $CuCl_2$ and 3×10^{-1} M of urea

5.2.5 Characterisation by BET of Copper Catalysts Prepared by Precipitation

In order to determine if any correlation existed between the surface area of the Cu catalysts prepared by precipitation and their activity for CH_4 oxidation BET analysis was carried out on three of the catalysts. Each of the three catalysts selected for analysis was prepared using a different Cu precursor. The results (table 5.7) show that the bipyramidal particles prepared with $CuCl_2$ have a surface area at 8 m^2/g, the needle- shaped particles prepared with $CuSO_4$ have a surface area of 6 m^2/g and the platelets prepared with $Cu(NO_3)_2$ a surface area of 4 m^2/g. The error associated with the equipment used to carry out BET analysis is ∓4 m^2/g. As such the three catalysts are considered to have comparable surface areas. From these results it can be concluded that the relative activity of the Cu catalysts prepared by precipitation is not determined by their surface area.

Table 5.7 Results of BET analysis carried out on Cu catalysts prepared by precipitation using various Cu precursors.

Precursor	Theoretical Morphology	Surface Area (m^2/g)	TOF (h^{-1})
$CuSO_4$	Needles	6	5.1
$Cu(NO_3)_2$	Platelets	4	1.4
$CuCl_2$	Bipyramids	7	1.3

Sulfate needles; 1.5×10^{-2} M $CuSO_4$ and 5×10^{-1} M urea
Nitrate platelets; 3×10^{-2} M $Cu(NO_3)_2$ and 1×10^{-1} M urea
Chloride bipyramids; 8×10^{-3} M $CuCl_2$ and 2×10^{-1} M urea

5.2.6 Characterisation by XPS of Copper Catalysts Prepared by Precipitation

XPS analysis was carried out on samples of the Cu catalysts prepared by precipitation in order to determine the oxidation state of the Cu present on the catalyst surface. The results of this analysis were considered to be of particular importance as previous work carried out by M. H. Ab Rahim on Cu catalysts for CH_4 oxidation found that oxygenate selectivity was dependant on the oxidation state of the Cu present in the catalyst.[1] In his thesis he compared the activity of CuO prepared by quick precipitation, the modified sol-gel method and precipitation (using $CuCl_2$ as precursor). He concluded that catalysts containing a mixture of Cu^{2+} and Cu^{1+} display superior selectivity to oxygenated products compared to catalysts that contain Cu in only the 2+ oxidation state. The mechanism of interaction between Cu^{1+} or Cu^{2+} with H_2O_2 is particularly complex with several different mechanisms being described in the literature.[15-18] However it is generally accepted that the reactive intermediate generated depend on the oxidation state of the Cu.[18] This is likely the cause of the difference in activity, observed here, between catalysts with a mixture of Cu^{1+}/Cu^{2+} and catalysts where only Cu^{2+} is present. An investigation was carried out to determine whether this theory could also be applied to the series of Cu catalysts prepared by precipitation.

The XPS spectra for 5 of the Cu catalysts prepared by precipitation are shown in figure 5.9.

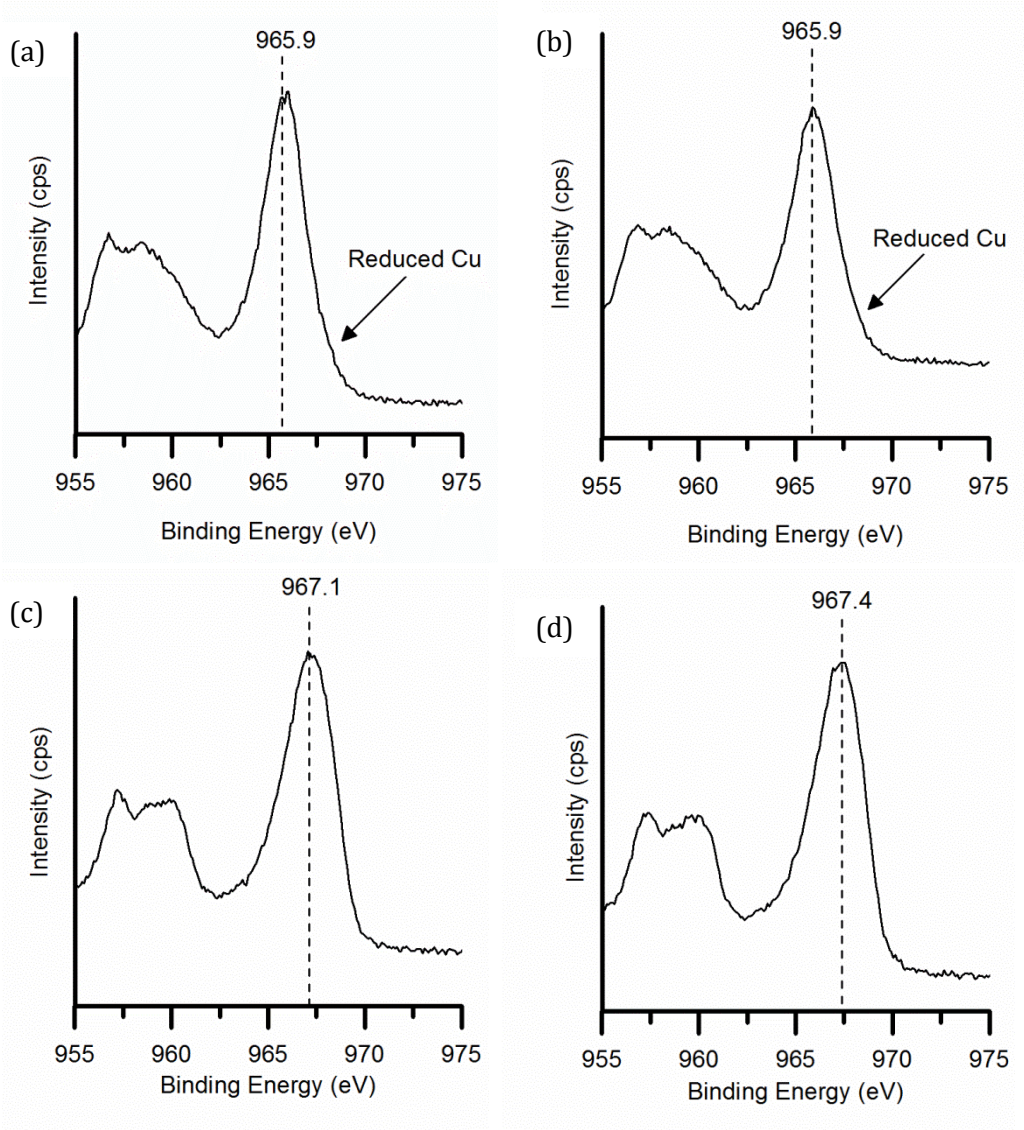

Figure 5.9 XPS spectra of Cu catalysts prepared by precipitation using either $CuSO_4$ and $Cu(NO_3)_2$ where various concentrations of the Cu precursor and urea were employed.

(a) Sulfate needles; 1.5×10^{-2} M $CuSO_4$ and 5×10^{-1} M urea
(b) Sulfate platelets; 1.2×10^{-3} M $CuSO_4$ and 3×10^{-1} M urea
(c) Nitrate spheres; 1.5×10^{-2} M $Cu(NO_3)_2$ and 2×10^{-1} M urea
(d) Nitrate platelets; 3×10^{-2} M $Cu(NO_3)_2$ and 1×10^{-1} M urea

Both catalysts prepared using $CuSO_4$ were found to contain reduced Cu. It is not possible to clearly differentiate between Cu^{1+} and Cu^0 in these spectra, Cu LMM Auger spectra are required to do so. However, as the metallic phase of Cu was not detected in XRD analysis of any of the catalysts it is assumed that the

reduced Cu species is Cu^{1+}. In the case of the needle-shaped particles 8% of the total copper present was calculated to be Cu^{1+} while the rest of the copper was in the 2+ oxidation state. The platelet shaped particles were found to contain the same amount of reduced copper (7%) within error. In neither of the two XPS spectra of the Cu catalysts prepared using $Cu(NO_3)_2$ was any reduced copper detected. Both catalysts prepared with $CuSO_4$ achieved oxygenate selectivities of >85% while the reactions carried out with catalysts prepared with $Cu(NO_3)_2$ displayed oxygenate selectivities of <85%. These results support the theory that catalysts containing a mixture of Cu^{1+} and Cu^{2+} have a greater tendency to produce oxygenated products than catalysts containing only Cu^{2+}.

Figure 5.10 shows the XPS spectrum of the bipyramidal particles prepared with $CuCl_2$.

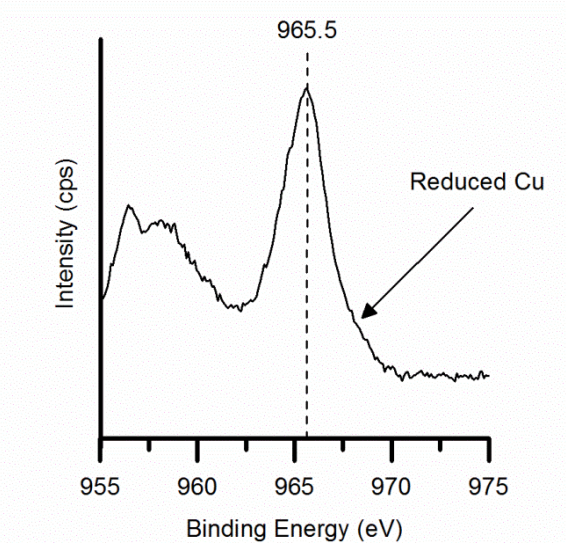

Figure 5.10 XPS spectra of Cu catalyst prepared by precipitation using different $CuCl_2$ and urea.

Chloride bipyramids; 8×10^{-3} M $CuCl_2$ and 2×10^{-1} M urea

This catalyst was not considered in the investigation of the effect of Cu oxidation state on oxygenate selectivity due to the high levels of Cu leaching observed for this catalyst during a standard CH_4 oxidation reaction (section 5.2.2). It is not clear what portion of the products detected after carrying out a CH_4 oxidation reaction with this catalyst are the result of heterogeneous or

homogeneous catalysis. It was determined that 18% of the Cu on the catalyst surface is present in a reduced oxidation state.

5.2.7 Effect of Aging on Copper Compounds Prepared by Precipitation

From the investigations into the use of Cu compounds prepared by precipitation as catalysts for CH_4 oxidation the compounds prepared using $CuSO_4$ were identified as being the most promising candidates for the production of CH_3OOH. Both catalysts produced high amounts of CH_3OOH (14.57 µmol for the needles and 9.71 µmol for the platelets) in the initial tests and insignificant amounts of Cu leaching were detected by MP-AES for both catalysts. Further testing was carried out with both catalysts approximately one week after the initial reactions (figure 5.11).

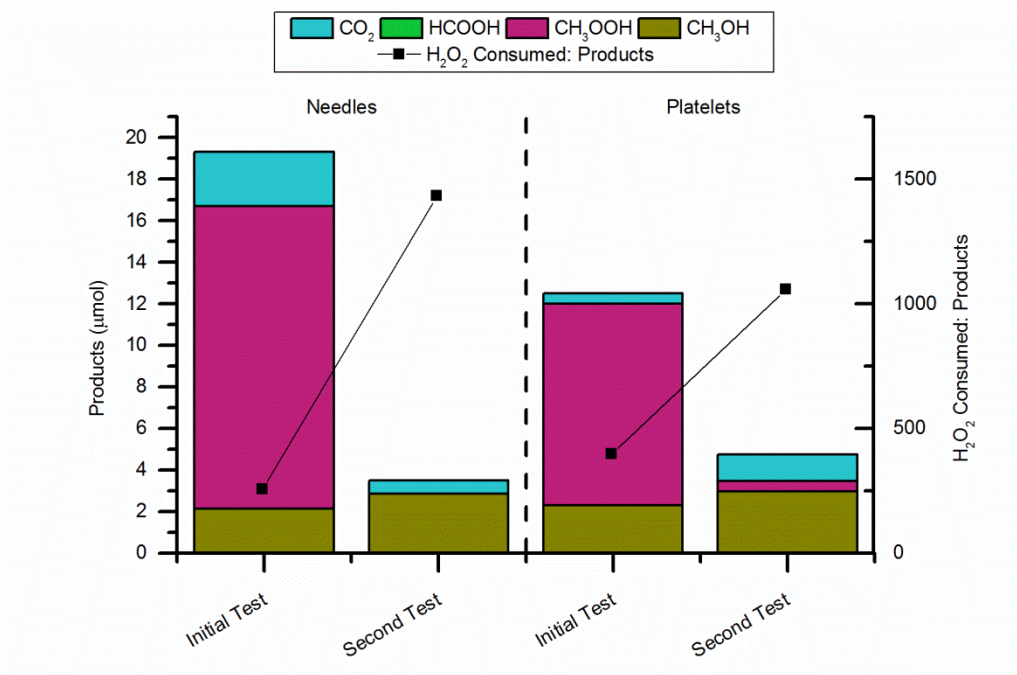

Figure 5.11 Effect of aging on activity of Cu catalysts prepared by precipitation using $CuSO_4$. Second test reaction was carried out one week after initial test.

Conditions; 28 mg catalyst, 5000 µmol H_2O_2, 50 ^{0}C, total volume 10ml, 30 bar CH_4, 30 min, 1500 rpm.
Sulfate needles; 1.5×10^{-2} M $CuSO_4$ and 5×10^{-1} M urea
Sulfate platelets; 1.2×10^{-3} M $CuSO_4$ and 3×10^{-1} M urea

In both instances a significant drop in activity was observed compared to the initial test. In the case of the needle- shaped particles the total amount of products produced dropped from 19.32 μmol to 3.49 μmol while for the platelets this amount dropped from 12.49 μmol to 4.14 μmol. These results show that aging causes a significant drop in the activity of these catalysts. It is possible that this is caused by oxidation of Cu^{1+} to Cu^{2+} as this ratio was found to have a significant effect on catalytic activity. As such it was determined that they were unsuitable for the purpose of producing CH_3OOH for use in further reactions due to the extent of variation expected in the amount of CH_3OOH produced by each reaction. It was therefore necessary to consider alternative catalysts for the production of CH_3OOH.

5.3 Methyl Hydroperoxide Production from Methane Oxidation using Cu/ZSM-5

It has previously been reported that high-temperature activated, commercial H-ZSM-5(SiO_2/Al_2O_3=30) displays significant activity for the oxidation of CH_4 with H_2O_2 under similar reaction conditions as those employed throughout this study.[6, 7, 19] This was shown to be due to the trace amounts of Fe present in the zeolite. Addition of Cu^{2+} to ZSM-5(30) does not affect the overall productivity of the system however it dramatically increases the selectivity towards CH_3OOH/CH_3OH. EPR studies found that ·OH radicals are not present during reactions catalysed by Cu containing ZSM-5(30) but are observed when standard commercial H-ZSM-5(30) is used. This indicates that the increase in selectivity to CH_3OOH/CH_3OH observed when Cu^{2+} is present in the reactor is caused by the drop in concentration of ·OH radicals.[6, 7] No HCOOH is produced when the reaction is catalysed by Cu/ZSM-5(30) as ·OH radicals are responsible for the further oxidation of CH_3OH to HCOOH.

As Cu/ZSM-5(30) is highly active for CH_4 oxidation and displays a high selectivity to CH_3OH/CH_3OOH (producing very little CO_2 and no HCOOH) it was considered an ideal candidate for the production of CH_3OOH. CH_3OOH is the primary product of the reaction which then undergoes subsequent reaction or

decomposition to form CH_3OH. As such it was determined that CH_3OOH selectivity could be increased compared to CH_3OH by reducing reaction time. In addition increasing the initial CH_4 pressure is also known to increase selectivity to CH_3OOH.[6, 20] The average results for 20 CH_4 oxidation reactions carried out over 10 min under 50 bar CH_4 using H_2O_2 and 1.25wt% Cu/ZSM-5(30) prepared by solid state ion exchange and calcined at 550 °C for 3 hours are shown in table 5.8. On average 8.91 μmol of CH_3OOH was produced per reaction. This was considered sufficient to carry out an investigation into the use of CH_3OOH for the activation of CH_4. The standard deviation of this value was found to be 29% while a standard deviation of 27% was calculated for the amount of CH_3OH produced by each reaction. As the magnitude of these standard deviations is not considered to be insignificant all liquid phase products were quantified for each reaction catalysed by Cu/ZSM-5(30) before the filtrate was utilised for subsequent CH_4 oxidation reactions.

Table 5.8 Average result of 20 CH_4 oxidation reactions carried out with Cu/ZSM-5 and H_2O_2 over 10 min.

	Product amount (μmol)			
	CH_3OH	CH_3OOH	HCOOH	Total
Average	37.82	8.91	0.00	46.73
Stan. dev.	10.30	2.58	0.00	13.26

Conditions; 28 mg catalyst, 5000 μmol H_2O_2, 50 ^{0}C, total volume 10 ml, 50 bar CH_4, 10 min, 1500 rpm.
Catalyst; 1.25 wt% Cu/ZSM-5 (30) prepared by solid state ion exchange.

As the filtrate from the Cu/ZSM-5(30) catalysed CH_4 oxidation reactions was to be used as for subsequent CH_4 oxidation reactions it was necessary to determine whether significant levels of Cu leaching occurred during the primary reaction. Cu leaching was quantified through analysis of the reaction liquid by MP-AES. It was determined that 0.12 mg/L of Cu leached from the Cu/ZSM-5(30) over the 10 min reaction period. As stated earlier (section 5.2.2) it was established that a CH_4 oxidation reaction carried out using 1 mg/L of homogeneous Cu ($Cu(NO_3)_2$) produced no liquid phase products and only 0.38 μmol of CO_2. As such the amount of Cu leached from Cu/ZSM-5(30) during the 10

min reaction was not considered to be sufficient to significantly affect the results of the second CH_4 oxidation reaction.

5.4 Investigation into the Use of Methyl Hydroperoxide for Methane Oxidation

CH_4 oxidation reactions were carried out using the filtrate from 10 min CH_4 oxidation reactions catalysed by Cu/ZSM-5(30). Once the catalyst was filtered out of the reaction liquid from the first reaction, standard analysis was carried out to determine the quantity of liquid phase products present (the gas phase was simply vented) and the amount of remaining H_2O_2. Taking into account the reduction in liquid volume caused by filtration and analysis, sufficient H_2O_2 was added to bring the oxidant concentration to the required amount and sufficient water was added to bring the total volume to 10ml. This liquid was then placed in a clean reactor and used to carry out CH_4 oxidation following the standard procedure outline in chapter 2. It should be noted that the reaction liquid was kept refrigerated during filtration and prior to use in the second reaction to minimise the decomposition of CH_3OOH.

The CH_3OOH system was used to carry out CH_4 oxidation reactions over various time lengths up to 120 min. This set of reactions were analysed using a 600Hz NMR spectrometer to enhance suppression of the solvent signal, water, which enabled the identification of the formaldehyde monohydrate, $CH_2(OH)_2$, signal at $\delta = 5.1$, as shown in figure 5.12 (see chapter 2 section 2.6.1 for all other signal assignments).

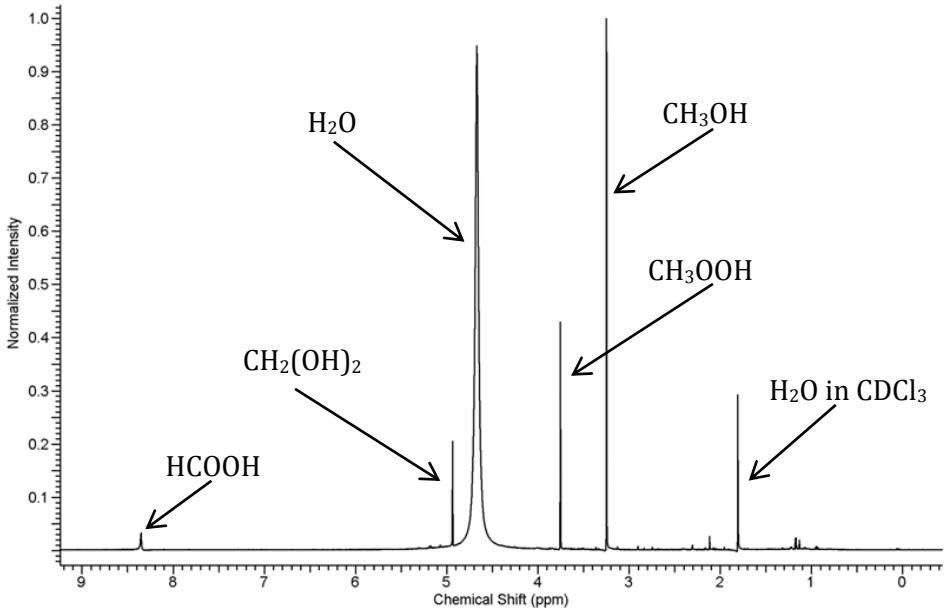

Figure 5.12 ^{1}H-NMR spectrum of CH_4 oxidation reaction carried out using CH_3OOH and H_2O_2 generated by 600Hz NMR spectrometer.

Conditions; 5000 µmol H_2O_2, 50 ^{0}C, total volume 10 ml, 30 bar CH_4, 30 min, 1500 rpm. Initial mixture formed through CH_4 oxidation with H_2O_2 and 1.25 wt% Cu/ZSM-5 (30) prepared by solid state ion- exchange using the following conditions; 28 mg catalyst, 5000 µmol H_2O_2, 50 ^{0}C, total volume 10 ml, 50 bar CH_4, 10 min, 1500 rpm.

$CH_2(OH)_2$ could not be routinely quantified in this work as in spectra obtained from the 500 Hz NMR the signal of the solvent, water, masks that of the $CH_2(OH)_2$. It can be assumed that $CH_2(OH)_2$ is produced in all CH_4 oxidation reaction carried out using CH_3OOH such that the percentage increase in reaction products reported for all reactions (apart from those in this time- on- line study and the reaction carried out under optimised conditions) is slightly lower than the total value. As an insert (capillary tube containing TMS and $CDCl_3$) cannot be used when using the 600 Hz NMR spectrometer, the $CH_2(OH)_2$ was quantified using the CH_3OH calibration signal as a reference which had previously been quantified using an insert and the 500 Hz NMR.

The temporal selectivity towards reaction products of this system is shown in figure 5.13.

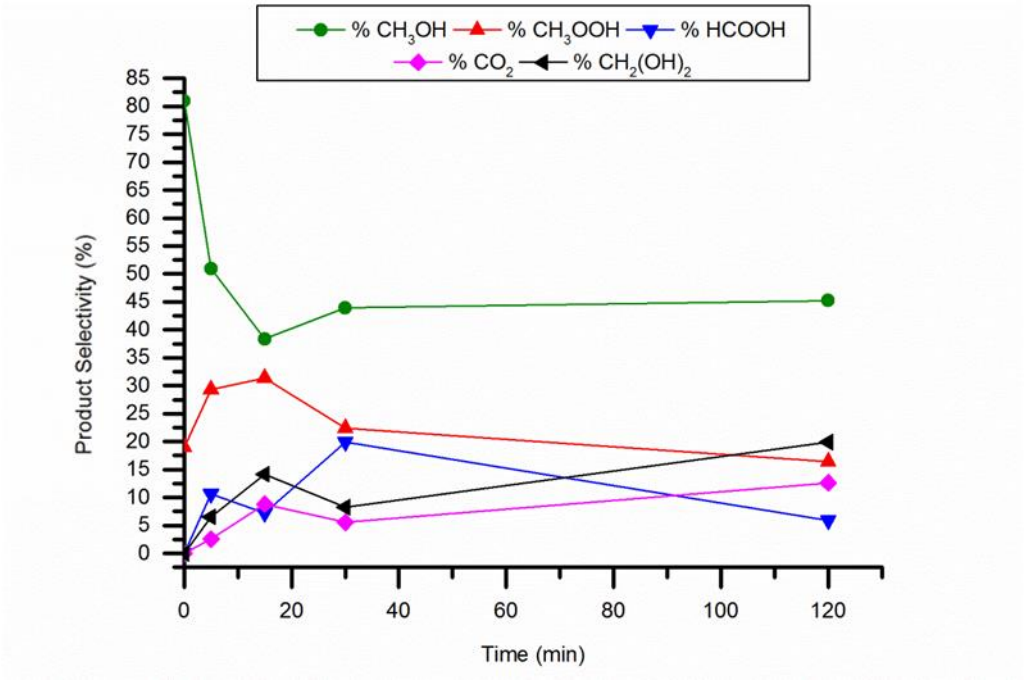

Figure 5.13 Temporal selectivity towards reaction products of CH_4 oxidation reaction carried out using CH_3OOH and H_2O_2.

Conditions; 5000 µmol H_2O_2, 50 ^{0}C, total volume 10 ml, 30 bar CH_4, 1500 rpm.
Initial mixture formed through CH_4 oxidation with H_2O_2 and 1.25 wt% Cu/ZSM-5(30) prepared by solid state ion- exchange using the following conditions; 28 mg catalyst, 5000 µmol H_2O_2, 50 ^{0}C, total volume 10ml, 50 bar CH_4, 10 min, 1500 rpm.

This is based on the final distribution of total products in the reaction liquid so includes the CH_3OOH and CH_3OH placed in the reactor at the start of the reaction however the average distribution of products at time = 0 min is also displayed. The selectivity towards CH_3OOH decreases with time as it undergoes subsequent reaction to form the secondary oxidation products. The major product of the reaction for all time lengths investigated is CH_3OH with the selectivity towards CH_3OH remaining stable above 35%. The selectivity towards HCOOH is comparable at time lengths of 5, 15 and 120 min (roughly 8% in each instance) however there is a spike to 20% in selectivity towards HCOOH at 30 min. As over-oxidation increases with time so does the selectivity towards CO_2. The selectivity to $CH_2(OH)_2$ also increases as the reaction proceeds indicating that it is a secondary reaction product.

Figure 5.14 displays the percentage increase in products as the reaction proceeds as well as the final percentage of oxygenated products and the percentage of the initial H_2O_2 remaining at the end of the reaction.

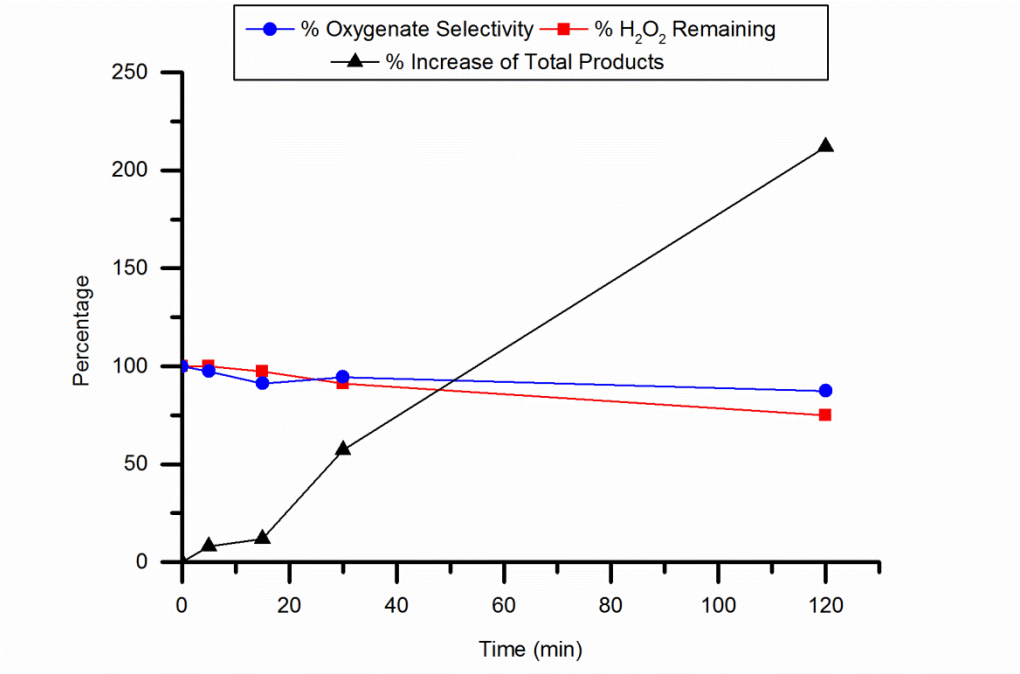

Figure 5.14 Time- on- line study of CH_4 oxidation reaction carried out using CH_3OOH and H_2O_2.

Conditions; 5000 µmol H_2O_2, 50 ^{0}C, total volume 10 ml, 30 bar CH_4, 1500 rpm.
Initial mixture formed through CH_4 oxidation with H_2O_2 and 1.25wt% Cu/ZSM-5(30) prepared by solid state ion- exchange using the following conditions; 28 mg catalyst, 5000 µmol H_2O_2, 50 ^{0}C, total volume 10 ml, 50 bar CH_4, 10 min, 1500 rpm.

The percentage increase in the total amount of products generated by the reaction steadily increases as the reaction proceeds. The 120 min reaction, for instance, began with 15.3 µmol of liquid phase products in the reactor and at the end of the reaction time the total amount of products detected was 59.63 µmol. Product distribution continuously favours the oxygenated products with overall oxygenate selectivity remaining above 85% for all reactions in the study. Low H_2O_2 consumption was observed for this system with reaction ≤30 min consuming <10% of the initial H_2O_2, increasing to 25% for a 120 min reaction.

5.4.1 Effect of Reaction Temperature

In order to investigate the effect of temperature on the CH_3OOH system CH_4 oxidation reactions were carried out over a range of temperatures from 30 to 90 °C (figure 5.15).

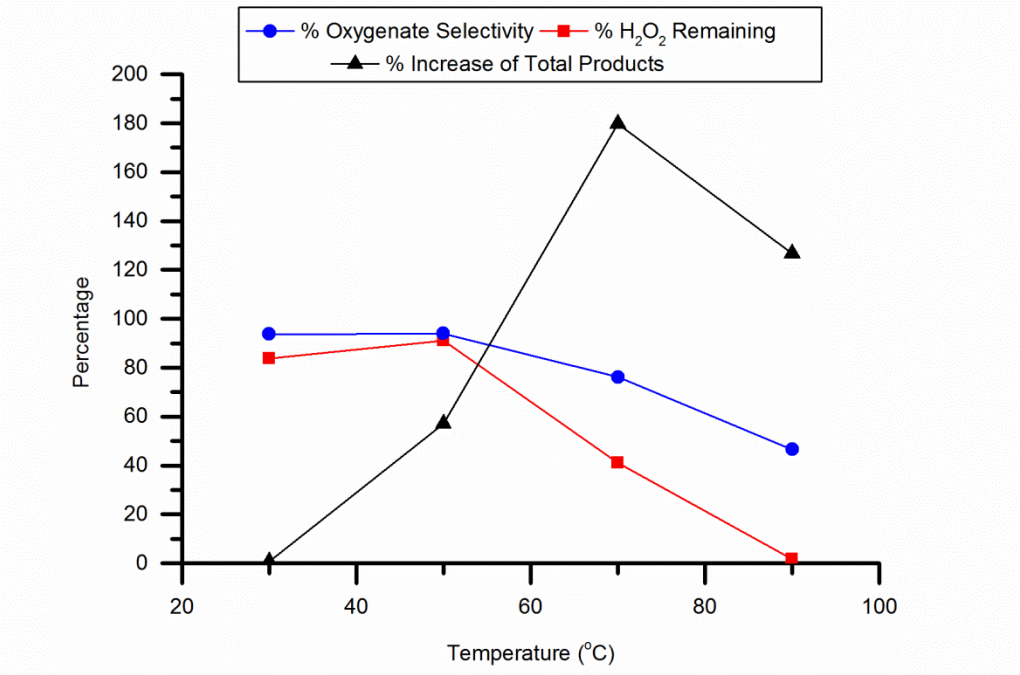

Figure 5.15 Effect of temperature on CH_4 oxidation reactions carried out using CH_3OOH and H_2O_2.

Conditions; 5000 µmol H_2O_2, total volume 10 ml, 30 bar CH_4, 30 min, 1500 rpm.
Initial mixture formed through CH_4 oxidation with H_2O_2 and 1.25wt% Cu/ZSM-5(30) prepared by solid state ion- exchange using the following conditions; 28 mg catalyst, 5000 µmol H_2O_2, 50 ^{0}C, total volume 10 ml, 50 bar CH_4, 10 min, 1500 rpm.

At 30 °C an increase of less than 1% in the total amount of products produced was observed compared to the amount of products present in the initial reaction liquid. The percentage increase in total products rises to 180% when the reaction is carried out at 70 °C then drops to 126% at 90%. This drop in activity is likely caused by the increased rate of over-oxidation to CO_2 and H_2O_2 decomposition observed as temperature is increased. Selectivity towards oxygenated products drops from 94 to 47% as the temperature is increased from 30 to 90 °C. As more over oxidation occurs less CH_3OOH is present in the reactor to activate CH_4

resulting in a drop in the amount of products produced. H_2O_2 consumption increased with reaction temperature with no residual H_2O_2 being detected at 90 °C. This is caused by the increased rate of H_2O_2 decomposition at higher reaction temperatures.

5.4.2 Effect of Methane Pressure

A series of CH_4 oxidation reactions were carried out using the CH_3OOH system at various initial pressures of CH_4 from 20 to 50 bar. The results of these reactions are shown in figure 5.16. The system displayed a selectivity towards oxygenated products of >85% for all initial pressures of CH_4 investigated. The percentage increase in the total amount of products generated compared to the initial amount present in the reaction liquid increased from 14 to 77% upon raising the CH_4 pressure from 20 to 40 bar. Further increasing the CH_4 pressure to 50 bar causes a sharp drop in this figure to 40%. It is hypothesised that this drop in activity of the system is caused by the increased stability of peroxy species with increasing CH_4 pressure. This has previously been observed in other work on CH_4 oxidation.[21, 22] The stabilisation of H_2O_2 by increased CH_4 pressure can be observed in the increase of 20% in the amount of H_2O_2 remaining at the end of the reaction upon raising the CH_4 pressure from 40 to 50 bar. In addition the same increase in CH_4 pressure causes the selectivity towards CH_3OOH to increase from 9.4 to 37.7%. When CH_3OOH and H_2O_2 are more stable they are less likely to react to activate the CH_4 and so less products are produced.

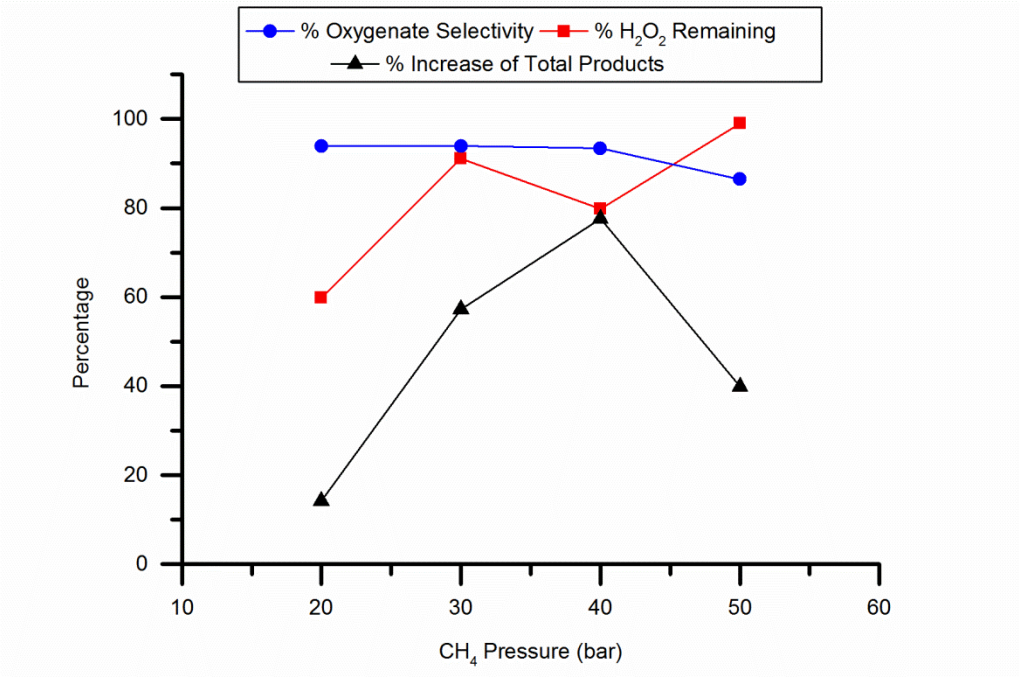

Figure 5.16 Effect of CH_4 pressure on CH_4 oxidation reactions carried out using CH_3OOH and H_2O_2.

Conditions; 5000 µmol H_2O_2, 50 ^{0}C, total volume 10 ml, 30 min, 1500 rpm.
Initial mixture formed through CH_4 oxidation with H_2O_2 and 1.25wt% Cu/ZSM-530) prepared by solid state ion- exchange using the following conditions; 28 mg catalyst, 5000 µmol H_2O_2, 50 ^{0}C, total volume 10 ml, 50 bar CH_4, 10 min, 1500 rpm.

5.4.3 Effect of Initial H_2O_2 Concentration

In order to establish the effect of initial H_2O_2 concentration on the activity of the CH_3OOH system, reactions were carried out where various amounts of H_2O_2 were added to the reactor. It should be noted that not all the H_2O_2 was consumed in the primary Cu/ZSM-5(30) catalysed reaction. As such after filtration, the amount of H_2O_2 reaming in the reaction liquid was quantified by titration (see chapter 2 section 2.6.3) and then sufficient additional H_2O_2 was added to the liquid to bring the H_2O_2 concentration to the desired level prior to being used for the second reaction. This meant that the effect of H_2O_2 concentrations lower than 2500 µmol could not be investigated. The results of the secondary reactions where various concentrations of H_2O_2 were employed are shown in figure 5.17. As the initial H_2O_2 concentration is raised the amount of products generated increases. The percentage increase in the amount of products formed compared

to the initial reaction liquid increases from 7% for a reaction where initially 2500 µmol of H_2O_2 are present in the reactor to 140% when 10,000 µmol are present at the start of the reaction. Both the percentage selectivity to oxygenated products and the percentage of the initial H_2O_2 remaining in the reactor are high for all reactions in the study, >80% of the initial oxidant remained and an oxygenate selectivity of >85% was observed for all reactions.

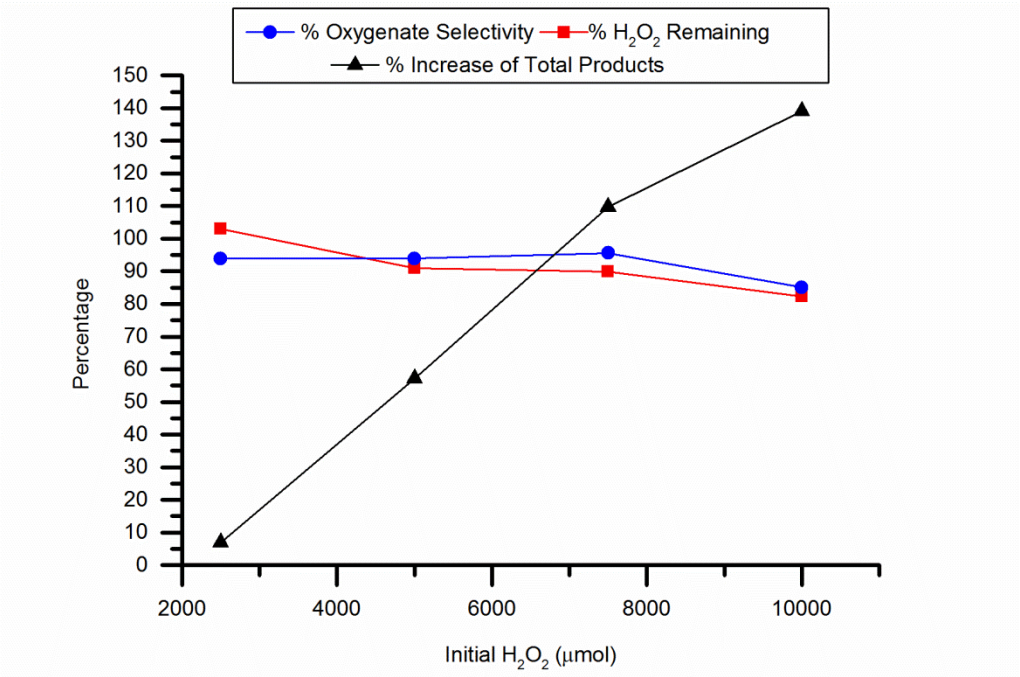

Figure 5.17 Effect of initial H_2O_2 concentration on CH_4 oxidation reactions carried out using CH_3OOH and H_2O_2.

Conditions; 50 ^{0}C, total volume 10 ml, 30 bar CH_4, 30 min, 1500 rpm.
Initial mixture formed through CH_4 oxidation with H_2O_2 and 1.25wt% Cu/ZSM-5 (30) prepared by solid state ion- exchange using the following conditions; 28 mg catalyst, 5000 µmol H_2O_2, 50 ^{0}C, total volume 10 ml, 50 bar CH_4, 10 min, 1500 rpm.

5.4.4 Optimised Reaction Conditions

The value for each of the reaction parameters for which the CH_3OOH system performed best was identified from the data reported in the preceding sections. These values were combined to form a set of optimised reaction conditions. The result of a reaction carried out using these conditions is shown in table 5.9 and compared with a reaction carried out under standard conditions. Under the

optimised reaction conditions a percentage increase of 260% in the total products produced was achieved compared to the initial reaction mixture whereas under standard conditions the increase in amount of products is only 71%. The CH_3OOH system maintains a high selectivity of 87% to oxygenated products under the optimised conditions which is comparable to the selectivity of 94% to oxygenated products under standard conditions. The H_2O_2 consumption for the optimised system is also favourable with 87% of the initial H_2O_2 remaining at the end of reaction compared with 91% for the reaction carried out under standard conditions.

Table 5.9 Comparison of standard and optimised reaction conditions for CH_4 oxidation reactions carried out using CH_3OOH and H_2O_2.

Conditions	Increase (%)	Oxygenated Products (%)	H_2O_2 Remaining (%)	H_2O_2 consumed/ Products
Standard	71	94	91	27
Optimised	260	87	87	57

Standard Conditions; 5000 μmol H_2O_2, 50 ^{0}C, total volume 10 ml, 30 bar CH_4, 30 min, 1500 rpm.
Optimised Conditions; 10,000 μmol H_2O_2, 70 ^{0}C, total volume 10 ml, 40 bar CH_4, 120 min, 1500 rpm.
Initial mixture formed through CH_4 oxidation with H_2O_2 and 1.25 wt% Cu/ZSM-5 (30) prepared by solid state ion- exchange using the following conditions; 28 mg catalyst, 5000 μmol H_2O_2, 50 ^{0}C, total volume 10 ml, 50 bar CH_4, 10 min, 1500 rpm.

5.5 Mechanistic Studies of Methyl Hydroperoxide System

Thus far it has been established that CH_3OOH can be used to oxidise CH_4 with H_2O_2 with the amount of products increasing by up to 260% compared to the amount of oxygenates initially present in the reactor. However the mechanism by which this reaction occurs is unclear. In this section the results of a preliminary investigation into the nature of this reaction mechanism are reported. Full understanding of this reaction will require a more in depth study then reported here and will likely involve an extensive study of the radicals that take part in this process by EPR. The aim of this section is to carry out some preliminary probing

of the mechanism by which this novel process occurs of which we, so far, have limited knowledge.

5.5.1 Oxidation of Isotopically Labelled Methane

In order to probe the mechanism by which CH_3OOH activates CH_4 and to confirm that the increase in products observed when a CH_4 oxidation reaction is carried out using CH_3OOH originates from CH_4, a CH_4 oxidation reaction was carried out using the CH_3OOH system where 12% of the $^{12}CH_4$ was replaced with $^{13}CH_4$. The initial reaction mixture was prepared as standard using Cu/ZSM-5(30) and 100% $^{12}CH_4$. The reaction conditions of the subsequent reaction were manipulated in order to increase the total amount of products produced to ensure that ^{13}C incorporation could be detected. The reaction was carried out at 70 °C with 10,000 μmol H_2O_2 for 6 hours. The NMR spectrum generated by the 600 Hz NMR spectrometer of the isotopically labelled reaction is shown in figure 5.18.

Incorporation of ^{13}C into the liquid phase products was observed. Of the total amount of products detected at the end of the reaction 10% of the CH_3OH, 14% of the CH_3OOH and 11% of the HCOOH contained ^{13}C. These results confirm that the reaction products originated from the CH_4. In addition the proportions of ^{13}C present in the liquid phase products indicate that they were all likely to have been generated during the second reaction. Therefore all of the liquid phase products present at the start of the reaction (10.14 μmol total) have undergone over-oxidation by the end of the 6 hour period. This is supported by the amount of CO_2 detected at the end of the reaction, 57.5 μmol.

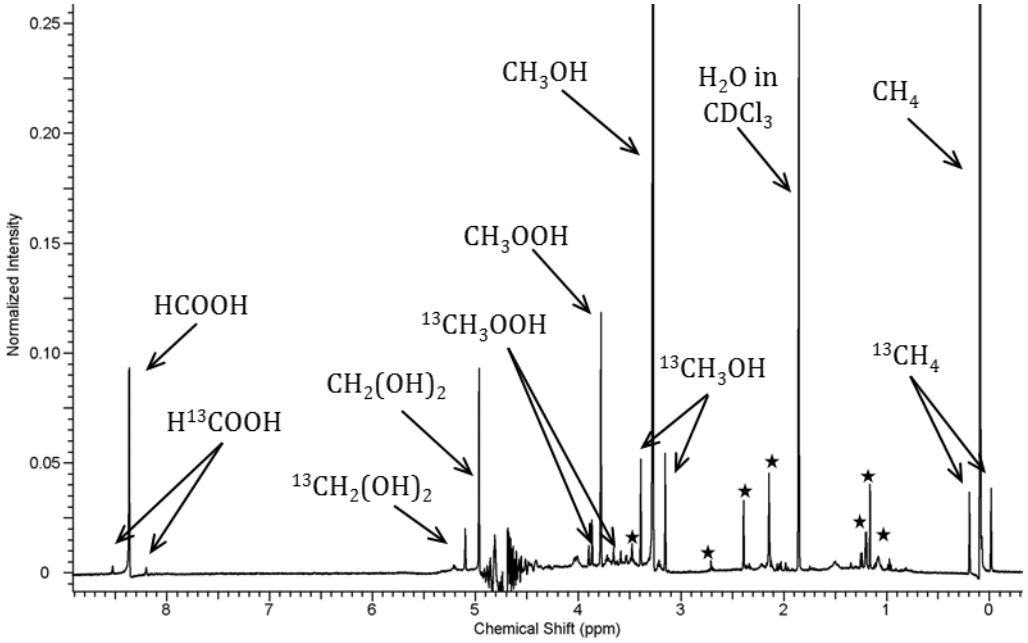

Figure 5.18 ^{1}H-NMR spectrum of CH_4 oxidation reaction carried out using CH_3OOH and H_2O_2 generated by 600Hz NMR spectrometer where a portion of the CH_4 was replaced with $^{13}CH_4$.

★ = peaks originating from contaminants
Conditions; 5000 µmol H_2O_2, 50 ^{0}C, total volume 10 ml, 30 bar CH_4, 30 min, 1500 rpm.
Initial mixture formed through CH_4 oxidation with H_2O_2 and 1.25 wt% Cu/ZSM-5 (30) prepared by solid state ion- exchange using the following conditions; 28 mg catalyst, 5000 µmol H_2O_2, 50 ^{0}C, total volume 10 ml, 50 bar CH_4, 10 min, 1500 rpm.

5.5.2 Producing Methyl Hydroperoxide Using H-ZSM-5

In order to determine the importance of the presence of Cu in the initial CH_4 oxidation reaction, reactions were carried out using H-ZSM-5(30) to produce the initial mixture of oxygenates in water. The H-ZSM-5(30) was removed by filtration and the filtrate was used to carry out subsequent CH_4 oxidation reactions. These subsequent reactions were carried out at 30 and 50 °C. The same procedure and conditions were employed as for a standard reaction using the CH_3OOH system where Cu/ZSM-5(30) was used to produce CH_3OOH. The results of the reactions carried out where H-ZSM-5(30) was used to produce the initial reaction mixture are shown in table 5.10. No increase in the amount of products present in the reactor was detected compared to the initial reaction mixture. In fact a slight decrease in the amount of products present in the reactor was observed but this is considered to be within the experimental error for

quantification of liquid products by NMR and CO_2 by GC-FID. This would imply that it is necessary to use a Cu catalyst to produce the initial reaction mixture in order for more products to be generated in the second reaction. It has previously been reported that ·OH radicals have been detected by EPR during CH_4 oxidation reactions catalysed by H-ZSM-5(30) but not when the same reaction is catalysed by Cu/ZSM-5(30).[6, 7] This would indicate that the presence of ·OH radicals interferes with the mechanism by which CH_3OOH activates CH_4.

Table 5.10 Results of CH_4 oxidation reaction carried out using CH_3OOH and H_2O_2 where the CH_3OOH was generated using H-ZSM-5.

Temp. (°C)		Product amounts (μmol)					Increase %	H_2O_2 remaining %
		CH_3OH	CH_3OOH	HCOOH	CO_2	Total		
30	Initial	5.22	10.41	14.77	-	30.41		
	Final	7.14	7.14	11.43	3.37	29.08	-4	77
50	Initial	2.86	7.05	9.56	-	19.46		
	Final	5.14	4.29	6.57	2.89	18.89	-3	67

Conditions; 5000 μmol H_2O_2, 50 ^{0}C, total volume 10 ml, 30 bar CH_4, 30 min, 1500 rpm. Initial mixture formed through CH_4 oxidation with H_2O_2 and H-ZSM-5(30) using the following conditions; 28 mg catalyst, 5000 μmol H_2O_2, 50 ^{0}C, total volume 10ml, 50 bar CH_4, 10 min, 1500 rpm.

It has already been established that the amount of Cu leaching that occurs during the initial Cu/ZSM-5(30) catalysed reaction (0.12 ppm) is too low to independently activate CH_4. However, these results show that the reaction does not proceed when H-ZSM-5(30) is used to produce the initial reaction mixture. It has been reported that homogeneous copper can act as a scavenger of ·OH radicals in CH_4 oxidation reactions catalysed by Fe/ZSM-5.[7] It was hypothesised that it is necessary for a small amount of homogeneous Cu, scavenging ·OH radicals, to be present in solution for the reaction to proceed. To investigate this possibility A solution of CH_3OH/CH_3OOH was generated using ZSM-5 using the standard conditions. 1 ppm homogeneous Cu was added to the solution which was then used to carry out a subsequent CH_4 oxidation reaction. No additional products were generated during the course of this 30 min reaction. A shift in product distribution towards secondary and over-oxidation products was

observed. This result demonstrates the role of the Cu in the Cu catalyst used to generate the initial reaction mixture is not simply to supply homogeneous Cu for the subsequent reaction. A more in-depth study of this reaction mechanism and the radicals which take part in it is required.

5.6 Conclusions

In this chapter CH_3OOH in combination with H_2O_2 has been successfully used to activate CH_4. The first step in this investigation involved identifying a suitable catalyst with which to produce CH_3OOH. With this aim in mind Cu catalysts were prepared by precipitation of $CuCl_2$ with urea, by the modified sol-gel method and by quick precipitation. The results of CH_4 oxidation reactions carried out with H_2O_2 showed that the most CH_3OOH was produced by the precipitation catalyst. This prompted an investigation into the effect of varying both the type of Cu salt and the precursor concentrations employed in the precipitation procedure. A series of Cu catalysts were prepared by precipitation, characterised and used to carry out CH_4 oxidation reactions.

It was determined that the catalysts prepared using $CuCl_2$ were unsuitable for this study due to the high levels of Cu leaching (>60 mg/L) detected in the reaction liquid by MP-AES. As the purpose of this investigation is to produce CH_3OOH for used in a subsequent CH_4 oxidation reactions the presence of high levels of homogeneous Cu in solution could potentially contribute to the formation of products in the second reaction. Neither Cu catalyst prepared using $Cu(NO_3)_2$ was considered for further study as both of them produced < 2 μmol of CH_3OOH over the course of a standard reaction. The Cu catalysts prepared with $CuSO_4$ appeared to be more promising, with each producing >9 μmol of CH_3OOH when they were first tested. However, the activity of the catalysts was severely affected by aging. One week after the initial tests the same catalysts were tested again but in this instance they both produced less than 4 μmol of total products. As such they were also discounted for further study.

Of the catalyst parameters investigated it was found that that the oxidation state of the Cu species had the most pronounced effect on the activity of the

copper catalysts investigated. Based on the results of this investigation it was concluded that a combination of Cu^{1+} and Cu^{2+} oxidation states is more effective for the oxidation of CH_4 compared to Cu^{1+} alone. It order to verify this hypothesis it is suggested that future study of CuO materials as catalysts for CH_4 oxidation involve investigating the effect of reducing them after preparation either by calcination under flowing hydrogen or by treatment with $NaBH_4$. It this way the effect of altering the oxidation state of the Cu could be investigated.

The effects of particle size and morphology on catalyst activity were also investigated but were not found to have a significant effect. The catalysts prepared by the precipitation method using $Cu(NO_3)_2$ were both identified as tenorite (CuO) and no reduced Cu was detected in either sample. However, the two catalysts displayed significantly different particle sizes and morphologies. The first catalyst comprised of spherical particles of average size 0.19 μm while the second displayed a platelet-type particle morphology with an average particle size of 312 μm (as determined by SEM). Despite these differences both catalysts displayed similar activity for the oxidation of CH_4 with the spherical particles producing a total of 3.39 μmol of reaction products and the platelet type particles producing 5.22 μmol. It would be possible to verify this theory through the preparation of additional Cu catalysts of different particle shapes and sizes. According to the literature it is possible to prepare spherical particles by the precipitation method using $CuCl_2$ by varying the concentrations of the $CuCl_2$ and urea.[8] This would provide a morphological comparison to the bipyramidal particles prepared in this study. The effect of particle size could be verified through the preparation of CuO catalysts by the modified sol-gel method which is reported to produce NiO particles varying in size between 8.4 and 22.2 nm depending on the pH at which they are prepared.[9] The information gathered from this study and those suggested could be used to inform the future design of Cu catalysts for the oxidation of methane.

H-ZSM-5(30) has previously been reported to display significant activity for CH_4 oxidation originating from the presence of trace amounts of Fe in the zeolite.[6, 7, 19] When Cu^{2+} is added to the system either in homogeneous form or as part of the solid catalyst further oxidation to HCOOH is dramatically reduced so

that the distribution of products is shifted towards CH_3OOH/CH_3OH.[6, 7] It was determined from this information that Cu/ZSM-5(30) should be considered for use in this study. By using a short reaction time and increased CH_4 pressure the product distribution of this reaction can be pushed further towards CH_3OOH. For the remainder of the study the standard procedure for producing CH_3OOH for use in subsequent CH_4 oxidation reactions was to carry out a CH_4 oxidation reaction with 1.25wt% Cu-ZSM-5(30) (prepared by solid state ion exchange) and 5,000 μmol H_2O_2 at 50 °C for 10 min under 50 bar CH_4 with a total liquid volume of 10 ml and a stirring speed of 1500 rpm. Using this system 8.91∓ 2.58 μmol of CH_3OOH is produced per reaction. MP-AES analysis was used to confirm that negligible amounts of Cu leaching occurs during these reactions.

Using the filtrate from the Cu/ZSM-5(30) catalysed reactions the ability of CH_3OOH to activate CH_4 was investigated. A time- on- line- investigation of this system showed that the amount of products present in the reactor increases by >200% over the course of a 2 hour reaction with 85% of the total products detected being oxygenated products. The effect of CH_4 pressure, initial H_2O_2 concentration and reaction temperature were investigated and from these investigations a set of optimised reaction conditions was identified. Using these reaction conditions an increase of 260% in the amount of products present in the reactor was observed. A reaction carried out using this system where a portion of $^{12}CH_4$ was replaced with $^{13}CH_4$ was found to produce products that contained ^{13}C in proportions that confirmed that the products generated during this reaction originate from CH_4. In addition it was shown that all of the liquid phase products initially present in the reactor had been over-oxidised to CO_2 by the end of the reaction. These results suggest the exciting possibility of producing CH_3OH from CH_4 without the presence of a metal catalyst. In addition as CH_3OOH thermally decomposes to CH_3OH there is no need to separate a catalyst from the products in this system.

5.7 References

1. M. H. Ab Rahim, PhD, Cardiff University, 2011.
2. A. C. Egerton, W. Emte and G. J. Minkoff, *Farad. Discuss.*, 1951, 278-282.
3. A. D. Kirk, *Can. J. Chem.*, 1965, 43, 2236-&.
4. Y. Shiota and K. Yoshizawa, *J. Am. Chem. Soc.*, 2000, 122, 12317-12326.
5. M. R. Lin, T. Hogan and A. Sen, *J. Am. Chem. Soc.*, 1997, 119, 6048-6053.
6. C. Hammond, R. L. Jenkins, N. Dimitratos, J. A. Lopez-Sanchez, M. H. ab Rahim, M. M. Forde, A. Thetford, D. M. Murphy, H. Hagen, E. E. Stangland, J. M. Moulijn, S. H. Taylor, D. J. Willock and G. J. Hutchings, *Chem. Eur. J.*, 2012, 18, 15735-15745.
7. C. Hammond, M. M. Forde, M. H. Ab Rahim, A. Thetford, Q. He, R. L. Jenkins, N. Dimitratos, J. A. Lopez-Sanchez, N. F. Dummer, D. M. Murphy, A. F. Carley, S. H. Taylor, D. J. Willock, E. E. Stangland, J. Kang, H. Hagen, C. J. Kiely and G. J. Hutchings, *Angew. Chem. Int. Ed.*, 2012, 51, 5129-5133.
8. S. K. Matijević and S. Kratohvil, *J. Mater. Res.*, 1991, 6, 766-777.
9. Y. H. Wu, Y.; Wu, T.; Chen, T.; Weng, W.; Wan, H. , *Mater. Lett.*, 2007, 61, 3174-3178., 61, 3174-3178.
10. J. Zhu, D. C. Li, X. H.; Yang, L. Lu and X. Wang, *Mater. Lett.*, 2004, 58, 3324-3327.
11. R. J. Candal, A. E. Regazzoni and M. A. Blesa, *J. Mater. Chem.*, 1992, 2, 657-661.
12. R. Rodriguezclemente, C. J. Serna, M. Ocana and E. Matijevic, *J. Cryst. Growth*, 1994, 143, 277-286.
13. D. Marani, J. W. Patterson and P. R. Anderson, *Water Res.*, 1995, 29, 1317-1326.
14. S. M. K, *Can. Mineral.*, 1975, 13, 127-132.
15. M. K. Eberhardt, G. Ramirez and E. Ayala, *J. Org. Chem.*, 1989, 54, 5922-5926.
16. T. Ozawa and A. Hanaki, *J. Chem. Soc., Chem. Commun.*, 1991, DOI: 10.1039/C39910000330, 330-332.
17. M. H. Robbins and R. S. Drago, *J. Catal.*, 1997, 170, 295-303.
18. A. N. Pham, G. Xing, C. J. Miller and T. D. Waite, *J. Catal.*, 2013, 301, 54-64.
19. A. K. M. L. Rahman, M. Kumashiro and T. Ishihara, *Catal. Comm.*, 2011, 12, 1198-1200.
20. M. H. Ab Rahim, M. M. Forde, R. L. Jenkins, C. Hammond, Q. He, N. Dimitratos, J. A. Lopez-Sanchez, A. F. Carley, S. H. Taylor, D. J. Willock, D. M. Murphy, C. J. Kiely and G. J. Hutchings, *Angew. Chem. Int. Ed.*, 2013, 52, 1280-1284.
21. M. M. Forde, B. C. Grazia, R. Armstrong, R. L. Jenkins, M. H. Ab Rahim, A. F. Carley, N. Dimitratos, J. A. Lopez-Sanchez, S. H. Taylor, N. B. McKeown and G. J. Hutchings, *J. Catal.*, 2012, 290, 177-185.
22. M. Ab Rahim, M. M. Forde, C. Hammond, R. L. Jenkins, N. Dimitratos, J. A. Lopez-Sanchez, A. F. Carley, S. H. Taylor, D. J. Willock and G. J. Hutchings, *Top. Catal.*, 2013, 56, 1843-1857.

Conclusions and Future Work 6

One of the aims of this thesis was to investigate the role of the support in the oxidation of CH_4 with H_2O_2 when catalysed by Au-Pd nanoparticles. It had previously been reported that Au-Pd/TiO_2 was an effective catalyst for this reaction.[1, 2] In this work it was found that when the Au-Pd nanoparticles are unsupported they are not only active for this reaction but in fact display superior activity compared to their supported counterparts. This is a significant result as the metal-support interface of supported gold nanoparticles is generally considered to have a beneficial influence on the catalytic activity of gold nanoparticles.[3, 4]

An investigation was carried out into the cause of the observed difference in activity between the supported and unsupported Au-Pd nanoparticles for the oxidation of CH_4. It was found that supporting the nanoparticles, on a variety of different materials, results in a significant increase in the rate of H_2O_2 decomposition during the CH_4 oxidation reaction. Consequently, less oxidant is available to oxidise CH_4 during the reactions carried out with supported Au-Pd nanoparticles. The combined amount of H_2O_2 consumed by the unsupported Au-Pd nanoparticles and by TiO_2 (without the presence of the nanoparticles) is less that the amount consumed by Au-Pd/TiO_2 under the same conditions. It can therefore be concluded that it is the metal-support interface itself that is responsible for the increased levels of H_2O_2 decomposition. This result will help inform future work on the design of catalysts for both the oxidation of CH_4 and H_2O_2 synthesis.

Once it was established that the unsupported Au-Pd nanoparticles were more active for the oxidation of CH_4 than their supported counterparts an investigation into the extent of the Au-Pd nanoparticles intrinsic activity for this reaction was carried out. By optimising the reaction parameters productivities of up to 74.4 mol kg^{-1}_{cat} h^{-1} were achieved. This productivity compares favourably with other methane oxidation catalysts reported in the literature showing that the Au-Pd nanoparticles themselves are exceptionally active for this reaction. The effects of various parameters associated with the preparation of the unsupported Au-Pd nanoparticles were investigated. In has previously been found that nanoparticle size can be controlled by varying the ratio of metal to stabiliser used in their preparation.[5-7] An investigation into the effect of varying the ratio of metal to supporting ligand was carried out with the intention of determining the effect of particle size on catalytic activity. It has previously been shown in other studies investigating the use of unsupported gold nanoparticles that particle size has a significant effect on catalytic activity.[8-10] However, in this work, the increased instability of the Au-Pd colloids at low ratios of metal to stabilising ligand meant that although the effect on particle size was only moderate these colloids were inactive for the oxidation of CH_4 with H_2O_2.

This highlights the primary disadvantage of the colloidal system, its instability. This problem has also been encountered in other studies of unsupported nanoparticles whereby particles were reported to agglomerate, leading to deactivation.[8, 10] It is proposed that a full investigation into the factors affecting the stability of the Au-Pd nanoparticles should be carried out. It's possible that using PVP of very high molecular weight or using an alternative stabilising ligand may significantly increase the colloids stability. The effect of particle size on this system is yet to be determined. It has been reported that varying the ratio of metal to reducing agent used in the preparation of nanoparticles can also alter particle size.[11, 12] As such it is recommended that future investigations of the effect of particle size on this system manipulate particle size in this manner (as opposed to varying the concentration of the stabiliser) so as to avoid increasing the instability of the nanoparticles.

As previously stated, instability is the primary disadvantage of the Au-Pd colloidal system for the oxidation of CH_4. Work carried out by Schüth *et al.* has shown that gold nanoparticles can be encapsulated in porous zirconia shells and used as catalysts for CO oxidation.[13, 14] This involves first preparing the gold particles and then coating them with a dense layer of silica by the Stöber process which produces mono-disperse silica spheres each containing a single gold particle. The silica is then coated in zirconia and the silica is leached out. It is recommended that an investigation be carried out into using the same methods to encapsulate the Au-Pd nanoparticles for the oxidation of CH_4. In this way the advantages of the colloidal system, high activity and efficient H_2O_2 usage, could be retained while avoiding the disadvantages of instability and the difficulty of separating the nanoparticles from the liquid phase products.

In this work the ability of CH_3OOH in combination with H_2O_2 to activate CH_4 has been demonstrated. It was found that up to 260% more products could be generated compared to the initial reaction mixture without the presence of a solid catalyst. Several copper catalysts were prepared and trialled for the production of CH_3OOH by CH_4 oxidation but ultimately Cu/ZSM-5 was found to be to be the most suitable catalyst tested for this purpose. The production of CH_3OOH is essential to this system of CH_4 activation as such it is advised that further research into the optimisation of this process be carried out. The mechanism by which this system activates CH_4 is as yet unknown. Therefore it is suggested that an in-depth examination of this reaction mechanism be carried out with the inclusion of investigations into the effect of various radical scavengers on the outcome of the reaction. In addition EPR studies will be required to determine the precise mechanism by which this reaction occurs. It is hypothesised that this system may also be able to oxidise the higher alkanes as such it is recommended that an investigation into this possibility be carried out.

Both of the systems described in this thesis for the oxidation of CH_4 utilise H_2O_2 as the source of oxygen. However the cost of H_2O_2 compared to the value of the desired product (CH_3OH) is not insignificant and as such a system that oxidises CH_4 using H_2O_2 as an oxidant would only be economically viable if very efficient H_2O_2 usage was achieved. Molecular oxygen, being both cheap and

environmentally favourable, would be the ideal oxidant for the direct oxidation of methane. Although the enzyme, methane monooxygenase,[15] can carry out this reaction efficiently there is as yet no industrially viable equivalent. Therefore it is recommended that future study of both of the systems described here should investigate the possibility of either entirely replacing the H_2O_2 with O_2 as the oxidant or to use H_2O_2 and O_2 in combination.

One possible method of improving H_2O_2 usage and avoiding the cost of buying pre-formed H_2O_2 is to generate the H_2O_2 *in situ*. It has previously been reported that a 5wt% Au-Pd/TiO_2 catalyst prepared by impregnation can carry out methane oxidation using a hydroperoxy species generated *in situ* from O_2 and H_2. This *in situ* method generated three times more products than an equivalent reaction carried out with pre-formed H_2O_2. Au-Pd nanoparticles have been shown to be highly active for the synthesis of H_2O_2.[2] As such it is likely that the colloidal Au-Pd PVP stabilised nanoparticles are also active for the synthesis of H_2O_2. This study has found that they display significantly lower activity for H_2O_2 decomposition compared to supported Au-Pd nanoparticles and so they are likely to be more efficient catalysts for H_2O_2 synthesis than their supported counterparts. For these reason it is suggested that the use of Au-Pd colloidal nanoparticles be investigated for the oxidation of CH_4 with *in situ* generation of peroxide.

It has been shown that Au-Pd nanoparticles are capable of catalysing the synthesis of H_2O_2[16] and the oxidation of the primary C-H bonds of toluene.[17] Both of these processes involve the activation of O_2 by the Au-Pd nanoparticles. This indicates that the use of the unsupported Au-Pd nanoparticles to activate O_2 for the oxidation of methane may also be feasible. Of the investigations proposed based on the results reported in this thesis, an investigation into this possibility is considered to be the most important.

6.1 References

1. M. Ab Rahim, M. M. Forde, C. Hammond, R. L. Jenkins, N. Dimitratos, J. A. Lopez-Sanchez, A. F. Carley, S. H. Taylor, D. J. Willock and G. J. Hutchings, *Top. Catal.*, 2013, 56, 1843-1857.
2. M. H. Ab Rahim, M. M. Forde, R. L. Jenkins, C. Hammond, Q. He, N. Dimitratos, J. A. Lopez-Sanchez, A. F. Carley, S. H. Taylor, D. J. Willock, D. M. Murphy, C. J. Kiely and G. J. Hutchings, *Angew. Chem. Int. Ed.*, 2013, 52, 1280-1284.
3. A. Haruta, *Chem. Rec.*, 2003, 3, 75-87.
4. M. Haruta, *Faraday Discuss.*, 2011, 152, 11-32.
5. T. Teranishi and M. Miyake, *Chem. Mater.*, 1998, 10, 594-600.
6. O. Masala and R. Seshadri, *Annu. Rev. Mater. Res.*, 2004, 34, 41-81.
7. X. Junyang, Hua, H., Jiang, Z., Ma, Y., Huang, H., *Langmuir*, 2012, 28, 6736-6741.
8. M. Comotti, C. Della Pina, R. Matarrese and M. Rossi, *Angew. Chem., Int. Ed.*, 2004, 43, 5812-5815.
9. H. Tsunoyama, H. Sakurai, Y. Negishi and T. Tsukuda, *J. Am. Chem. Soc.*, 2005, 127, 9374-9375.
10. A. Villa, D. Wang, D. S. Su and L. Prati, *Chemcatchem*, 2009, 1, 510-514.
11. F. Porta, L. Prati, M. Rossi and G. Scari, *J. Catal.*, 2002, 211, 464-469.
12. S. Biella, F. Porta, L. Prati and M. Rossi, *Catal. Lett.*, 2003, 90, 23-29.
13. F. Schuth, *Chem. Mater.*, 2014, 26, 423-434.
14. R. Palkovits, M. Antonietti, P. Kuhn, A. Thomas and F. Schuth, *Angew. Chem. Int. Ed.*, 2009, 48, 6909-6912.
15. J. Colby, D. I. Stirling and H. Dalton, *Biochem. J.*, 1977, 165, 395-402.
16. J. K. Edwards, E. Ntainjua N, A. F. Carley, A. A. Herzing, C. J. Kiely and G. J. Hutchings, *Angew. Chem. Int. Ed.*, 2009, 48, 8512-8515.
17. L. Kesavan, R. Tiruvalam, M. H. Ab Rahim, M. I. bin Saiman, D. I. Enache, R. L. Jenkins, N. Dimitratos, J. A. Lopez-Sanchez, S. H. Taylor, D. W. Knight, C. J. Kiely and G. J. Hutchings, *Science*, 2011, 331, 195-199.